NASA Contractor Report 3677

Results of Winglet Development Studies for DC-10 Derivatives

Carl A. Shollenberger, John W. Humphreys,
Frank S. Heiberger, and Robert M. Pearson

NASA

NASA Contractor Report 3677

Results of Winglet Development Studies for DC-10 Derivatives

Carl A. Shollenberger, John W. Humphreys,
Frank S. Heiberger, and Robert M. Pearson
McDonnell Douglas Corporation
Long Beach, California

NASA

National Aeronautics
and Space Administration

**Scientific and Technical
Information Branch**

1983

FOREWORD

This document presents the results of a contract study performed for the National Aeronautics and Space Administration (NASA) by Douglas Aircraft Company of McDonnell Douglas Corporation. This work was part of Phase II of the Energy Efficient Transport (EET) project of the Aircraft Energy Efficiency (ACEE) program.

The support and guidance given by the following persons is gratefully acknowledged; T. G. Gainer, the NASA technical monitor for the contract, of the Energy Efficient Transport Project Office at the Langley Research Center, and J. R. Tulinius, the on-site NASA representative, as well as Dr. R. T. Whitcomb of the Langley Research Center for his technical advice. Also acknowledged are the director and staff of the NASA-Ames Research Center for providing the facilities at which some of the test programs of this study were conducted.

The Douglas Aircraft Company personnel who made significant contributions to this work were:

M. Klotzsche	ACEE Program Manager
A. B. Taylor	EET Project Manager
J. T. Callaghan	Principal Staff Engineer for DC-10/EET
R. S. Bird	Aerodynamics
M. G. Brislawn	Aerodynamics
J. E. Donelson	Aerodynamics
N. A. Dodge	Aerodynamics
F. S. Heiberger	Aerodynamics
J. W. Humphreys	Aerodynamics
R. M. McCullough	Aerodynamics
J. K. Nomura	Structural Mechanics
R. M. Pearson	Structural Mechanics
E. G. Salamacha	Aerodynamics
C. A. Shollenberger	Aerodynamics
D. R. Summers	Aerodynamics

CONTENTS

ILLUSTRATIONS

ILLUSTRATIONS (Continued)

ILLUSTRATIONS (Continued)

ILLUSTRATIONS (Continued)

TABLES

SUMMARY

The results of investigations into the application of winglets to the DC-10 aircraft are presented. The DC-10 winglet configuration was developed and its cruise performance determined in a previous investigation. This study included high-speed and low-speed wind tunnel tests to evaluate aerodynamic characteristics, and a subsonic flutter wind tunnel test with accompanying analysis and evaluation of results. Additionally, a configuration integration study employed the results of the wind tunnel studies to determine the overall impact of the installation of winglets on the DC-10 aircraft. Conclusions derived from the high-speed and low-speed tests indicate that the winglets had no significant effects on the DC-10 stability characteristics or high-speed buffet and had a small improvement on outboard aileron effectiveness. It was determined that winglets had a minimal effect on aircraft lift characteristics and improved the low-speed aircraft drag under high-lift conditions. A winglet leading edge device was evaluated at low speed; it did not benefit performance but did delay winglet flow separation. The winglets affected the DC-10 flutter characteristics by reducing the flutter speed of the basic critical mode and introducing a new critical mode involving outer wing torsion and longitudinal bending. Further good agreement was obtained between flutter predictions and test results, thereby validating the prediction methods for analysis of winglet configurations. The overall impact of winglets was determined to be of sufficient benefit to merit flight evaluation.

SYMBOLS

The longitudinal aerodynamic characteristics presented in this report are referred to the stability-axis system. Force and moment data have been reduced to coefficient form based on trapezoidal wing area. All dimensional values are given in both International System of Units (SI) and U.S. Customary Units, the principal measurements and calculations using the latter.

Coefficients and symbols used herein are defined as follows:

AR	wing aspect ratio
b	wing span
$C_{D_{TO}}$	drag coefficient with tail removed
ΔC_D	incremental drag coefficient between winglet installed and baseline configurations
c	airfoil chord
$\bar{c}$	mean aerodynamic chord
C_ℓ	rolling moment coefficient
ΔC_ℓ	incremental aircraft rolling moment coefficient between given δ_a and $\delta_a = 0$ DEG
C_{ℓ_β}	derivative of rolling moment coefficient with respect to sideslip angle
$C_{L_{BUFFET}}$	buffet lift coefficient
$C_{L_{MAX}}$	maximum lift coefficient
$\Delta C_{L_{MAX}}$	incremental aircraft maximum lift coefficient between winglet installed and baseline configurations
C_L	aircraft lift coefficient
$C_{L_{TO}}$	aircraft lift coefficient with tail removed
$\Delta C_{L_{TO_{MAX}}}$	incremental tail-off maximum lift coefficient between winglet installed and baseline configurations
$C_{m_{\bar{c}/4}}$	pitching moment coefficient referenced to quarter chord of the mean aerodynamic chord
$\Delta C_{m_{\bar{c}/4}}$	incremental aircraft pitching moment coefficient between winglet installed and baseline configurations
$C_{m_{C_L}}$	derivative of pitching moment coefficient with respect to lift coefficient
$C_{m_{o_{TO}}}$	pitching moment coefficient at zero lift with tail removed

3

C_n	yawing moment coefficient
ΔC_n	incremental yawing moment coefficient between winglet installed and baseline configurations
C_{n_β}	derivative of yawing moment coefficient with respect to sideslip angle
C_P	pressure coefficient
$C_{P_{TE}}$	trailing edge pressure coefficient
C_Y	side force coefficient
ΔC_Y	incremental side force coefficient between winglet installed and baseline configurations
C_{Y_β}	derivative of side force coefficient with respect to sideslip angle
E	Young's modulus of elasticity
f	longitudinal displacement, forward positive
g	acceleration due to gravity
g_s	structural damping coefficient
G	shear modulus of elasticity
h	vertical displacement, down positive
i_H	incidence angle of horizontal stabilizer
I_{xx}	pitch mass moment of inertia
I_{yy}	roll mass moment of inertia
I_{zz}	yaw mass moment of inertia
I_{xy}, I_{yz}, I_{xz}	products of inertia
J	polar moment of inertia
l	lateral displacement, outboard positive
M	Mach number
M_x, M_y, M_z	mass of bay multiplied by displacement
q	free-stream dynamic pressure
R	Reynolds number per unit length
R_{mac}	Reynolds number based on mean aerodynamic chord
S	reference wing area
V	speed
V-g	airspeed and load factor flight envelope

V_2	aircraft takeoff safety speed which is 20 percent in excess of the stall speed
x	spanwise coordinate, positive outboard
X_{ea}, X_{EA}	spanwise coordinate of elastic axis
y	longitudinal coordinate, positive aft
Y_{ea}	longitudinal coordinate of elastic axis
z	vertical coordinate, positive up
Z_{ea}	vertical coordinate of elastic axis
α_F	fuselage angle of attack
β	sideslip angle
δ_a	aileron deflection angle
$\delta_{a_{LH}}$	deflection angle of left outboard aileron
$\delta_{a_{RH}}$	deflection angle of right outboard aileron
δ_F	flap deflection angle
δ_S	slat deflection angle
θ	roll angle, pylon mode
ψ	yaw angle, pylon mode

ABBREVIATIONS

Abbreviations used herein are defined as follows:

ACEE	Aircraft Energy Efficiency
AIC	aerodynamic influence coefficient
AND	airplane nose down
ANU	airplane nose up
CG	center of gravity
DAC	Douglas Aircraft Company
EA	elastic axis
EET	Energy Efficient Transport
FRP	fuselage reference plane
GAW	general aviation Whitcomb airfoil
GVT	ground vibration test
LWD	left wing down
MAC	mean aerodynamic chord
NASA	National Aeronautics and Space Administration
RWD	right wing down
SIC	structural influence coefficient
TED	aileron trailing edge down
TEU	aileron trailing edge up
T.O.	takeoff
WLA	wing load alleviation

INTRODUCTION

One of the latest technological advances to be considered for energy savings in transport aircraft is the winglet concept developed by Dr. R. T. Whitcomb, of the National Aeronautics and Space Administration (NASA). In this concept, the winglet is a near-vertical wing tip surface whose geometry is optimized to achieve a measure of drag reduction with less penalty on the wing bending material than a wing tip extension of equivalent performance.

The original NASA experimental investigation, reported in Reference 1, was carried out at high subsonic speeds on a wind tunnel model of what eventually became the DC-10, a second-generation jet transport having a wide body. However, more intensive explorations with improved winglets were conducted on a representative first-generation, narrow-bodied jet transport (Reference 2). The latter work led to the NASA-USAF KC-135 flight test program which has demonstrated substantial performance gains at full scale, and has verified conventional analytical methods and wind tunnel testing techniques.

Although the NASA experiments and KC-135 development showed much promise, the application of winglets to a representative second-generation transport required further investigation primarily because of a difference in the wing designs.

The second-generation, wide-bodied transport wings tend to be less tip-loaded (more twisted) and therefore do not offer as much potential for induced drag improvement from a wing tip device as the more elliptically loaded first-generation wings. Also, the newer wings are associated with advanced high-lift systems, resulting in significantly higher lift coefficients in the low-speed regime. While this affords greater opportunity for winglet-related induced drag reduction, the possibility of flow separation and hence adverse viscous effects on winglet performance and potential low-speed buffet is introduced. This distinction also separates transport winglet applications from those of some current production corporate aircraft which do not achieve such high-lift coefficients, such as the Gulfstream III, Learjet 55, and the Westwind 2. Although the winglets employed on these aircraft exhibit some geometric similarities to those which stemmed from transport winglet development (planform, location, and supercritical airfoil section), careful refinements are necessary to tailor the flow characteristics to the particular wing and its required flight conditions.

Flutter characteristics have also been found to be highly dependent on the specific winglet application. The significance of this is illustrated by the study conducted on the Boeing 747 (Reference 3) which concluded that the weight and cost penalty for correcting flutter speed degradations could be excessive. The potential sensitivity of flutter provisions was further shown in an Energy Efficient Transport (EET) study of an optimized wing/winglet transport configuration, reported in Reference 4.

In the light of these considerations, the EET project sponsored wind tunnel tests and analyses using the DC-10. The first program, reported in Reference 5, developed a satisfactory cruise configuration of upper and lower winglets through wind tunnel tests. Evaluations were made of the DC-10 Series 10 and the extended-span Series 30 models. It was concluded that the cruise drag reduction potential of winglets was close to the analytical prediction. The second program, which is the subject of this report, was intended to further the technology to a point at which evaluations could be made for production application, or, if necessary, any further development requirements could be identified.

This second program consisted of four separate studies to determine the effects of winglets on DC-10 performance. These included:

- High-speed stability and control tests made on a full-span model in the NASA Ames 11-Foot Tunnel.

- Low-speed tests, made on a full-span model in the NASA 12-Foot Tunnel, to determine the effects on both performance and stability and control characteristics.

- Flutter tests made on an elastically scaled semispan model in the Northrop 7- by 10-Foot Subsonic Tunnel. These tests provided data on flutter speeds, damping, and frequency characteristics that could be correlated with predicted results using available analytical techniques.

- An analytical investigation to determine how the findings of the aerodynamic and flutter investigations might affect the most significant performance characteristics of the DC-10. The results of available Douglas structural studies were utilized in this investigation.

Each investigation is described in a separate section of this report. The tests were made on models of a DC-10 Series 30 aircraft; however, the results in general are considered to be applicable to the shorter span DC-10 Series 10 aircraft as well.

HIGH-SPEED INVESTIGATIONS

Investigation Objectives

A high-speed wind tunnel test was conducted in March and April of 1980 to aid in evaluating the impact of winglets on the high-speed stability characteristics of the DC-10 Series 30 aircraft. The specific objectives of this investigation were to:

- Evaluate the effect of winglets on the basic aircraft longitudinal, lateral, and directional stability characteristics.

- Determine the change in outboard aileron effectiveness resulting from the winglets.

- Estimate the effect of winglets on the cruise buffet boundary.

- Observe the flow quality on the winglet and outer wing upper surface.

Experimental Apparatus and Procedures

The model employed during this test was a 3.25-percent scale representation of the DC-10 Series 30 aircraft including all cruise configuration components which had been employed in previous tests. The tail surfaces and the aft engine nacelle/pylon were removable from the model fuselage. The wing was equipped with removable nacelles and pylons for the General Electric CF6 engines. Additionally, the wing was fitted with movable outboard ailerons. The DC-10 Series 30 wing tips were modified for the installation of winglets. One set of upper and lower winglets was available for installation to the wing tips. The geometric characteristics of these winglets, given in Figures 1 and 2, were determined from the winglets utilized in the study of Reference 5. The minor differences between the winglets of Reference 5 and the present study were the result of on-site modifications made during the winglet configuration development process. The upper winglets were positionable at incidence angles of 0, −2, and −4 degrees (positive defined as toe-in), but only the −2-degree setting was employed during this program to reflect the selected configuration of Reference 5.

The test was conducted at the Unitary Plan Wind Tunnel at NASA-Ames Research Center. The test section employed in this test program is 3.4 meters (11 feet) high by 3.4 meters wide by 6.7 meters (22 feet) long. The walls are slotted on all four sides of the test section, resulting in a fixed wall porosity of 6 percent to reduce shock wave reflection and provide boundary-layer removal. The main tunnel drive system consists of four 34-Megawatt (45,000 horsepower) electric motors rotating a three-stage axial flow compressor. The Ames 11-Foot Wind Tunnel is capable of operating over a Mach Number range of approximately 0.6 to 1.4, a stagnation pressure of 0.5 to 2.25 atmospheres, a maximum stagnation temperature of 322 K (580° R), Reynolds numbers of 5.6×10^6 per meter (1.7×10^6 per foot) to 30.8×10^6 per meter (9.4×10^6 per foot), and dynamic pressures of 11,970 Pascals (250 lb/ft^2) to 95,760 Pascals (2,000 lb/ft^2).

DIMENSIONS IN CENTIMETERS (INCHES) MODEL SCALE
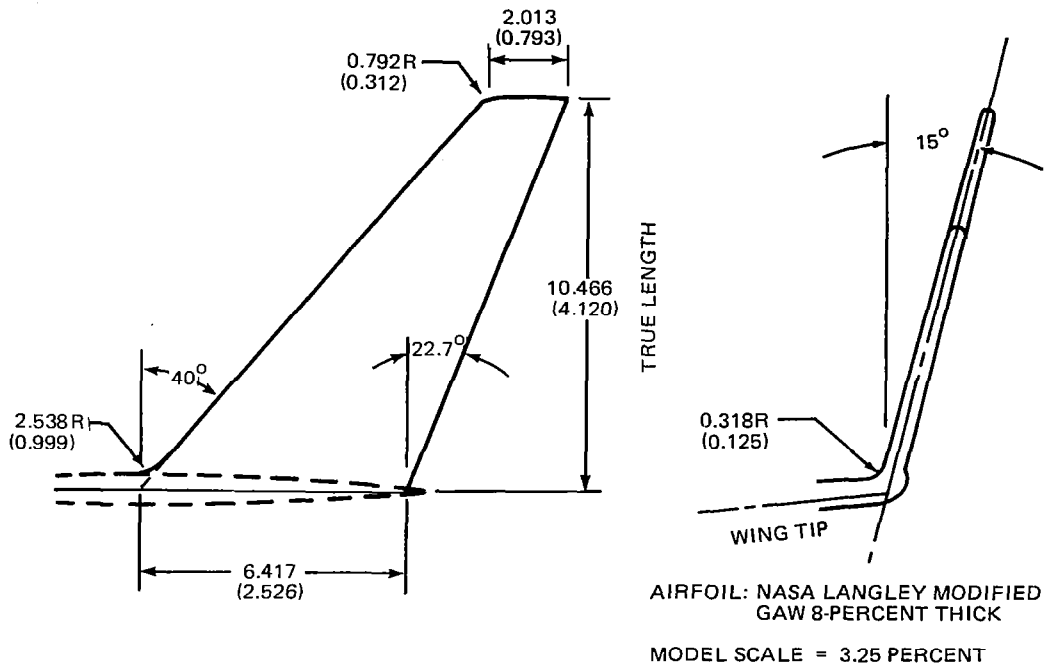
FIGURE 1. UPPER WINGLET GEOMETRIC CHARACTERISTICS FOR THE DC-10 SERIES 30
HIGH-SPEED WIND TUNNEL MODEL

DIMENSIONS IN CENTIMETERS (INCHES) MODEL SCALE
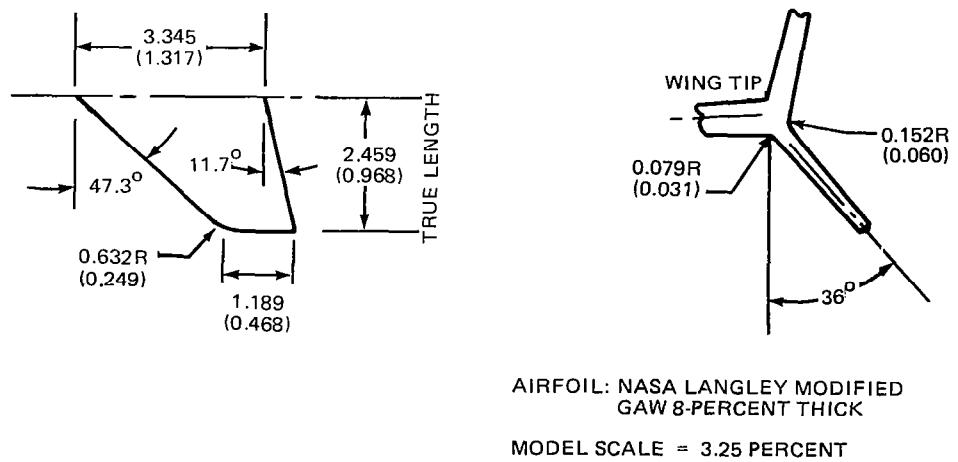
FIGURE 2. LOWER WINGLET GEOMETRIC CHARACTERISTICS FOR THE DC-10 SERIES 30 HIGH-SPEED
WIND TUNNEL MODEL

12

The DC-10 Series 30 model was mounted on the Task Mark XB 6.35-cm (2.50-inch) internal strain gage balance and supported by the Douglas J011601 sting, as shown in Figure 3. As indicated in the figure, the support system included the Ames 10-degree adaptor and 102-cm (40-inch) extension. Model alignment in pitch and roll was checked by using the bubbles embedded in the model, whereas yaw alignment was checked by dropping plumb bob lines from known points on the side of the fuselage. A photograph of the model installed in the test section is shown in Figure 4.

The model instrumentation consisted of the Task Mark XB 6.35-cm (2.50-inch) internal model balance, root-bending moment gages, strain gages on the dynamics damper beam, and a model ground indicator. Pressure orifices were located on the wing and winglets, in the sting and balance cavities, and on the base areas.

Wing pressure orifice rows were located at 23.5, 31.1, 42.3, 56.4, 67.6, 79.9, and 93.0 percent semispan stations on the wing. Additionally, rows of pressure orifices were located at 12 and 80 percent span locations on the upper winglets. Tubing from the orifices was connected to two six-module scanivalve units located in the fuselage nose. The scanivalves were equipped with 103,000-Pascal (15 lb/in.^{2}) differential pressure transducers.

Six-component balance data, sting cavity pressures, model base pressures, and wing root bending moments were recorded for all runs, whereas wing and winglet pressures were recorded only for selected runs. The balance data were reduced to force and moment coefficients referenced to the stability axes. Force and moment coefficients were corrected for the effect of the deviation of model base and sting cavity pressures from free-stream static pressure. All coefficients were based on free-stream dynamic pressure and scaled-down geometric constants for the DC-10 Series 30 aircraft.

In order to investigate and record the flow quality on the upper winglet, the lower winglet outboard surface, and the wing tip upper surface, a mini-tuft visualization technique was employed (Reference 6). Nylon monofilament tufts of 0.0025-cm (0.0010-inch) diameter and approximately 0.64-cm (0.25-inch) long and treated with fluorescent dye were applied to the subject areas in spanwise rows. The tuft patterns were recorded by employing an ultraviolet flash unit and two remotely operated cameras.

The wind tunnel program was divided into two main parts: the first part focused on the baseline DC-10 Series 30 aircraft without winglets to establish basic characteristics, and the second examined the characteristics of the winglet-equipped aircraft. In each part, tail-on and tail-off investigations were conducted beginning with (1) longitudinal stability evaluations employing pitch runs, (2) lateral-directional stability evaluations employing pitch runs at a fixed sideslip angle, and (3) yaw sweeps at a fixed pitch angle. Two horizontal stabilizer incidence angles were investigated in the tail-on tests. These stability and control tests were conducted over a Mach

DIMENSIONS IN CENTIMETERS (INCHES) MODEL SCALE

TS = TUNNEL STATION

MS = MODEL STATION
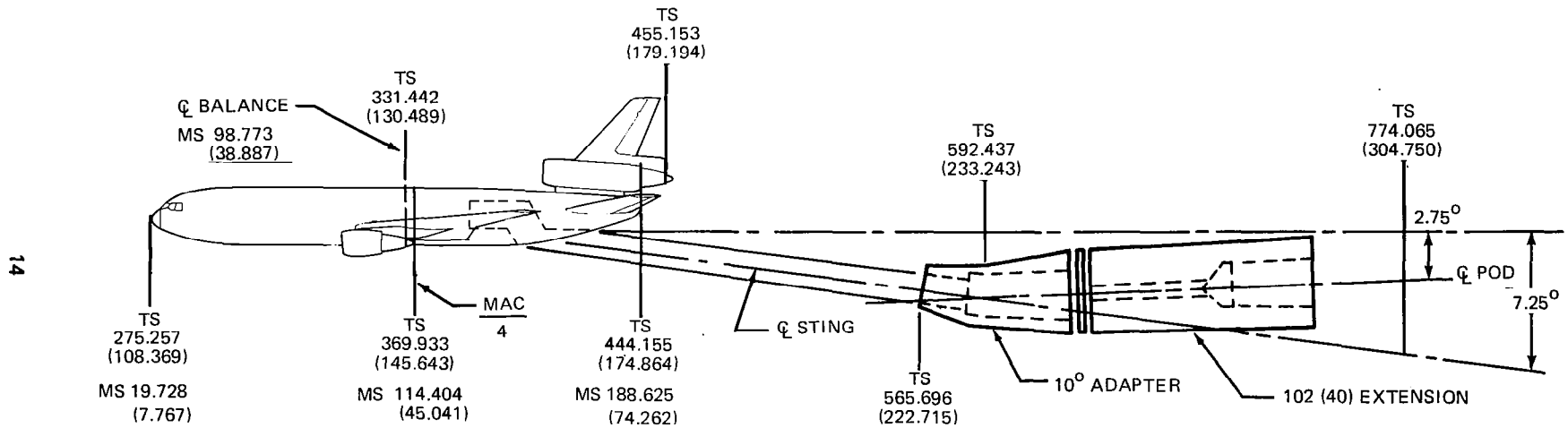
FIGURE 3. INSTALLATION OF DC-10 SERIES 30 HIGH-SPEED MODEL IN NASA AMES RESEARCH CENTER 11-FOOT WIND TUNNEL
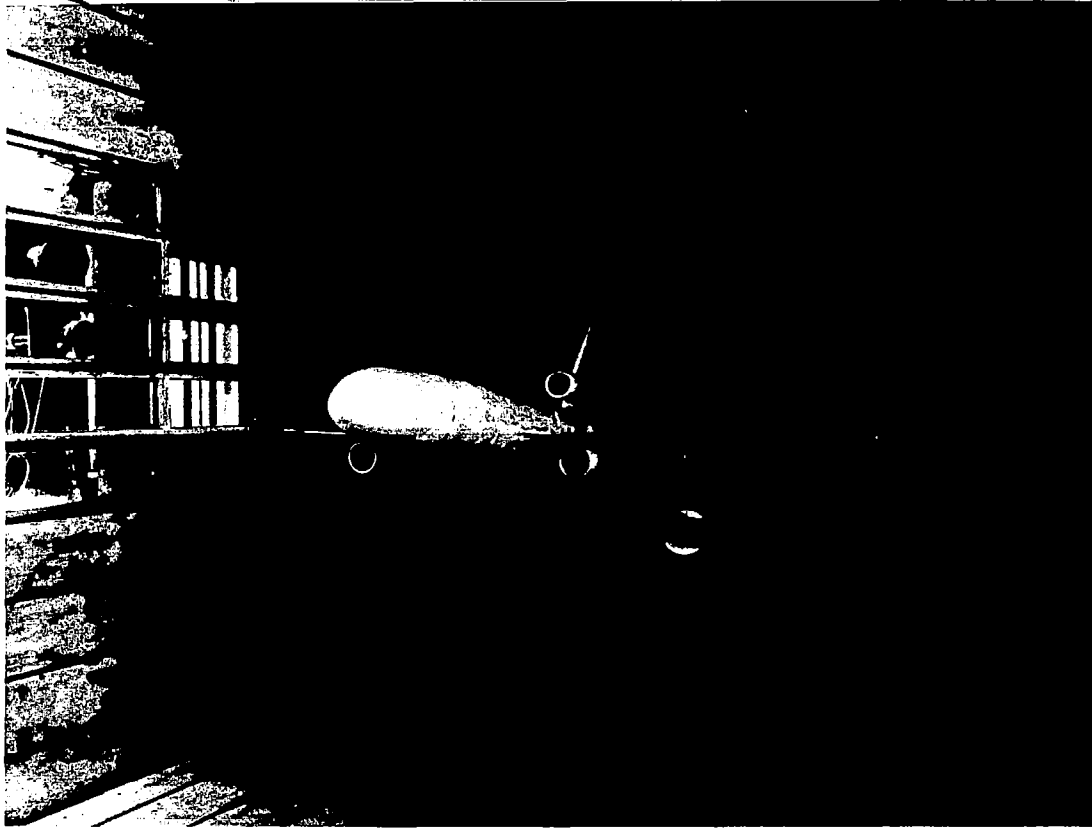
FIGURE 4. DC-10 SERIES 30 HIGH-SPEED MODEL WITH WINGLETS INSTALLED IN AMES RESEARCH CENTER 11-FOOT WIND TUNNEL

number range of 0.60 to 0.95 at a Reynolds number of 19.7×10^6 per meter (6.0×10^6 per foot). Additional angles of attack were inserted into the tail-off, pitch runs at a Mach number of 0.82 to facilitate the determination of buffet lift coefficient. Also, tail-off runs were conducted with one outboard aileron deflected upward at angles of 5, 10, and 15 degrees to evaluate the aileron effectiveness in the presence of the winglet. The mini-tuft flow visualization tests were conducted at Mach numbers of 0.60 and 0.82.

Results and Discussion

Stability and control characteristics — The primary flight regime evaluated was cruise. Basic pitch and yaw sweeps were made to allowable balance limits to study the longitudinal and directional characteristics as functions of angle of attack and sideslip. Additional pitch sweeps were made with the model yawed at 2 degrees sideslip and yaw sweeps were made with the model at an angle of attack of approximately 4 degrees. Outboard aileron effectiveness was studied at deflections of −5, −10, and −15 degrees trailing edge up to determine the effects of winglets on lateral control for possible active control applications. Representative results and comparisons are presented in the following text.

The effect of winglets on the slope of the pitching moment curves, C_{mC_L}, is given in Figure 5, where C_{mC_L} is plotted as a function of Mach number for both tail-on and tail-off configurations, with and without winglets. These data show that the addition of winglets to the basic DC-10 Series 30 had a stabilizing effect on C_{mC_L}. The winglet contributed a fairly constant increment of C_{mC_L} of approximately −0.02 for both tail-on and tail-off configurations. The magnitude of this increment was equivalent to that which would be produced by a forward shift in the aircraft center-of-gravity location of about 2 percent mean aerodynamic chord. The tail-off zero-lift pitching moment coefficient, $C_{m_{0TO}}$, shows a fairly constant increment of 0.004 due to the winglets over most of the Mach number range (Figure 6). The stability increase exhibited in Figure 5 due to winglets increased with angle of attack, as evidenced by Figures 7 through 9, and was maintained up to the highest angle of attack tested, which was well past buffet onset for all Mach numbers.
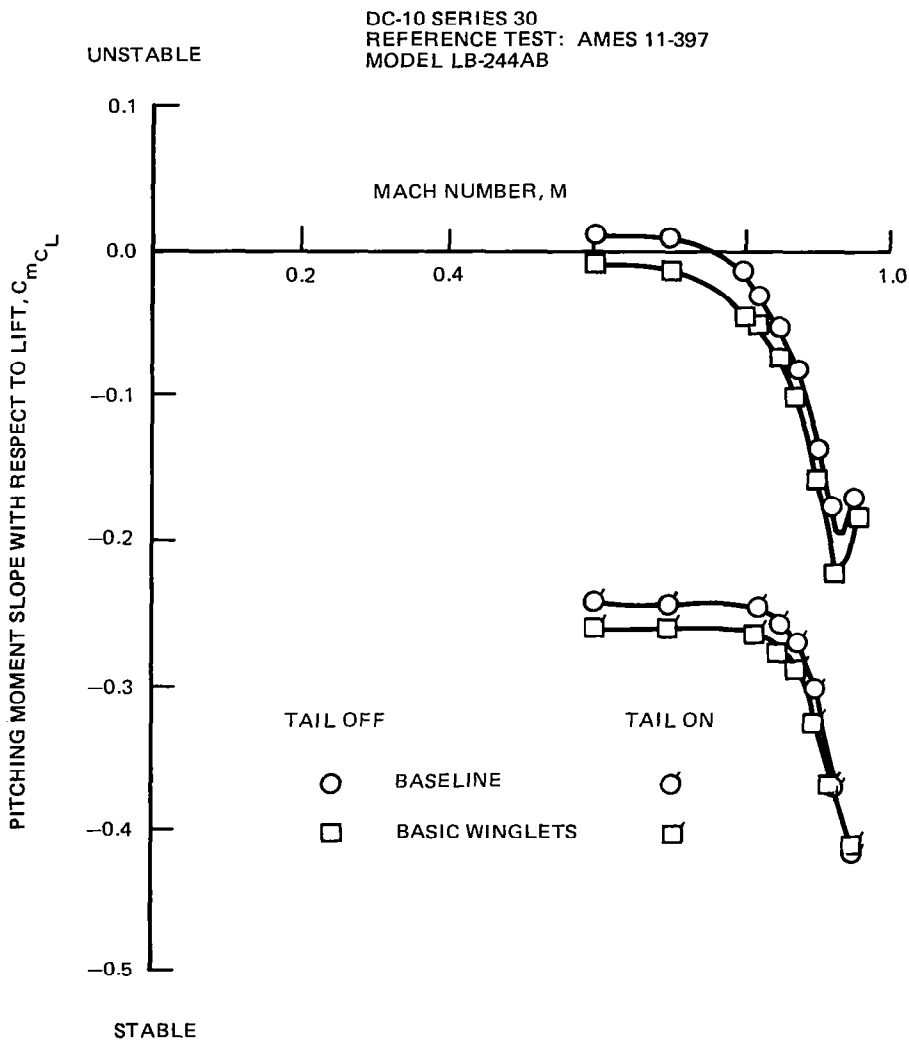
FIGURE 5. EFFECT OF WINGLETS ON PITCHING MOMENT SLOPE
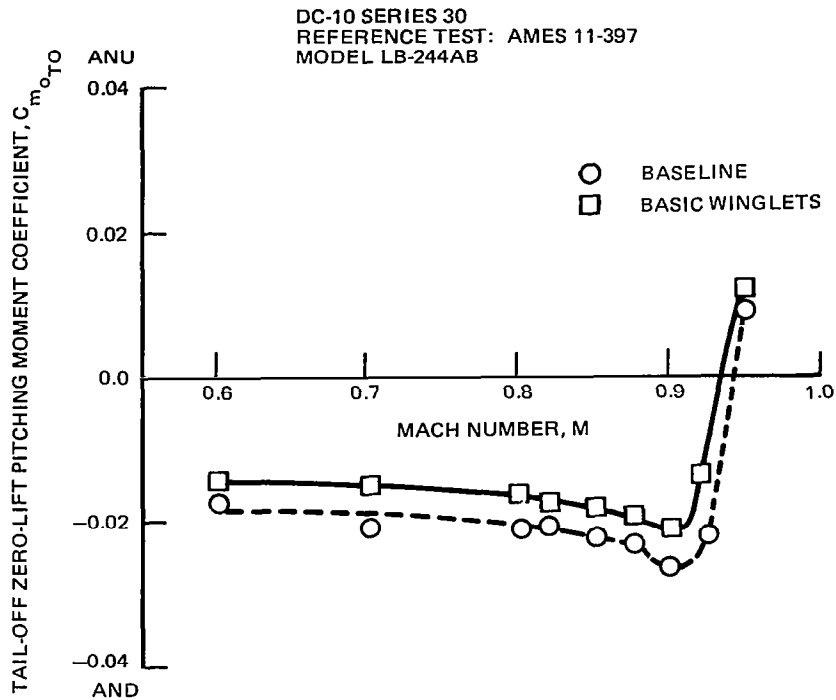
FIGURE 6. EFFECT OF WINGLETS ON TAIL-OFF ZERO-LIFT PITCHING MOMENT
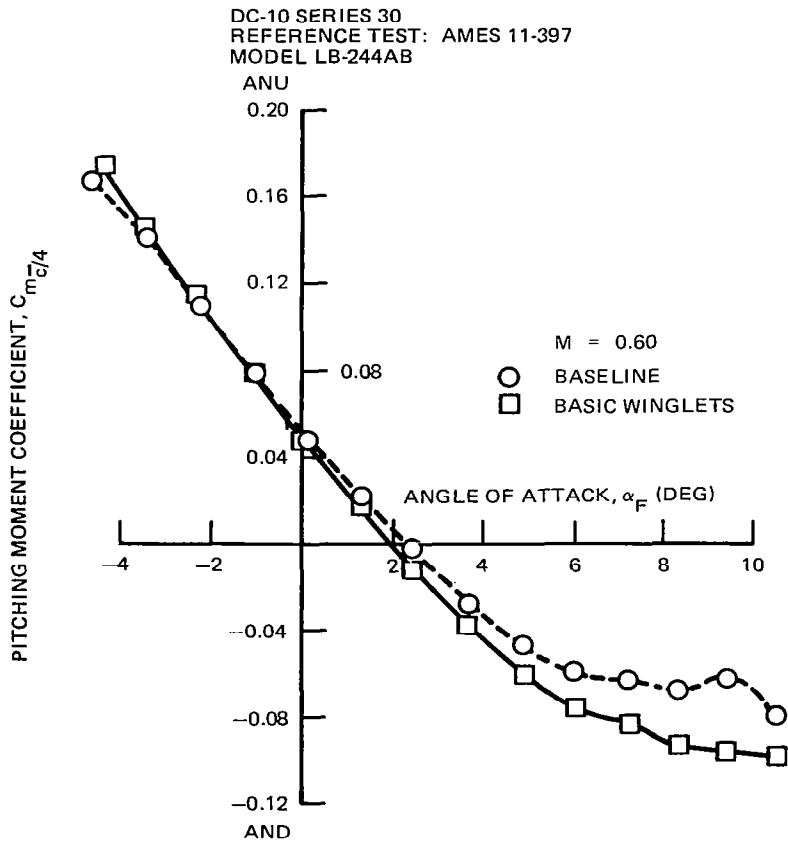
FIGURE 7. EFFECT OF WINGLETS ON PITCHING MOMENT CHARACTERISTICS (M = 0.60)

ANU
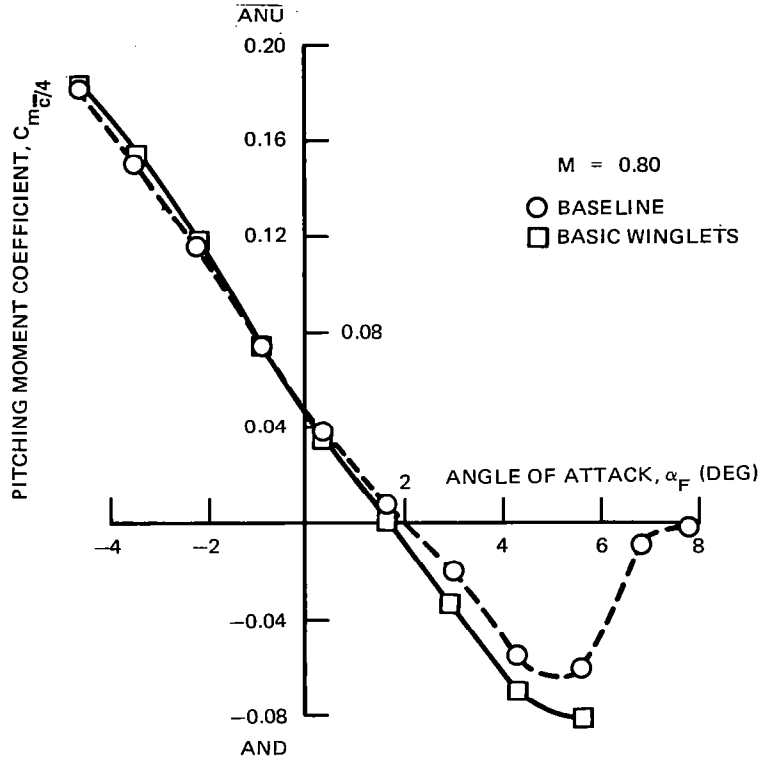
FIGURE 8. EFFECT OF WINGLETS ON PITCHING MOMENT CHARACTERISTICS (M = 0.80)

Tail-on and tail-off dihedral effect, C_{l_β}, with and without winglets, is shown in Figure 10. The winglets increased the tail-on effective dihedral by about 12 percent between Mach numbers of 0.6 and 0.9. The winglet effect reduced to zero at Mach 0.95. Figures 11 through 13 show the effect of winglets as a function of angle of attack for Mach numbers of 0.6, 0.8, and 0.9 for sideslip angles of 0 and 2 degrees. The rolling moment increment due to winglets remained fairly constant throughout the angle-of-attack range at Mach 0.6 and 0.8, but varied with angle of attack at Mach 0.9.

Tail-on and tail-off directional stability, C_{n_β}, with and without winglets, is presented in Figure 14. The winglets increased the tail-on directional stability by approximately 15 percent for Mach numbers between 0.6 and 0.8, with a gradual reduction to about 7 percent at Mach 0.95. The incremental change in C_{n_β} due to winglets shown in Figure 14 is independent of angle of attack, as illustrated in Figures 15 and 16. Yawing moment coefficient as a function of angle of attack was plotted for Mach 0.8 and 0.9 for angles of sideslip of 0 and 2 degrees. These data showed a fairly constant stabilizing increment in yawing moment of approximately 10 percent over the angle-of-attack range for 2 degrees sideslip at both Mach numbers.
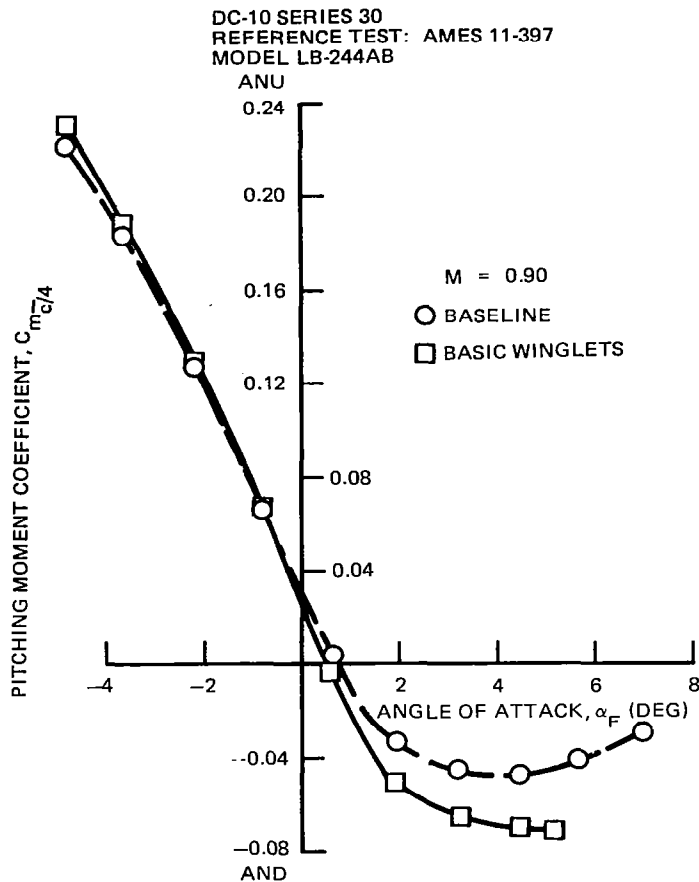
FIGURE 9. EFFECT OF WINGLETS ON PITCHING MOMENT CHARACTERISTICS (M = 0.90)

The tail-on and tail-off side force derivative, C_{Y_β}, with and without winglets, is presented in Figure 17. Adding the winglets increased the tail-on derivative by about 10 percent between Mach 0.6 and 0.9 and by about 5 percent at Mach 0.95. Figures 18 and 19 present the side force coefficient as a function of angle of attack for Mach numbers of 0.8 and 0.9 at both 0 and 2 degrees of sideslip, with and without winglets. These data indicate the side force coefficient increment, ΔC_Y, due to winglets was essentially independent of angle of attack in anticipated cruise range sideslip angles.

The changes in the lateral-directional sideslip derivatives have an insignificant effect on the lateral-directional dynamics. Static directional stability, C_{m_β}, became more positive with the winglets and static lateral stability, C_{l_β}, became more negative. The combination of the two derivatives leaves the lateral-directional dynamics, Dutch roll, and spiral mode stability essentially unchanged.

Although the current DC-10 outboard aileron is locked in the faired position at high speed, the influence of winglets on high-speed outboard aileron effectiveness was investigated for possible active control applications. It was determined that the outboard aileron effectiveness in the

$\alpha_F = 0$ DEG
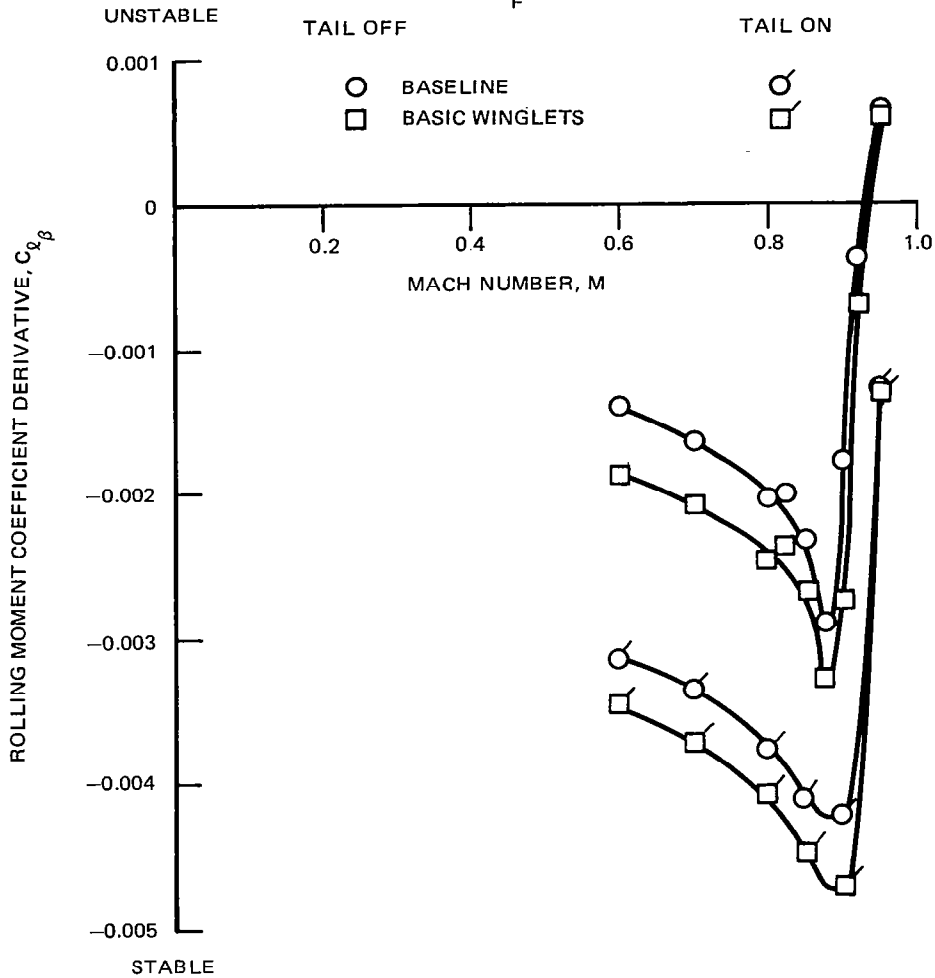
FIGURE 10. CHANGE IN DIHEDRAL EFFECT DUE TO WINGLETS

cruise configuration at intermediate Mach numbers of 0.60 to 0.82 is essentially unaffected by the winglets. At higher Mach numbers, the winglets provided a significant improvement in aileron power, as exhibited in Figure 20 which presents incremental rolling moment as a function of Mach number for a trailing edge-up aileron deflection of −10 degrees. Figures 21 and 22 show the angle-of-attack trends at Mach 0.875 and 0.92 for control deflections of −5, −10, and −15 degrees trailing edge-up, with and without winglets. The greatest increase in aileron power was noted in the 1- through 3-degree angle-of-attack range.

Cruise buffet characteristics — An evaluation of the cruise buffet lift coefficient was conducted at a Mach number of 0.82 for both the baseline and winglets-installed configurations. Figure 23 gives the lift curves for the baseline and winglet configurations. Lift curve break was employed to determine buffet onset lift coefficient for the baseline and winglet aircraft. This method of buffet onset determination has correlated well with flight test data. Figure 23 shows that the winglets had very little effect on the buffet lift coefficient. Similar trends in buffet onset deter-
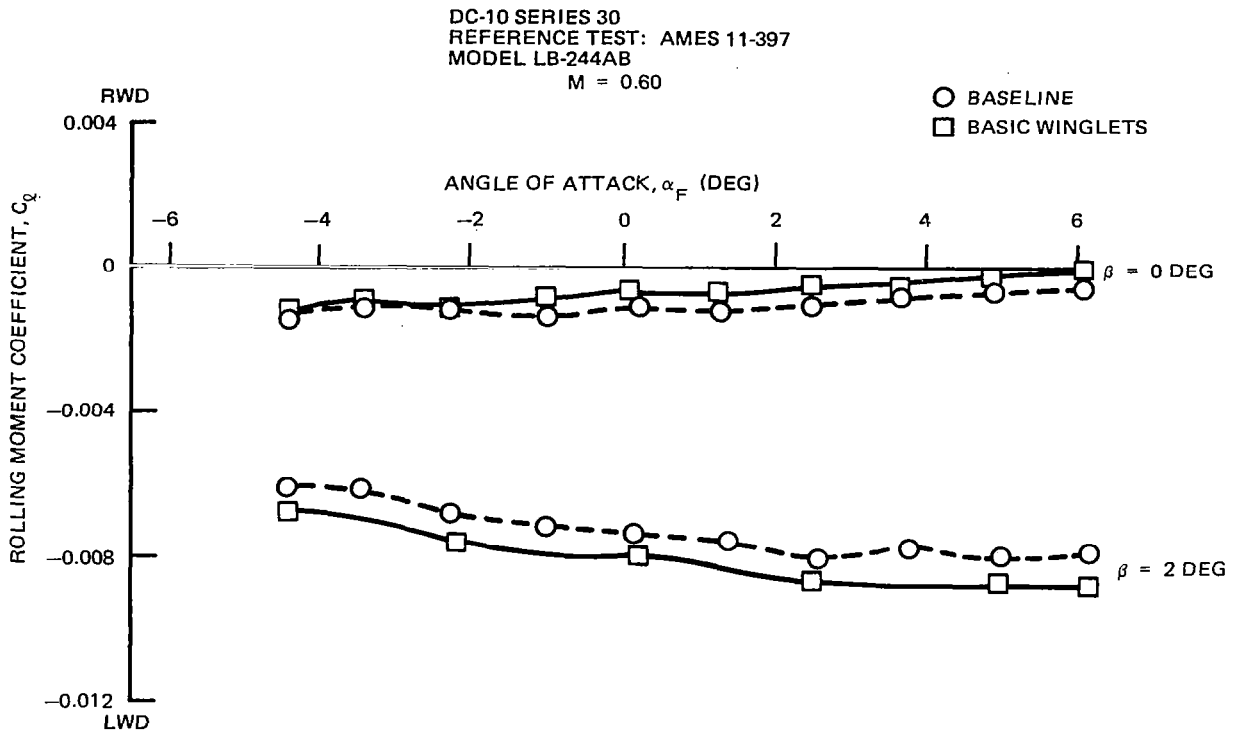
FIGURE 11. EFFECT OF WINGLETS ON ROLLING MOMENT (M = 0.60, β = 0 AND 2 DEG)
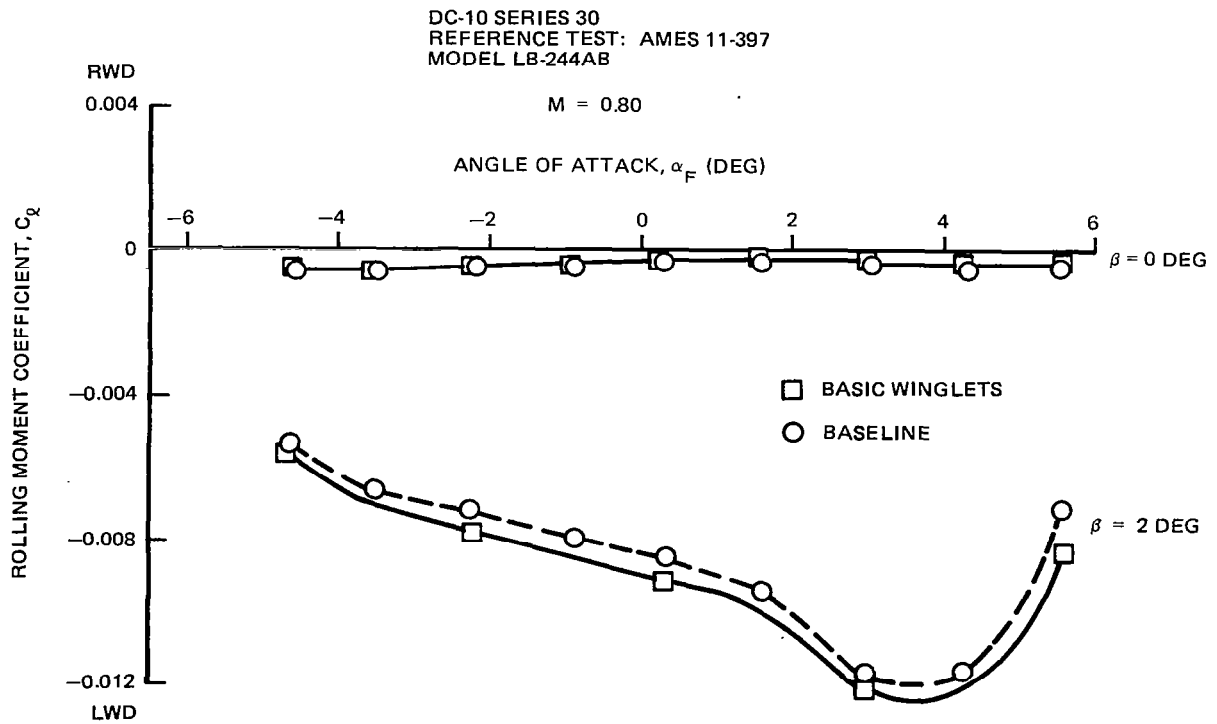
FIGURE 12. EFFECT OF WINGLETS ON ROLLING MOMENT (M = 0.80, β = 0 AND 2 DEG)

21

RWD

0.004

M = 0.90

ANGLE OF ATTACK, α_F (DEG)

ROLLING MOMENT COEFFICIENT, C_ℓ

-6   -4   -2   0   2   4   6

0

β = 0 DEG

-0.004

β = 2 DEG

-0.008

☐ BASIC WINGLETS

○ BASELINE

-0.12

LWD
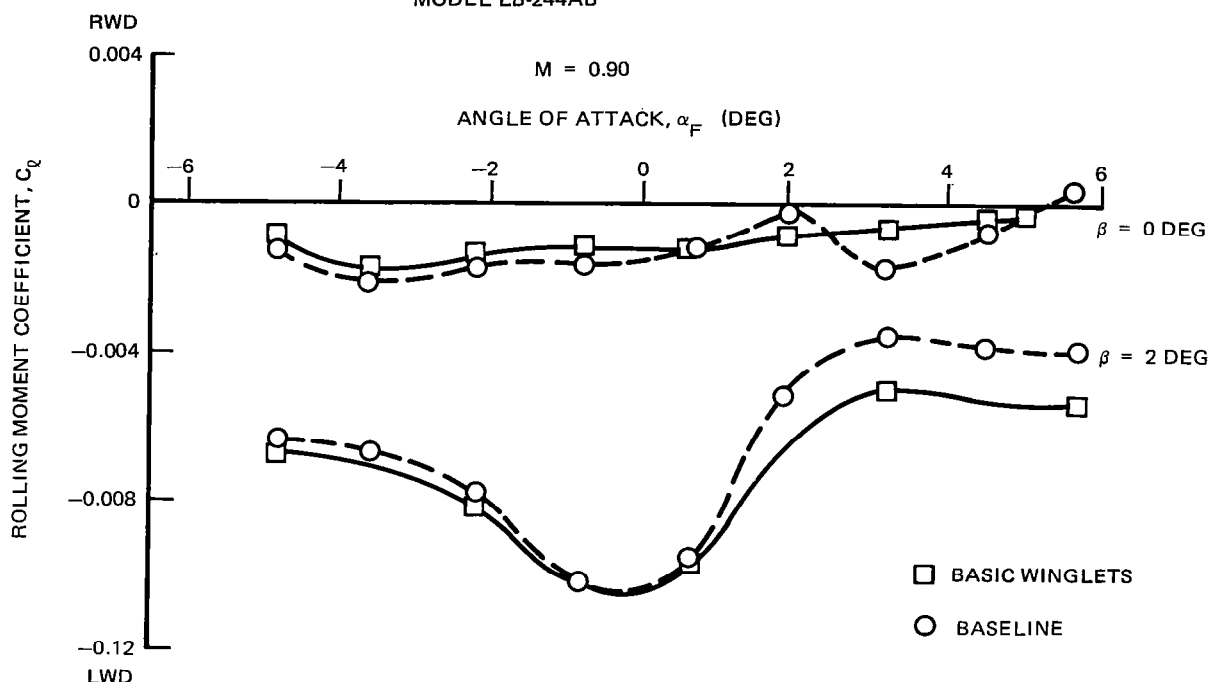
FIGURE 13. EFFECT OF WINGLETS ON ROLLING MOMENT (M = 0.90, β = 0 AND 2 DEG)

mined from pitching moment curve break are given in Figure 24. This minor variation in buffet lift coefficient — resulting from the winglet — which was within the degree of accuracy to which buffet lift coefficient can be determined, was also confirmed by analysis of wing trailing edge pressures. The wing trailing edge pressures at the buffet-critical wing spanwise station are shown in Figure 25 for both the baseline and winglet-installed cases. In this figure, the winglets are shown to have had no effect on the trailing edge pressure break at the critical wing station. Further, there was no break in the winglet trailing edge pressure curve at lifts less than buffet onset. Consequently, it is apparent that the winglet was not buffet-limiting and that the buffet-critical wing station was not affected by the installation of the winglet.

Mini-tuft flow visualization results verified the buffet results described previously. Flow visualization results indicated good flow quality on the winglet and the wing-winglet juncture at angles of attack ranging from cruise through buffet onset. Figures 26 and 27 give sample flow visualization results at a cruise lift coefficient of approximately 0.5. Aerodynamic buffet was caused by flow separation on the wing which was not changed by the winglets. The pressure measurements and flow visualization results indicated that the winglet flow was still attached at buffet conditions where the wing outer panel was experiencing flow separation.
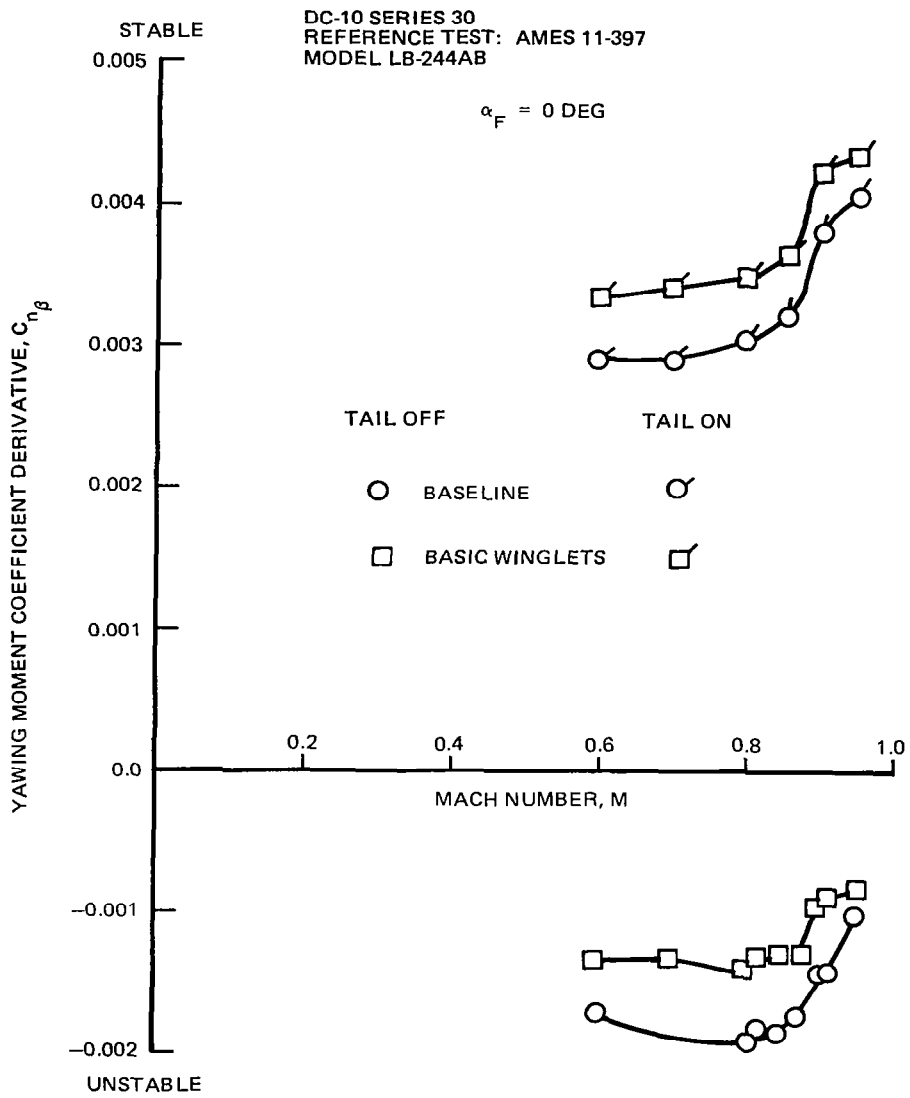
FIGURE 14. EFFECT OF WINGLETS ON YAWING MOMENT DERIVATIVE

DC-10 SERIES 30
REFERENCE TEST: AMES 11-397
MODEL LB-244AB
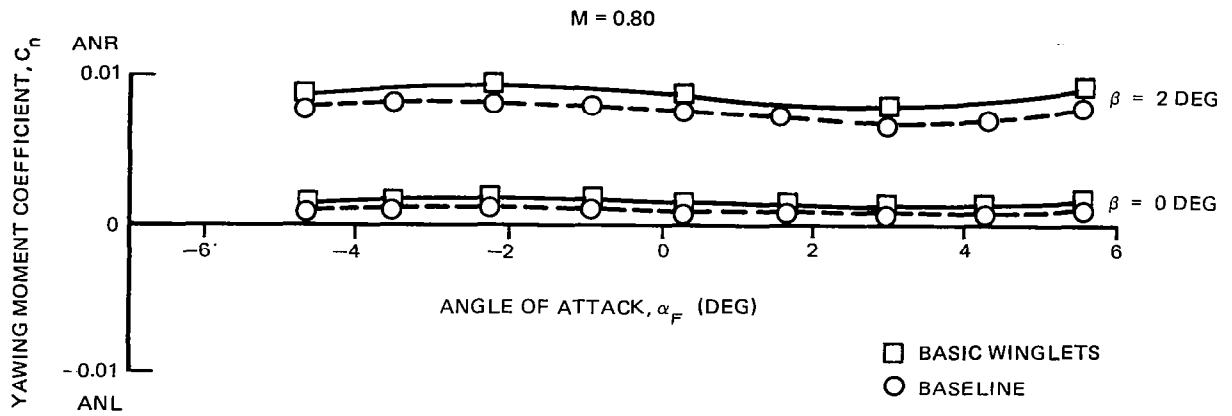
M = 0.80

FIGURE 15. EFFECT OF WINGLETS ON YAWING MOMENT (M = 0.80, β = 0 AND 2 DEG)

DC-10 SERIES 30
REFERENCE TEST: AMES 11-397
MODEL LB-244AB
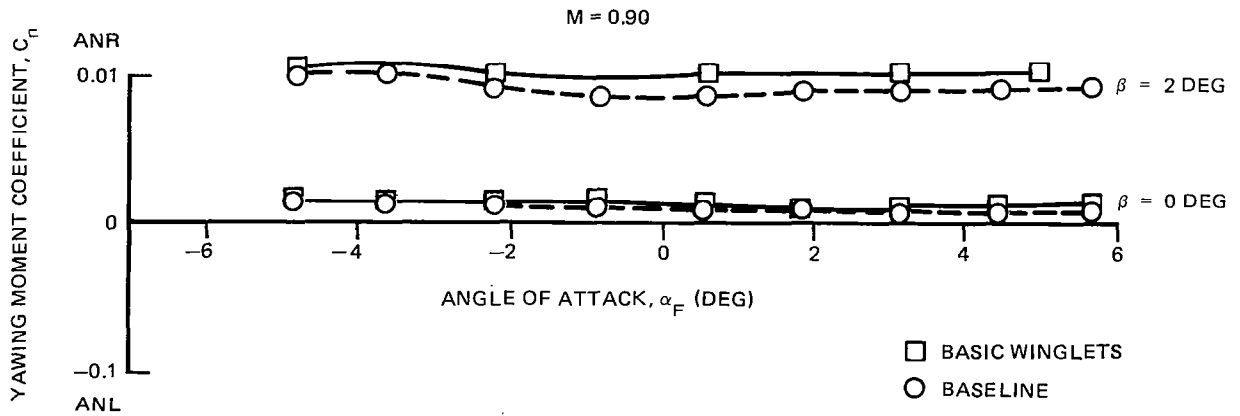
M = 0.90

FIGURE 16. EFFECT OF WINGLETS ON YAWING MOMENT (M = 0.90, β = 0 AND 2 DEG)

24

DC-10 SERIES 30
REFERENCE TEST: AMES 11-397
MODEL LB-244AB

MACH NUMBER, M
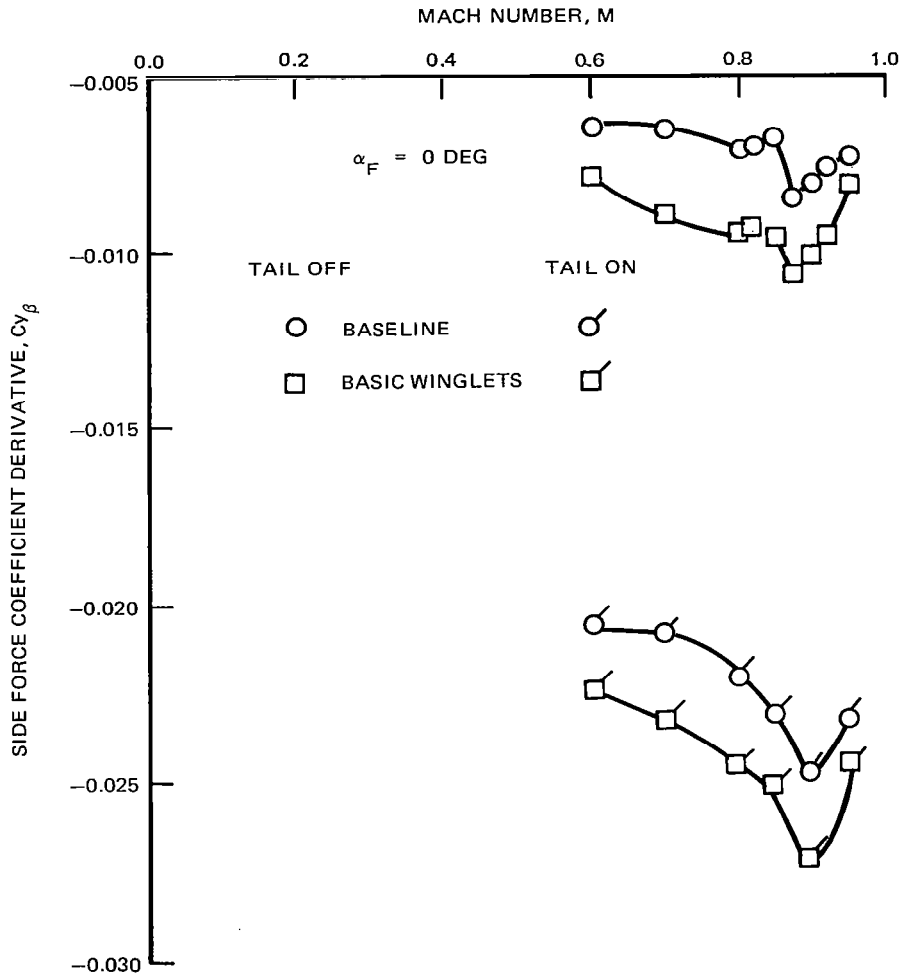
FIGURE 17. EFFECT OF WINGLETS ON SIDE FORCE DERIVATIVE

DC-10 SERIES 30
REFERENCE TEST: AMES 11-397
MODEL LB-244AB
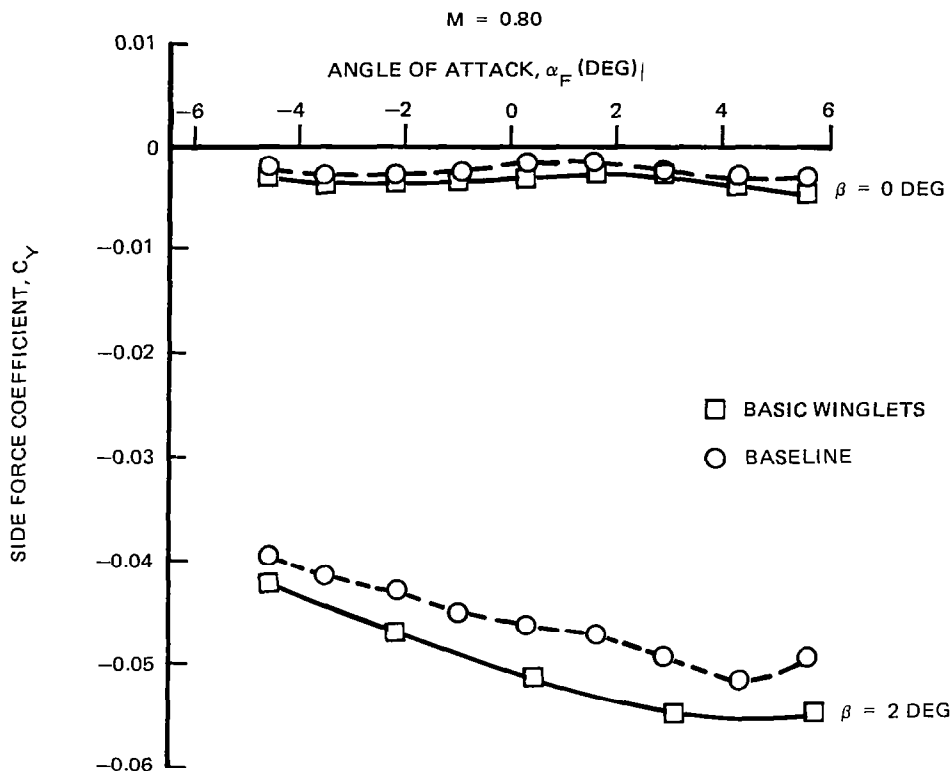
FIGURE 18. EFFECT OF WINGLETS ON SIDE FORCE (M = 0.80, β = 0 AND 2 DEG)

Conclusions

The following conclusions have been reached regarding the high-speed aerodynamic characteristics with winglets installed:

- Winglets added a small but stabilizing increment of pitching moment, and they also increased the lateral-directional coefficients by a small amount. The trend of the winglet stability data closely approximated the baseline data. Winglets had a negligible impact on the high-speed stability characteristics of the airplane.

- For possible future versions of the DC-10 in which the outboard ailerons may be used at high speed instead of locked in the faired position as it is presently, it was found that winglets essentially did not change the outboard aileron effectiveness for Mach numbers up to 0.82. At higher Mach numbers up to 0.95, an improvement in aileron effectiveness was shown.

- Winglets had no impact on cruise buffet characteristics and did not change the flow mechanism which causes buffet onset.

DC-10 SERIES 30
REFERENCE TEST: AMES 11-397
MODEL LB-244AB

M = 0.90

ANGLE OF ATTACK, α_F (DEGREES)

□ BASIC WINGLETS

○ BASELINE

SIDE FORCE COEFFICIENT, C_Y

β = 0 DEG

β = 2 DEG
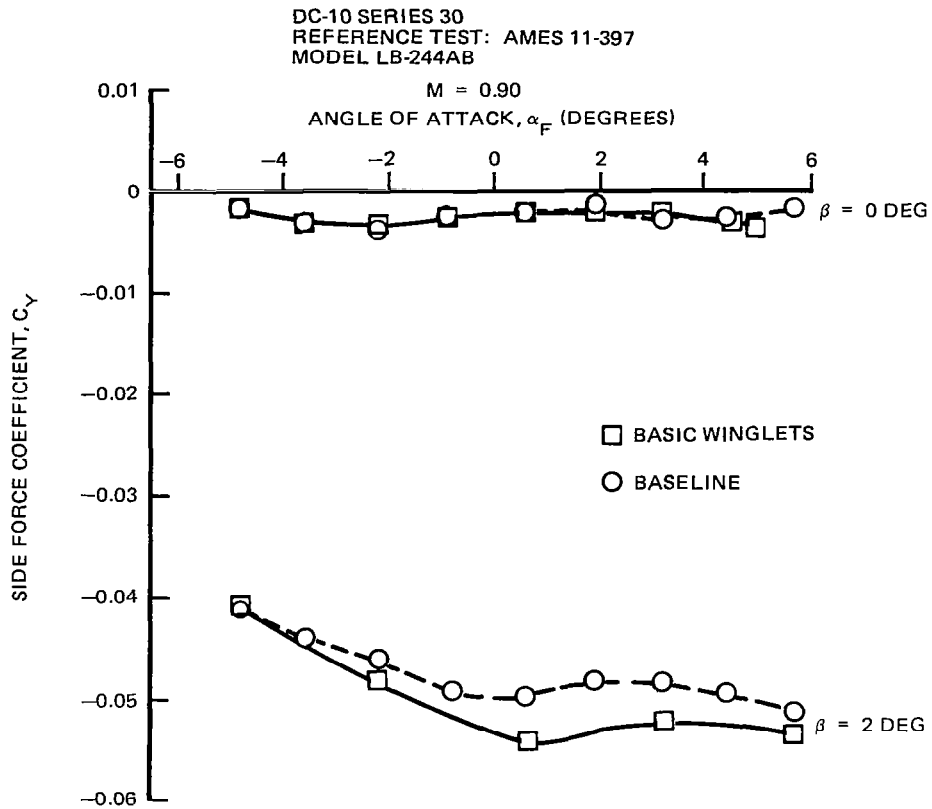
FIGURE 19. EFFECT OF WINGLETS ON SIDE FORCE (M = 0.90, β = 0 AND 2 DEG)

DC-10 SERIES 30
REFERENCE TEST: AMES 11-397
MODEL LB-244AB

RWD

α_F = 1 DEG

δ_a^{RH} —10 DEG (TEU)

□ BASIC WINGLETS

○ BASELINE

TAIL OFF

INCREMENTAL ROLLING MOMENT COEFFICIENT DUE TO RH OUTBD AILERON, ΔC_ℓ

MACH NUMBER, M

LWD
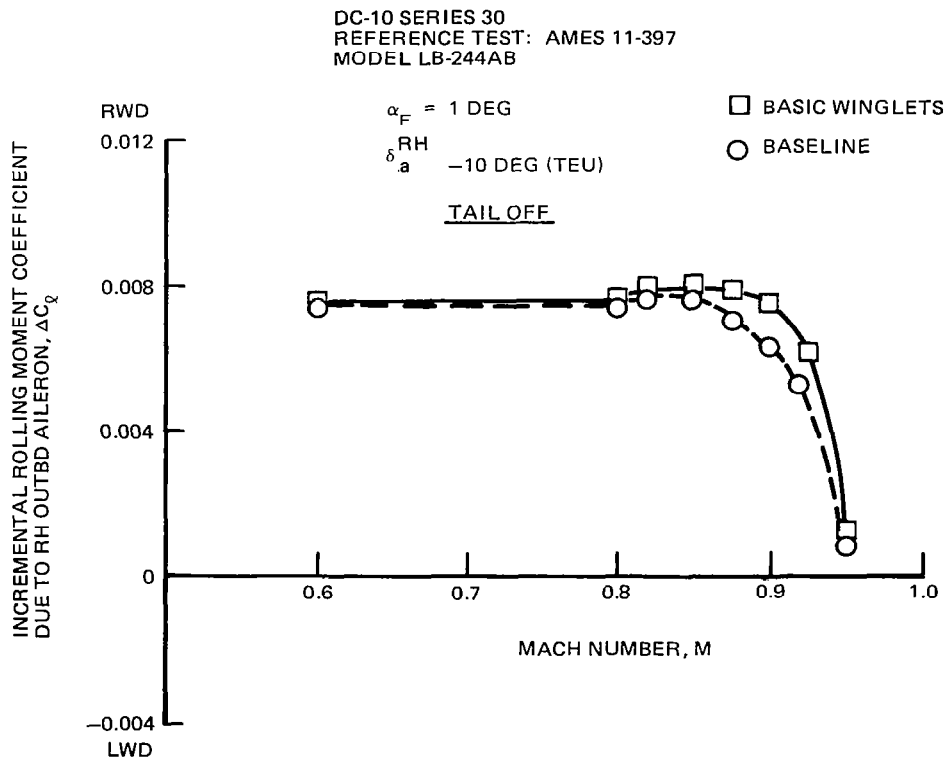
FIGURE 20. CHANGE IN AILERON EFFECTIVENESS DUE TO WINGLETS

27
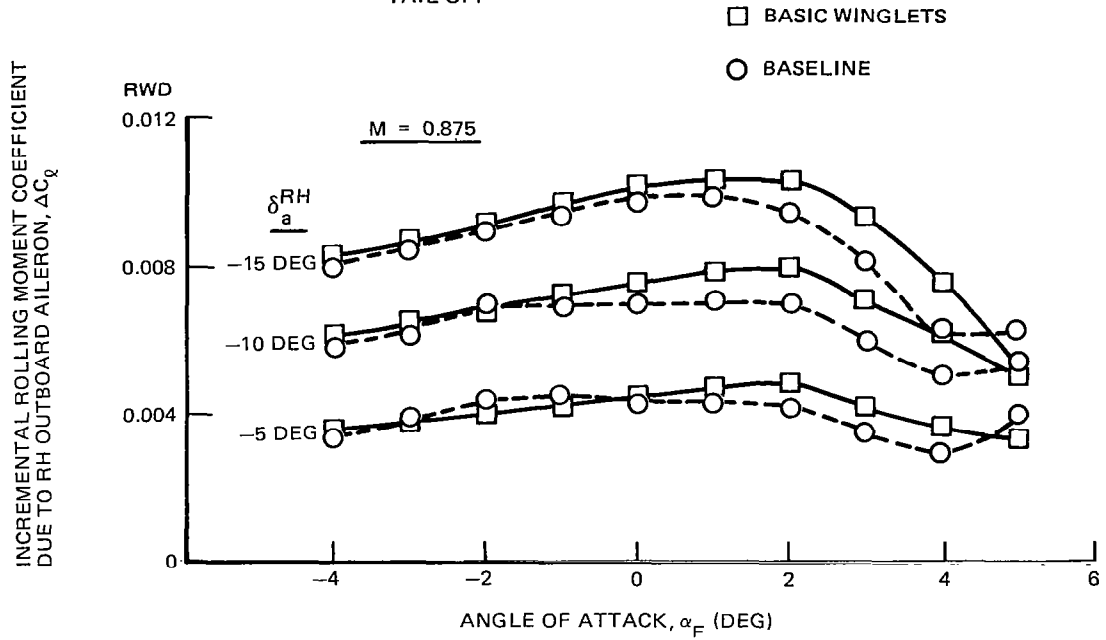
FIGURE 21. CHANGE IN AILERON EFFECTIVENESS DUE TO WINGLETS (M = 0.875).
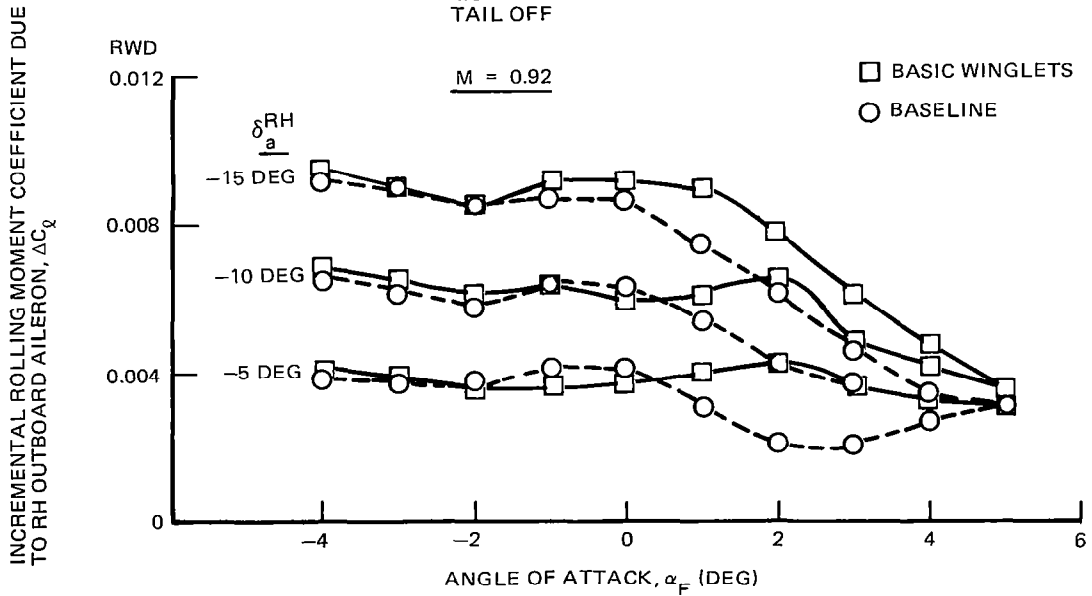
FIGURE 22. CHANGE IN AILERON EFFECTIVENESS DUE TO WINGLETS (M = 0.92)

DC-10 SERIES 30
REFERENCE TEST: AMES 11-397
MODEL LB-244AB
TAIL OFF
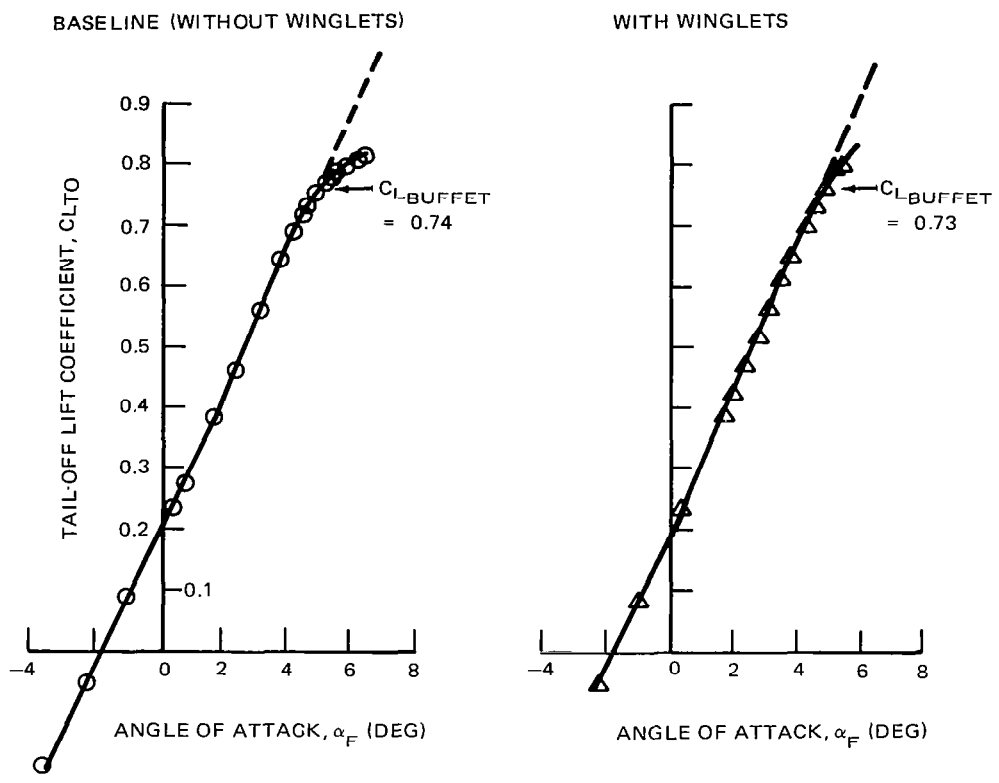
FIGURE 23. CRUISE BUFFET ESTIMATION WITH AND WITHOUT WINGLETS AT MACH NUMBER OF 0.82

DC-10 SERIES 30
REFERENCE TEST: AMES 11-397
MODEL LB-244AB
TAIL OFF

BASELINE (WITHOUT WINGLETS)   WITH WINGLETS
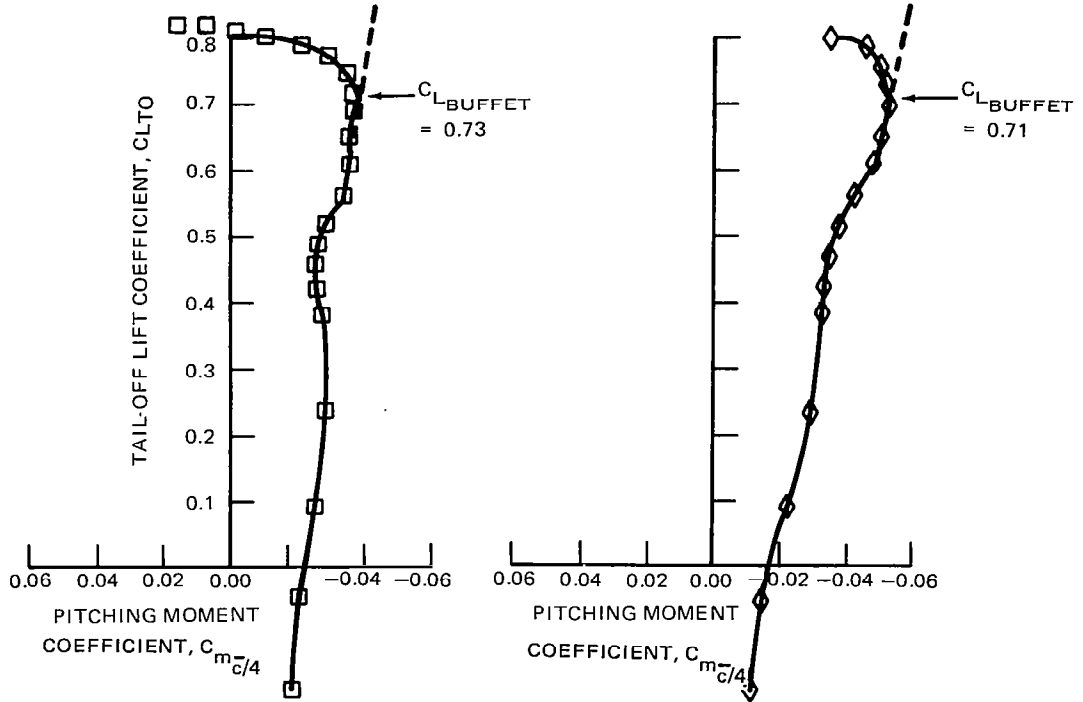
FIGURE 24. CRUISE BUFFET ESTIMATION BY PITCHING MOMENT WITH AND WITHOUT WINGLETS AT MACH NUMBER OF 0.82

DC-10 SERIES 30
REFERENCE TEST: AMES 11-397
MODEL LB-244AB

O WING, 68% SEMISPAN   BASELINE
□ WING, 68% SEMISPAN }
△ WINGLET, 12% SPAN   } WINGLET INSTALLED
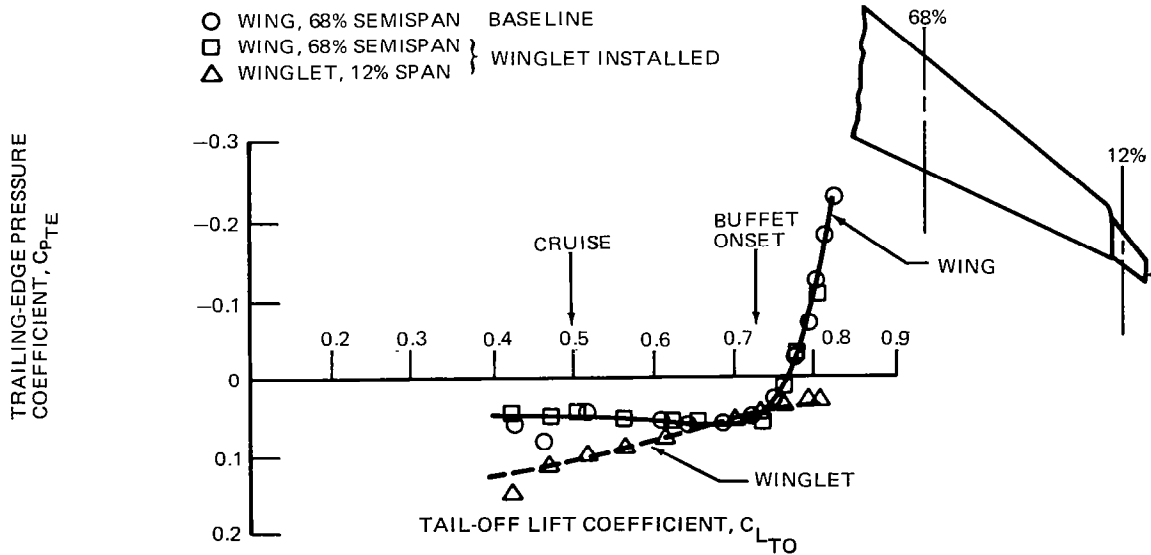
FIGURE 25. WING AND WINGLET TRAILING-EDGE PRESSURE COEFFICIENT VARIATION WITH LIFT COEFFICIENT AT MACH NUMBER OF 0.82
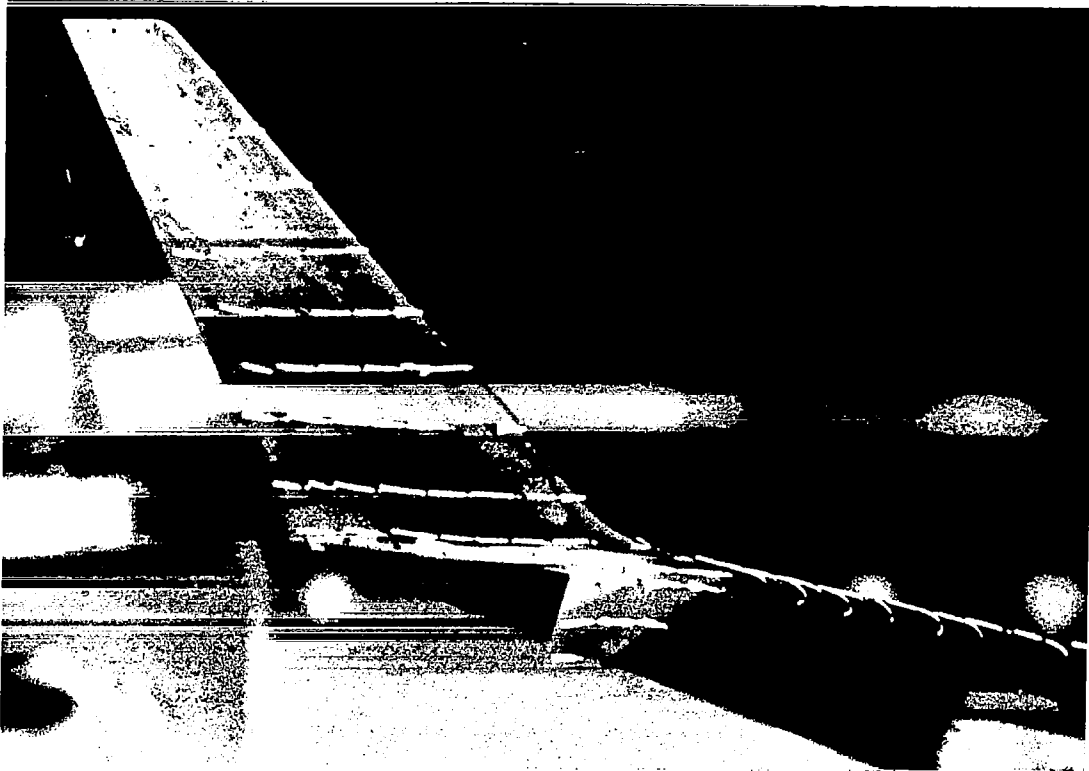
FIGURE 26. MINI-TUFT FLOW VISUALIZATION OF WINGLET OUTBOARD SURFACES AT ANGLE OF ATTACK = 2.47 DEGREES AND MACH NUMBER OF 0.82

FIGURE 27. MINI-TUFT FLOW VISUALIZATION OF WING TIP AND WINGLET INBOARD SURFACE AT ANGLE OF ATTACK = 2.47 DEGREES AND MACH NUMBER OF 0.82

LOW-SPEED INVESTIGATIONS

Investigation Objectives

Two wind tunnel tests were conducted between August 1979 and April 1981 to aid in the evaluation of the low-speed aerodynamic characteristics of the DC-10 Series 30 aircraft with winglets installed.

The initial test was intended to identify early any potential problem associated with the winglet installation as well as obtain basic longitudinal and lateral-directional aircraft characteristics. The specific objectives were to:

- Estimate basic performance of the winglet DC-10 aircraft relative to the baseline aircraft characteristics for a range of flap/slat deflections representative of takeoff and landing configurations.

- Determine the merit of an upper winglet slat for the aircraft with winglets installed.

- Evaluate longitudinal, lateral, and directional stability, outboard aileron control effectiveness, and longitudinal stabilizer effectiveness for the aircraft with winglets.

- Observe the flow quality on the inner surface of the upper winglet and correlate with quantitative behavior.

The second low-speed test involved a detailed examination of the installation effects of winglets, including additional flap/slat settings. The test also included evaluation of a winglet with a smaller span than the basic configuration, such a reduction having been proposed in separate studies as having potential for retrofit on certain DC-10 applications (see the section on Configuration Integration Analysis). The specific test objectives were:

- Evaluate in detail the impact of basic and reduced-span winglets on low-speed performance.

- Evaluate longitudinal, lateral, and directional stability and outboard aileron control effectiveness with either basic or reduced-span winglets installed.

- Obtain pressure data on the wing and winglet at low speed for loads estimation and diagnostic purposes.

- Examine the impact on performance and characteristics of simulated ice accumulation on the upper winglet and determine the requirement for leading edge ice protection.

- Observe the flow quality on the inner surface of the upper winglet and correlate with measured aircraft characteristics.

Experimental Apparatus and Procedures

The model utilized in this investigation was a 4.7-percent scale representation of the DC-10 Series 30 configuration including high-lift components. The model, which had previously been used in numerous DC-10 Series 30 high-lift studies, was modified to accept upper and lower winglets on each wing tip. Model components other than the winglets (fuselage, wing, wing slats, flaps, nacelles, pylons, empennage, gear, etc.) were the same as employed in other DC-10 low-speed investigations.

As stated in the objectives, two winglet configurations were evaluated during the test program. The first, referred to as the basic winglet, was the winglet installation of the cruise configuration development test. The second configuration, known as the reduced-span winglet, was a truncated version of the first winglet planform. Figure 28 illustrates the principal dimensions of the basic and reduced-span winglets.

Each upper-surface winglet had provisions for installation of a leading edge slat and appropriate slat undersurface leading edge contour. The winglet slat deflection was fixed at 30 degrees with gap and overhang of 1.75 and −1.0-percent chord, respectively. Although three winglet incidences were provided by the model design, the values of −2 degrees incidence angle (positive defined as toe-in) for the upper winglet and 0 degrees incidence angle for the lower winglet were

DIMENSIONS IN CENTIMETERS (INCHES) MODEL SCALE

FIGURE 28. UPPER AND LOWER WINGLET GEOMETRIC CHARACTERISTICS FOR THE DC-10 SERIES 30 LOW-SPEED WIND TUNNEL MODEL
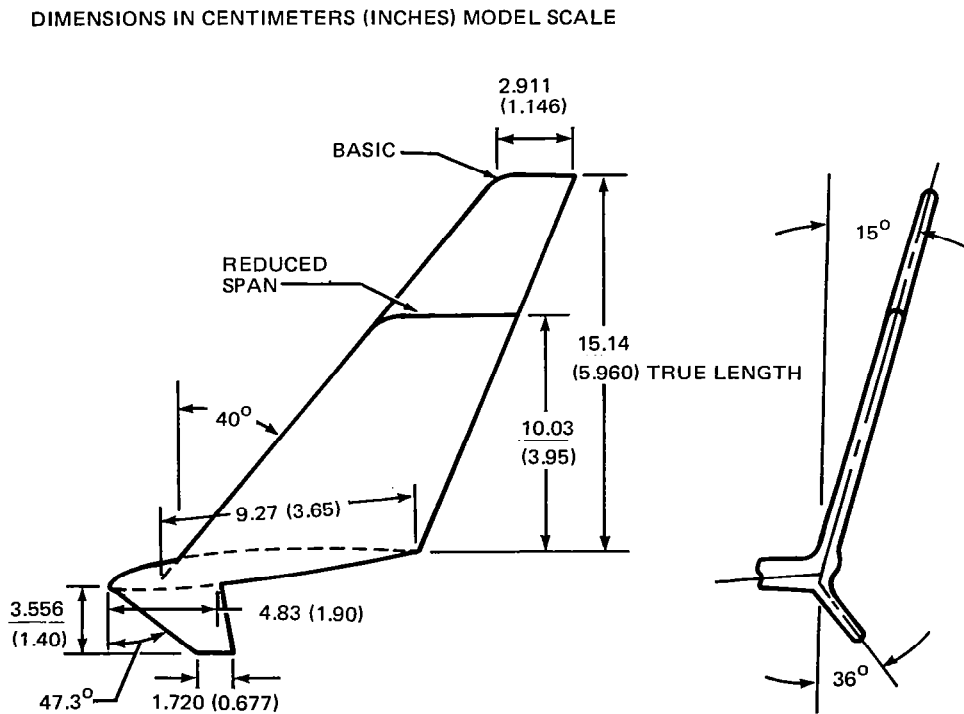
used for the low-speed tests as well as for the high-speed tests. The incidence angles were derived in the development program of Reference 5. Pressure instrumentaion was utilized on the wing and winglet during this investigation. Wing chordwise pressure orifice rows were located at 16, 27, 36, 53, 67, 79, and 87 percent of the wing semispan. Additionally, pressures were measured along the 12.5- and 80-percent span stations of the upper winglet.

A constant-section wooden leading edge attachment was used to simulate ice accumulation on the upper winglet and determine its effect on aircraft characteristics. The ice shape employed represented an estimate of the contour resulting from 45 minutes of holding during maximum continuous icing conditions.

The investigation was conducted in the NASA-Ames Research Center 12-Foot Pressure Wind Tunnel, which is a variable-density low-turbulence tunnel that operates at subsonic speeds up to slightly less than a Mach number of 1.0. The test section was 3.44 meters (11.3 feet) high, the same width, and 5.49 meters (18.0 feet) long. The wind tunnel is powered by a two-stage, axial-flow fan. Eight fine-mesh screens in the settling chamber, together with the large contraction ratio of 25 to 1, provide a low turbulence level in the test section.

The DC-10 model was supported in the test section by a tandem-strut support system, shown in Figure 29. A Task Mark IVA 10-cm- (4-inch)-diameter balance was installed in the rear center section of the fuselage to measure forces and moments about all axes. The fuselage angle of attack was adjustable from 0 to 10 degrees with the pitch control strut locked, thereby keeping the balance aligned with the test section axis for these angles of attack. Therefore, for the angle of attack range of 0 to 10 degrees, the drag force was determined solely from the balance axial component, avoiding inherent inaccuracies resulting from resolution of both normal and axial components into the drag direction. Beyond the 0-to-10-degree range, pitch of the model is achieved by the usual manner of actuating the pitch strut. Yaw of the model was obtained by rotating the tunnel test section turntable. Photographs of the model installed in the test section are given in Figures 30 and 31 and photographs of the winglet installations are presented in Figures 32 and 33.

All tests were conducted at a nominal test section Mach number of 0.2. A nominal Reynolds number of 19.7×10^6 per meter (6.0×10^6 per foot) was used for all tests except for Reynolds number influence investigations and a few conditions where balance loads became critical at full Reynolds number and high sideslip angles. At the nominal value of 19.7×10^6 per meter (6.0×10^6 per foot), the Reynolds number of the model based on the mean aerodynamic chord was 6.95×10^6, the value based on the basic upper winglet tip chord was 5.73×10^5, and the value based on the winglet slat tip chord was 8.60×10^4.

Measurements recorded during the test program included the six-component force and moment data measured by the internal model balance. In reduced form, all forces and moments were

DIMENSIONS IN CENTIMETERS (INCHES) MODEL SCALE

MS = 28.532
(11.233)

AMES TASK
MK IVA BALANCE

BALANCE
CENTER

MS = 161.986 (63.774)
Z = 0.833 (0.328)

FRP (Z = 0)

TUNNEL ℄
Z = −2.151 (−0.847)

DATA REFERENCE
CENTER

MS = 165.448 (65.137)
Z = −3.104 (−1.222)

MS = MODEL STATION
TS = TUNNEL STATION
Z = HEIGHT ABOVE MODEL FRP

MS = 188.250 (74.114)
TS = 306.616 (120.715)
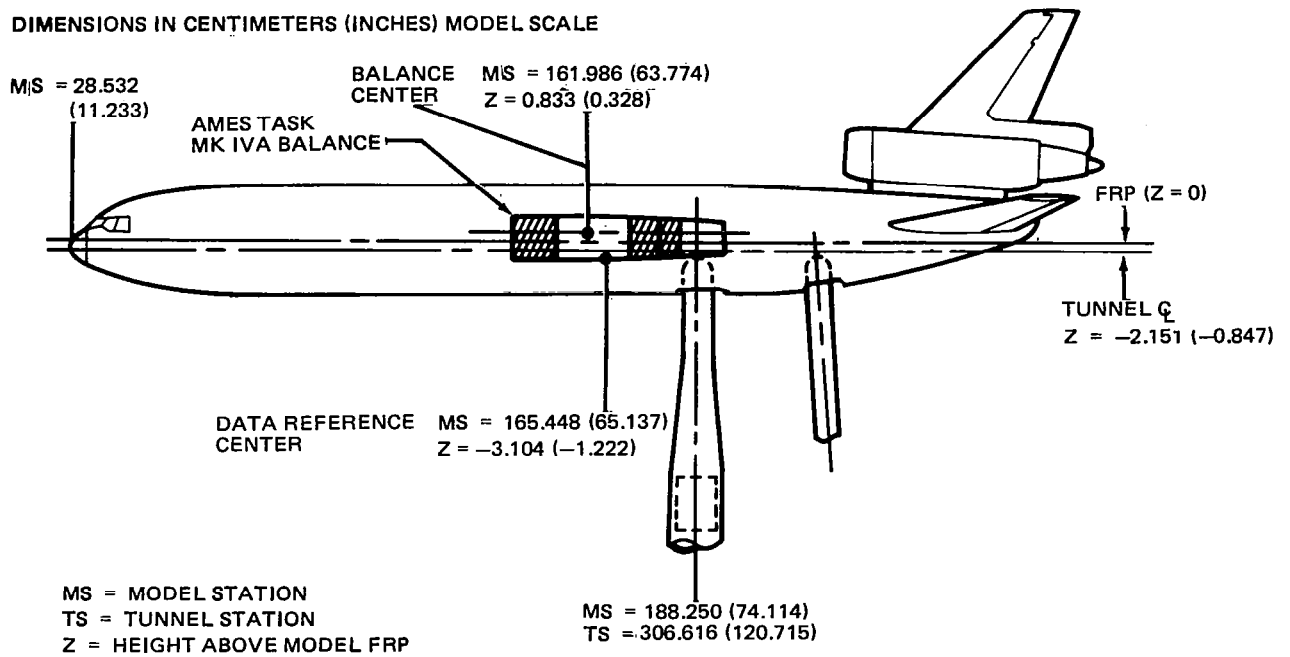
FIGURE 29. TANDEM SUPPORT INSTALLATION OF DC-10 SERIES 30 HIGH-LIFT MODEL IN AMES RESEARCH CENTER 12-FOOT WIND TUNNEL
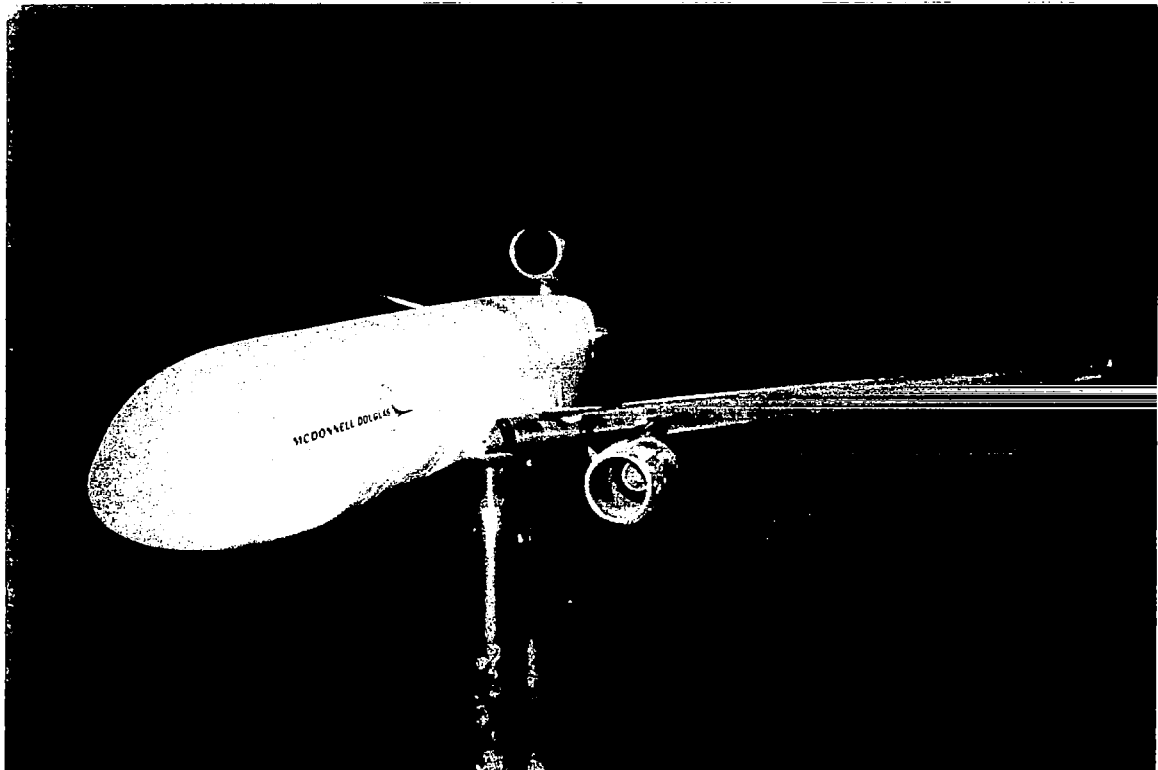
FIGURE 30. FRONT VIEW OF DC-10 SERIES 30 HIGH-LIFT MODEL WITH BASIC WINGLETS INSTALLED IN AMES RESEARCH CENTER 12-FOOT WIND TUNNEL

36
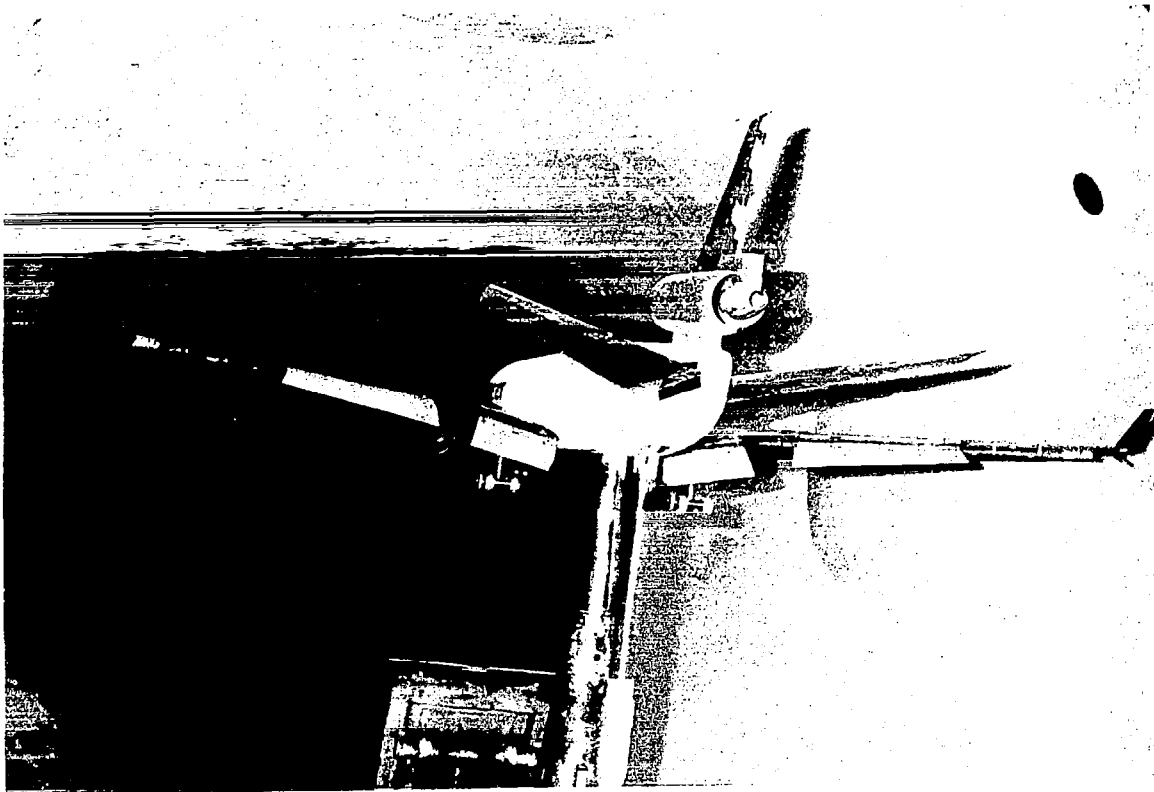
FIGURE 31. AFT VIEW OF DC-10 SERIES 30 HIGH-LIFT MODEL WITH REDUCED-SPAN WINGLETS INSTALLED IN AMES RESEARCH CENTER 12-FOOT WIND TUNNEL
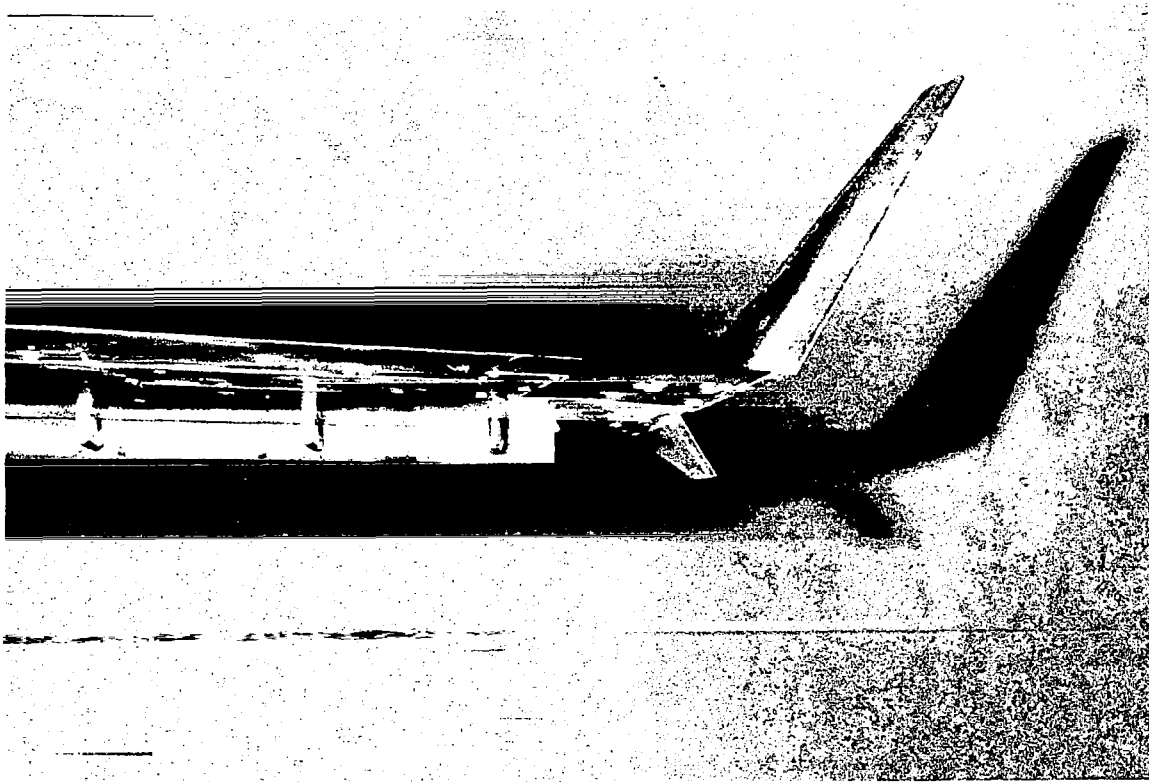
FIGURE 32. BASIC UPPER WINGLET INSTALLED ON DC-10 SERIES 30 HIGH-LIFT MODEL

37
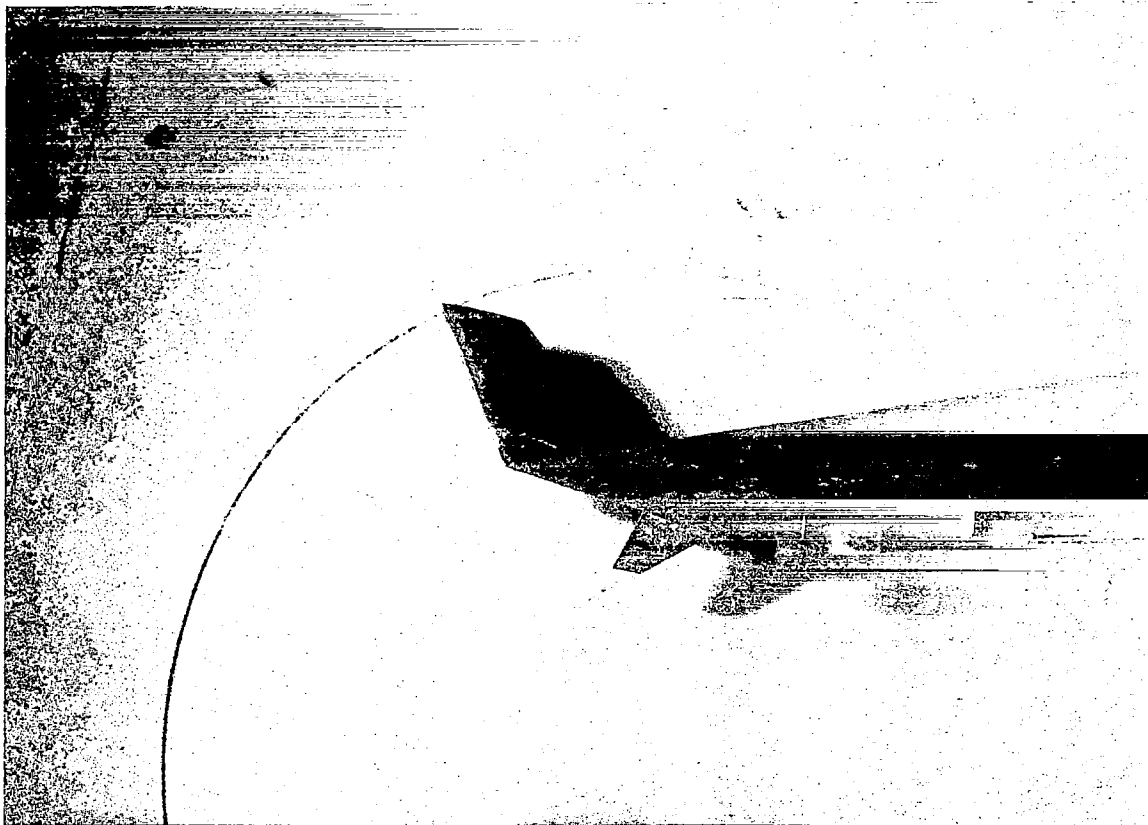
FIGURE 33. REDUCED-SPAN UPPER WINGLET INSTALLED ON DC-10 SERIES 30 HIGH-LIFT MODEL

referred to the stability axes and all moments were referred to a center at the 25-percent position of the wing mean aerodynamic chord in the plane of symmetry and 3.10 cm (1.22 inches) below the fuselage reference plane. All coefficients were based on free-stream dynamic pressure and geometric constants of the DC-10 Series 30 wing. Final stability axis coefficients account for model weight tare effects and wind tunnel wall interference corrections. Additional measurements included static pressures along chordwise rows at seven spanwise locations on the wing and two chordwise rows along the winglet span. Also, trailing edge pressures were measured at four winglet spanwise stations.

In order to investigate and record the flow patterns on the upper winglet inner surface and wing tip upper surface, a mini-tuft flow visualization technique was employed (Reference 6). Nylon monofilament tufts of 0.0025-cm (0.0010-inch) diameter and approximately 1.3 cm (0.5 inch) in length, treated with fluorescent dye, were applied to the subject areas in spanwise rows. As in the high-speed investigations, the tuft patterns were recorded by an ultraviolet flash unit and a remotely operated camera.

Five wing flap/slat configurations were utilized to investigate relevant takeoff and landing conditions. The flap/slat configurations are designated by the nominal flap setting (0, 15, 25, or 50 degrees) and slat positions (retracted, takeoff, or landing). The flap/slat configurations which were the subject of this investigation are described in Table 1.

TABLE 1
FLAP/SLAT CONFIGURATION DEFINITION FOR DC-10 SERIES 30
WINGLET DEVELOPMENT LOW-SPEED WIND TUNNEL MODEL

DESIGNATION	FLAP DEFLECTION, δ_F (DEG)		SLAT DEFLECTION, δ_S (DEG)	
	INBOARD	OUTBOARD	INBOARD	OUTBOARD
0/RETRACT (0/0)	0	0	0	0
0/TAKEOFF (0/T.O.)	0	0	15	25
15/TAKEOFF (15/T.O.)	15	13	15	25
25/TAKEOFF (25/T.O.)	25	22	15	25
50/LANDING (50/LND)	50	45	19	30

For each winglet configuration, an initial evaluation was made of the winglet slat effectiveness with the empennage removed. After the best winglet slat position (extended or retracted) was selected, tests were conducted at all flap/slat settings for the baseline (no winglets) and for both winglet configurations (basic and reduced-span) to determine drag and maximum-lift characteristics.

At selected flap/slat configurations, pitch variations were conducted tail-on and tail-off for investigating longitudinal stability characteristics. Also, lateral-directional stability was investigated by varying pitch at a fixed sideslip angle and varying yaw at a fixed pitch angle. Additionally, tail-on tests were conducted with one outboard aileron deflected −20, −10, +10, and +20 degrees (positive trailing edge down) to evaluate the aileron effectiveness in the presence of the winglet at high-lift conditions. Some yaw cases were run at reduced Reynolds number conditions because maximum balance roll capability was attained at the maximum Reynolds number condition.

Accumulation of ice on the leading edge of the upper winglet was simulated for the primary takeoff and landing flap settings. Mini-tuft flow visualization was conducted during most of the low-speed investigation.

Results and Discussion

Flow visualization results — Mini-tuft flow visualization for a typical takeoff flap/slat setting is given in Figures 34 through 39. The mini-tuft flow observations of these figures indicate a progression of flow quality from well-behaved, attached flow at low angles of attack (8 degrees and below) to degraded and separated flow at high angles of attack. Intermediate angles of attack display varying degrees of flow separation. Generally, the upper winglet leading edge slat delayed the onset of flow separation to higher angles of attack for the entire upper winglet inner surface. Figure 38 indicates, for a lift coefficient beyond that associated with V_2, nearly total flow separation for the winglet slat retracted case, whereas the corresponding slat-extended case exhibits attached flow over a significant portion of the upper winglet surface.
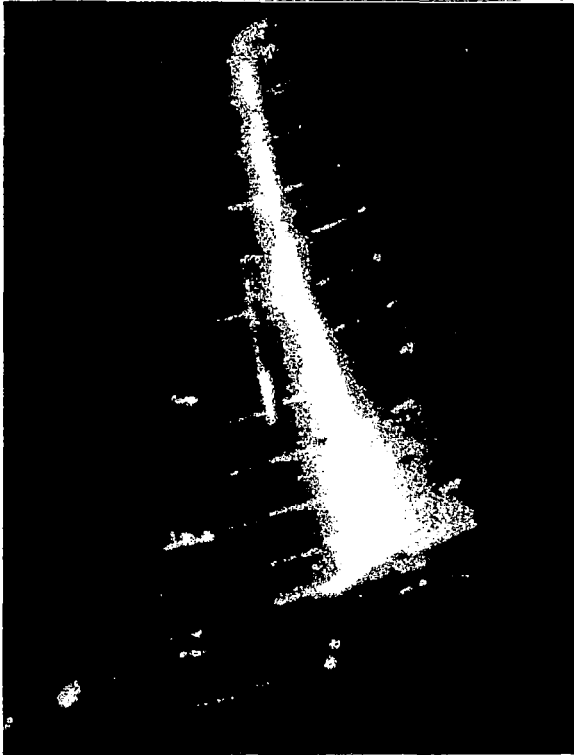
WINGLET SLAT RETRACTED
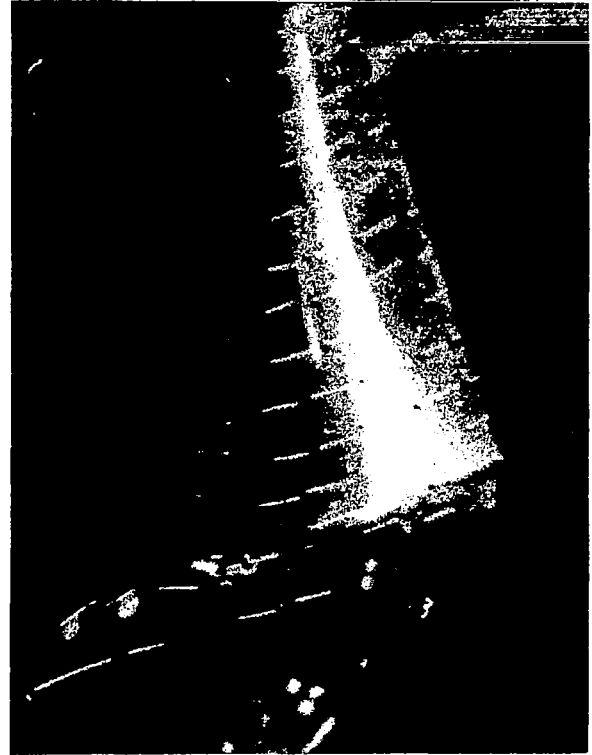
WINGLET SLAT EXTENDED

FIGURE 34. MINI-TUFT FLOW VISUALIZATION FOR THE BASIC WINGLET AIRCRAFT IN THE 15/TAKEOFF CONFIGURATION AT 0-DEGREE ANGLE OF ATTACK

WINGLET SLAT RETRACTED
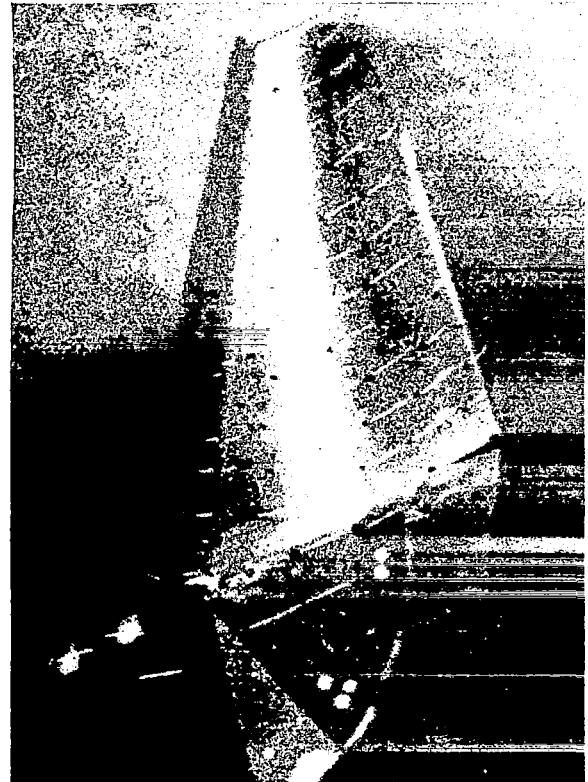
WINGLET SLAT EXTENDED

FIGURE 35. MINI-TUFT FLOW VISUALIZATION FOR THE BASIC WINGLET AIRCRAFT IN THE 15/TAKEOFF CONFIGURATION AT 8-DEGREE ANGLE OF ATTACK
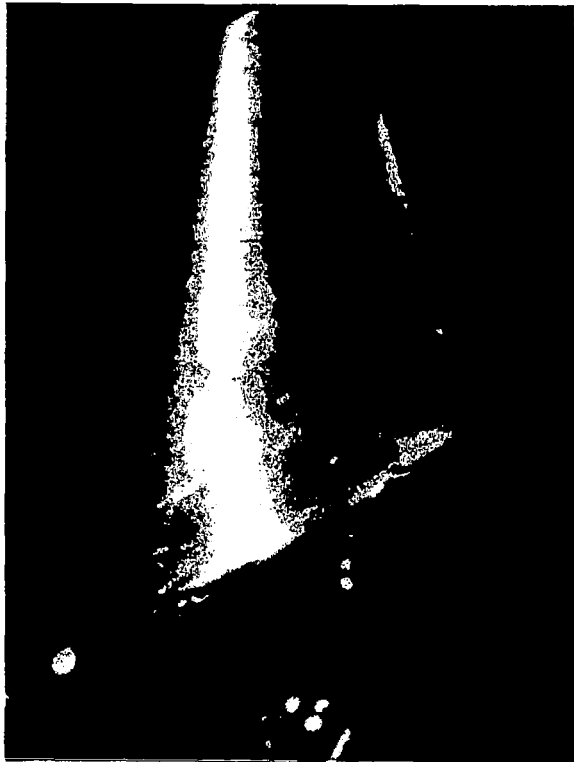
WINGLET SLAT RETRACTED   **WINGLET SLAT EXTENDED**

FIGURE 36. MINI-TUFT FLOW VISUALIZATION FOR THE BASIC WINGLET AIRCRAFT IN THE
15/TAKEOFF CONFIGURATION AT 12-DEGREE ANGLE OF ATTACK

WINGLET SLAT RETRACTED   **WINGLET SLAT EXTENDED**

FIGURE 37. MINI-TUFT FLOW VISUALIZATION FOR THE BASIC WINGLET AIRCRAFT IN THE
15/TAKEOFF CONFIGURATION AT 13-DEGREE ANGLE OF ATTACK

41
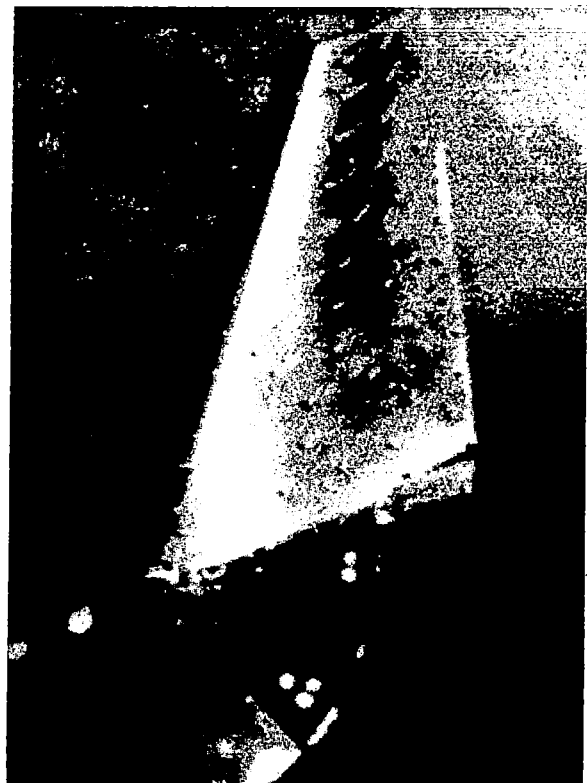
WINGLET SLAT RETRACTED
WINGLET SLAT EXTENDED

FIGURE 38. MINI-TUFT FLOW VISUALIZATION FOR THE BASIC WINGLET AIRCRAFT IN THE 15/TAKEOFF CONFIGURATION AT 14-DEGREE ANGLE OF ATTACK
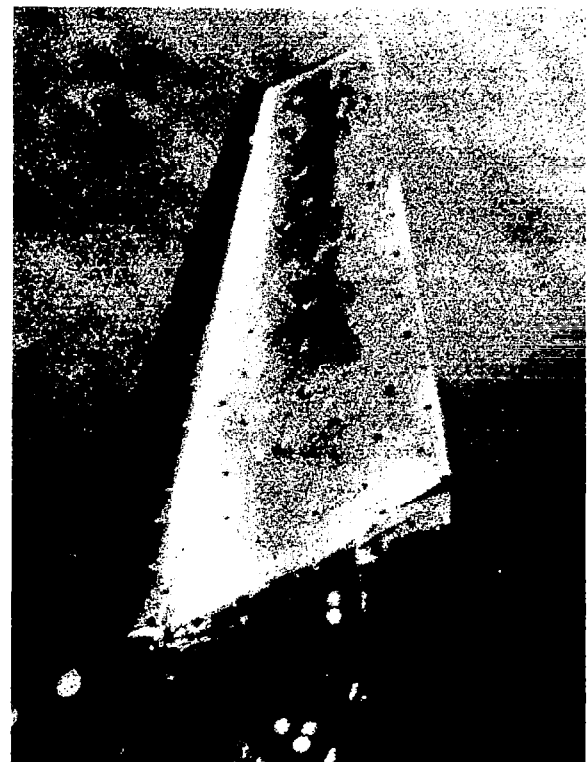
WINGLET SLAT RETRACTED
WINGLET SLAT EXTENDED

FIGURE 39. MINI-TUFT FLOW VISUALIZATION FOR THE BASIC WINGLET AIRCRAFT IN THE 15/TAKEOFF CONFIGURATION AT 15-DEGREE ANGLE OF ATTACK

A second flow visualization sequence is given in Figures 40 through 46 where a comparison of flow visualization results is given for the inboard surface of the basic and reduced-span upper winglets at a landing flap setting of 50 degrees. A general winglet flow progression with increasing angle of attack from attached streamwise flow to spanwise directed flow and eventually to separated winglet flow is indicated in these figures for both winglet configurations. At the condition representative of landing approach (Figure 43, $\alpha = 7°$), the flow is completely attached on the winglet and wing tip. The spanwise winglet flow appears to originate at the winglet root trailing edge and spread outboard with increasing angle of attack. Spanwise winglet flow was generally noted over a larger percentage of the basic winglet than of the reduced-span winglet at the same aircraft angle of attack. Although the spanwise flow originates near the winglet root trailing edge region, actual flow separation, as evidenced by reversed tufts, appears to originate at the winglet tip, as indicated in Figures 45 and 46. Also, Figure 46 indicates that when the winglet flow is completely separated, the wing tip flow remains reasonably well behaved.

Lift characteristics — Figures 47 through 49 show the tail-off lift characteristics for the baseline, basic winglet with winglet slat retracted, and basic winglet with winglet slat extended configurations. The data presented are representative of the clean wing, takeoff, and landing configurations investigated. These figures indicate that the impact of the basic winglet on the baseline aircraft maximum lift coefficient and lift curve slope was very small, and in no case detrimental. Similarly, the impact of the winglet slat on lift characteristics was inconsequential. A slight increase in lift curve slope and a negligible impact on maximum lift coefficient are typical of the winglet influence for all flap settings.

BASIC WINGLET   REDUCED-SPAN WINGLET
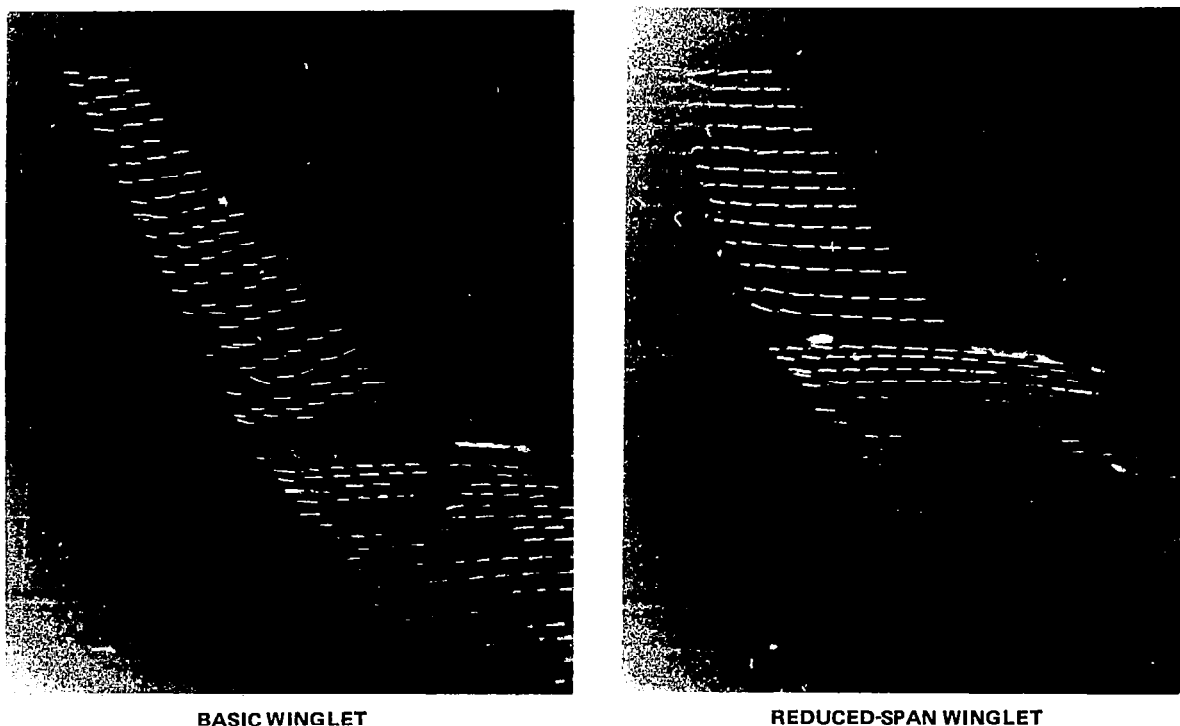
FIGURE 40. MINI-TUFT FLOW VISUALIZATION FOR THE BASIC AND REDUCED-SPAN WINGLETS IN THE 50/LANDING CONFIGURATION AT 0.7-DEGREE ANGLE OF ATTACK
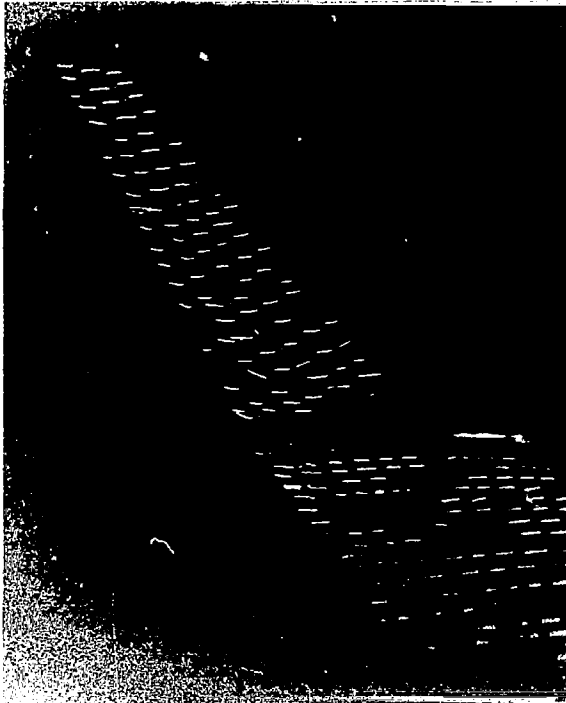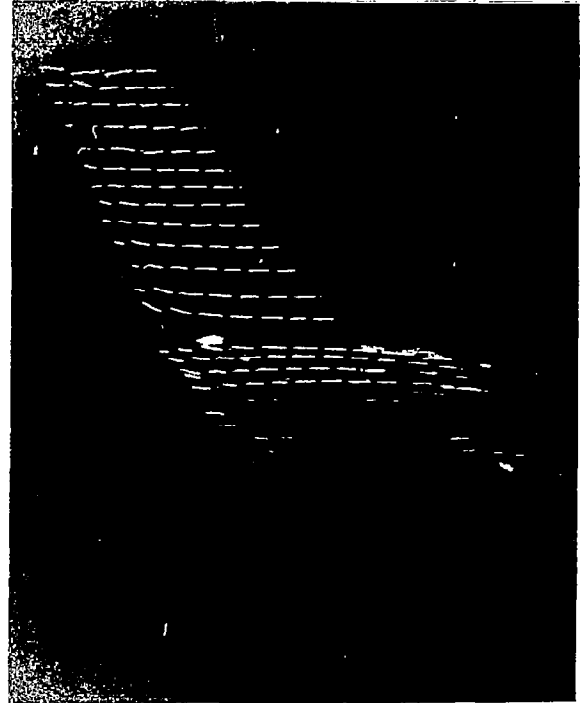
BASIC WINGLET

REDUCED-SPAN WINGLET

FIGURE 41. MINI-TUFT FLOW VISUALIZATION FOR THE BASIC AND REDUCED-SPAN WINGLETS IN THE 50/LANDING CONFIGURATION AT 2.8-DEGREE ANGLE OF ATTACK
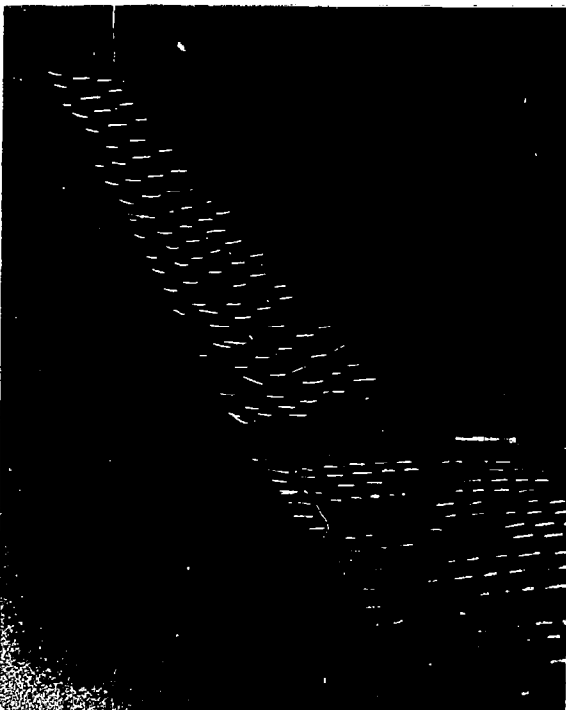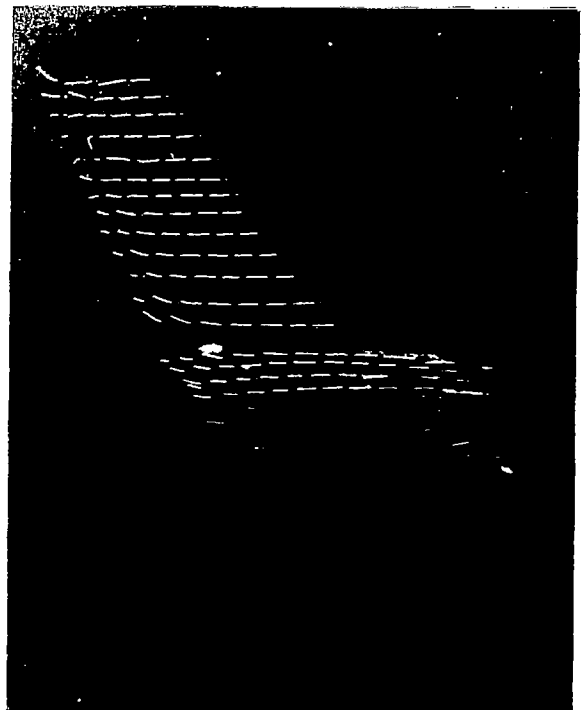
BASIC WINGLET

REDUCED-SPAN WINGLET

FIGURE 42. MINI-TUFT FLOW VISUALIZATION FOR THE BASIC AND REDUCED-SPAN WINGLETS IN THE 50/LANDING CONFIGURATION AT 4.9-DEGREE ANGLE OF ATTACK
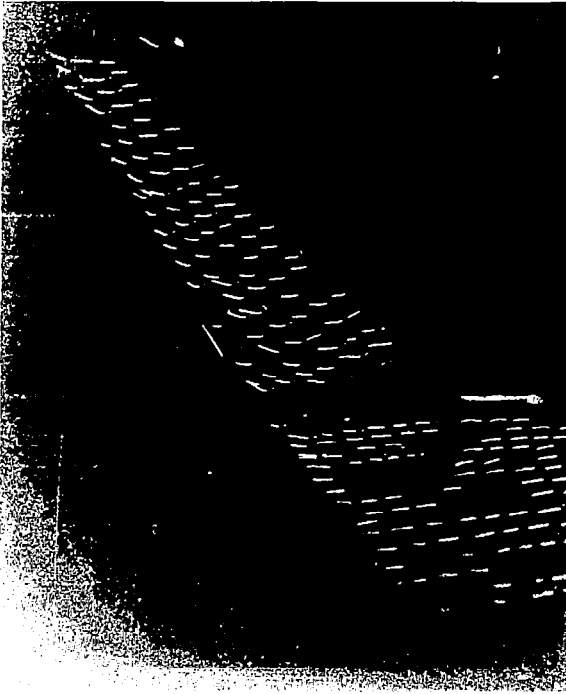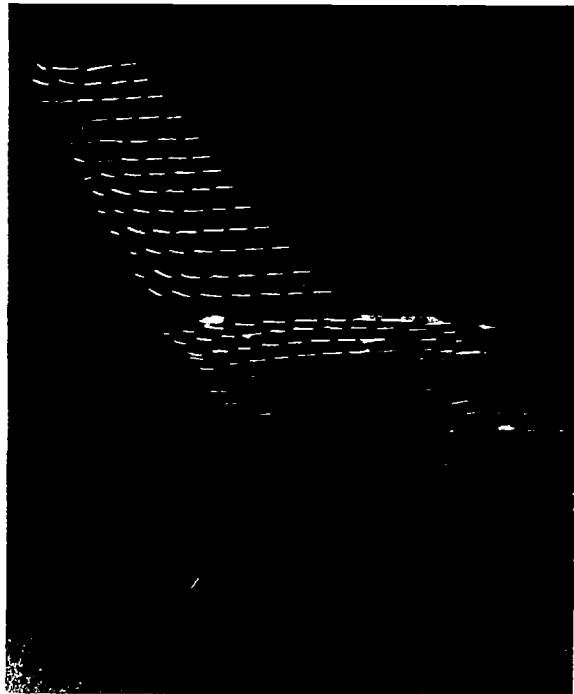
BASIC WINGLET   REDUCED-SPAN WINGLET

FIGURE 43. MINI-TUFT FLOW VISUALIZATION FOR THE BASIC AND REDUCED-SPAN WINGLETS IN THE 50/LANDING CONFIGURATION AT 7.0-DEGREE ANGLE OF ATTACK
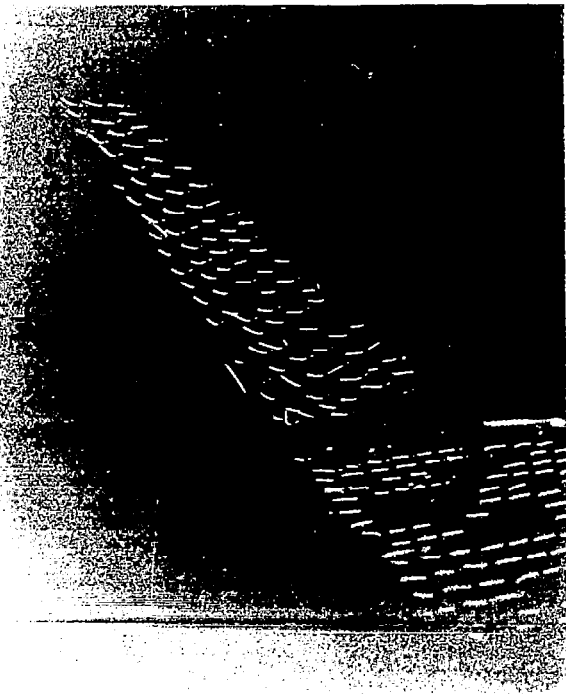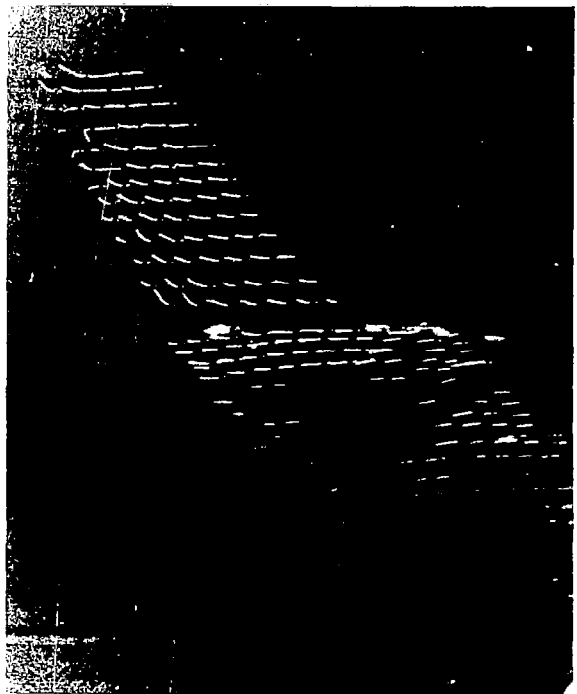
BASIC WINGLET   REDUCED-SPAN WINGLET

FIGURE 44. MINI-TUFT FLOW VISUALIZATION FOR THE BASIC AND REDUCED-SPAN WINGLETS IN THE 50/LANDING CONFIGURATION AT 9.1-DEGREE ANGLE OF ATTACK
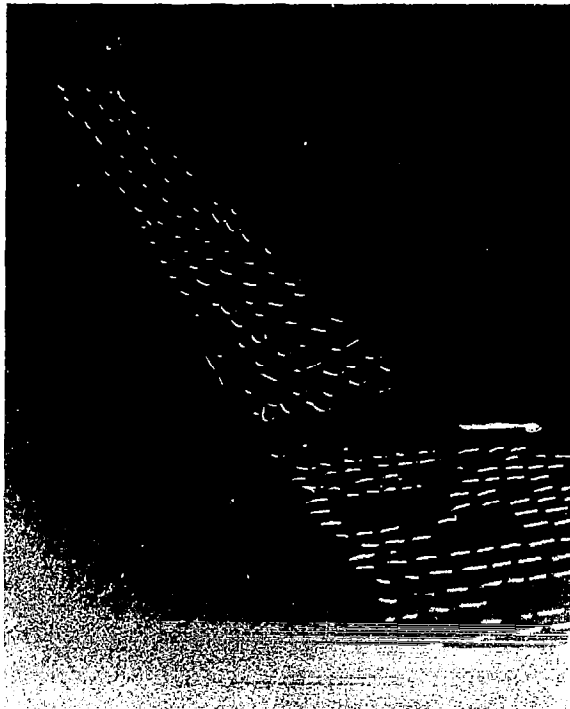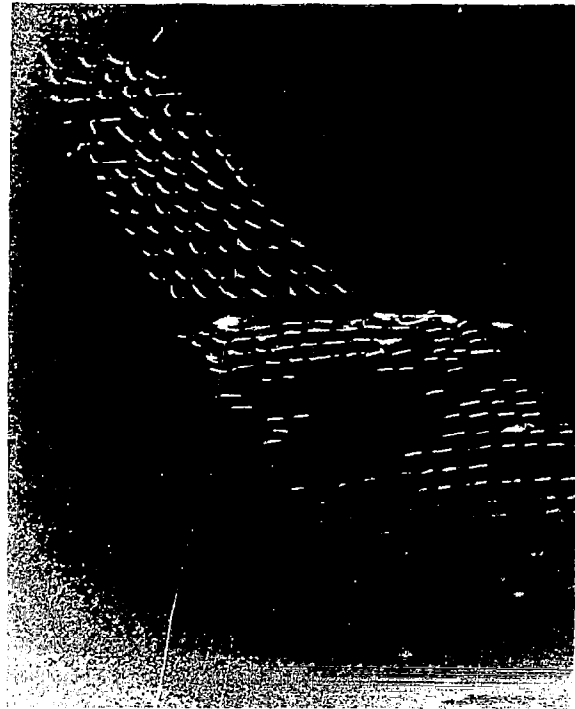
BASIC WINGLET

REDUCED-SPAN WINGLET

FIGURE 45. MINI-TUFT FLOW VISUALIZATION FOR THE BASIC AND REDUCED-SPAN WINGLETS IN THE 50/LANDING CONFIGURATION AT 11.2-DEGREE ANGLE OF ATTACK
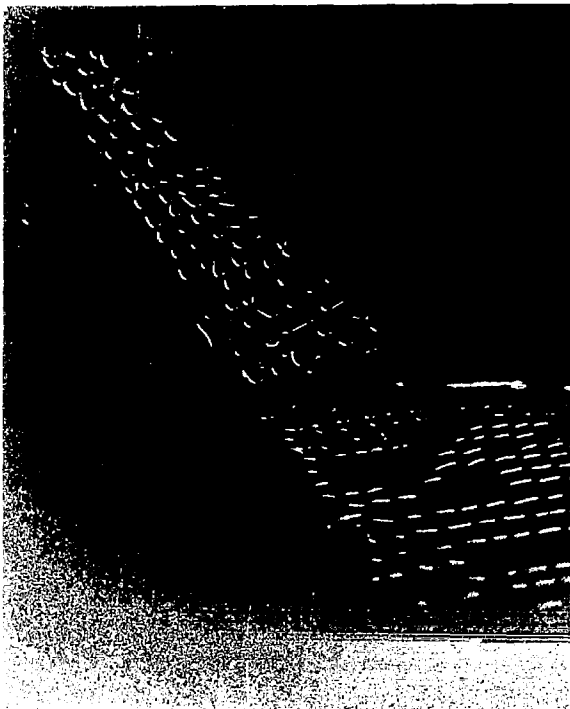
BASIC WINGLET

REDUCED-SPAN WINGLET

FIGURE 46. MINI-TUFT FLOW VISUALIZATION FOR THE BASIC AND REDUCED-SPAN WINGLETS IN THE 50/LANDING CONFIGURATION AT 13.3-DEGREE ANGLE OF ATTACK
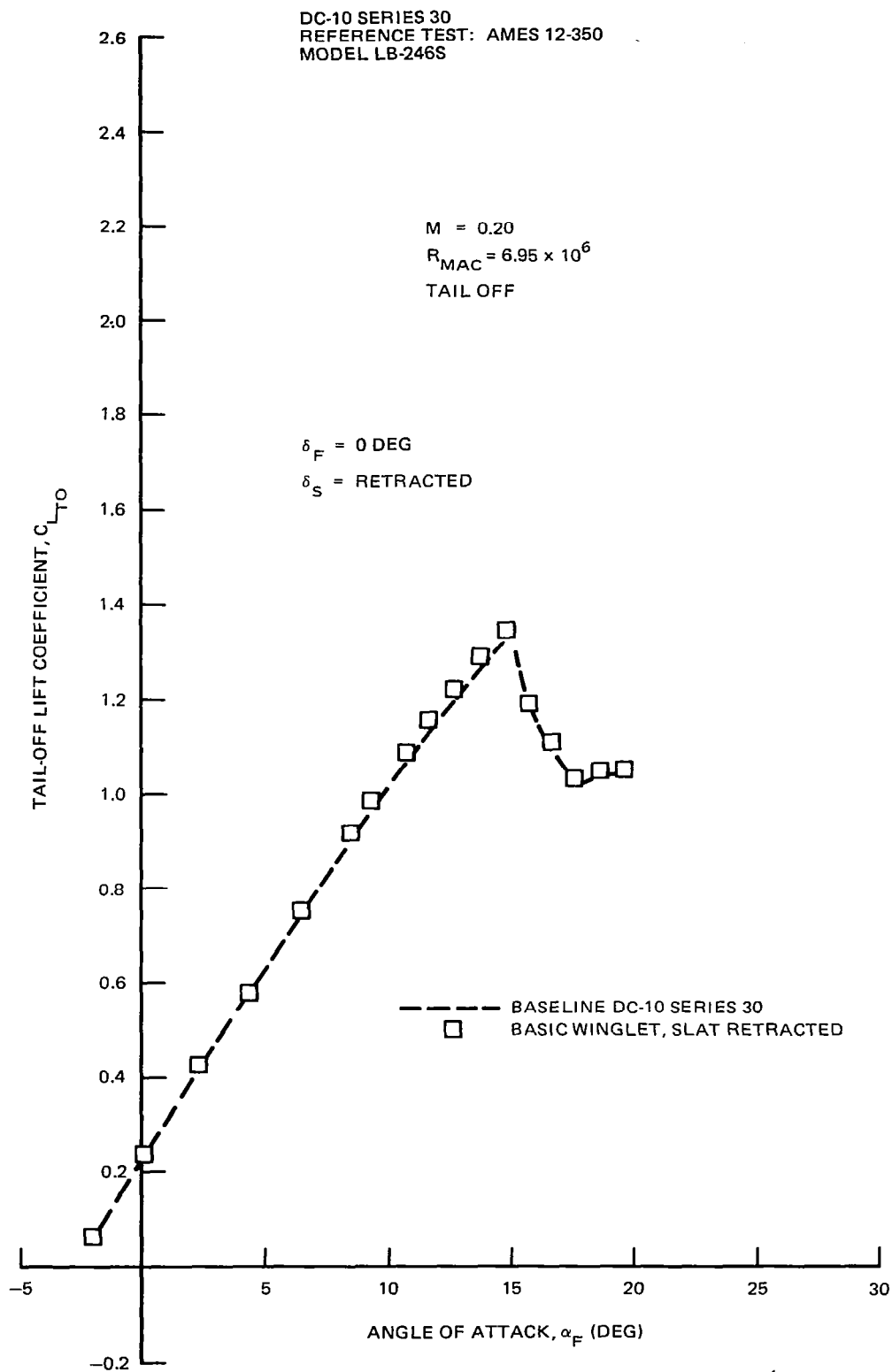
FIGURE 47. BASELINE AND BASIC WINGLET AIRCRAFT LIFT CHARACTERISTICS FOR CLEAN WING CONFIGURATION

47
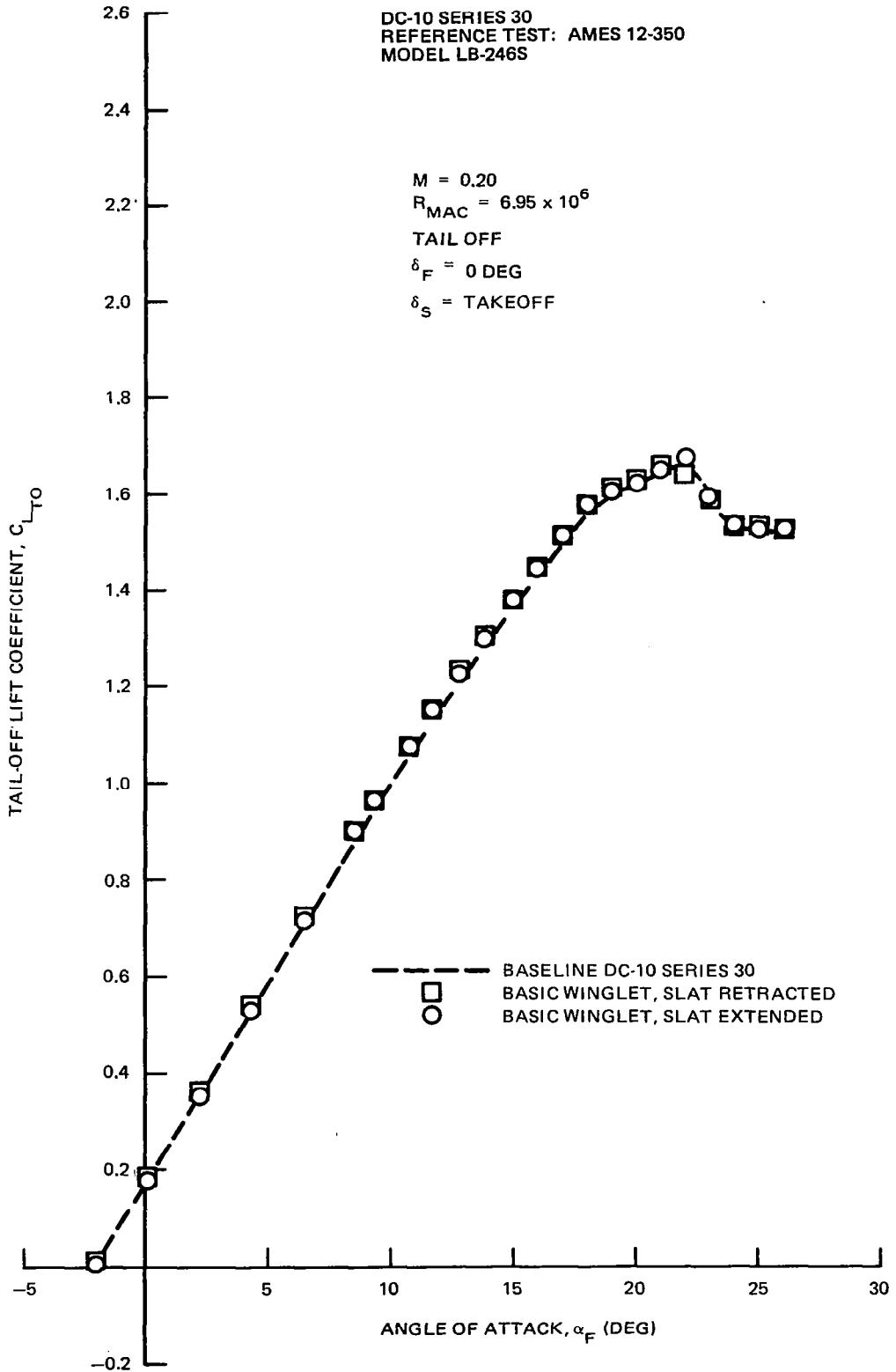
FIGURE 48. BASELINE AND BASIC WINGLET AIRCRAFT LIFT CHARACTERISTICS FOR RETRACTED FLAPS AND EXTENDED SLATS CONFIGURATION
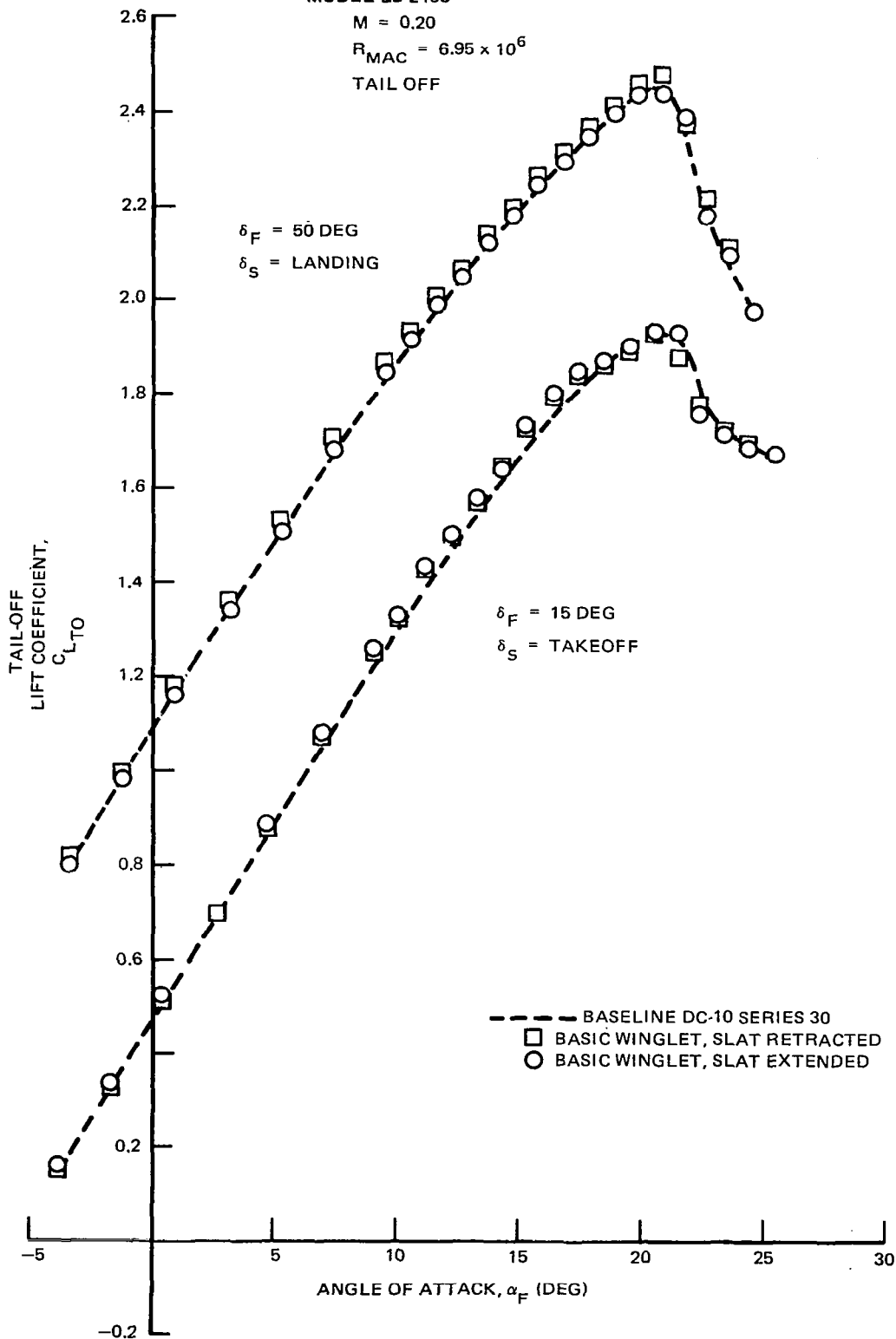
FIGURE 49. BASELINE AND BASIC WINGLET AIRCRAFT LIFT CHARACTERISTICS FOR TAKEOFF AND LANDING CONFIGURATIONS

49

Figure 50 reflects essentially the same trend in a comparison of basic and reduced-span winglet influence on the baseline lift characteristics for a flaps-retracted, slats-extended configuration. A summary of winglet impact on maximum lift characteristics is presented in Figure 51, which indicates negligible impact throughout the flap deflection range for the basic and reduced-span winglets with the winglet slat extended.

Drag characteristics — As expected, the drag characteristics of the baseline configuration were significantly improved by the winglets. Figures 52 through 54 show the results obtained during the winglet slat investigation conducted in the first of the two wind tunnel tests. Figure 53 includes a comparison of basic winglet flow quality and drag reduction for a takeoff (15/takeoff) flap/slat configuration. This comparison will be discussed later. Substantial drag improvement from the baseline was realized for the winglet configuration for the operational lift range of each flap/slat deflection tested. Also, the impact of the winglet slat on drag was minor, although slightly degraded drag characteristics were observed for the slat extended compared with the slat retracted. On the basis of these lift and drag results, it was decided to conduct all subsequent tests with the winglet slat retracted inasmuch as the extended slat, with its associated complexity, provided no performance advantage. It was recognized, however, that the winglet slat could be of benefit in minimizing the extent of separation-induced buffet, should this condition be encountered.

Typical winglet drag reductions determined from the second wind tunnel test are given in Figures 55 through 59 for the basic and reduced-span winglet configurations along with the basic winglet benefit defined in the first test. The difference in the drag reductions between the reduced-span and basic winglets was, in most cases, approximately proportional to the difference in winglet span. Exceptions to this trend are given in Figures 56 and 58 where the drag reductions for the basic and reduced-span winglets for the given flap/slat deflections are about equal. The relative performance of the two winglet configurations is in agreement with analytical predictions.

At takeoff flap deflections, the drag reduction levels between the two different tests, LB-246S and LB-246AD, were in reasonably good agreement. However, the agreement between the two tests was progressively poorer with increasing flap deflection. The differences between the two tests were less than could be expected between separate tests, but comparison of the two tests for the landing configuration of Figure 59 indicates a slightly lower degree of repeatability than for the takeoff flap settings.

Figure 53 shows the winglet incremental drag improvement for the winglet slat in the extended and retracted positions for the 15/takeoff configuration. Also, an approximate flow quality indication, based on the tuft flow visualization, is provided. For this takeoff flap/slat deflection, it appears that the winglet slat retracted case is superior to the slat extended configuration. Additionally, the maximum drag advantage is realized for middle lift coefficients near the operational
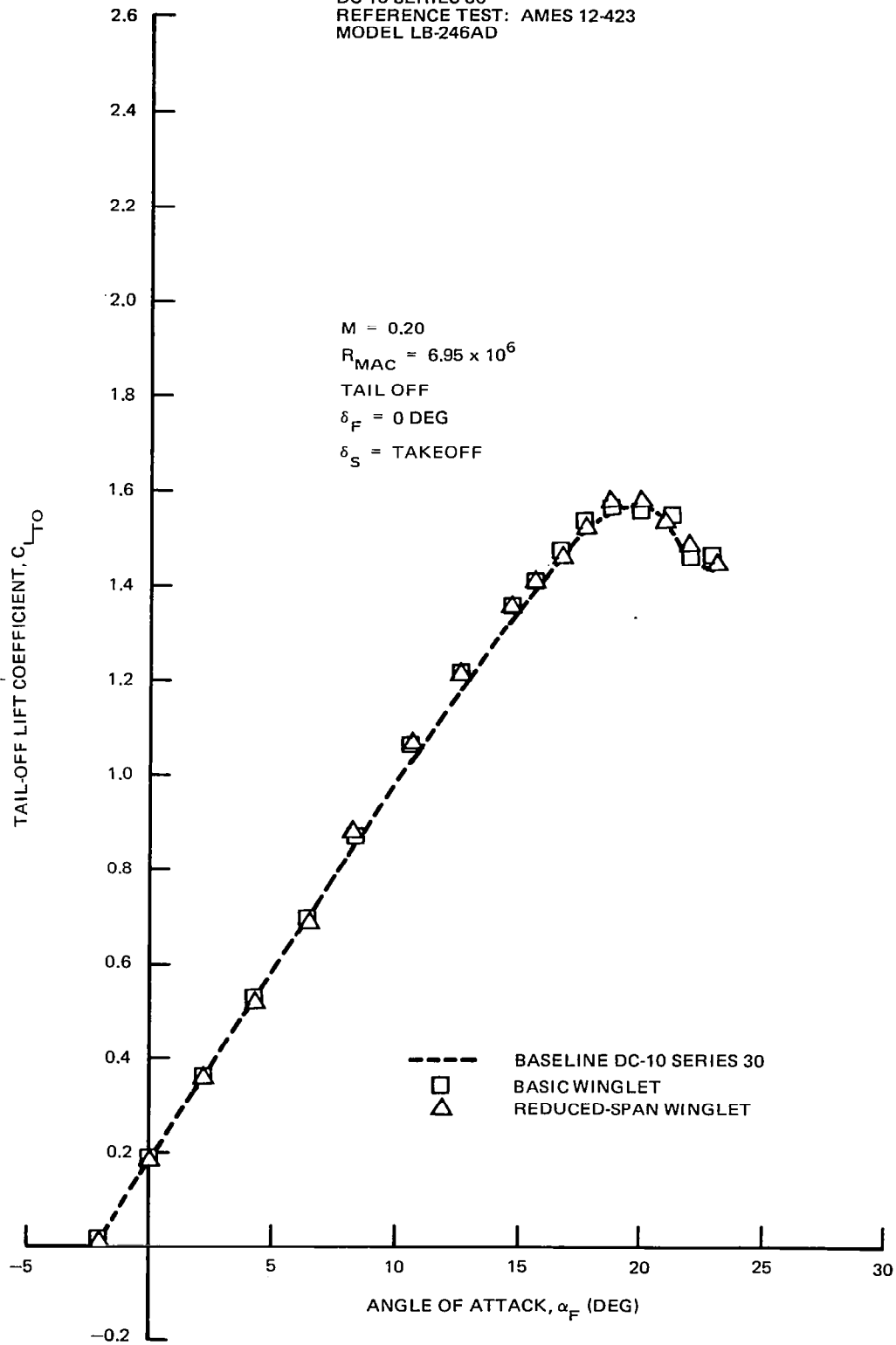
FIGURE 50. EFFECT OF BASIC AND REDUCED-SPAN WINGLETS ON LIFT CHARACTERISTICS FOR CONFIGURATION WITH RETRACTED FLAPS AND TAKEOFF SLATS

DC-10 SERIES 30
REFERENCE TEST: AMES 12-423
MODEL LB-246AD

$M = 0.20$
$R_{MAC} = 6.95 \times 10^6$
□ BASIC WINGLET
△ REDUCED-SPAN WINGLET

FLAGGED SYMBOLS — SLATS RETRACTED
UNFLAGGED SYMBOLS — SLATS EXTENDED

IMPROVEMENT

INCREMENTAL MAXIMUM TAIL-OFF LIFT COEFFICIENT, $\Delta C_{L_{TO_{MAX}}}$

FLAP DEFLECTION, δ_F (DEG)
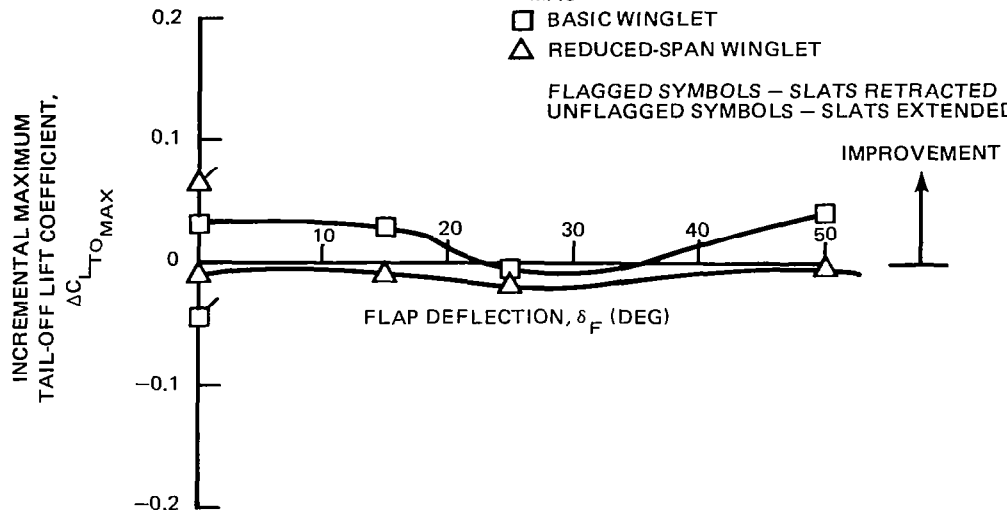
FIGURE 51.   EFFECT OF WINGLETS ON TAIL-OFF MAXIMUM LIFT COEFFICIENT

DC-10 SERIES 30
REFERENCE TEST: AMES 12-350
MODEL LB-246S

$M = 0.20$
$R_{MAC} = 6.95 \times 10^6$

TAIL OFF

$\delta_F = 0$ DEG

$\delta_S = $ TAKEOFF

□ BASIC WINGLET, SLAT RETRACTED
○ BASIC WINGLET, SLAT EXTENDED

INCREMENTAL DRAG COEFFICIENT, ΔC_D

IMPROVEMENT

TAIL-OFF LIFT COEFFICIENT, $C_{L_{TO}}$
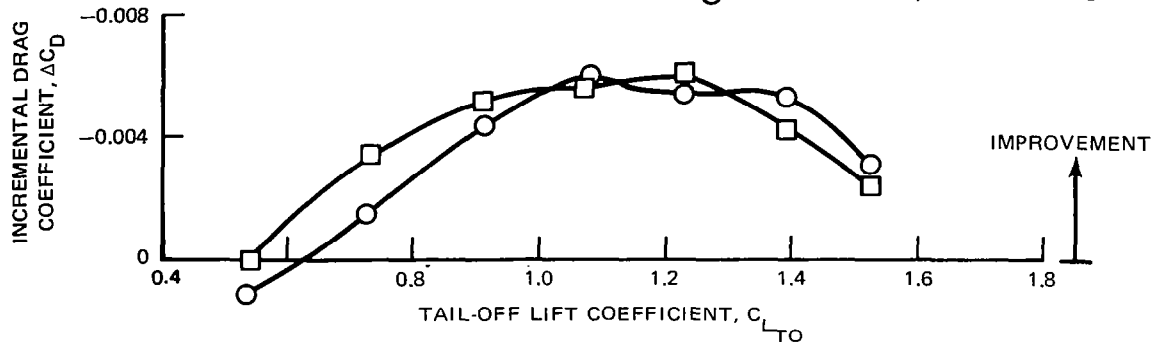
FIGURE 52.   EFFECT OF WINGLET SLAT ON BASIC WINGLET AIRCRAFT DRAG IMPROVEMENT WITH RETRACTED FLAPS AND TAKEOFF SLATS

DC-10 SERIES 30
REFERENCE TEST: AMES 12-350
MODEL LB-246S

$M = 0.20$
$R_{MAC} = 6.95 \times 10^6$
TAIL-OFF
$\delta_F = 15$ DEG
$\delta_S =$ TAKEOFF

□ BASIC WINGLET, SLAT RETRACTED
○ BASIC WINGLET, SLAT EXTENDED

TYPICAL V_2 ENGINE OUT CLIMB

IMPROVEMENT

$C_{L\ MAX_{TO}}$

TAIL-OFF LIFT COEFFICIENT, $C_{L_{TO}}$

WINGLET FLOW QUALITY

| RETRACTED | ATTACHED | DEGRADED | SEPARATED |
| EXTENDED | ATTACHED | DEGRADED | SEPARATED |
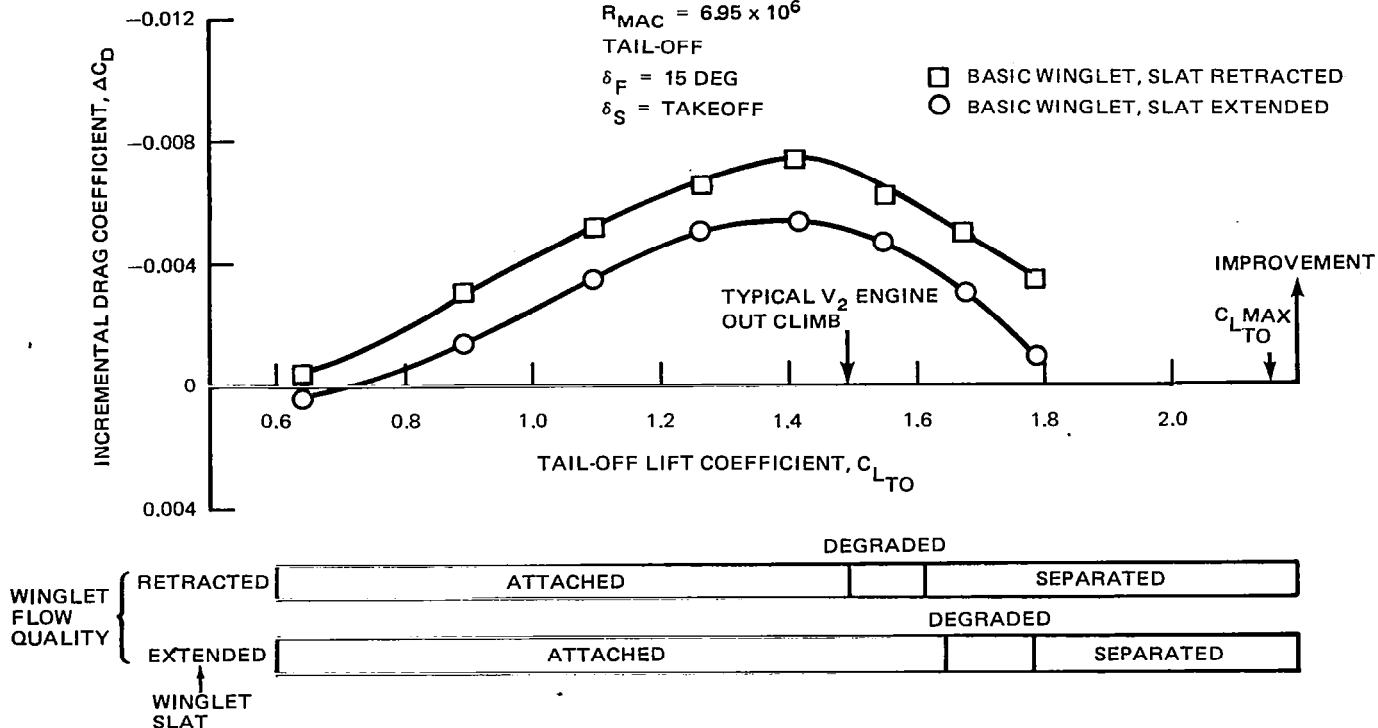
WINGLET SLAT

FIGURE 53. EFFECT OF WINGLET SLAT ON BASIC WINGLET DRAG IMPROVEMENT FOR TAKEOFF CONFIGURATION ($\delta_F = 15$ DEG)

V_2 lift value for engine inoperative climb. Significant winglet inner-surface flow separation is disclosed by the tuft observations for the winglet slat-retracted configuration, but this occurs at lift coefficients beyond that associated with V_2. This flow separation results in the winglet drag improvement being significantly degraded at lift coefficients greater than that associated with V_2.

However, the presence of separated flow near the operational range of the aircraft raises concern of low-speed buffet. Although only verifiable by flight test, the extent and impact of winglet flow separation are anticipated to be less at flight Reynolds numbers than at wind tunnel conditions. Nevertheless, it is recommended that a winglet leading edge device be provided for any flight evaluation in the event that adverse winglet flow is encountered.

A second set of summary results is given in Figures 60 and 61 where the impact of winglet slat and winglet span on the DC-10 drag and lift characteristics is shown for the range of flap settings available. These results are trimmed for a center-of-gravity location of 8 percent mean aerodynamic chord. A significant improvement in low-speed drag performance is available over the entire range of flap deflections. Consistent with the untrimmed lift results of Figure 51, the impact of winglets on maximum lift coefficient is insignificant for the trimmed results of Figures 60 and 61.

53

M = 0.20

R_{MAC} = 6.95 x 10^6

TAIL OFF

□ BASIC WINGLET, SLAT RETRACTED

δ_F = 50 DEG

○ BASIC WINGLET, SLAT EXTENDED

δ_S = LANDING

INCREMENTAL DRAG COEFFICIENT, Δc_D

-0.012

-0.008

-0.004

0

0.004

IMPROVEMENT

0.6   1.0   1.2   1.4   1.6   1.8   2.0

TAIL-OFF LIFT COEFFICIENT, $C_{L_{TO}}$
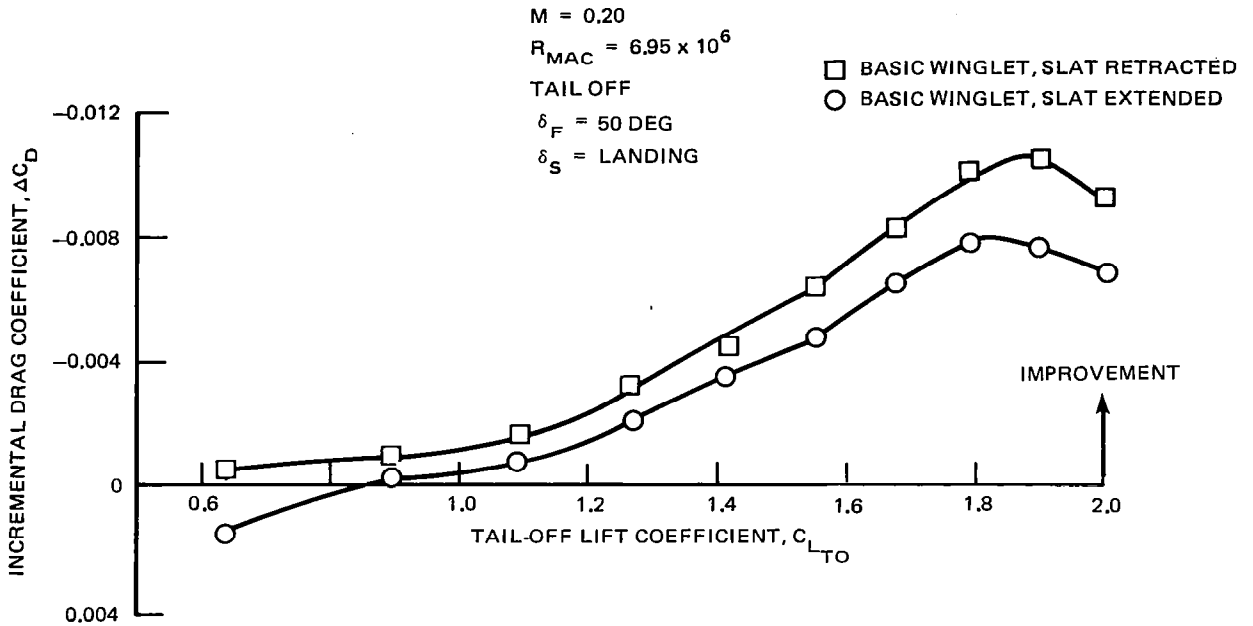
FIGURE 54. EFFECT OF WINGLET SLAT ON BASIC WINGLET DRAG IMPROVEMENT FOR LANDING CONFIGURATION

DC-10 SERIES 30

M = 0.20

R_{MAC} = 6.95 x 10^6

TAIL OFF

δ_F = 0 DEG

δ_S = RETRACTED

□ BASIC WINGLET (LB-246AD)

△ REDUCED-SPAN WINGLET (LB-246AD)

□ BASIC WINGLET (LB-246S)

INCREMENTAL DRAG COEFFICIENT, Δc_D

-0.008

-0.004

0

IMPROVEMENT

0.4   0.6   0.8   1.0   1.2   1.4   1.6   1.8

TAIL-OFF LIFT COEFFICIENT, $C_{L_{TO}}$
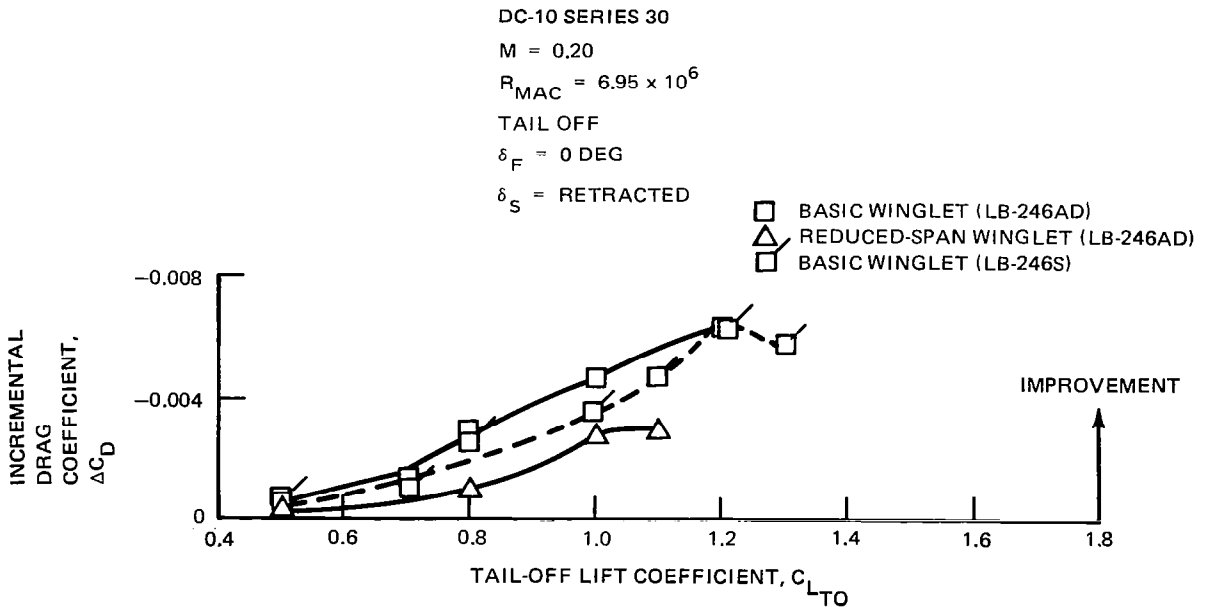
FIGURE 55. EFFECT OF WINGLETS ON DRAG FOR CLEAN WING CONFIGURATION

M = 0.20

R_{MAC} = 6.95 x 10⁶

TAIL OFF

δ_F = 0 DEG

δ_S = TAKEOFF

□ BASIC WINGLET (LB-246AD)
△ REDUCED-SPAN WINGLET (LB-246AD)
⬠ BASIC WINGLET (LB-246S)

INCREMENTAL DRAG COEFFICIENT, Δc_D

TAIL-OFF LIFT COEFFICIENT, $C_{L_{TO}}$

IMPROVEMENT
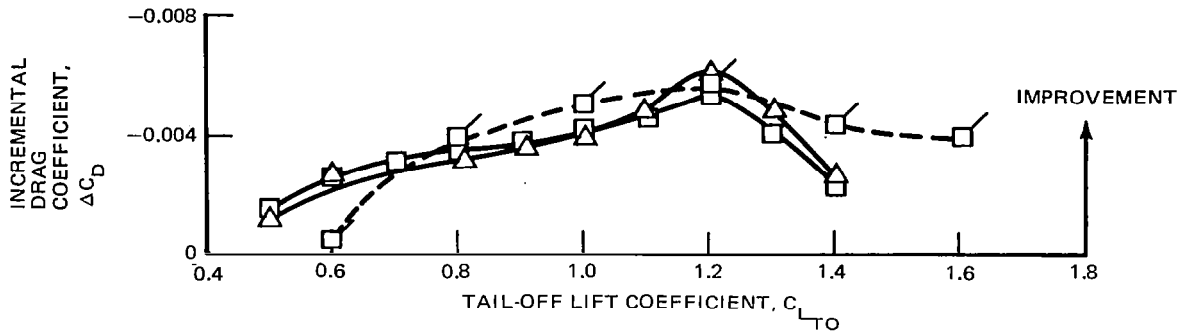
FIGURE 56. EFFECTS OF WINGLETS ON DRAG WITH TAKEOFF SLATS AND RETRACTED FLAPS

DC-10 SERIES 30

M = 0.20

R_{MAC} = 6.95 x 10⁶

TAIL OFF

δ_F = 15 DEG

δ_S = TAKEOFF

□ BASIC WINGLET (LB-246AD)
△ REDUCED-SPAN WINGLET (LB-246AD)
⬠ BASIC WINGLET (LB-246S)

INCREMENTAL DRAG COEFFICIENT, Δc_D

TAIL-OFF LIFT COEFFICIENT, $C_{L_{TO}}$

IMPROVEMENT
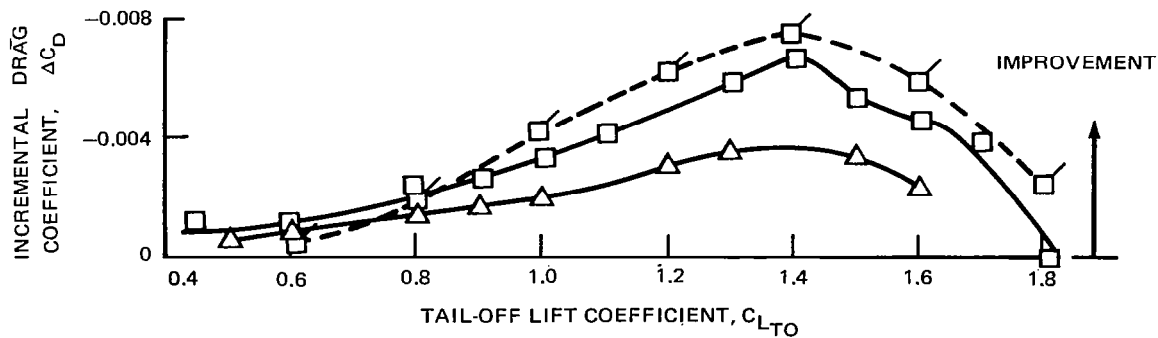
FIGURE 57. EFFECT OF WINGLETS ON DRAG FOR TAKEOFF CONFIGURATION (δ_F = 15 DEG)

INCREMENTAL DRAG COEFFICIENT ΔC_D

M = 0.20
R_{MAC} = 6.95 x 10^6
TAIL OFF
δ_F = 25 DEG
δ_S = TAKEOFF

☐ BASIC WINGLET (LB-246AD)
△ REDUCED-SPAN WINGLET (LB-246AD)

IMPROVEMENT

-0.008

-0.004

0

0.4   0.6   0.8   1.0   1.2   1.4   1.6   1.8   2.0

TAIL-OFF LIFT COEFFICIENT, $C_{L_{TO}}$
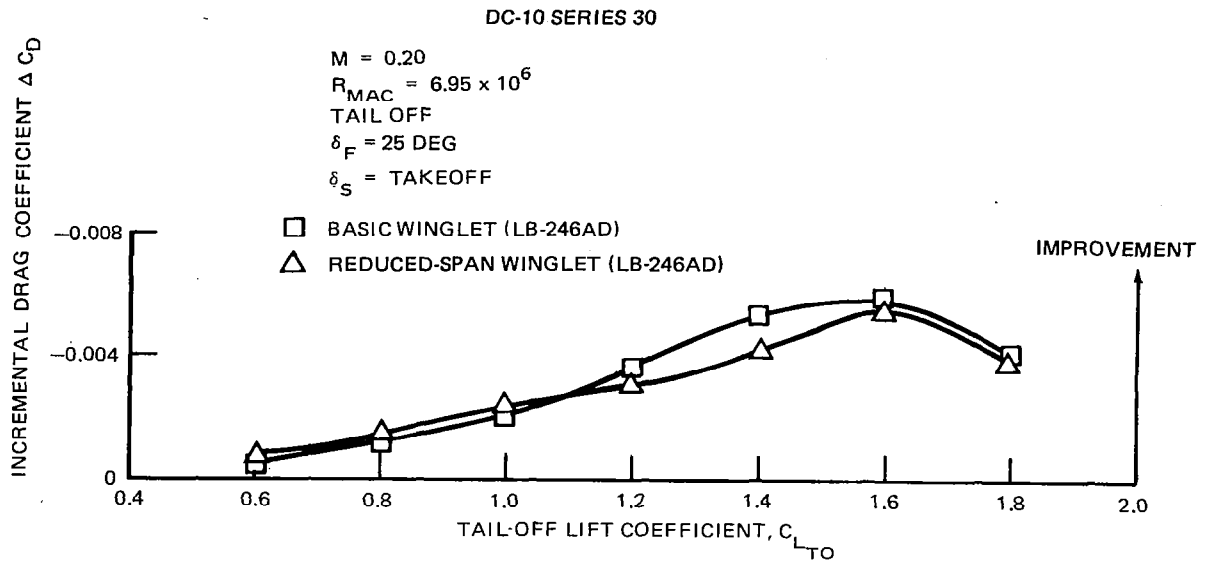
FIGURE 58. EFFECT OF WINGLETS ON DRAG FOR TAKEOFF CONFIGURATION (δ_F = 25 DEG)

DC-10 SERIES 30
M = 0.20
R_{MAC} = 6.95 x 10^6
TAIL OFF
δ_F = 50 DEG
δ_S = LANDING

☐ BASIC WINGLETS (LB-246AD)
△ REDUCED-SPAN WINGLETS (LB-246AD).
◻ BASIC WINGLETS (LB-246S)

INCREMENTAL DRAG COEFFICIENT, ΔC_D

-0.012

-0.008

-0.004

0

IMPROVEMENT

0.6   0.8   1.0   1.2   1.4   1.6   1.8   2.0

TAIL-OFF LIFT COEFFICIENT, $C_{L_{TO}}$
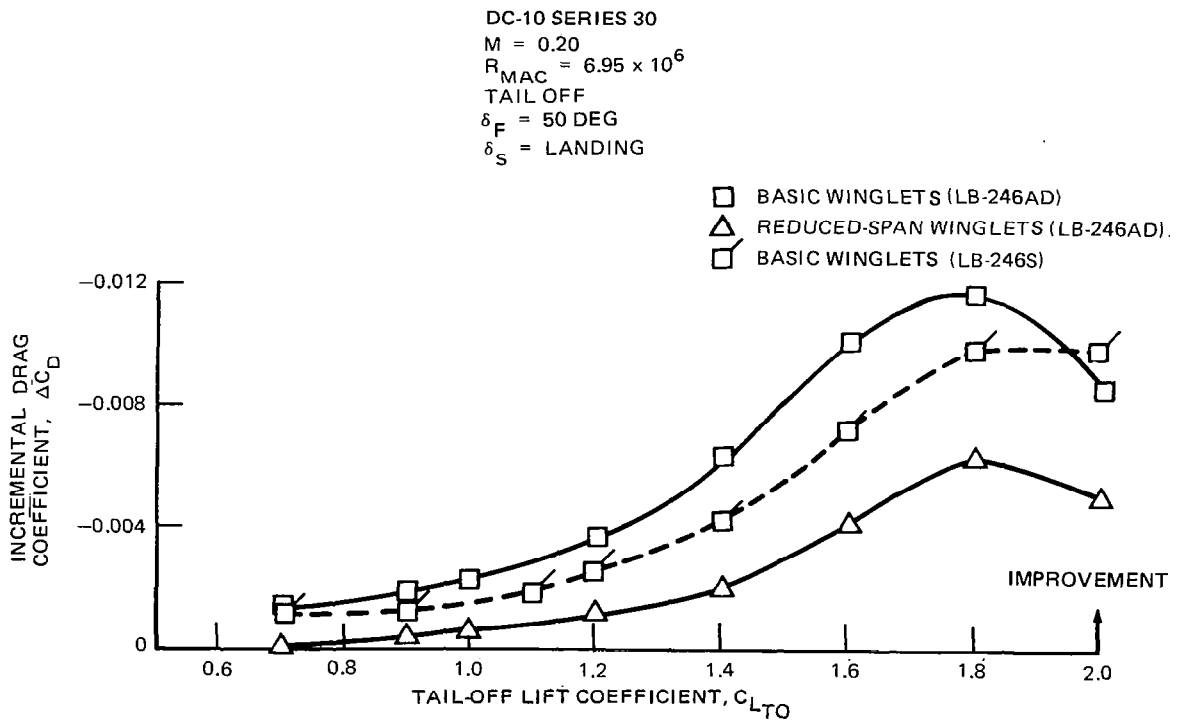
FIGURE 59. EFFECT OF BASIC AND REDUCED-SPAN WINGLETS ON DRAG FOR LANDING CONFIGURATION (δ_F = 50 DEG)
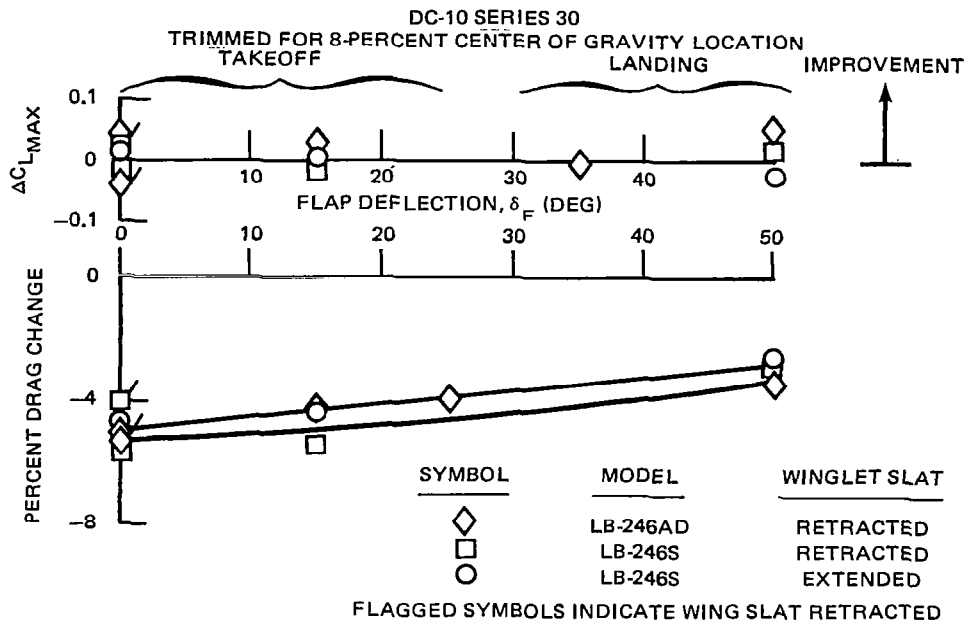
DC-10 SERIES 30
TRIMMED FOR 8-PERCENT CENTER OF GRAVITY LOCATION

FIGURE 60. EFFECT OF BASIC WINGLET AND WINGLET SLAT ON TRIMMED MAXIMUM
LIFT AND DRAG
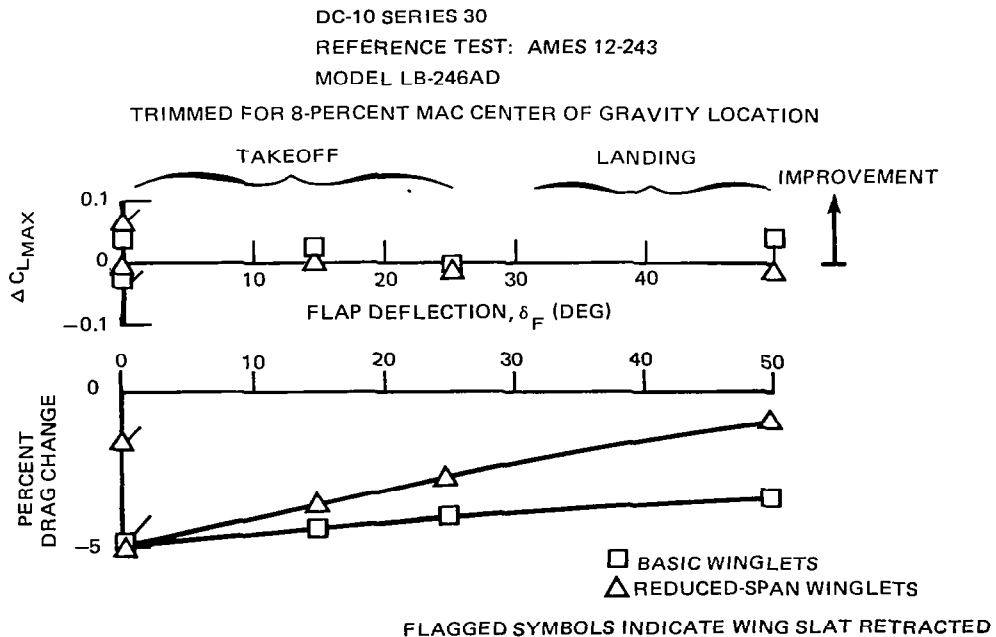
DC-10 SERIES 30
REFERENCE TEST: AMES 12-243
MODEL LB-246AD

TRIMMED FOR 8-PERCENT MAC CENTER OF GRAVITY LOCATION

FIGURE 61. EFFECT OF WINGLETS ON TRIMMED MAXIMUM LIFT AND DRAG

57

Pressure distributions — A significant portion of the second low-speed wind tunnel test was devoted to the measurement of wing and winglet pressure distributions. Figures 62 through 64 present examples of measured pressures for the takeoff case of 15 degrees of flap deflection. The most outboard wing chordwise row of pressure orifices are given in Figure 62 whereas the two winglet rows are given in Figures 63 and 64. The lift values selected for use in these figures represent (1) a low lift value ($C_L = 1.05$), (2) a value near the maximum winglet drag reduction value ($C_L = 1.55$), and (3) a value well beyond the maximum drag reduction point where the winglet effectiveness is eroding ($C_L = 1.83$).

DC-10 SERIES 30

REFERENCE TEST: AMES 12-423
MODEL LB-246AD
M = 0.20
$R_{MAC} = 6.95 \times 10^6$
TAIL OFF
$\delta_F = 15$ DEG
$\delta_S =$ TAKEOFF

SYM	ANGLE OF ATTACK, α_F (DEG)	$C_{L_{TO}}$
O	6.65	1.05
□	13.0	1.55
△	18.1	1.83

PRESSURE COEFFICIENT, C_P

CHORDWISE POSITION
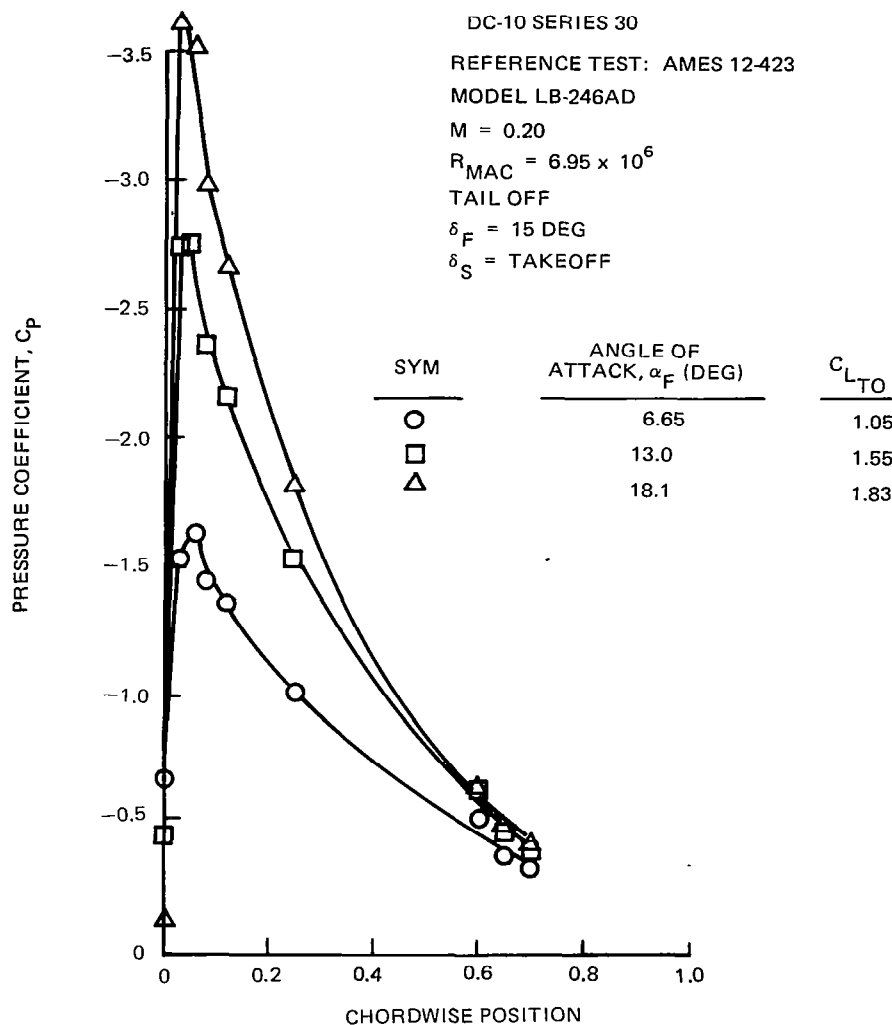
FIGURE 62. UPPER SURFACE WING PRESSURE DISTRIBUTION AT 87-PERCENT SEMI-SPAN LOCATION FOR TAKEOFF CONFIGURATION
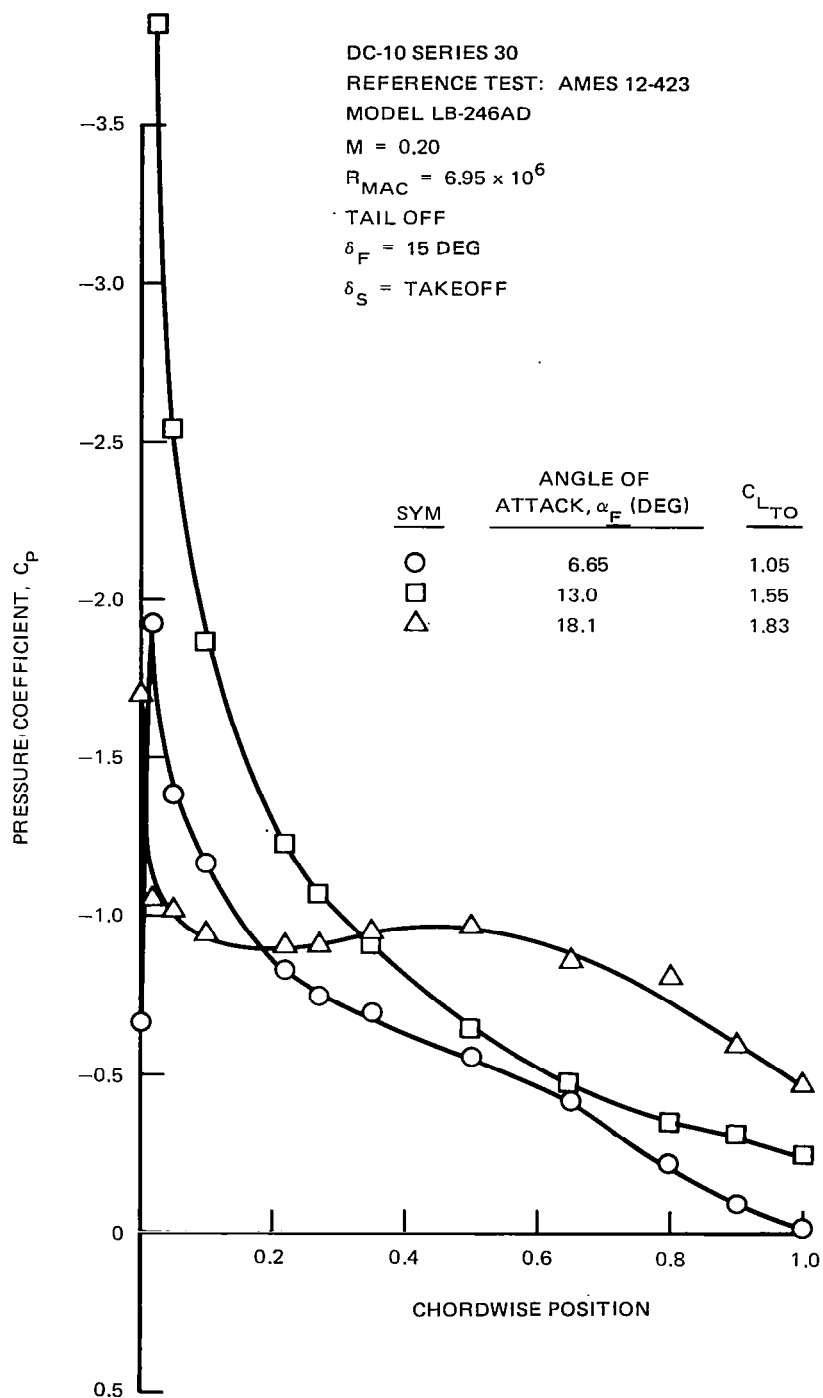
FIGURE 63. INBOARD SURFACE WINGLET PRESSURE DISTRIBUTION AT 12-PERCENT SPAN LOCATION FOR TAKEOFF CONFIGURATION
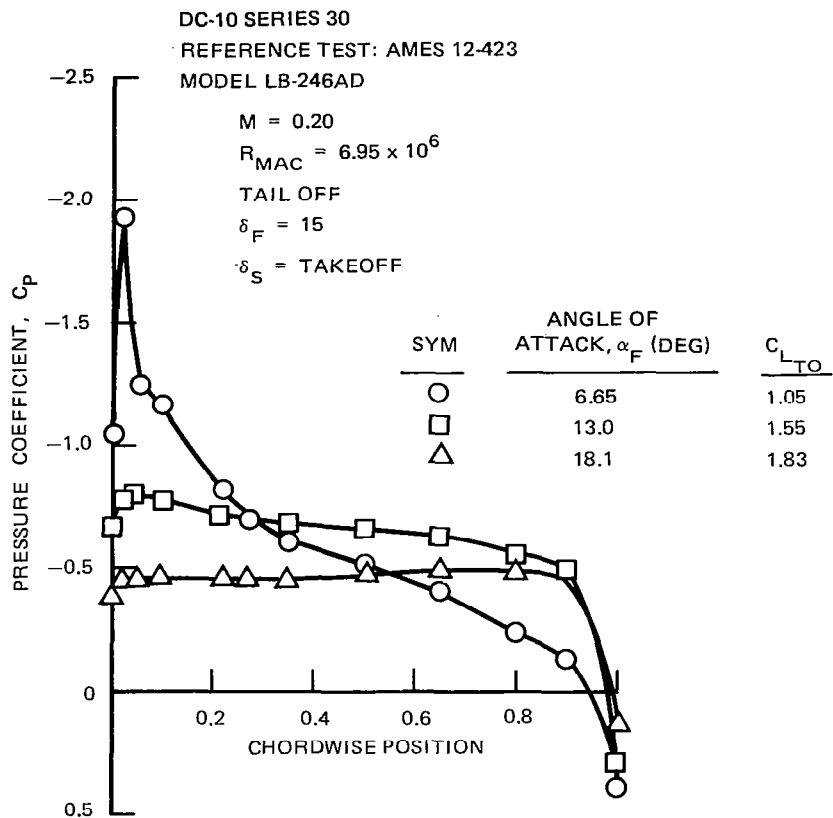
FIGURE 64. INBOARD SURFACE WINGLET PRESSURE DISTRIBUTION AT 80-PERCENT SPAN LOCATION FOR TAKEOFF CONFIGURATION

Figure 62 shows that the flow over the wing outboard station remains attached with good pressure recovery for the range of lift values presented. However, the outboard winglet station pressure distribution given in Figure 64 indicates a weakening of the flow recovery and loss of lift at the two higher lift values. Finally, the inboard winglet pressure distribution of Figure 63 indicates that this station carries a substantial load at the lower aircraft lift values but experiences a loss of lift with little pressure recovery at the highest lift value presented. From these observations, it is evident that the winglet flow separates before the wing stall and that the winglet flow separation originates at its tip and progresses to the root. These pressure results have been correlated with tuft observations and measured aircraft characteristics to examine the impact of winglet flow behavior on the DC-10. The winglet flow behavior encountered in flight may differ significantly from the test findings since the flow character is strongly dependent on Reynolds number. The relatively low winglet Reynolds number of this investigation may have resulted in premature winglet flow separation. Such separation could be delayed to higher lift values for flight Reynolds number conditions. However, the extent of winglet flow separation and its impact on low-speed buffet and performance can only be conclusively determined in flight.

Upper winglet ice simulation — The shape of the upper winglet leading edge attachment used to simulate icing is shown in Figure 65. Also shown are the measured incremental maximum lift coefficient and drag coefficient resulting from the ice. The ice impact on maximum lift coefficient was minimal for the two flap deflections studied. The two flap settings investigated are representative of landing approach and landing climb (go-around). The drag detriment of the upper winglet ice is shown to be small and of insignificant magnitude to seriously degrade the aircraft performance. Based on these lift and drag results, it would appear that the complication of providing ice protection to the upper winglet leading edge would be unnecessary for a production application.

The effect of winglet leading edge ice on pitch stability is presented in Figure 66. Winglet icing causes an insignificant decrease in longitudinal stability. This effect diminishes with increasing angle of attack.

Stability and control characteristics — A major portion of the low-speed wind tunnel test program was devoted to the investigation of winglet effects on stability and control characteristics. Low-speed stability and control characteristics were evaluated for the five flap/slat deflection combinations defined in Table 1 for the winglets-installed and baseline aircraft. Specifically, pure pitch sweeps were made through stall plus 5 degrees to investigate longitudinal effects.

DC-10 SERIES 30
REFERENCE TEST: AMES 12-423
MODEL LB-246AD
M = 0.20
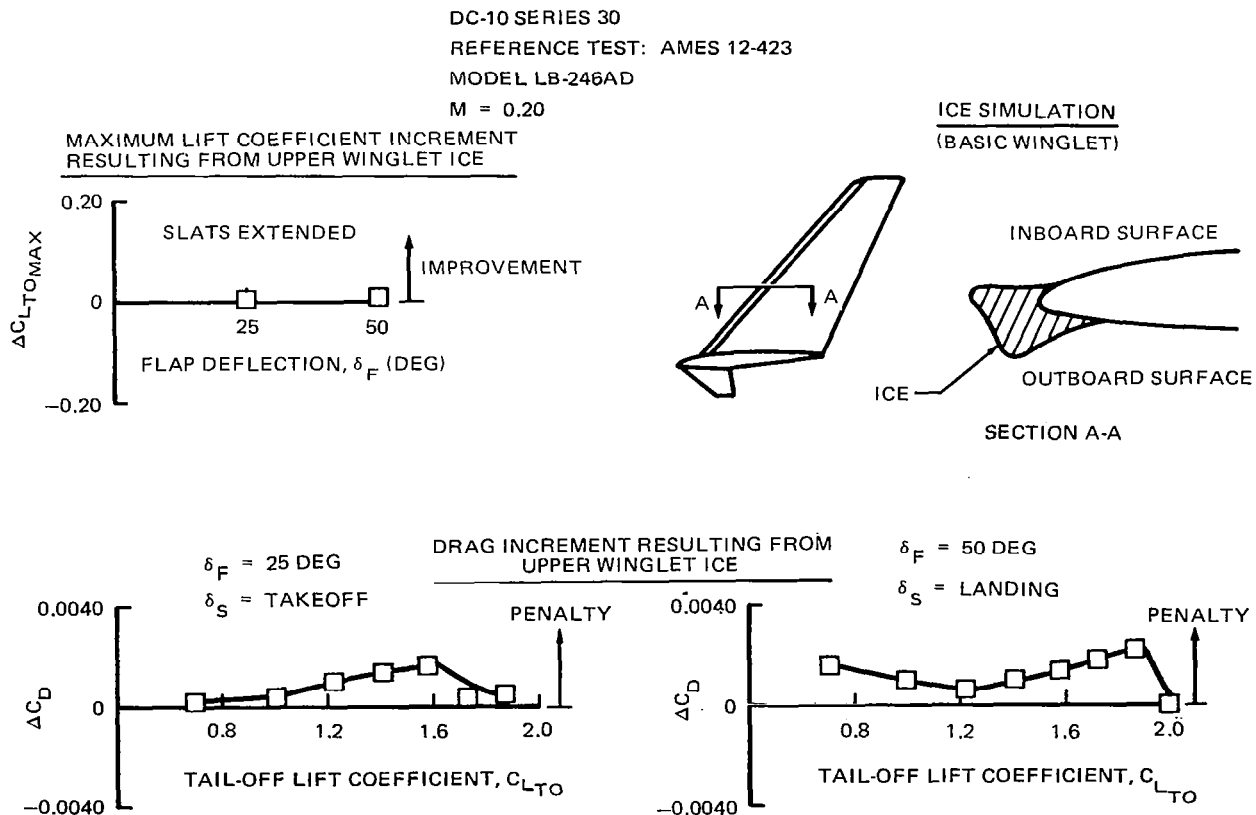
FIGURE 65. EFFECT OF UPPER WINGLET ICE ACCUMULATION ON PERFORMANCE
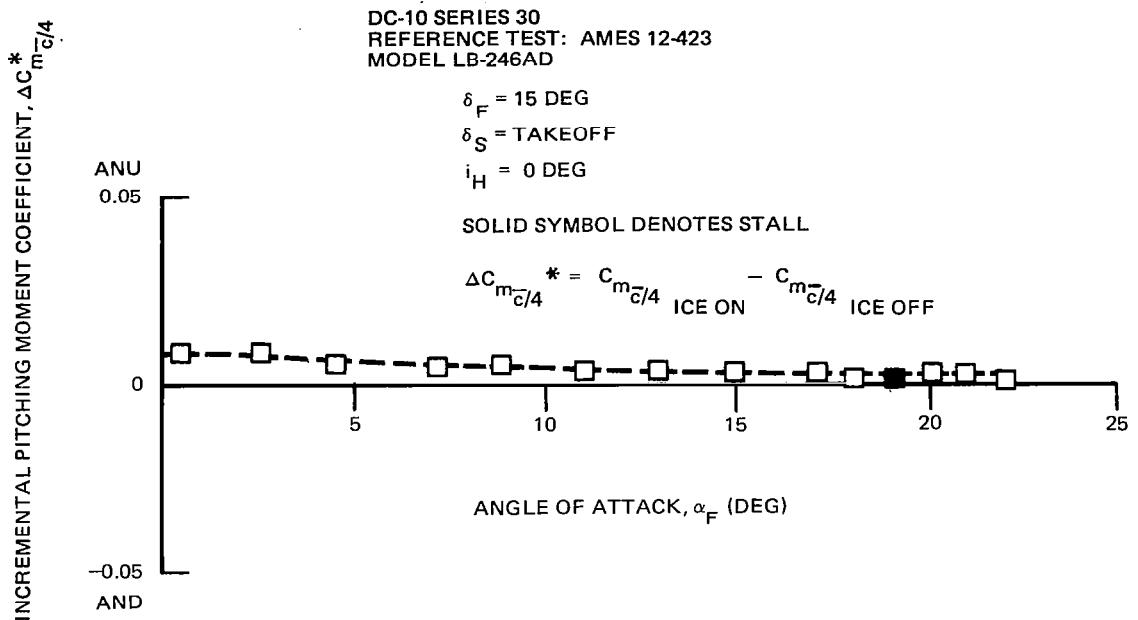
FIGURE 66. INCREMENTAL PITCHING MOMENT DUE TO SIMULATED ICE ON UPPER WINGLET

Additional pitch and yaw sweeps were made to determine the variation in directional stability with angle of attack and sideslip. Pitch sweeps were made with the model yawed 4 and 6 degrees, and yaw sweeps were made with the model at approximately 0, 8, and 13 degrees angle of attack. Outboard aileron effectiveness was studied to determine the effect of winglets on lateral control. Test runs were made in some instances on both the basic and reduced-span winglet configuration. The impact of winglets on the DC-10 Series 30 was small and caused insignificant changes in the basic stability and control characteristics. Representative results and comparisons are presented.

The configurations examined for stability and control had flap/slat settings of 15/takeoff and 25/takeoff. Figure 67 presents a comparison of the incremental pitching moments due to winglets from the two low-speed tests. The agreement is excellent until stall, after which the correlation becomes somewhat erratic as might be expected.

Figure 68 shows the pitching moment coefficient increments due to both the basic and reduced-span winglets for a 25-degree flap deflection with the leading edge slats extended in the takeoff position. In general, the basic winglets produced a negative pitching moment coefficient increment at angles of attack below about 20 degrees, and a positive increment above 20 degrees. The reduced-span winglets produced a smaller negative increment than the basic winglet and the increment became positive above about 15 degrees. The reduced-span winglet configuration appears to delay the stall by approximately 1 degree (Figure 69), which caused a spike in the pitching moment increment between the baseline and reduced-span winglet configurations, as shown in Figure 68. This delay in stall was not observed in the basic winglet configuration (Figure 70). The pitching moment curves (Figures 69 and 70) are very similar, and the winglet
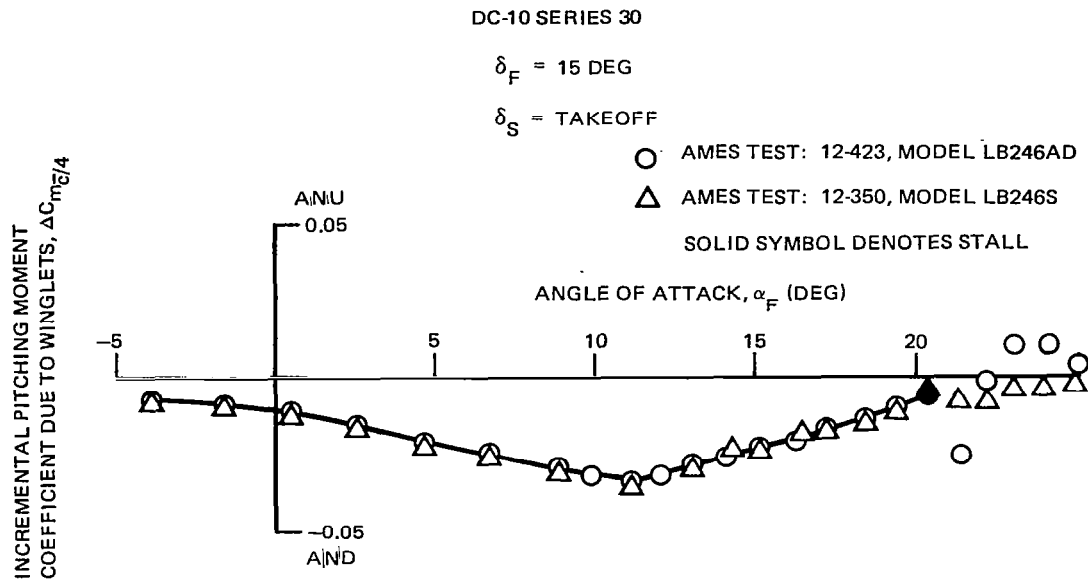
FIGURE 67. DATA REPEATABILITY BETWEEN TESTS — EFFECT OF BASIC WINGLETS ON TAIL-OFF INCREMENTAL PITCHING MOMENT
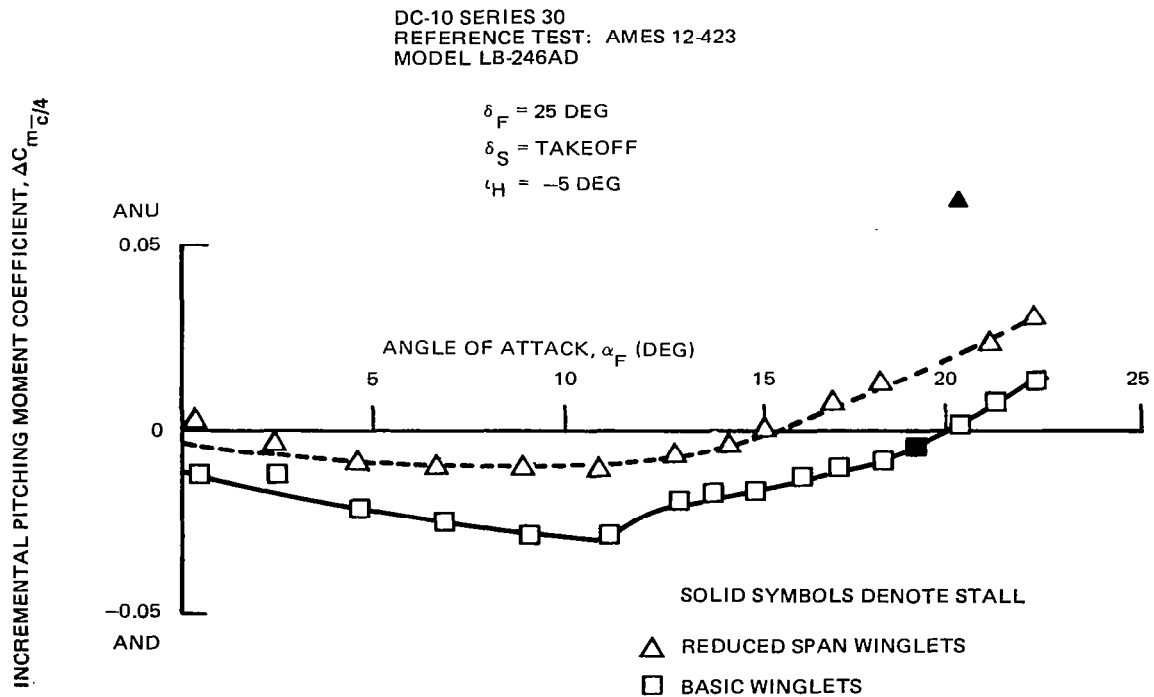
FIGURE 68. EFFECT OF WINGLET SPAN ON INCREMENTAL PITCHING MOMENT
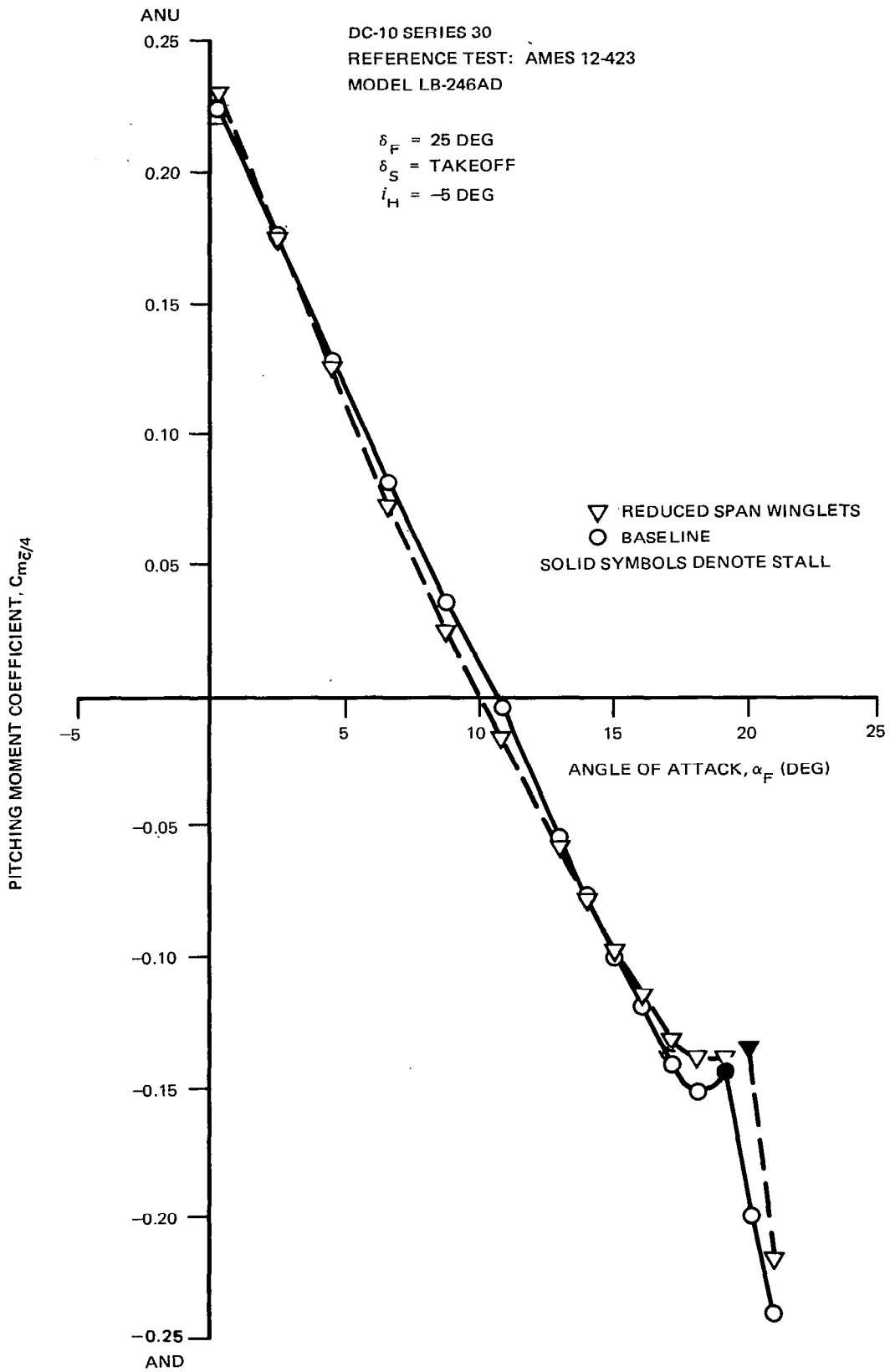
FIGURE 69. EFFECT OF REDUCED-SPAN WINGLETS ON PITCHING MOMENT
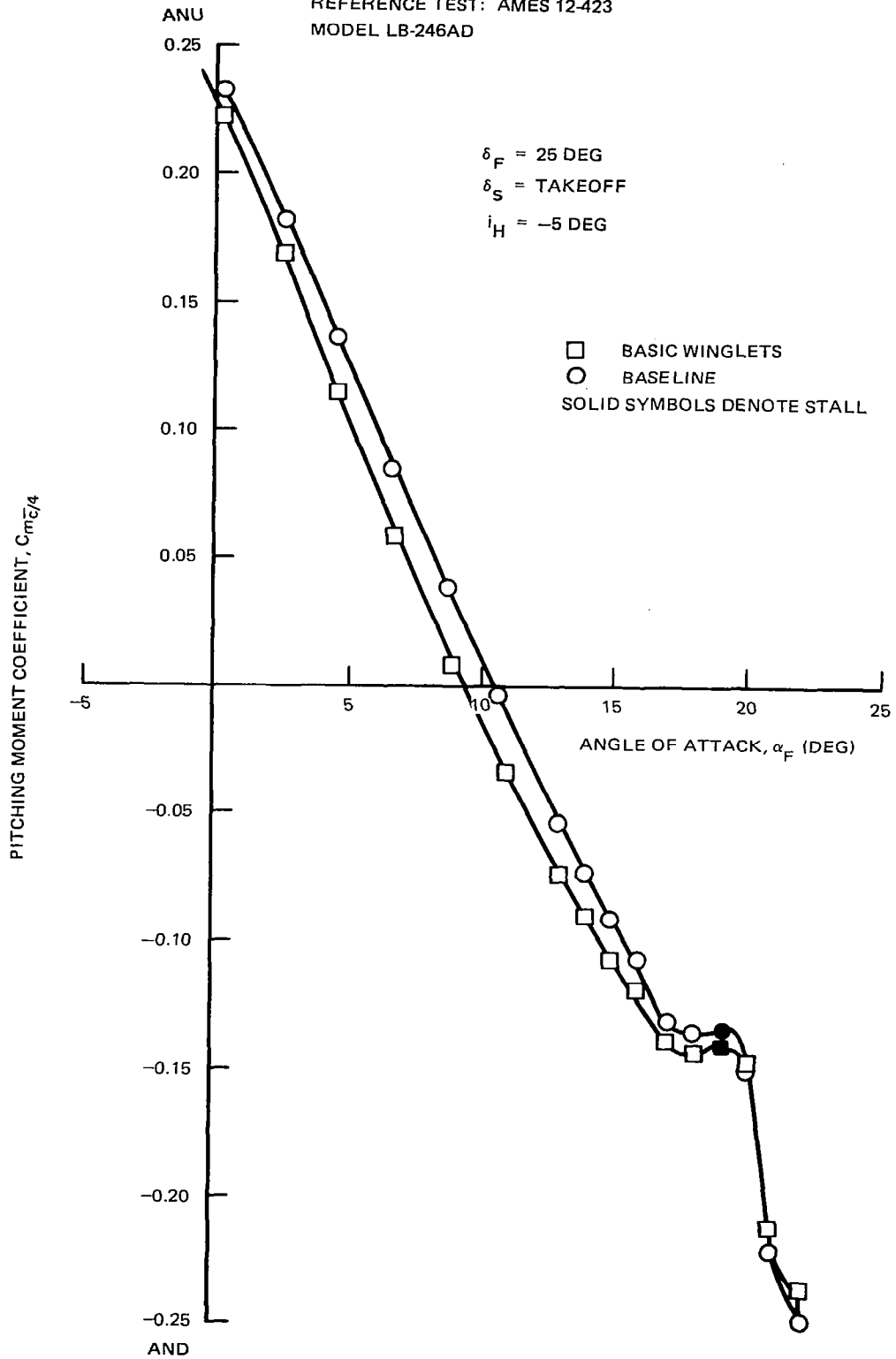
FIGURE 70. EFFECT OF BASIC WINGLETS ON PITCHING MOMENT

does not significantly alter the characteristics at stall. In general, the results presented for the 25/takeoff configuration are similar to those for the other flap/slat configurations tested.

Figure 71 shows incremental pitching moment coefficients due to the winglets for three flap/slat deflections. Basically, the winglets had a stabilizing effect (airplane nose-down moment) before stall for all flap/slat settings, decreasing to nearly zero effect at and above stall angle of attack. The trends of the incremental data after the stall were caused by the slightly different shapes of the plotted data and do not necessarily indicate a change in pitching moment characteristics. For example, the positive pitching moment increment for the 15/takeoff setting can be attributed to the winglet delaying stall by 1 degree beyond the baseline (Figure 72).

The effect of winglets on lateral and directional stability is presented in Figures 73 through 97. A small winglet effect is shown in these figures when comparing the winglet to the baseline configuration. Figures 73 through 81 present the side force, yawing moment, and rolling moment coefficients for yaw sweeps at angles of attack of 0 and 12.9 degrees. The winglets provided a small increase in side force, yawing moment, and rolling moment. The incremental effect due to winglets for these coefficients for both angles of attack is presented in Figures 79 through 81. For all three coefficients, the winglet incremental effect diminished with increasing angle of attack and was not particularly sensitive to sideslip angles beyond 15 degrees.
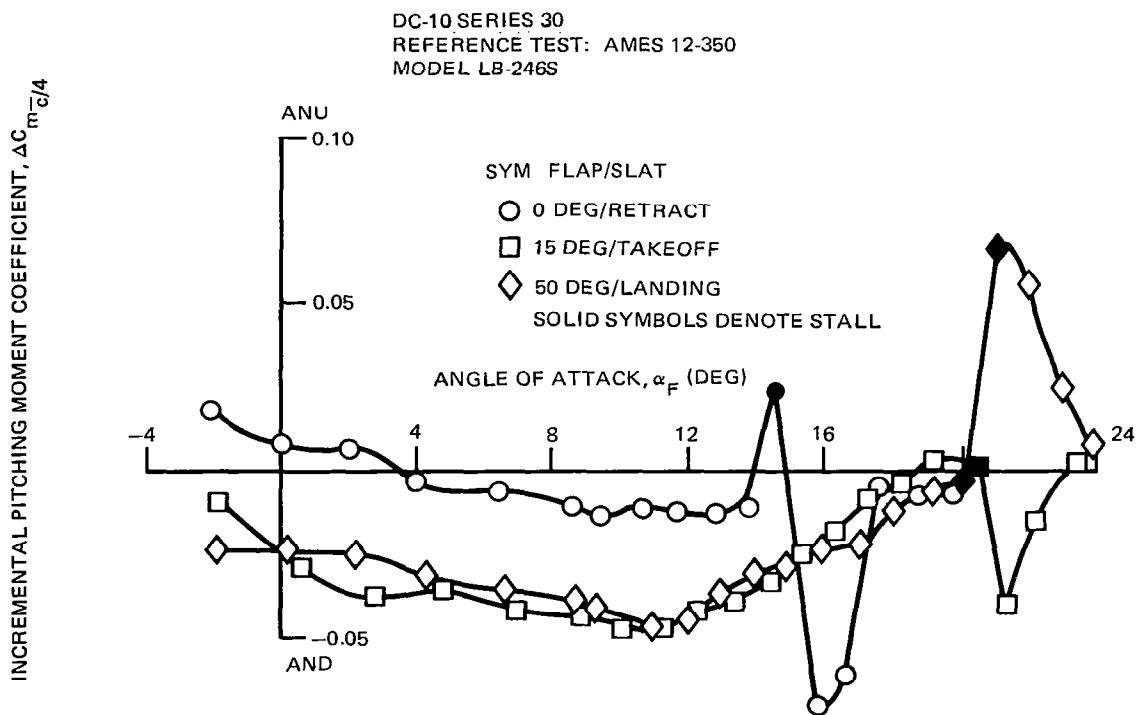
FIGURE 71. EFFECT OF FLAP/SLAT DEFLECTION ON INCREMENTAL PITCHING MOMENT DUE TO BASIC WINGLETS
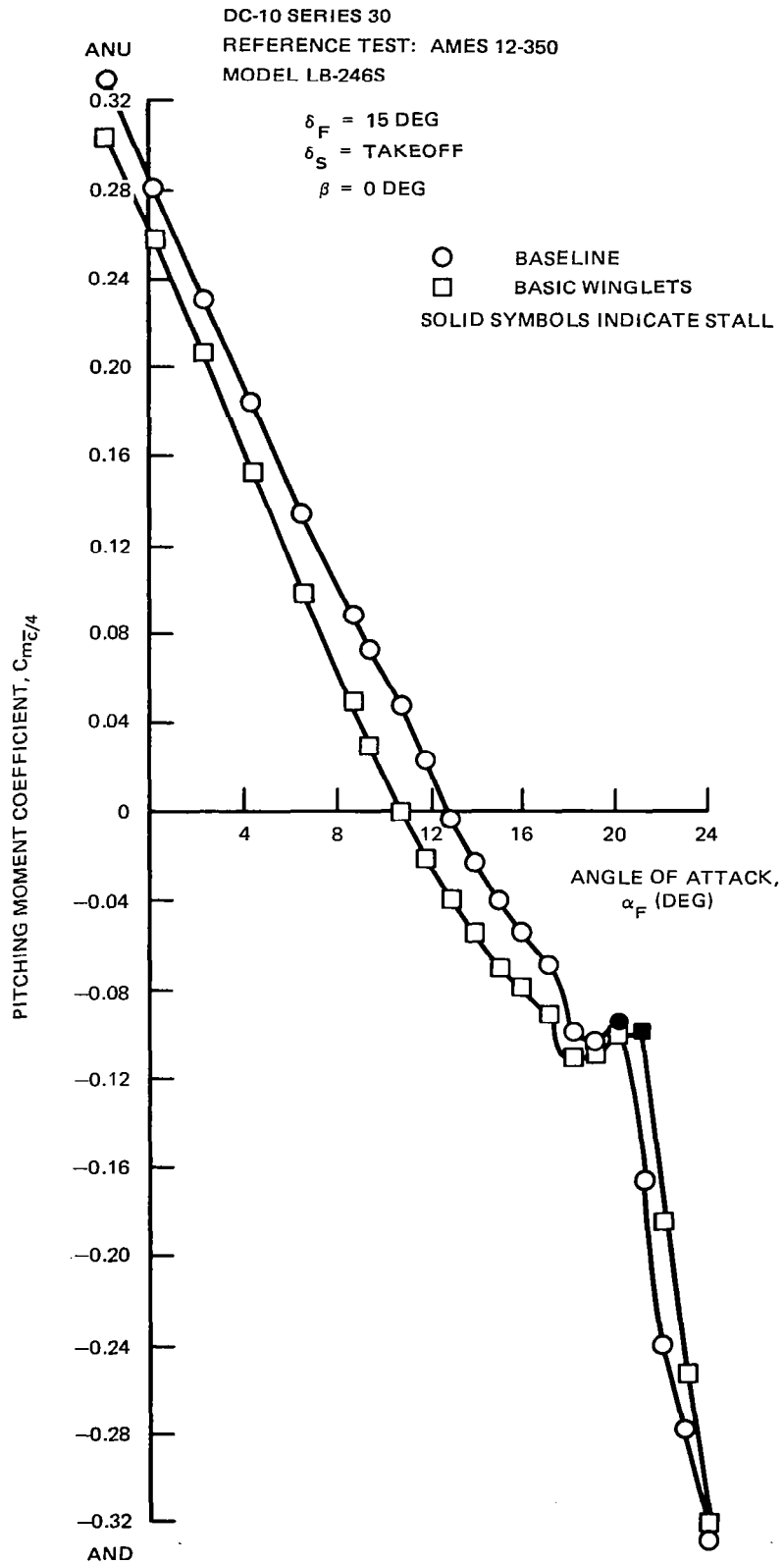
FIGURE 72. EFFECT OF BASIC WINGLETS ON PITCHING MOMENT FOR TAKEOFF CONFIGURATION

δ_F = 15 DEG

δ_s = TAKEOFF

i_H = −5 DEG

α_F = 0 DEG

SIDESLIP ANGLE, β (DEG)

SIDE FORCE COEFFICIENT, C_Y

□ BASIC WINGLETS

○ BASELINE
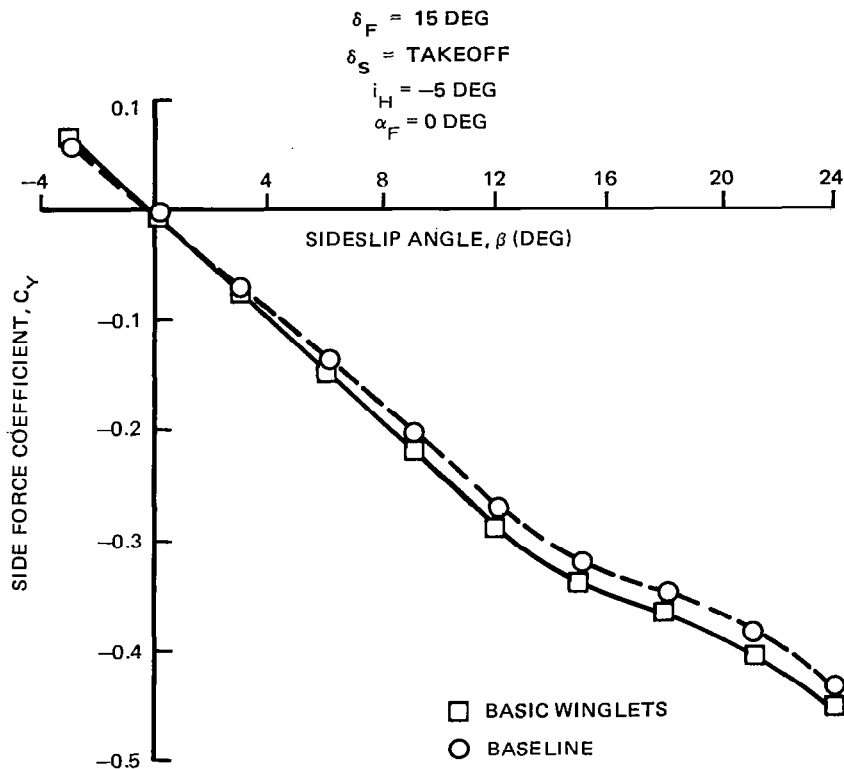
FIGURE 73. EFFECT OF BASIC WINGLETS ON SIDE FORCE (α_F = 0 DEG)

Figures 82 through 84 show the effects of winglet span on side force, yawing moment, and rolling moment, respectively, at a flap/slat deflection of 25/takeoff and an angle of attack of 7.7 degrees. In general, the data indicate small increases in the three coefficients with increased winglet span. Figures 85 through 87 show the winglet effect for three flap/slat deflections for the basic winglet. The variation of winglet incremental effects with flap/slat setting was small; about the only noticeable effect is on the yawing moments in Figure 86, where the 0/takeoff setting yielded slightly higher yaw increments than the other two settings.

Figures 88 and 89 show the winglet and baseline airplane lateral-directional coefficients for a pitch sweep at a 6-degree sideslip angle. The incremental effects of winglets were taken from these curves and are presented in Figures 90 and 91. In each case, the incremental effect of winglets and their variations was small with angle of attack. Figures 92 through 94 show the winglet effect on yawing moment for a pitch sweep at a 4-degree sideslip angle for three flap/slat settings; i.e., 0/takeoff, 25/takeoff, and 50/landing. In each case, the winglet effect was negligible. Figures 95 through 97 show the winglet effect on rolling moment for the same three flap settings at a 4-degree sideslip angle. The effect of winglets was to slightly increase the rolling

DC-10 SERIES 30
REFERENCE TEST: AMES 12-350
MODEL LB-246S

STABLE

δ_F = 15 DEG

δ_S = TAKEOFF

i_H = –5 DEG

α_F = 12.9 DEG

☐ BASIC WINGLETS
○ BASELINE

YAWING MOMENT COEFFICIENT, C_n

SIDESLIP ANGLE, β (DEG)

UNSTABLE
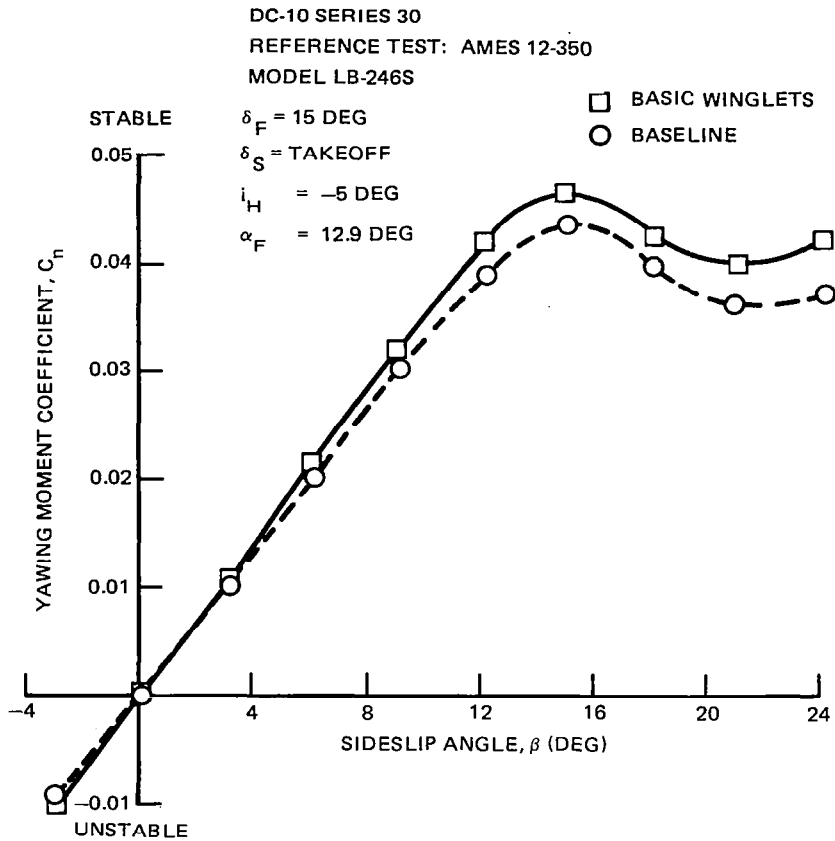
FIGURE 74. EFFECT OF BASIC WINGLETS ON YAWING MOMENT (α_F = 0 DEG)

UNSTABLE

DC-10 SERIES 30

REFERENCE TEST: AMES 12-350

MODEL LB-246S

δ_F = 15 DEG i_H = –5 DEG

δ_S = TAKEOFF

α_F = 0 DEG

SIDESLIP ANGLE, β (DEG)

ROLLING MOMENT COEFFICIENT, C_ℓ

○ BASELINE
☐ BASIC WINGLETS

STABLE
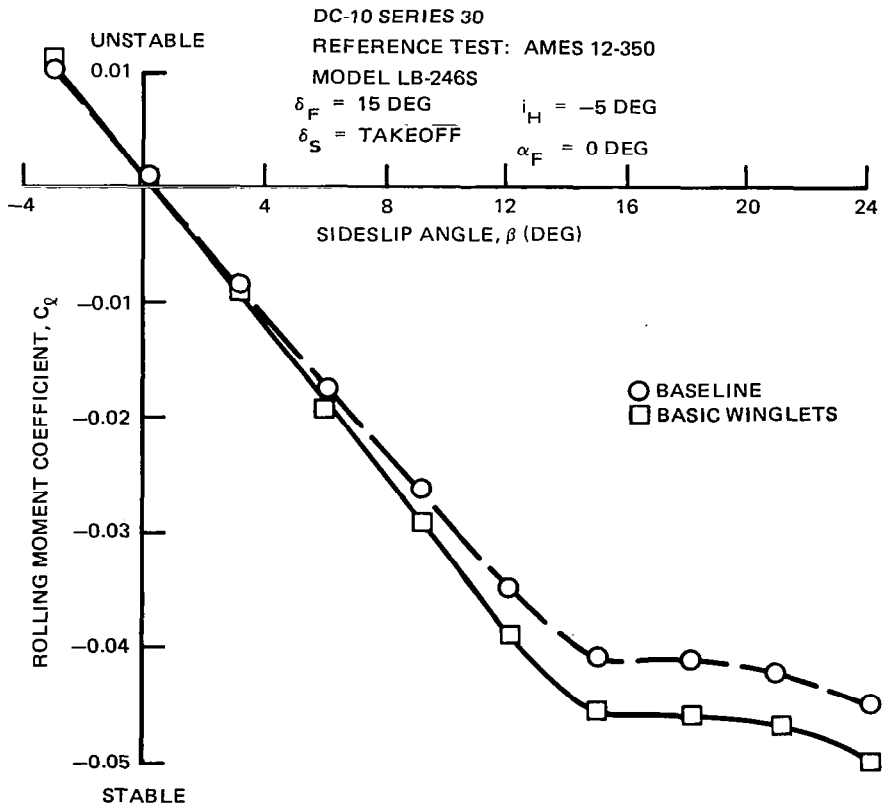
FIGURE 75. EFFECT OF BASIC WINGLETS ON ROLLING MOMENT (α_F = 0 DEG)

69
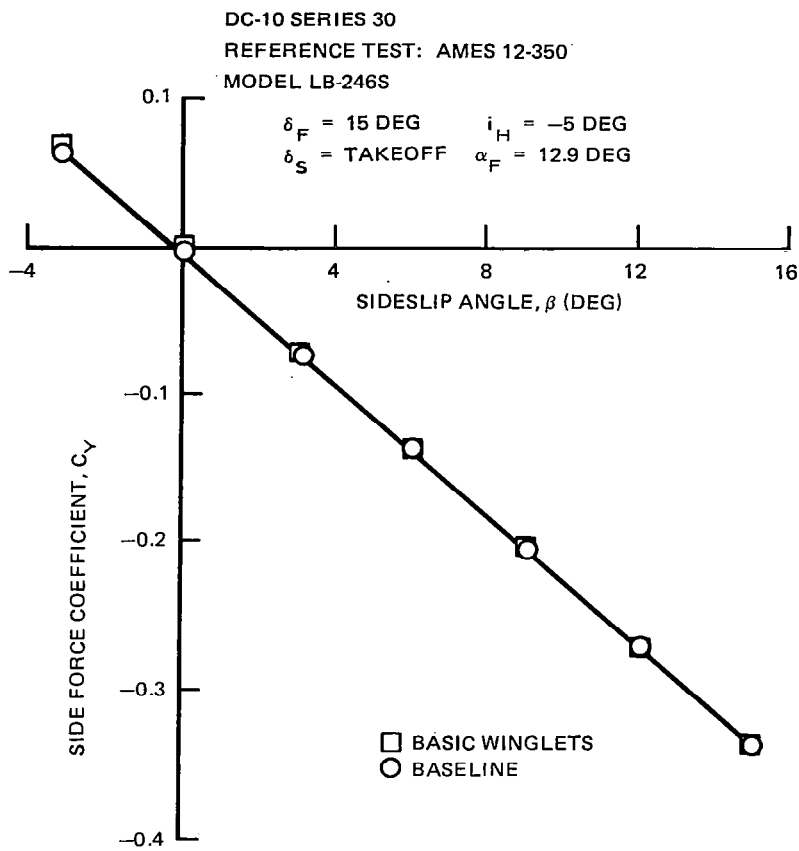
FIGURE 76. EFFECT OF BASIC WINGLETS ON SIDE FORCE (α_F = 12.9 DEG)
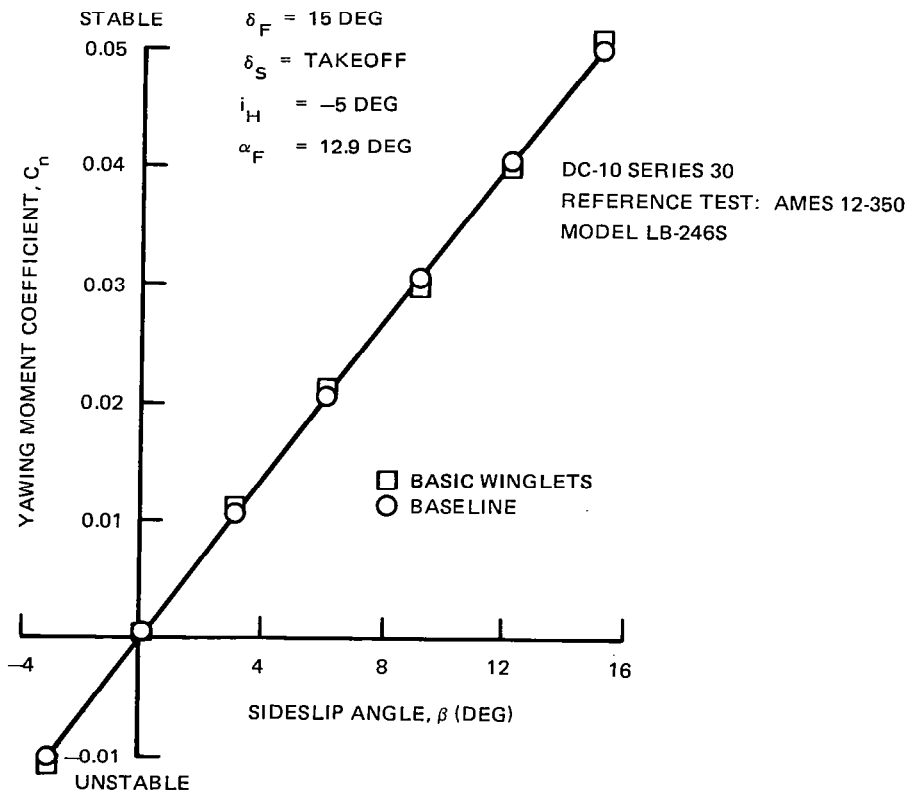
FIGURE 77. EFFECT OF BASIC WINGLETS ON YAWING MOMENT (α_F = 12.9 DEG)

DC-10 SERIES 30
REFERENCE TEST: AMES 12-350
MODEL LB-246S

δ_F = 15 DEG
δ_S = TAKEOFF
i_H = −5 DEG
α_F = 12.9 DEG

□ BASIC WINGLETS
○ BASELINE
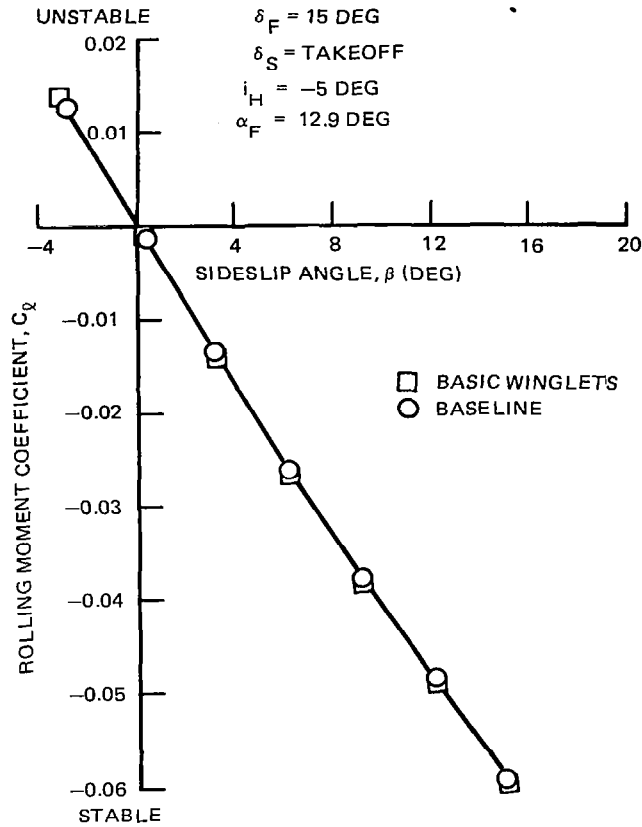
FIGURE 78. EFFECT OF BASIC WINGLETS ON ROLLING MOMENT (α_F = 12.9 DEG)

DC-10 SERIES 30
REFERENCE TEST: AMES 12-350
MODEL LB-246S

δ_F = 15 DEG
δ_S = TAKEOFF
i_H = 5 DEG

○ α_F = 13 DEG
□ α_F = 0 DEG
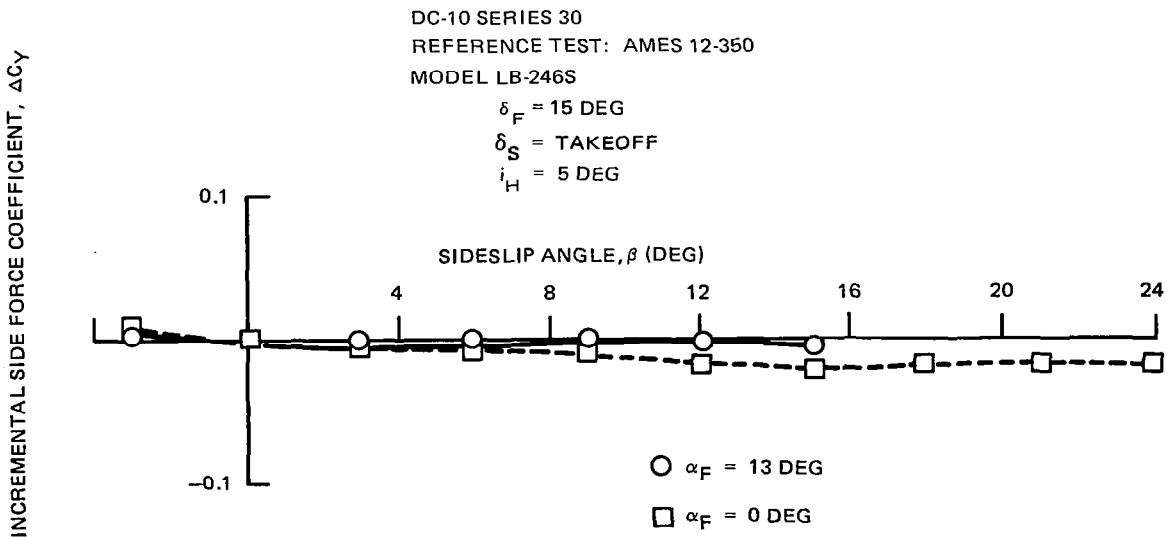
FIGURE 79. EFFECT OF SIDESLIP ON INCREMENTAL SIDE FORCE DUE TO BASIC WINGLETS
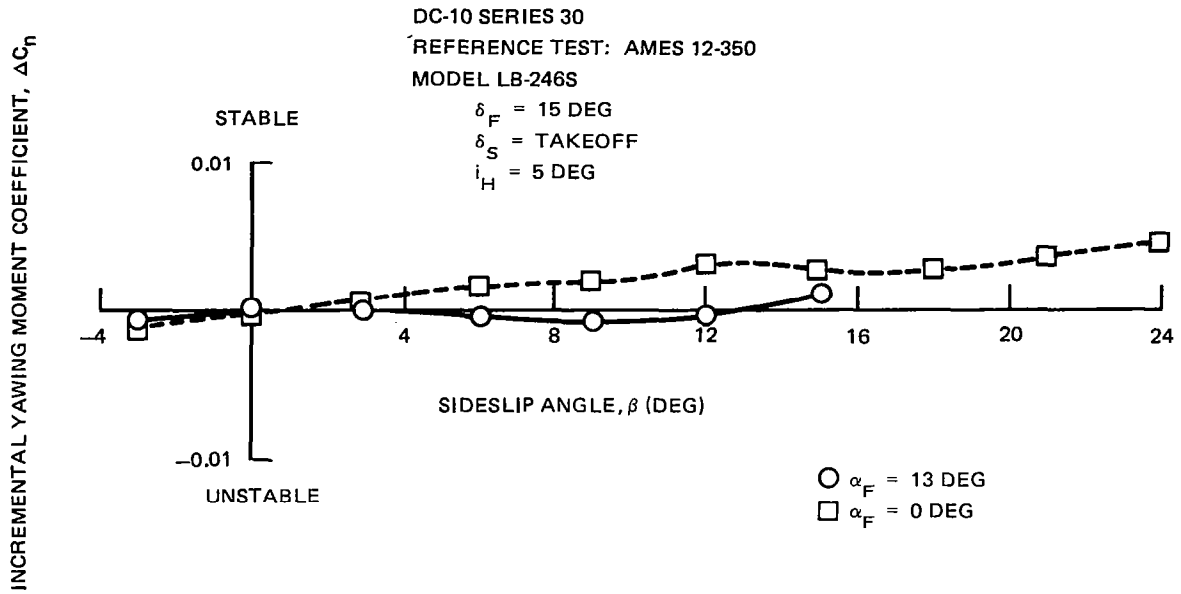
FIGURE 80. EFFECT OF SIDESLIP ON INCREMENTAL YAWING MOMENT DUE TO BASIC WINGLETS
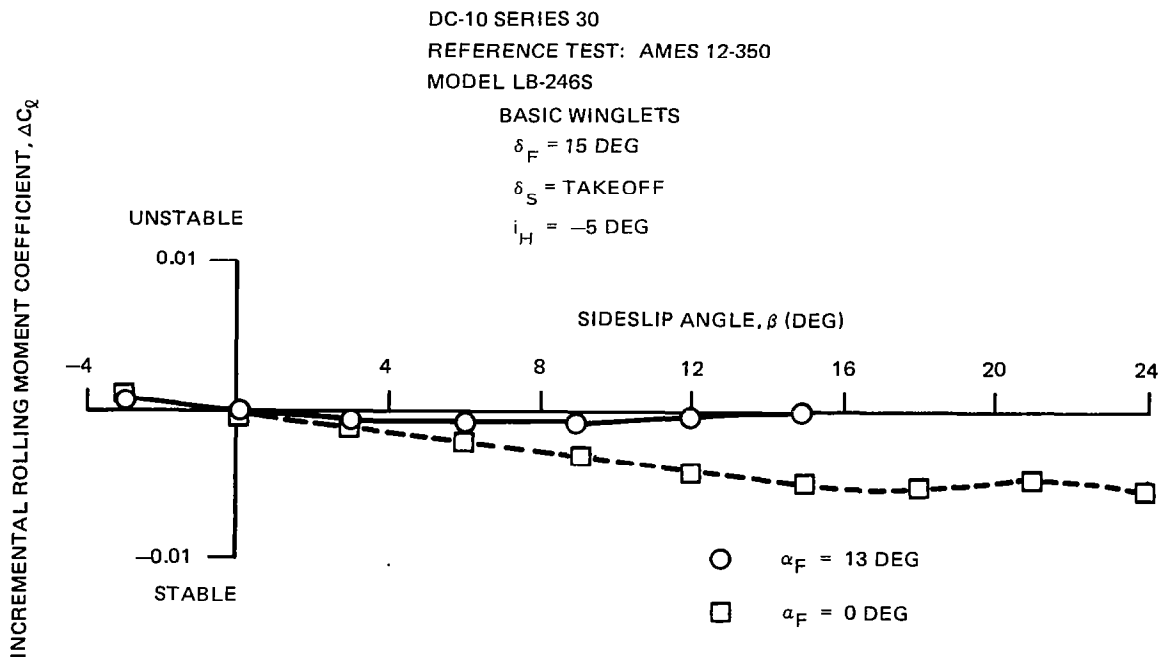
FIGURE 81. EFFECT OF SIDESLIP ON INCREMENTAL ROLLING MOMENT DUE TO BASIC WINGLETS
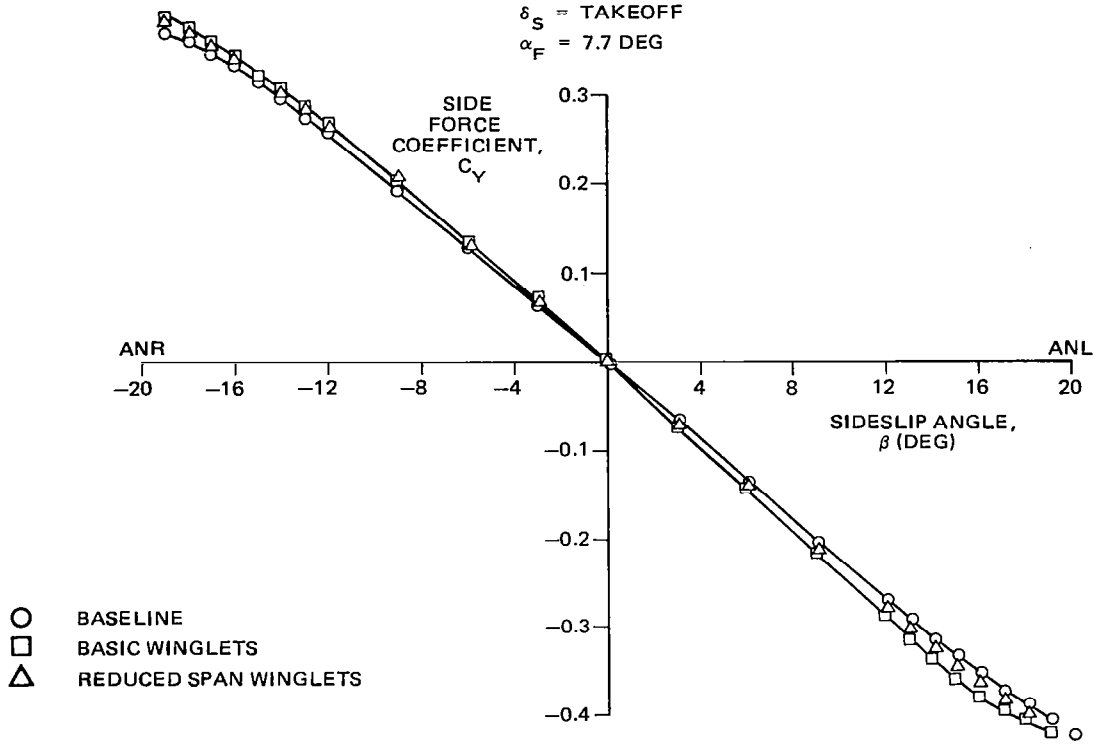
FIGURE 82. EFFECT OF WINGLET SPAN ON SIDE FORCE (α_F = 7.7 DEG)
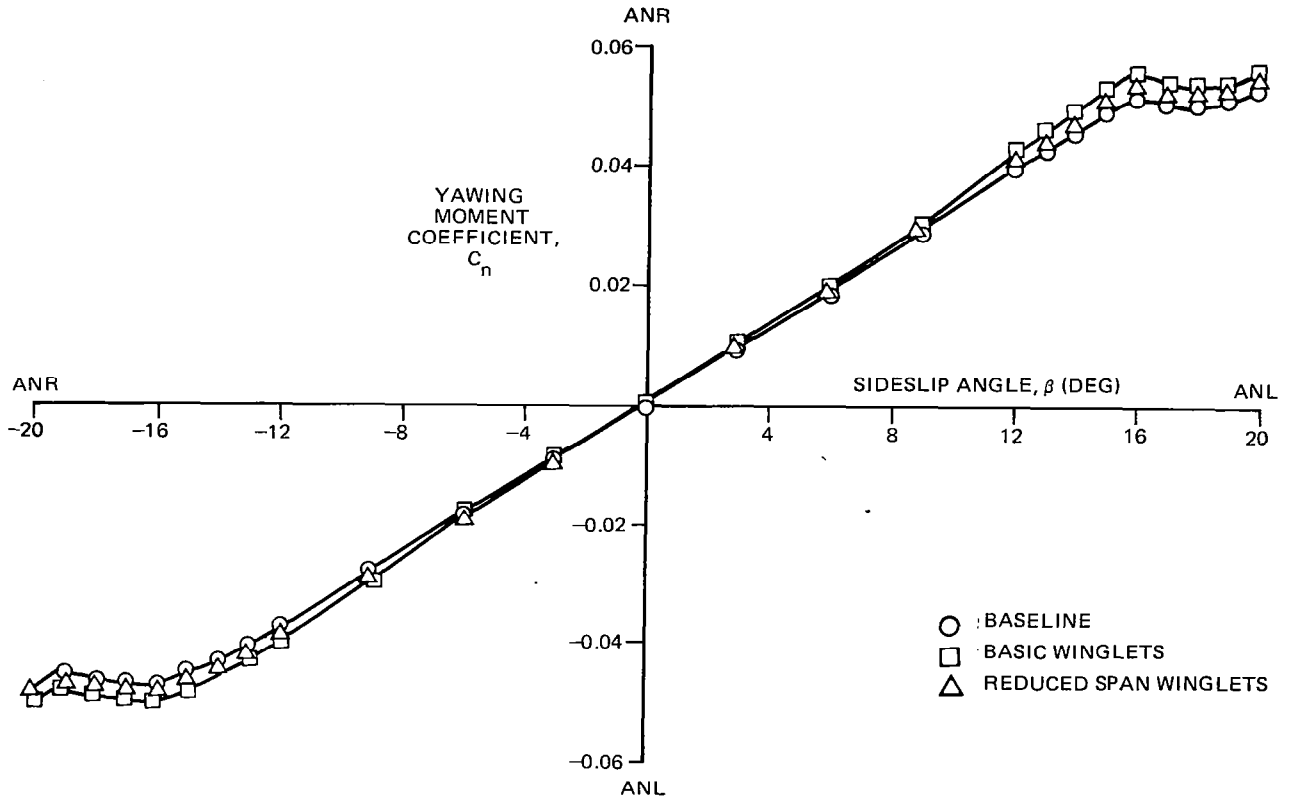
FIGURE 83. EFFECT OF WINGLET SPAN ON YAWING MOMENT (α_F = 7.7 DEG)

DC-10 SERIES 30
REFERENCE TEST: AMES 12-423
MODEL LB-246AD

δ_F = 25 DEG

δ_S = TAKEOFF

$\alpha_F \approx 7.7$ DEG

RWD

SIDESLIP ANGLE, β (DEG)

ANR

ANL

ROLLING MOMENT COEFFICIENT, C_ℓ

LWD

☐ BASELINE
○ BASIC WINGLETS
△ REDUCED SPAN WINGLETS
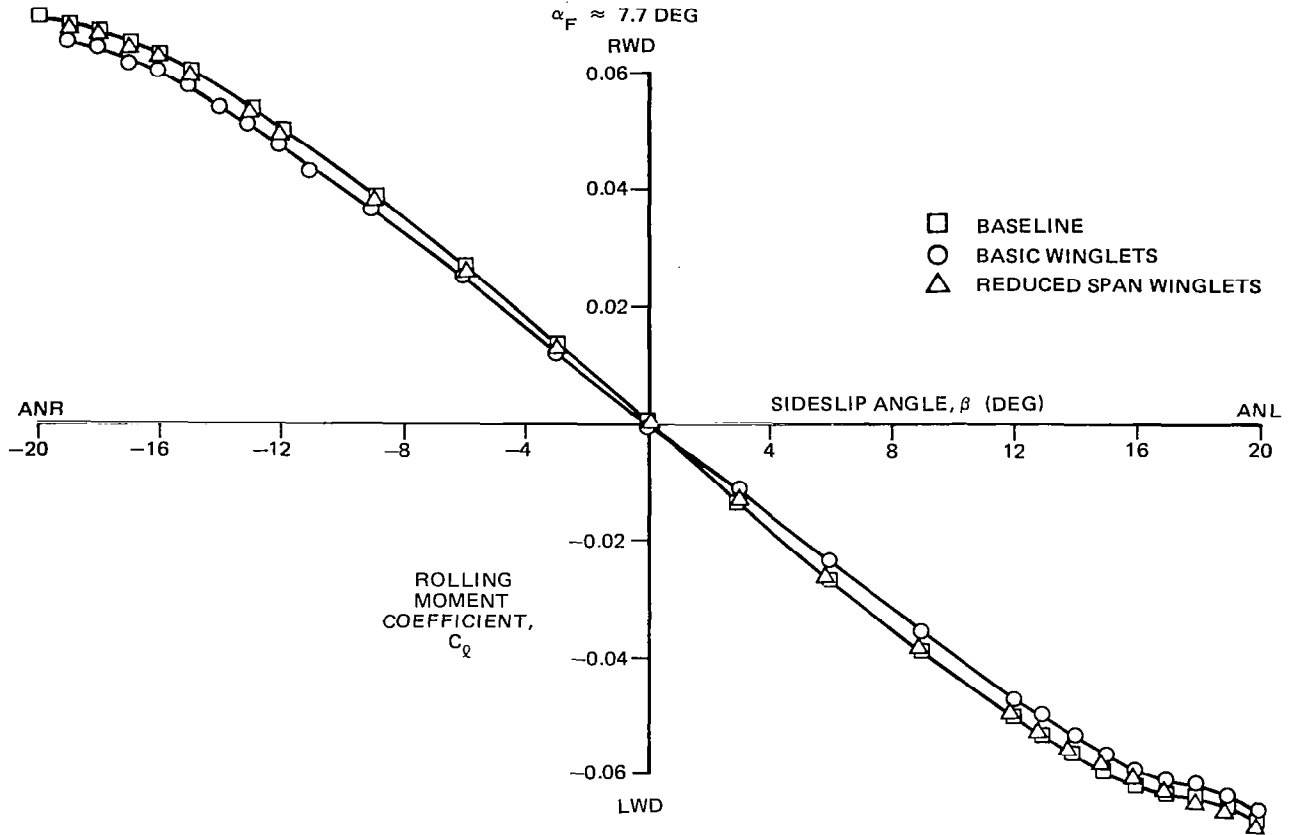
FIGURE 84. EFFECT OF WINGLET SPAN ON ROLLING MOMENT (α_F = 7.7 DEG)

α_F = 7.7 DEG

INCREMENTAL
SIDE FORCE
COEFFICIENT,
ΔC_Y

SIDESLIP ANGLE, β (DEG)

ANL

ANR

SYM	FLAP/SLAT
O	0 DEG/TAKEOFF
X	25 DEG/TAKEOFF
△	50 DEG/LANDING
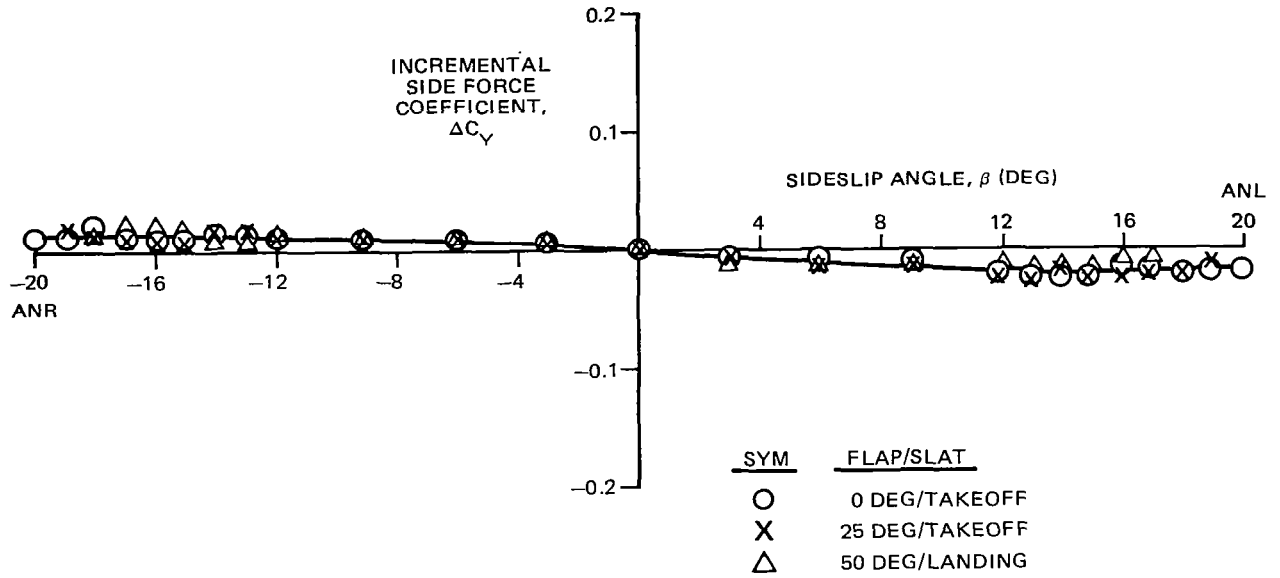
FIGURE 85. EFFECT OF FLAP/SLAT DEFLECTIONS ON INCREMENTAL SIDE FORCE DUE TO BASIC
WINGLETS (α_F = 7.7 DEG)

DC-10 SERIES 30
REFERENCE TEST: AMES 12-423
MODEL LB-246AD

$\alpha_F = 7.7$ DEG

FIGURE 86. EFFECT OF FLAP/SLAT DEFLECTIONS ON INCREMENTAL YAWING MOMENT DUE TO BASIC WINGLETS ($\alpha_F = 7.7$ DEG)

DC-10 SERIES 30
REFERENCE TEST: AMES 12-423
MODEL LB-246AD
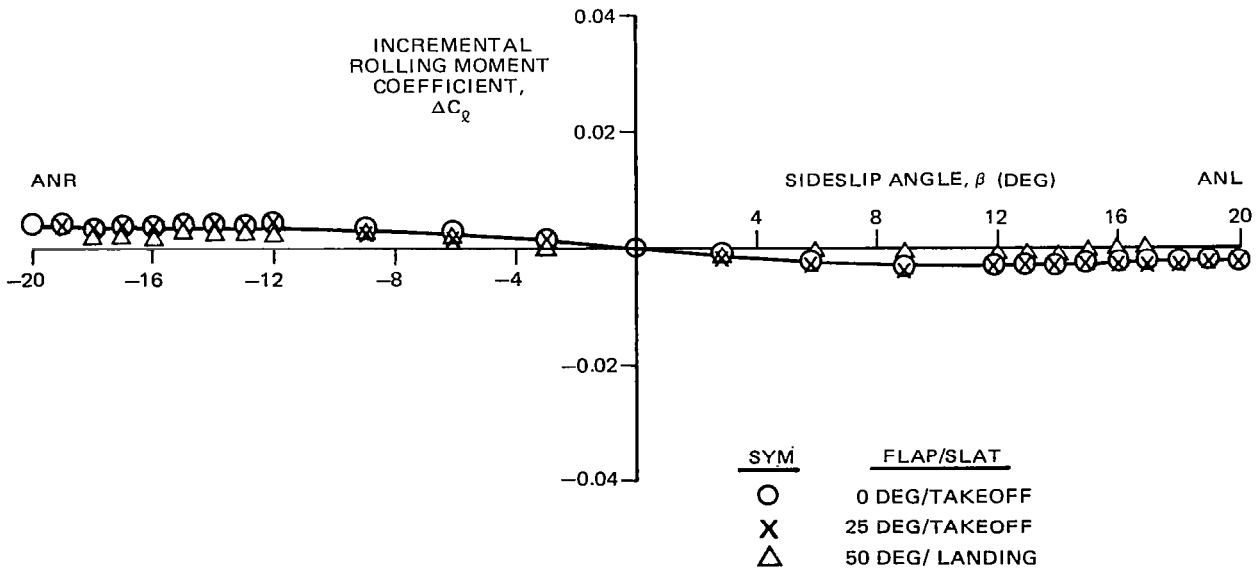
$\alpha_F = 7.7$ DEG

FIGURE 87. EFFECT OF FLAP/SLAT DEFLECTION ON INCREMENTAL ROLLING MOMENT DUE TO BASIC WINGLETS ($\alpha_F = 7.7$ DEG)
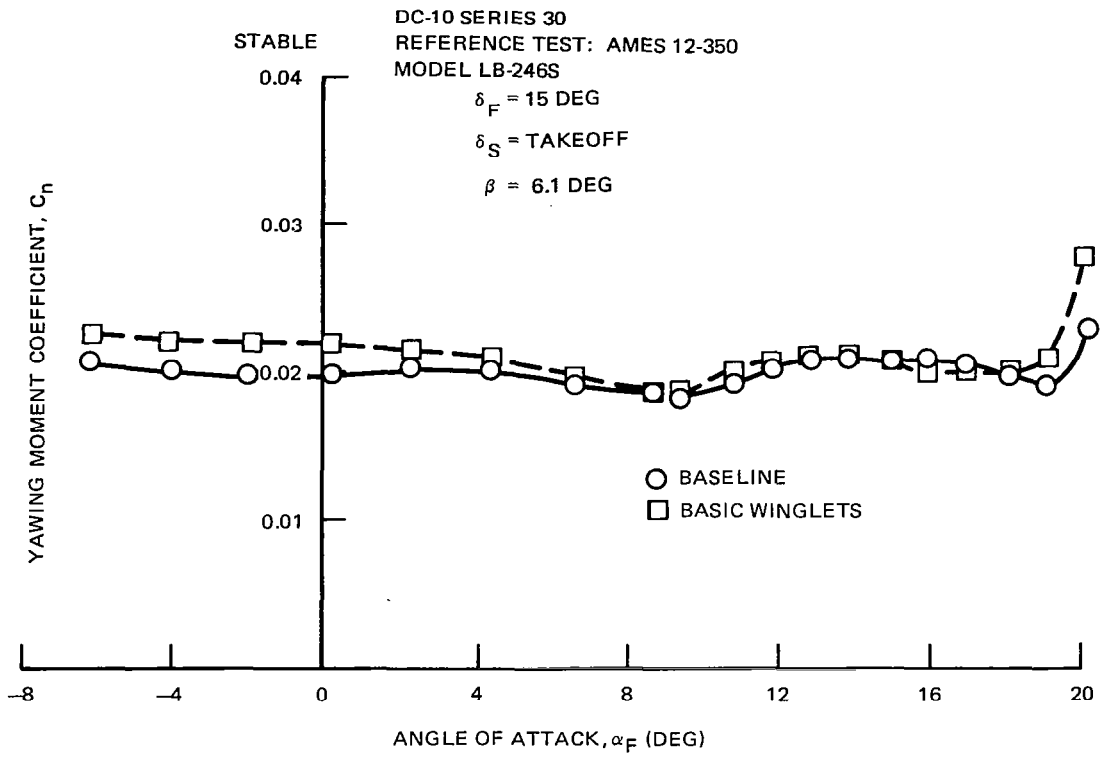
FIGURE 88. EFFECT OF BASIC WINGLETS ON YAWING MOMENT (β = 6.1 DEG)
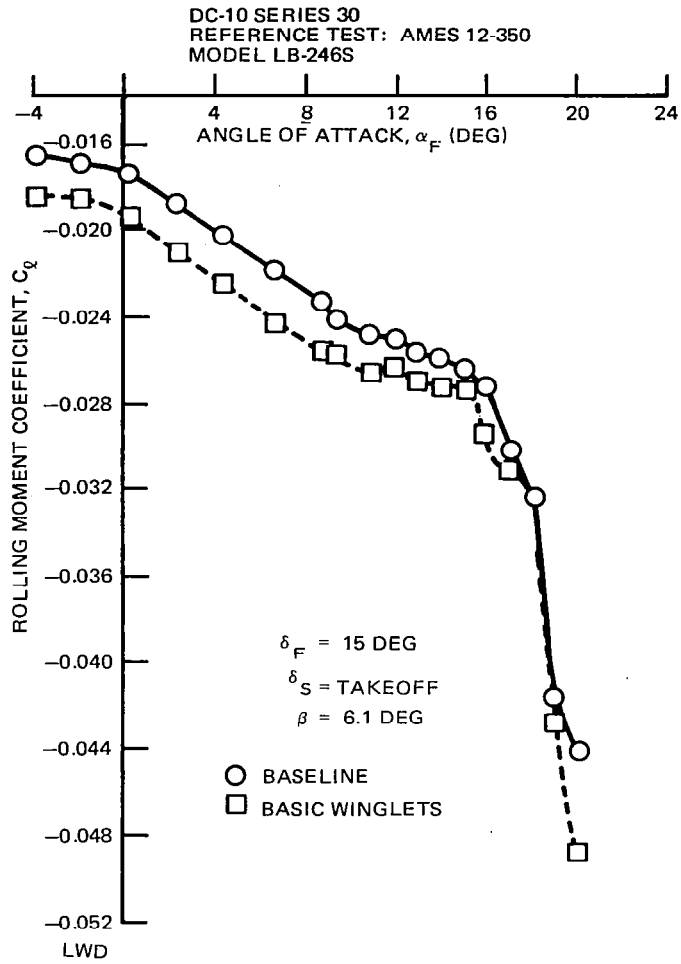
FIGURE 89. EFFECT OF BASIC WINGLETS ON ROLLING MOMENT (β = 6.1 DEG)
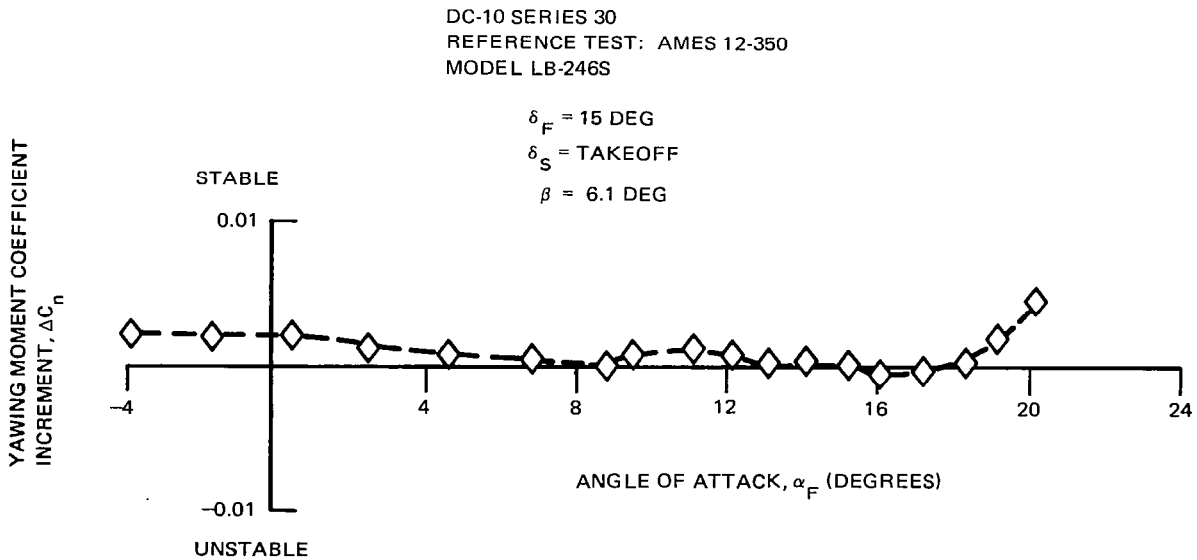
FIGURE 90. EFFECT OF BASIC WINGLETS ON YAWING MOMENT (β = 6.1 DEG)

DC-10 SERIES 30
REFERENCE TEST: AMES 12-350
MODEL LB-246S

δ_F = 15 DEG
δ_S = TAKEOFF
β = 6.1 DEG
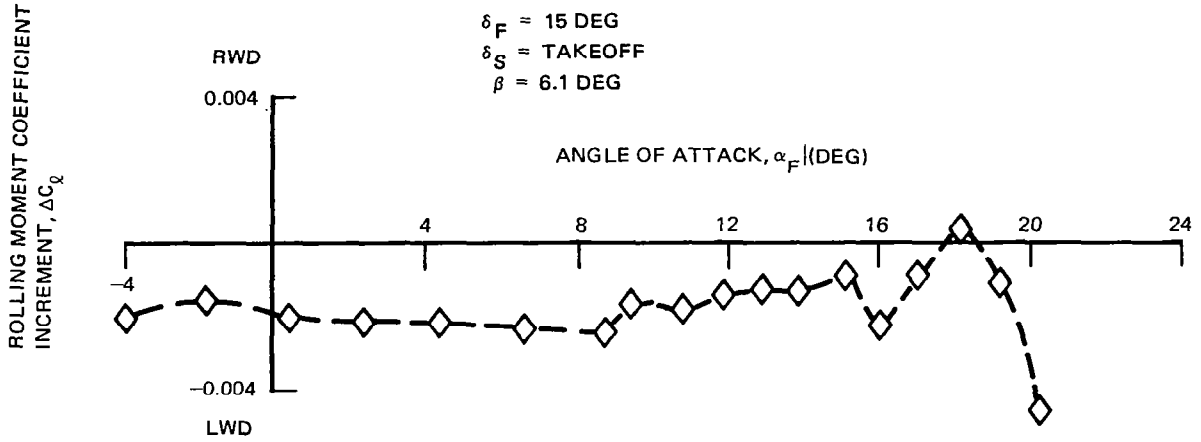
FIGURE 91.   EFFECT OF BASIC WINGLETS ON ROLLING MOMENT (β = 6.1 DEG)

DC-10 SERIES 30
REFERENCE TEST: AMES 12-423
MODEL LB-246AD

δ_F = 0 DEG
δ_S = TAKEOFF
β = 4 DEG

○ BASELINE
□ BASIC WINGLETS
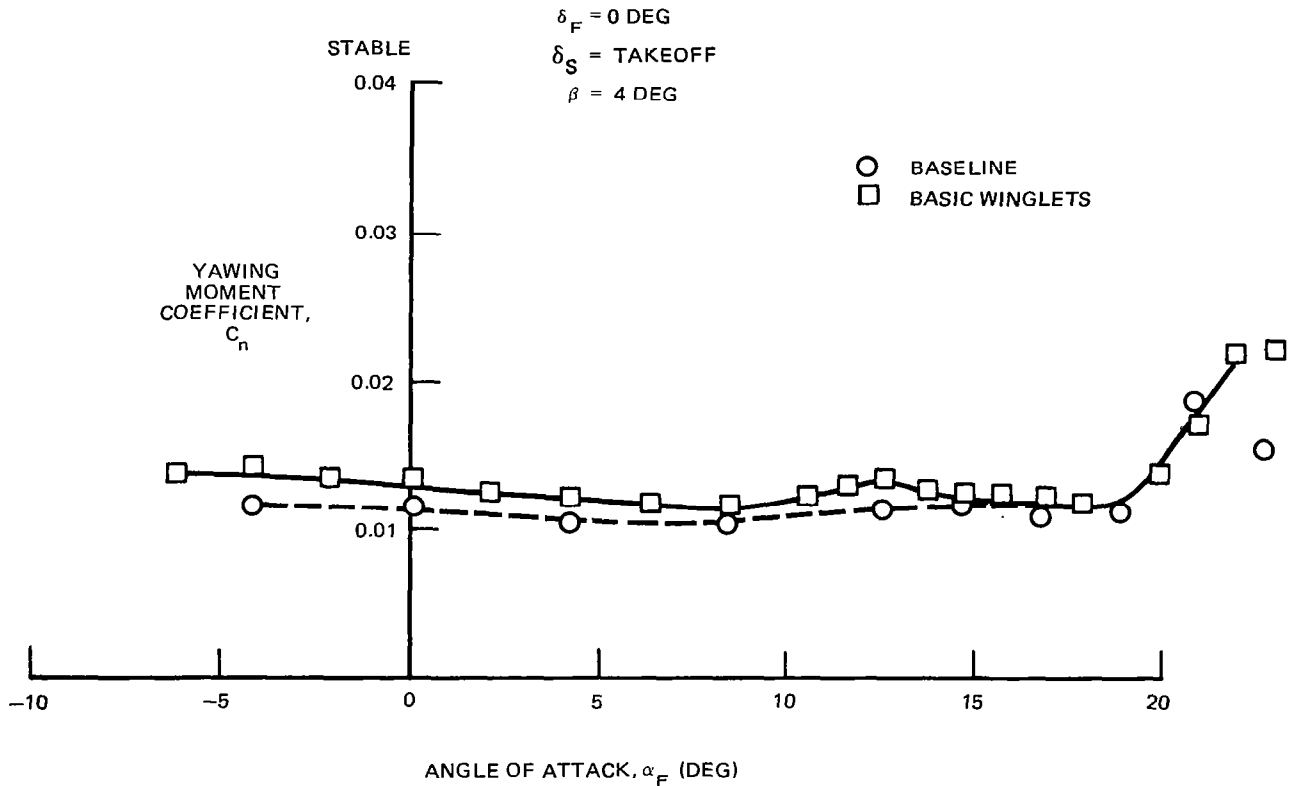
FIGURE 92. EFFECT OF BASIC WINGLETS ON YAWING MOMENT FOR TAKEOFF SLATS
AND RETRACTED FLAPS CONFIGURATION (β = 4 DEG)
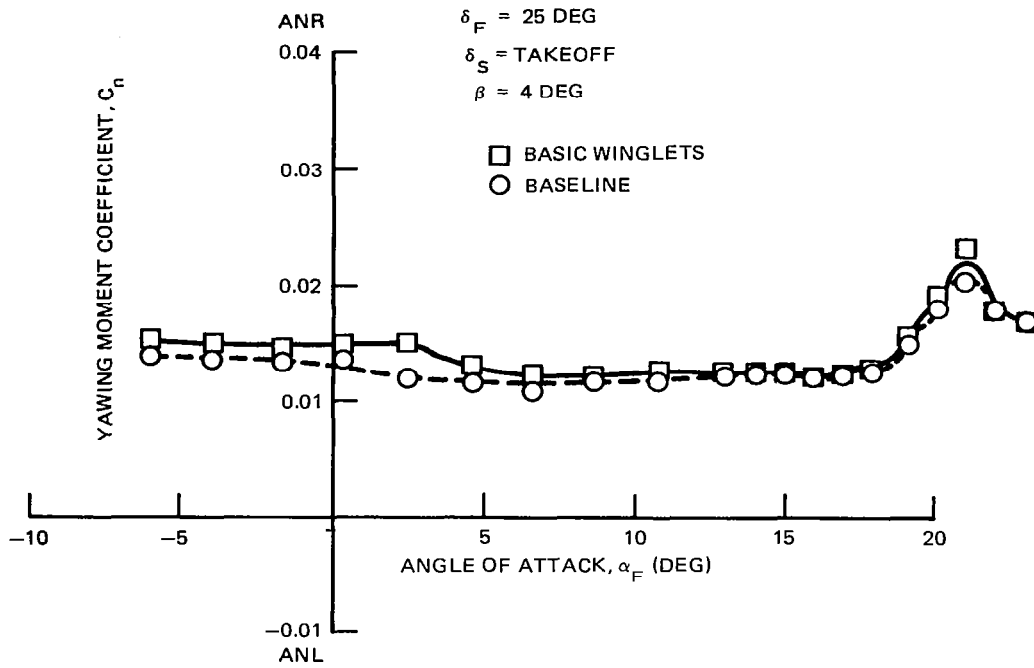
FIGURE 93. EFFECT OF BASIC WINGLETS ON YAWING MOMENT FOR TAKEOFF CONFIGURATION (β = 4 DEG)
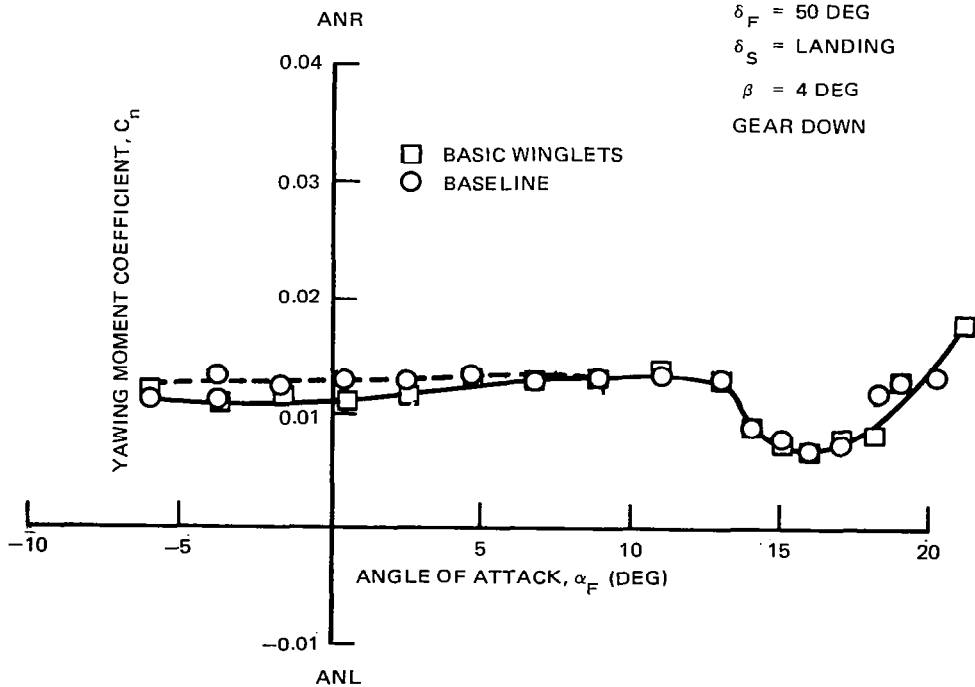
FIGURE 94. EFFECT OF BASIC WINGLETS ON YAWING MOMENT FOR LANDING CONFIGURATION (β = 4 DEG)

81
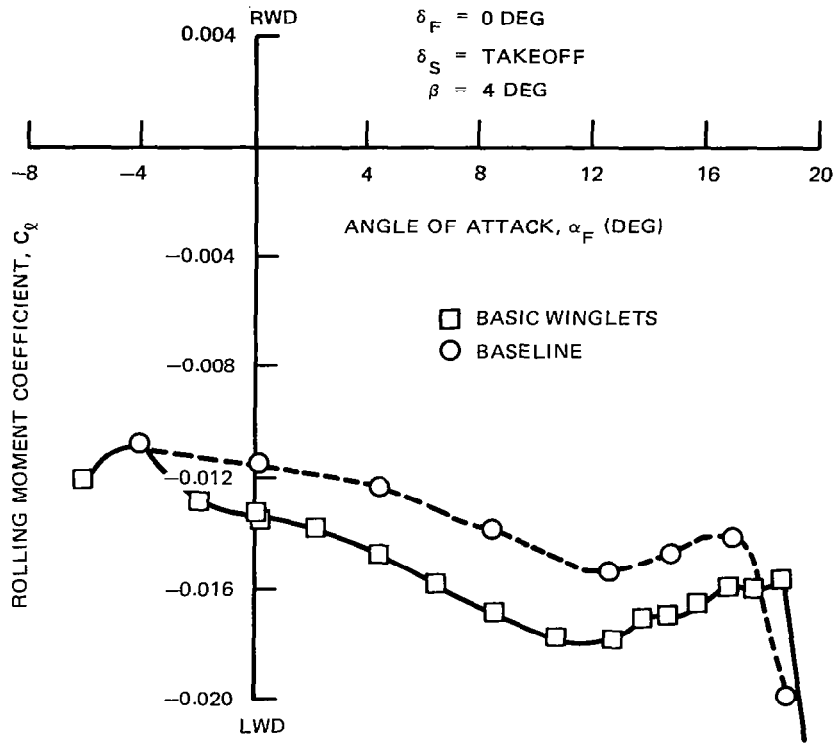
FIGURE 95. EFFECT OF BASIC WINGLETS ON ROLLING MOMENT FOR TAKEOFF SLATS AND RETRACTED FLAPS CONFIGURATION (β = 4 DEG)

ANGLE OF ATTACK, α_F (DEG)

ROLLING MOMENT COEFFICIENT, C_ℓ

δ_F = 25 DEG

δ_S = TAKEOFF

i_H = −5 DEG

β = 4 DEG

O BASIC WINGLETS
☐ BASELINE

LWD
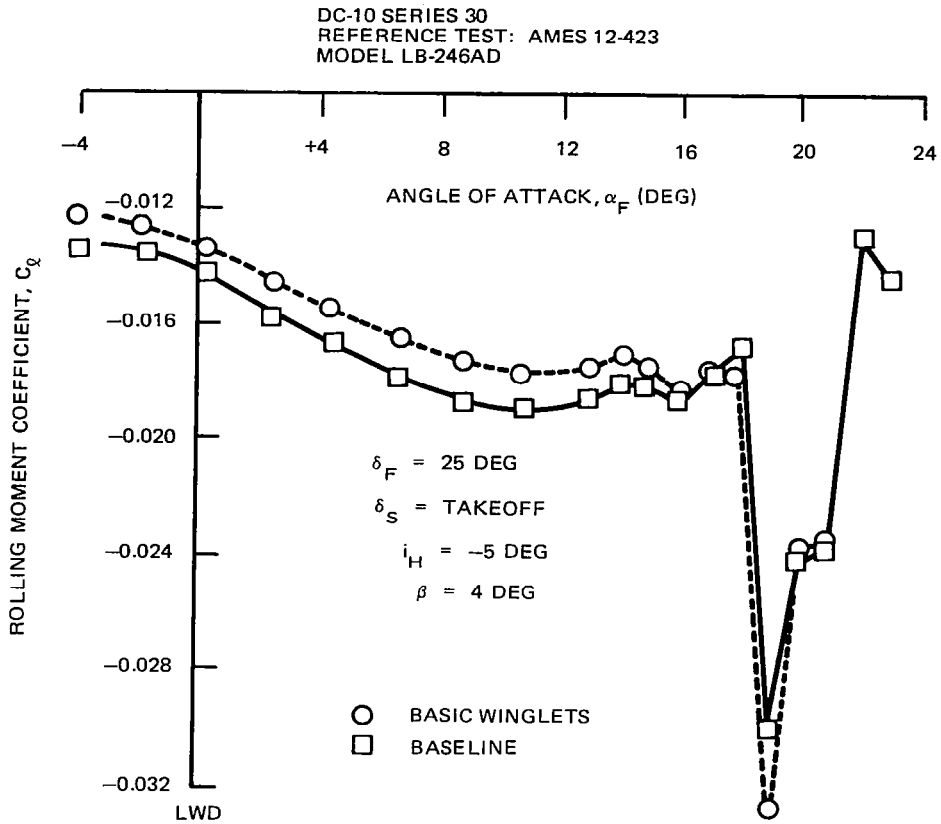
FIGURE 96. EFFECT OF BASIC WINGLETS ON ROLLING MOMENT FOR TAKEOFF CONFIGURATION (β = 4 DEG)

DC-10 SERIES 30
REFERENCE TEST: AMES 12-423
MODEL LB-246AD

RWD δ_F = 50 DEG

0.01 δ_S = LANDING

β = 4 DEG

GEAR DOWN

ANGLE OF ATTACK, α_F (DEG)

ROLLING MOMENT COEFFICIENT, C_ℓ

☐ BASIC WINGLETS
O BASELINE

LWD
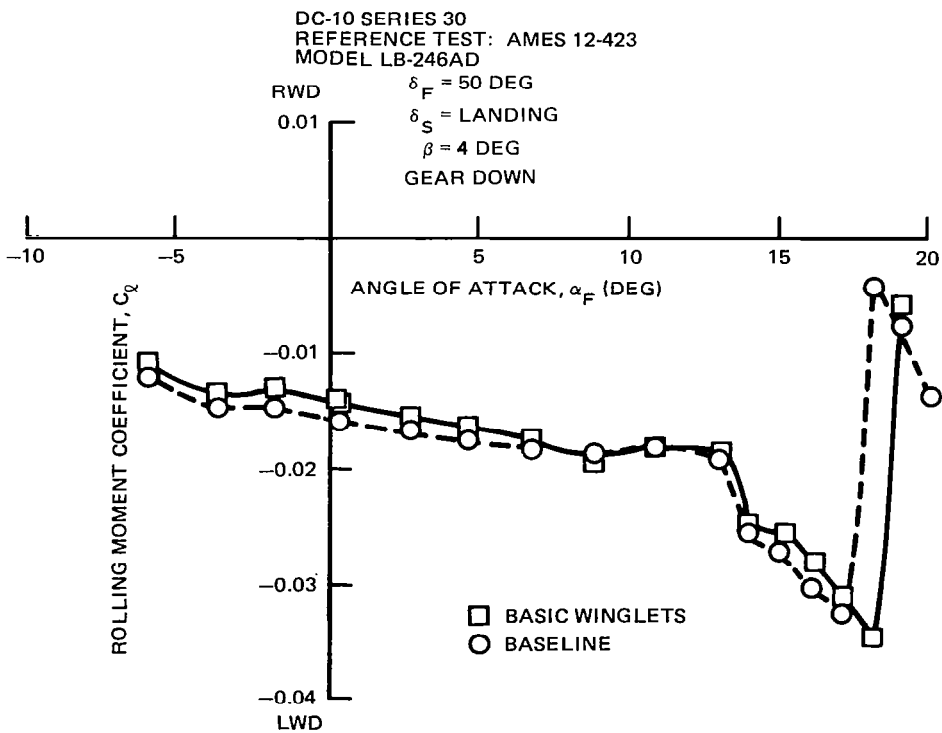
FIGURE 97. EFFECT OF BASIC WINGLETS ON ROLLING MOMENT FOR LANDING CONFIGURATION (β = 4 DEG)

moments at 50 degrees flaps. There was some question as to the validity of the 50-degree flap data because of an unplugged cavity in the wing-under-slat-surface area. Nevertheless, the trend of the data indicated that the rolling moment increment decreases with greater flap/slat settings, and the winglet effect on lateral and directional characteristics was small.

The winglet impact on aileron effectiveness for a 15-degree flap/takeoff slat configuration is presented in Figures 98 through 101. The rolling moment data for the baseline and winglet configuration are presented in Figures 98 and 99 with the right outboard aileron surface deflected to +20, −20, and 0-degree positions during pitch surveys.The trends of the data for both configurations were quite similar even through stall where large rolling moments, caused by asymmetric wing stall, are present in the wind tunnel data. Figure 100 shows the rolling moment increment for aileron deflections of +20 and −20 degrees measured from the 0-degree aileron position. The changes in aileron effectiveness due to winglets, taken from this plot, are presented in Figure 101. In this figure, the change in rolling moment resulting from the winglet is shown for deflections of +20 and −20 degrees. An increase in aileron effectiveness was noted up to approximately 12 degrees angle of attack for both positive and negative deflections. Above 12 degrees, a small loss of effectiveness was observed up to the stall vicinity for a 20-degree trailing edge down (TED) aileron deflection and a minor increase for 20 degrees trailing edge up (TEU). During and after stall, the data became somewhat erratic.

Additional data for the changes in outboard aileron effectiveness due to winglets are presented in Figures 102 through 104 for the 0-, 25-, and 50-degree flap settings as a function of angle of attack for the left aileron deflected alone. In general, the winglets increased aileron effectiveness at angles of attack below about 12 degrees, and reduced aileron effectiveness at angles of attack above this angle. This produced no significant change in the aircraft handling characteristics.

The impact of winglets on the basic characteristics of the DC-10 Series 30 aircraft was observed to be small and nearly negligible for all stability and control parameters which were examined during the wind tunnel tests.

Conclusions

The following conclusions have been reached regarding the low-speed characteristics with winglets installed:

- The basic and reduced-span winglets had minimum effects on the baseline DC-10 Series 30 aircraft lift characteristics.

- Significant reductions in drag from the baseline DC-10 Series 30 aircraft were obtained for winglet configurations at all flap deflections. In most cases, the reduced-span winglet produced a proportionally lower level of drag reduction than the basic winglet.
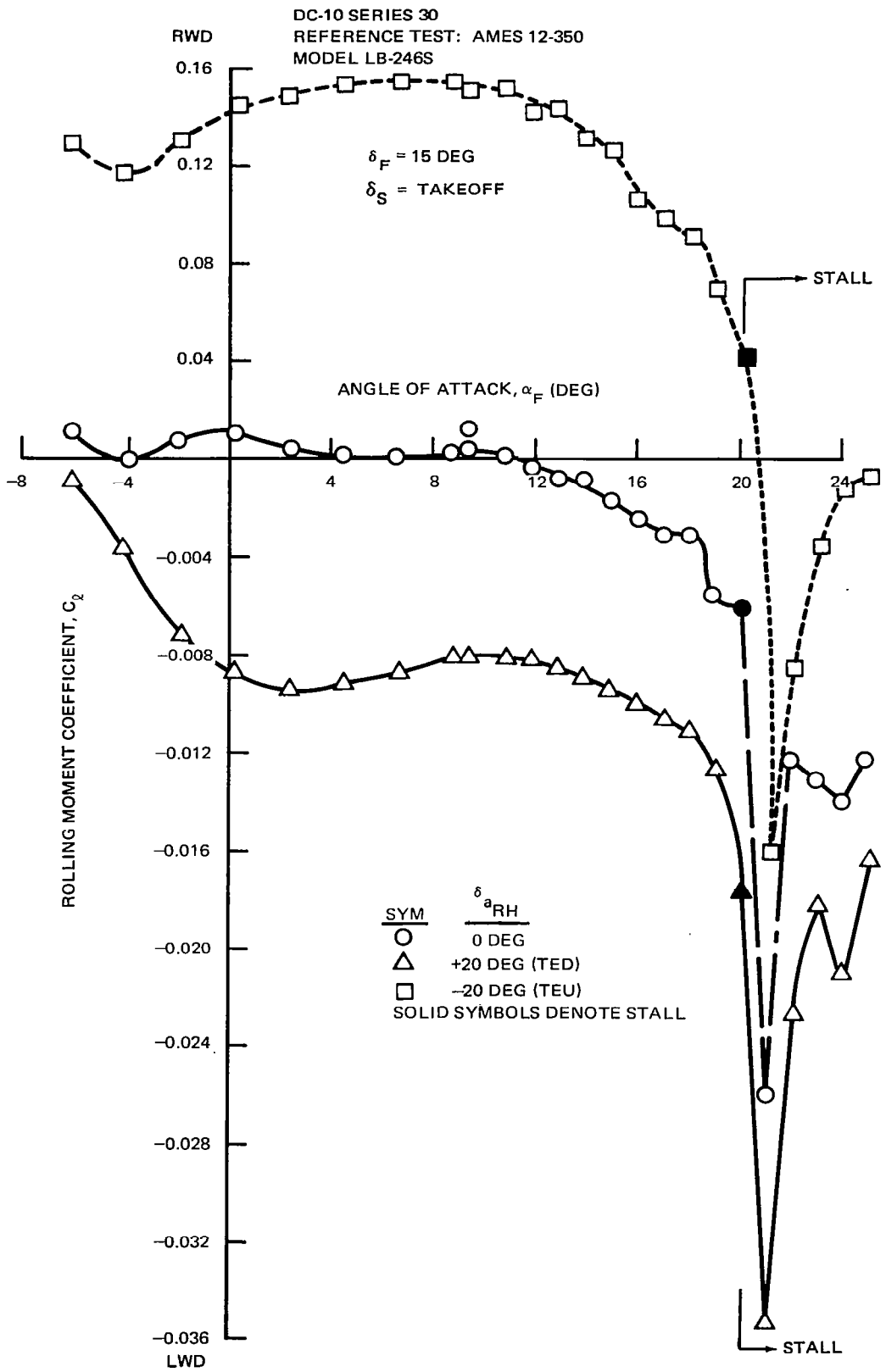
FIGURE 98. EFFECT OF AILERON DEFLECTION ON BASELINE AIRCRAFT ROLLING MOMENT
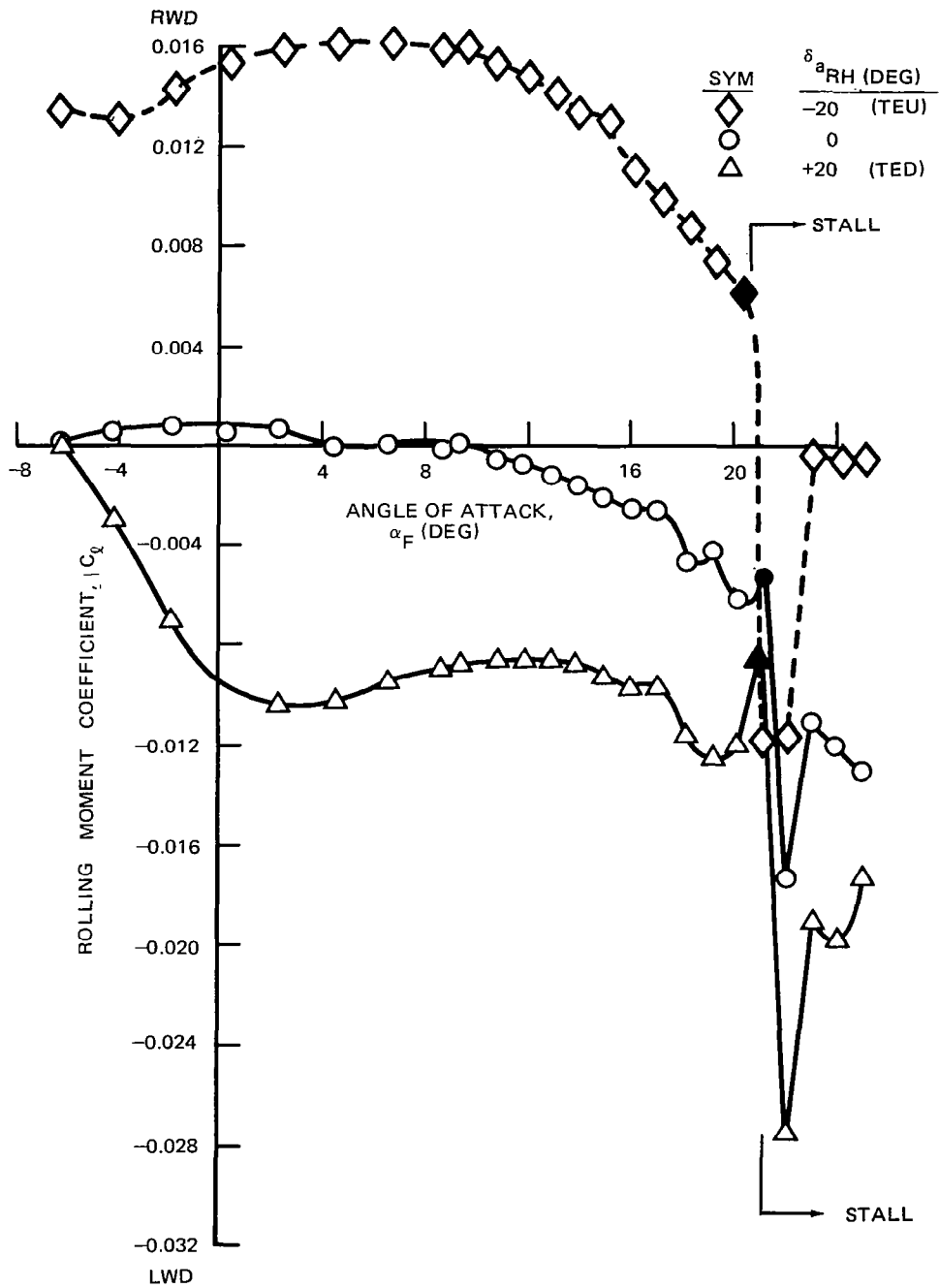
FIGURE 99. EFFECT OF AILERON DEFLECTION ON BASIC WINGLET AIRCRAFT ROLLING MOMENT
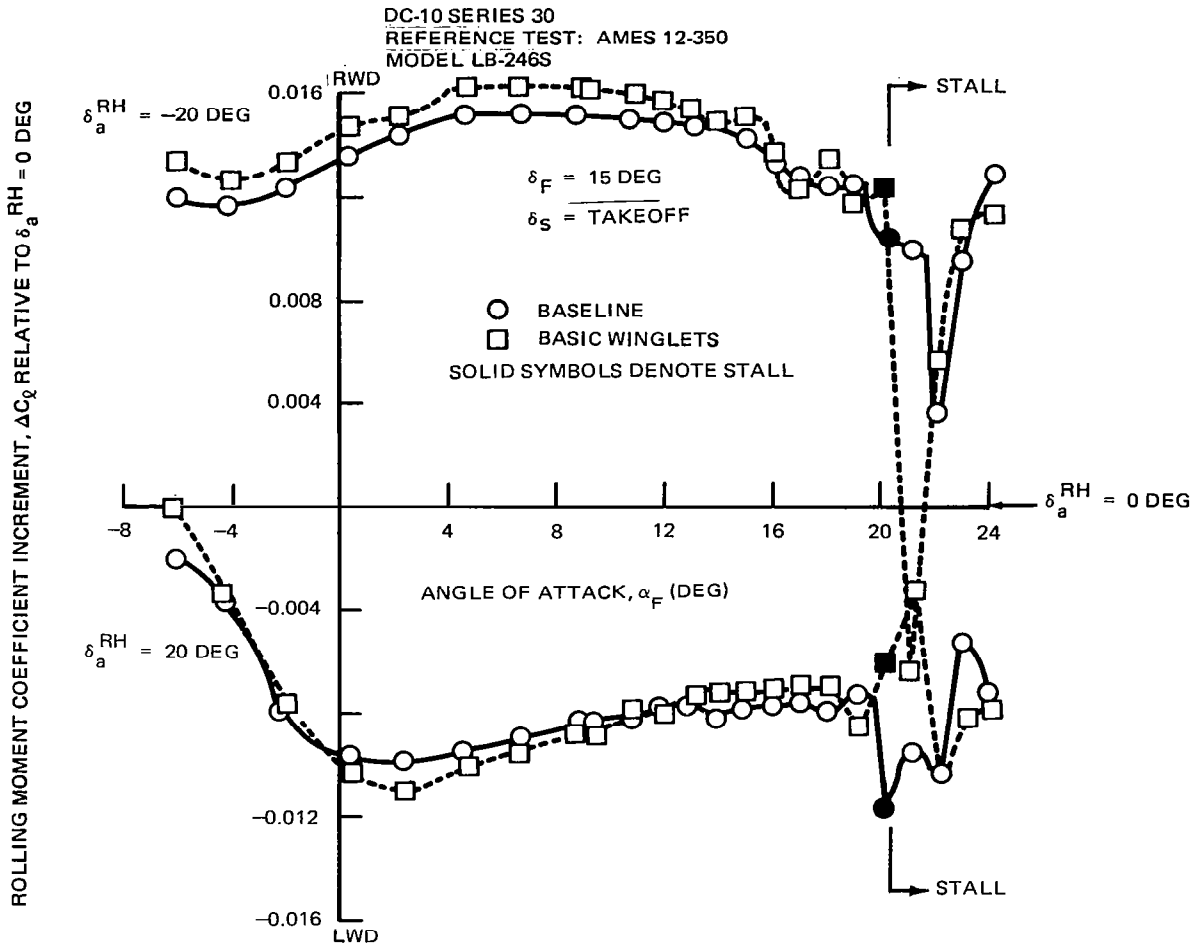
FIGURE 100. EFFECT OF BASIC WINGLETS ON AILERON EFFECTIVENESS
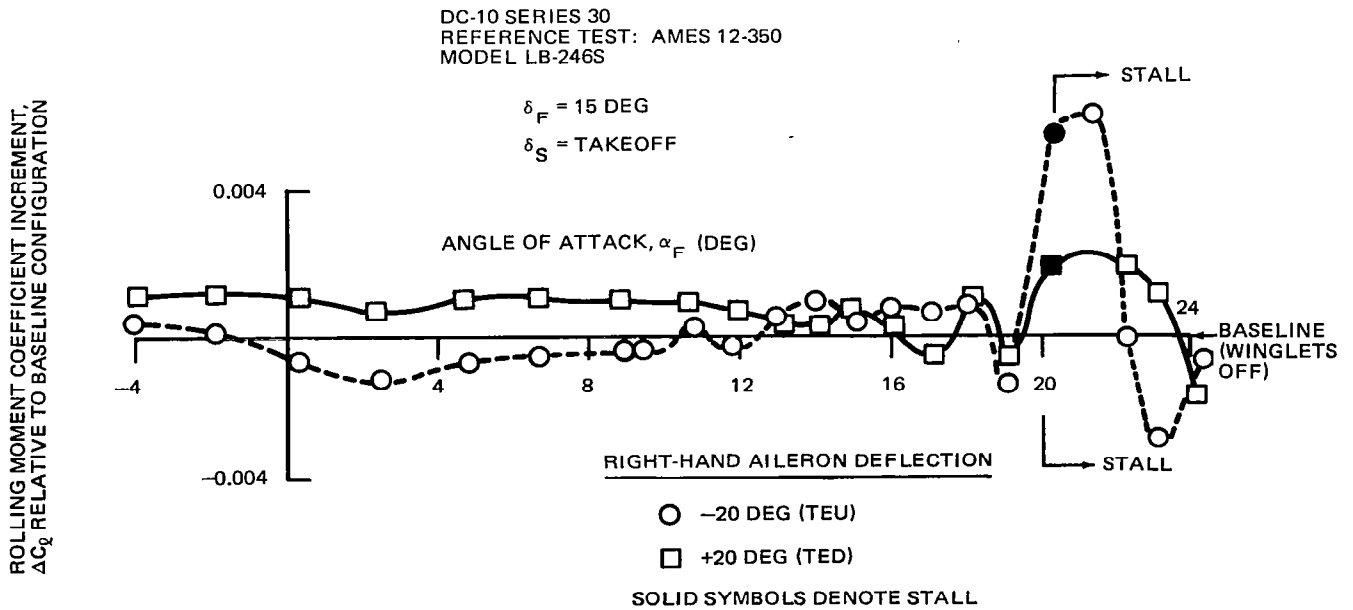
FIGURE 101. EFFECT OF BASIC WINGLETS ON ROLLING MOMENT INCREMENT WITH AILERON DEFLECTIONS OF ± 20 DEGREES
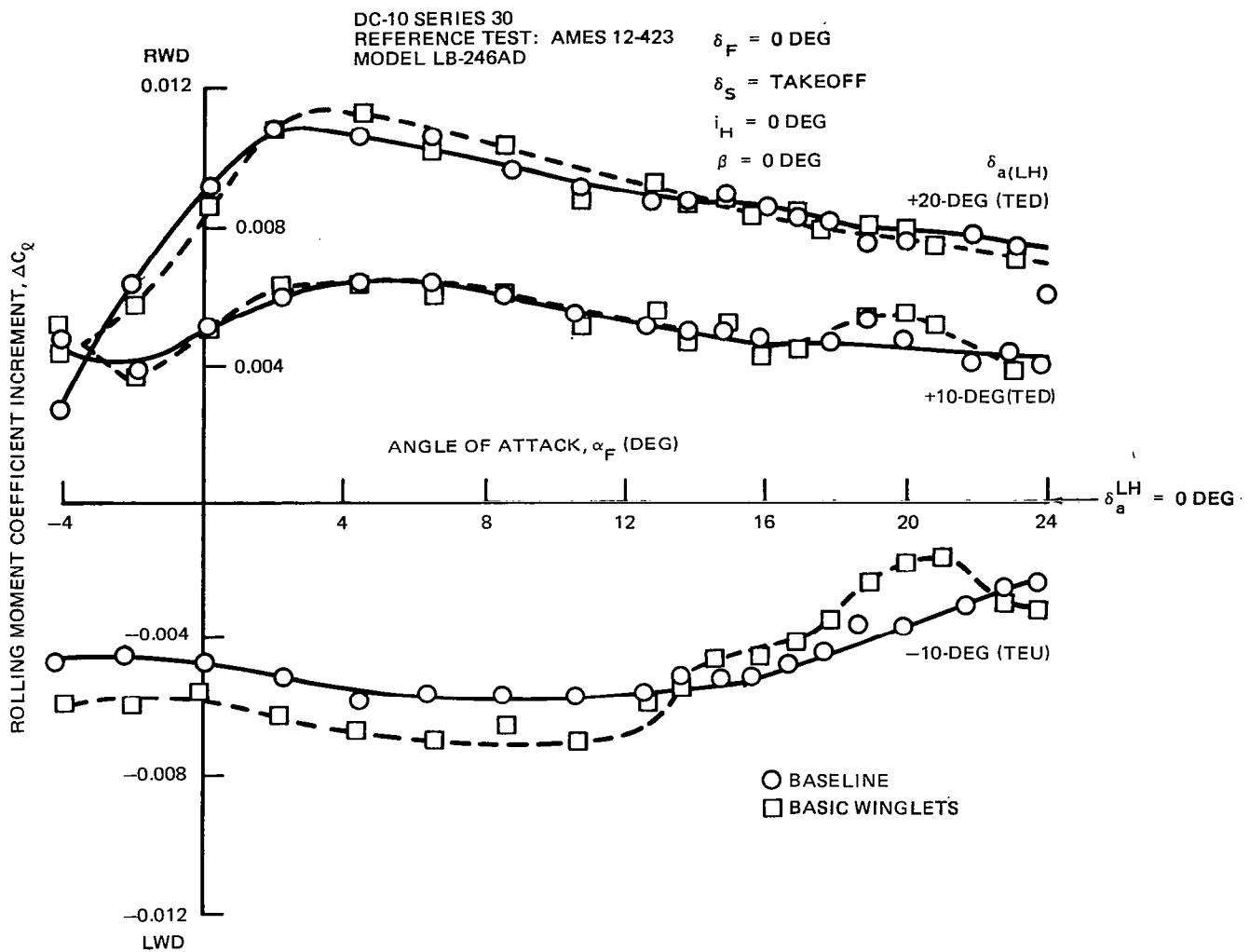
FIGURE 102. CHANGE IN AILERON EFFECTIVENESS DUE TO BASIC WINGLETS FOR RETRACTED FLAPS AND TAKEOFF SLATS

- Winglet pressure distributions and flow visualization results indicated that, at wind tunnel Reynolds numbers, the upper winglet encountered flow separation before the wing stalled.

- Evaluation of a winglet leading edge slat showed that it delayed flow separation on the upper winglet to higher angles of attack. The winglet slat had a minor effect on aircraft lift and drag characteristics. The impact of winglet flow separation on aircraft buffet and performance at flight Reynolds number can be determined only by flight evaluation. A winglet leading edge device should be included as a contingency in any flight evaluation program.

88

DC-10 SERIES 30
REFERENCE TEST: AMES 12-423
MODEL LB 246AD

RWD

ROLLING MOMENT COEFFICIENT INCREMENT, ΔC_ℓ

0.012

δ_F = 25 DEG

δ_S = TAKEOFF

○ BASELINE
□ BASIC WINGLETS

0.008

i_H = −5 DEG

β = 0 DEG

$\frac{\delta_a}{}$(LH)

0.004

+10-DEG (TED)

−4   4   8   12   16   20   24 δ_a^{LH} = 0 DEG

ANGLE OF ATTACK, δ_F (DEG)

−0.004   −10-DEG (TEU)

−20-DEG (TEU)

−0.012

−0.016

−0.020

LWD
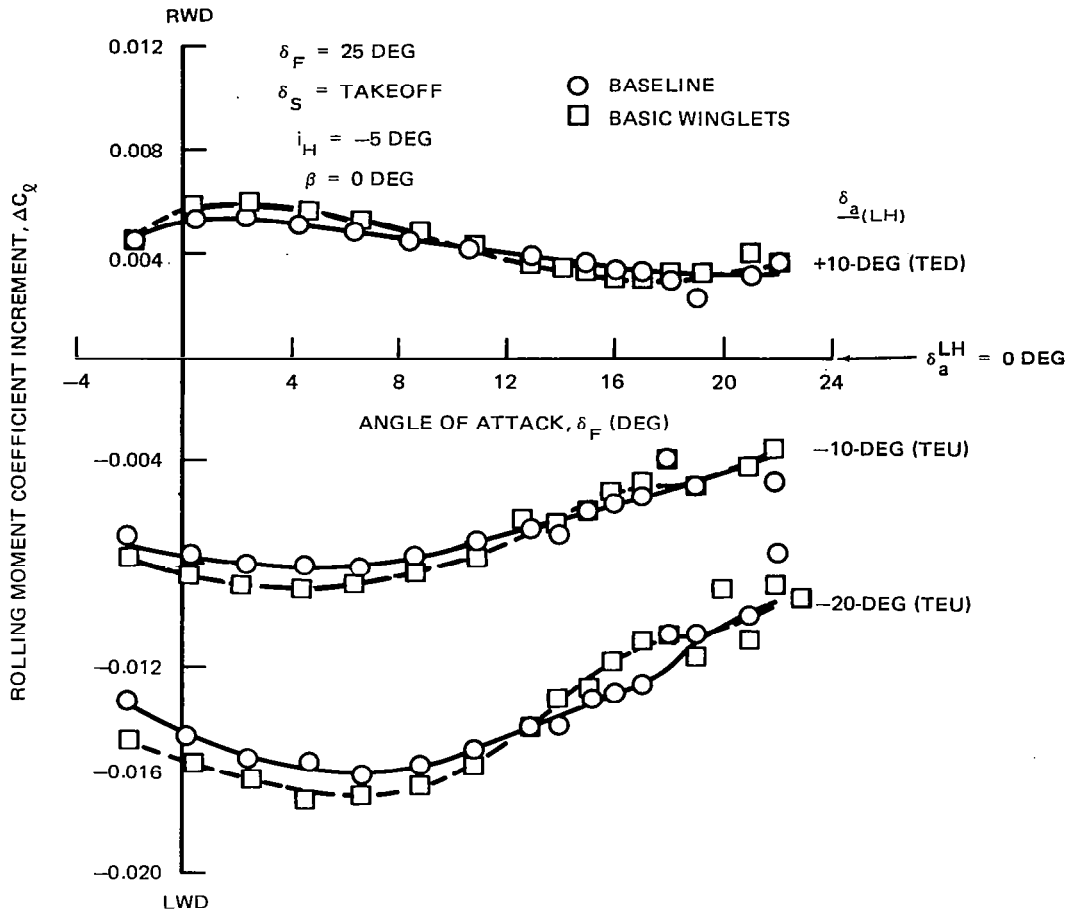
FIGURE 103.   CHANGE IN AILERON EFFECTIVENESS DUE TO BASIC WINGLETS FOR
TAKEOFF CONFIGURATION

• The simulated ice accumulation on the upper winglet leading edge had very little effect on the lift, drag, or pitching moment characteristics, so that ice protection would probably not be required for the leading edge.

• The addition of winglets to the aircraft resulted in no adverse effects on stability, control, or flying qualities.

• Winglets generally resulted in an improvement in outboard aileron effectiveness.

DC-10 SERIES 30
REFERENCE TEST: AMES 12-423
MODEL LB-246AD

δ_F = 50 DEG

δ_S = LANDING

i_H = −10 DEG   ○ BASELINE
β = 0 DEG   □ BASIC WINGLETS

RWD

0.012

0.008

0.004

−0.004

−0.012

−0.020

LWD

ROLLING MOMENT COEFFICIENT INCREMENT, ΔC_ℓ

LH δ_a = +10 (TED)

LH δ_a = −10 (TEU)

LH δ_a = −20 (TEU)

ANGLE OF ATTACK, α_F (DEG)

−4   4   8   12   16   24

δ_a^{LH} = 0 DEG

*RESULTS QUESTIONABLE
DUE TO UNPLUGGED CAVITY
IN WSS AREA
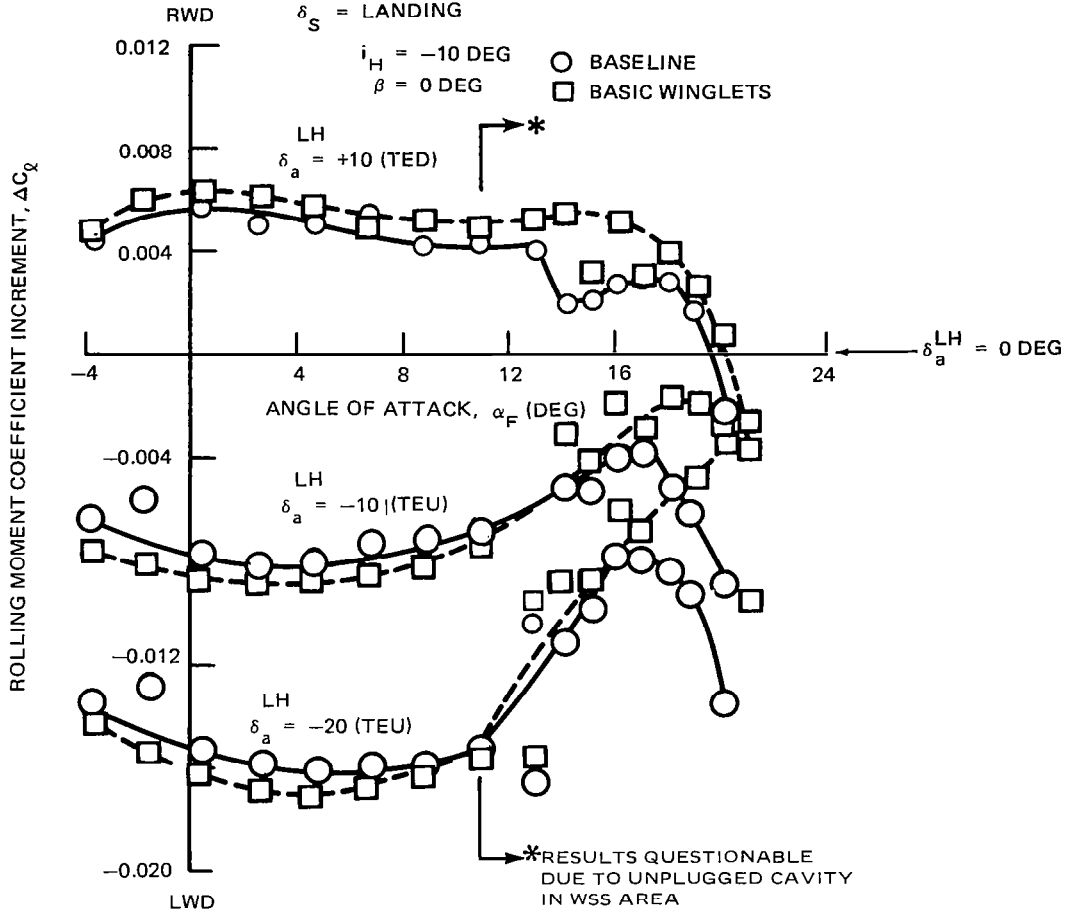
FIGURE 104.   CHANGE IN AILERON EFFECTIVENESS DUE TO BASIC WINGLETS FOR
LANDING CONFIGURATION

90

SUBSONIC FLUTTER INVESTIGATIONS

Investigation Objectives

A low-speed flutter model test program of a simple cantilevered wing/winglet configuration was conducted in May and June of 1979. The objectives of the test program were to: (1) perform a flutter analysis of the model; (2) obtain test data with a dynamically similar model of the DC-10 Series 30; and (3) correlate test results with analytical predictions.

The analyses and tests covered the basic wing without winglets, the wing with winglets installed, and the wing with dummy winglets installed. The dummy winglets were designed to simulate the mass and inertia of the winglets and yet have a minimal aerodynamic effect. Each of these configurations was tested and analyzed for an entire representative fuel schedule, as transport wing flutter is generally sensitive to fuel state. Other parametric variations evaluated in the test phase were winglet dihedral, engine weight, and wing angle of attack.

Experimental Apparatus and Procedures

The left wing of an existing 4.5-percent scale low-speed DC-10 Series 30 flutter model was modified to accommodate a winglet. The wing was designed as an equivalent beam model in which the wing stiffness distribution was represented by a single aluminum spar. The wing geometry was represented by segments built up from balsa wood and thin plywood. These sections were covered by Mylar sheets to provide aerodynamic continuity. Mass and inertia properties were simulated by lead ballast.

The mass of the winglet simulated a full-scale surface density of 39.059 kg/m^2 (8 lb/ft^2). The rigidity of the winglet was not simulated; it was effectively rigid in the important wing modes. The winglet geometry is shown in Figure 105. The winglet was designed so that the winglet dihedral angle could be easily changed and so that the winglet could be easily removed and replaced by a dummy. The dummy winglet, which was designed to isolate inertial from aerodynamic effects, is also shown in Figure 105.

The engine nacelle of the flutter model was a flow-through type representing the General Electric CF6-50 engine. The nacelle/pylon was a single-beam flexure. Several pylons were built representing different rigidity values.

Realistic root aerodynamic boundary conditions were achieved by a nonstructural fairing which simulated a typical fuselage cross section installed at the wing root.

Modal vibration tests were conducted in the laboratory before the model entered the wind tunnel. The wing was cantilevered at the root similar to the wind tunnel installation. A block diagram of the vibration test is shown in Figure 106.

DIMENSIONS IN CENTIMETERS (INCHES) MODEL SCALE
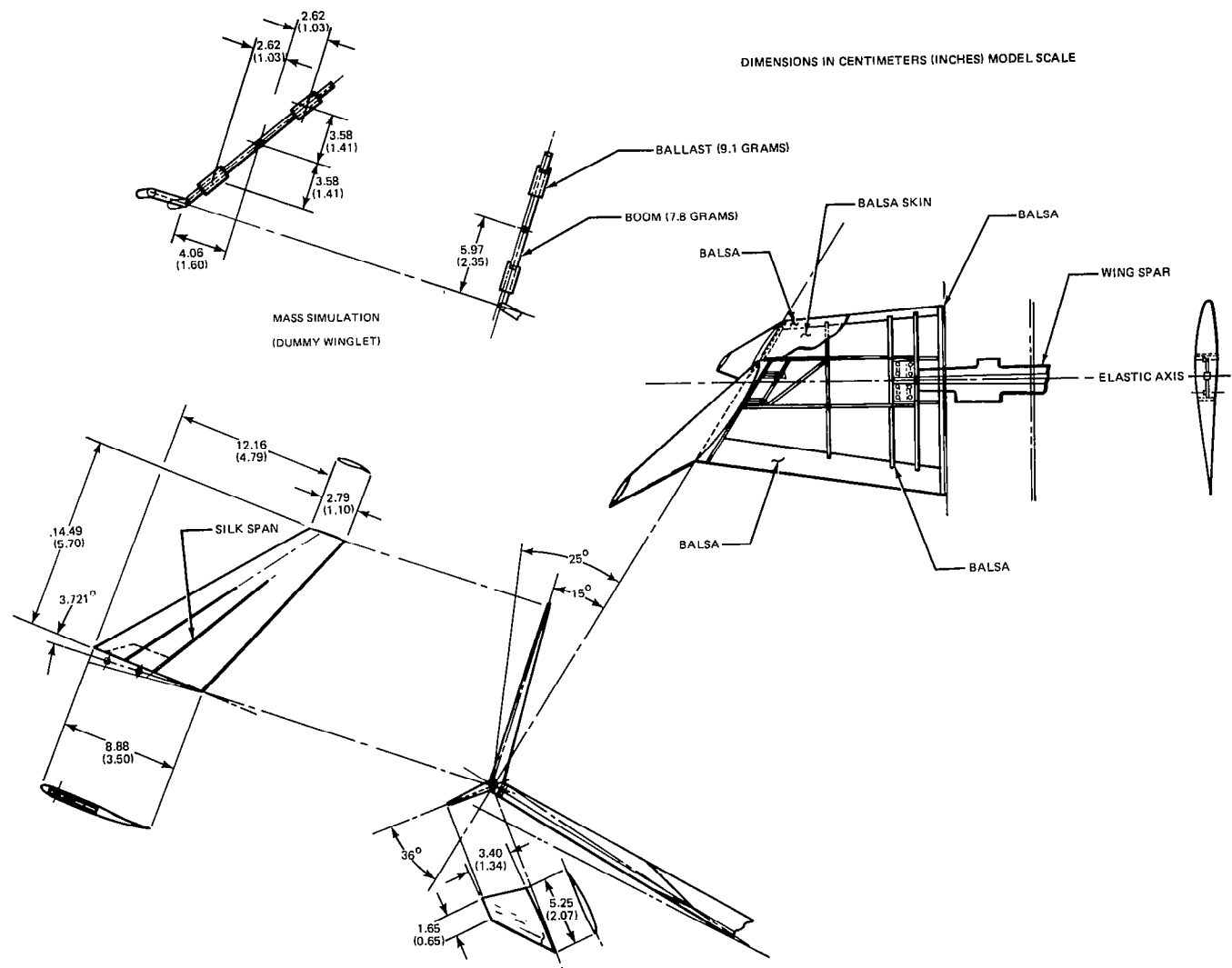
FIGURE 105. LOW-SPEED FLUTTER MODEL WINGLET GEOMETRY

92
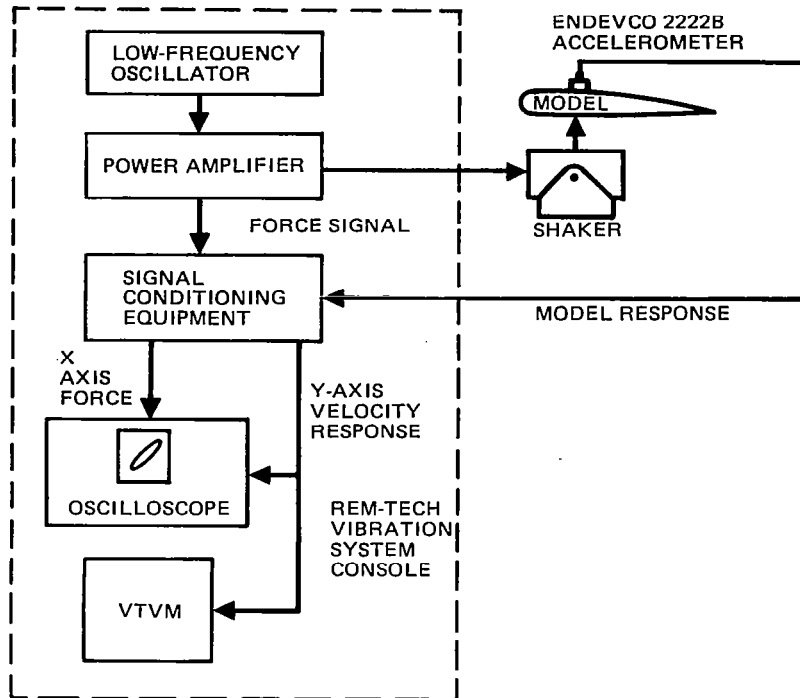
FIGURE 106. VIBRATION TEST SETUP FOR SEMISPAN WINGLET FLUTTER MODEL

Eight modes of vibration (i.e., shapes and frequencies) of the wing/winglet installation were measured for both zero- and full-fuel configurations. These modes of vibration were also measured for both zero and full fuel without the winglet installed. Some of the mode shapes and frequencies were remeasured after installation in the tunnel to ensure that no significant difference in root restraint existed. Also, modal frequency checks were made with the dummy winglet installed.

The wind tunnel test was conducted in the Northrop 7- by 10-Foot Subsonic Tunnel. Figures 107 and 108 show the wind tunnel installation. Figure 109 is a photograph of the model installed in the tunnel.

Tunnel speed was increased in increments until flutter onset (zero damping) was observed or a maximum speed of 67 meters per second (130 knots) was reached. To ensure detection of the neutral point and to obtain subcritical damping at each speed increment, the model was excited by sharp manual pulses applied through small-diameter flexible steel cables attached to the wing tip and nacelle. These lines were also used to snub the model after flutter occurred.

Periodic frequency measurements were made during the test to ensure model structural integrity. Zero-speed damping measurements were made for each run by recording model response to pulse inputs.
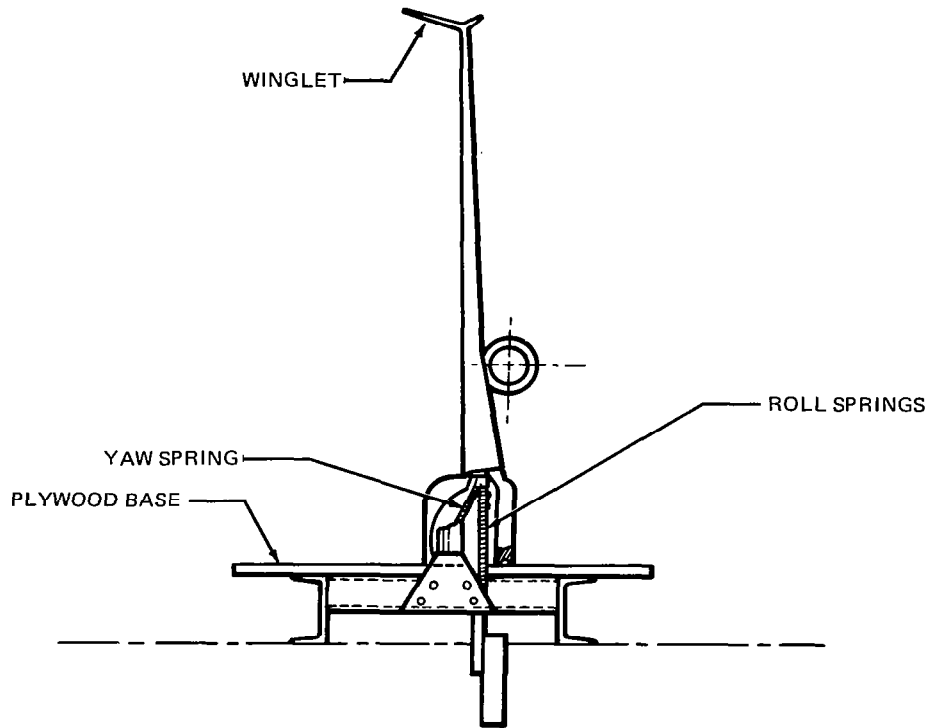
FIGURE 107. FRONT VIEW OF INSTALLATION OF DC-10 SERIES 30 FLUTTER MODEL IN NORTHROP 7- BY 10-FOOT WIND TUNNEL
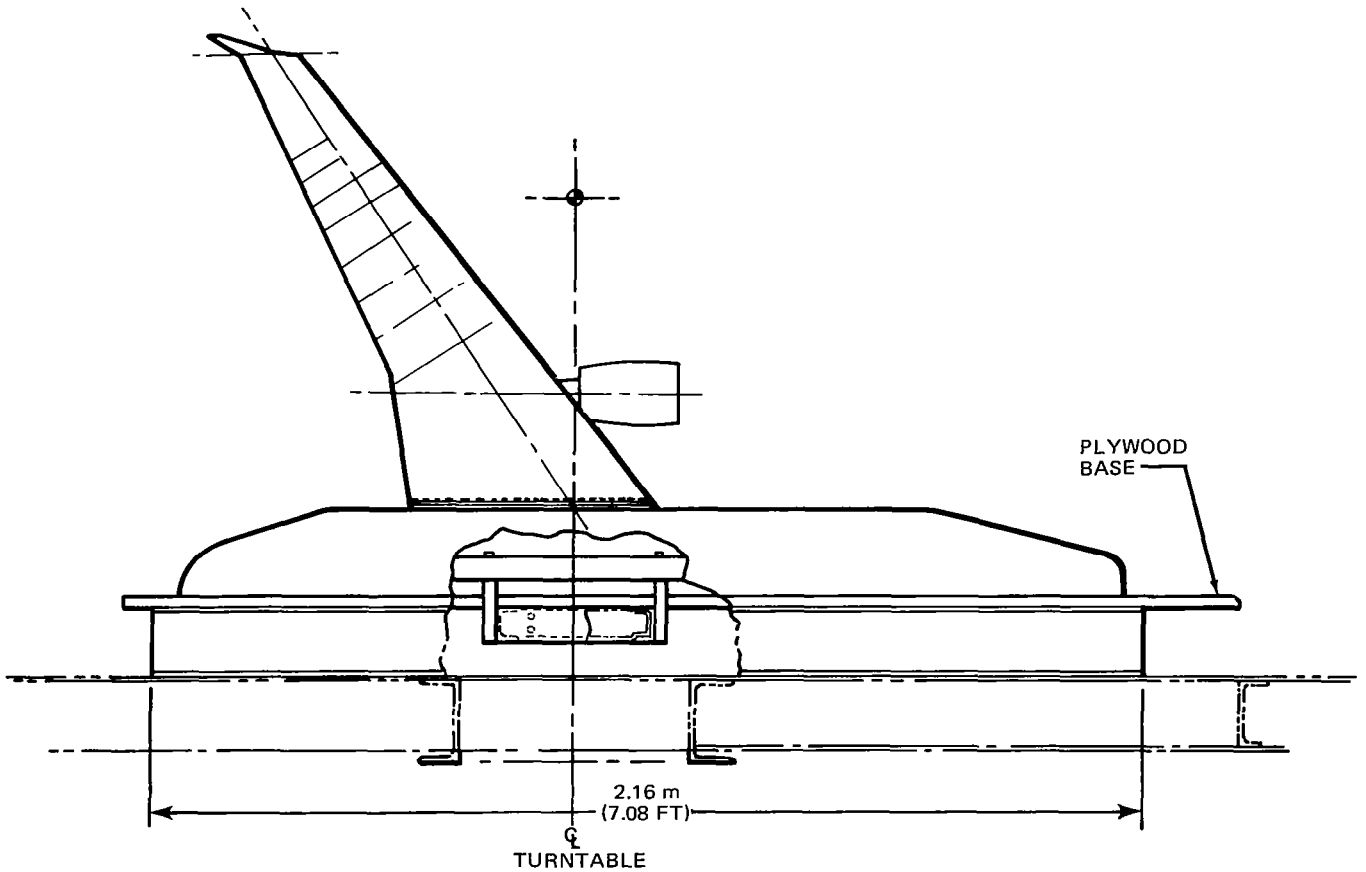
FIGURE 108. SIDE VIEW OF INSTALLATION OF DC-10 SERIES 30 FLUTTER MODEL IN NORTHROP 7-BY 10-FOOT WIND TUNNEL
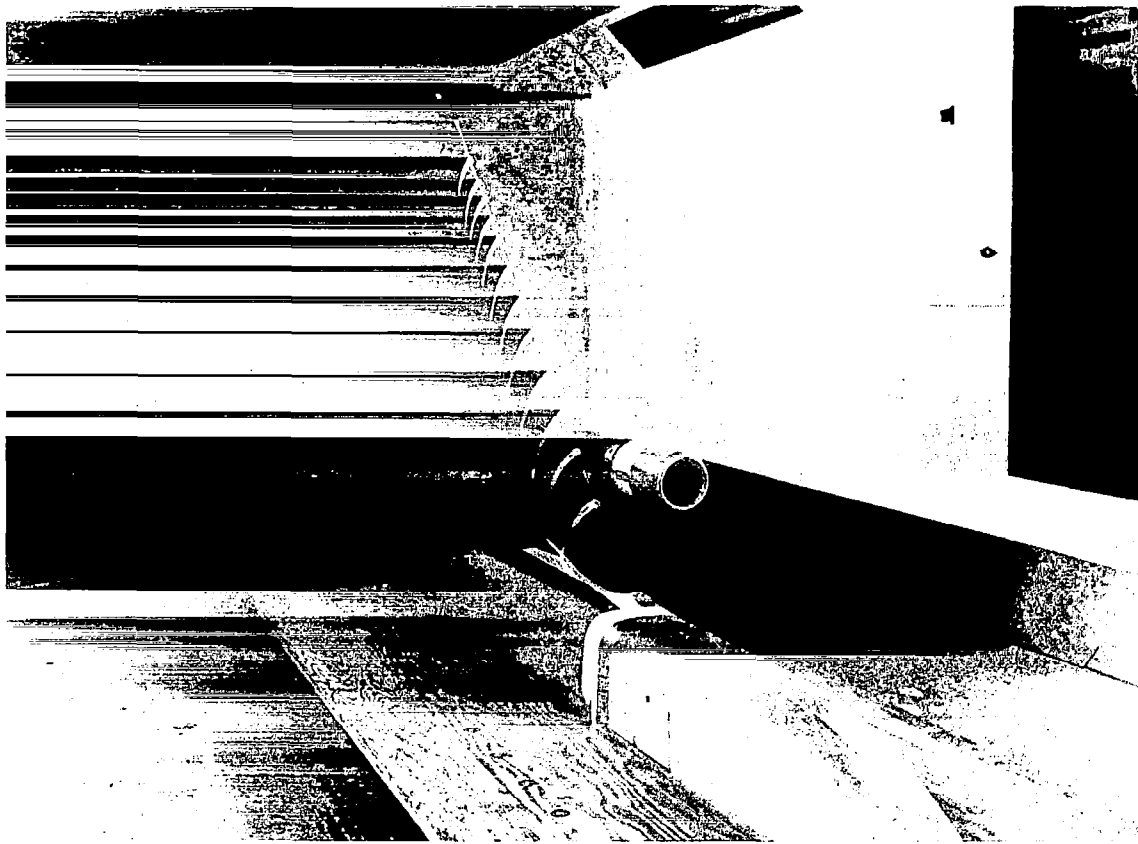
FIGURE 109. PHOTOGRAPH OF MODEL IN TUNNEL

The configurations tested are listed in Table 2.

The base engine weight represented a General Electric CF6-50 engine. The base pylon resulted in cantilevered component nacelle/pylon frequencies of 6.64 Hertz in lateral pylon bending and 16.27 Hertz in pylon vertical bending.

The instrumentation setup is shown in Figure 110. All instrumentation and electronic test equipment go through periodic maintenance and calibration procedures in the Douglas Calibration Laboratory using standards which are traceable to the National Bureau of Standards.

The model responses to pulse inputs were recorded on an oscillograph. These transient decay traces were manually reduced to obtain frequency and damping values. The test data were plotted to show frequency and damping as a function of speed. The test speeds were also summarized in the form of plots of flutter speed as a function of each parametric variation.

TABLE 2
FUEL QUANTITIES TESTED FOR VARIOUS CONFIGURATIONS
AND PARAMETRIC INVESTIGATIONS

CONFIGURATION / TEST	FUEL QUANTITY TESTED (PERCENT)							
	0	10	15	21.5	40	60	80	100
BASELINE (NO WINGLET)	●	●		●		●		●
LOWER WINGLET ONLY	●	●	●	●	●	●	●	●
BASIC WINGLET / 75 DEGREES DIHEDRAL	●	●	●	●	●	●	●	●
BASIC WINGLET / 65, 90 DEGREES DIHEDRAL	●	●	●	●		●		●
DUMMY MASS WINGLET	●	●	●	●		●		
ENGINE WEIGHT VARIATION						●		●
PYLON STIFFNESS VARIATION		●						
WING ANGLE OF ATTACK		●						●
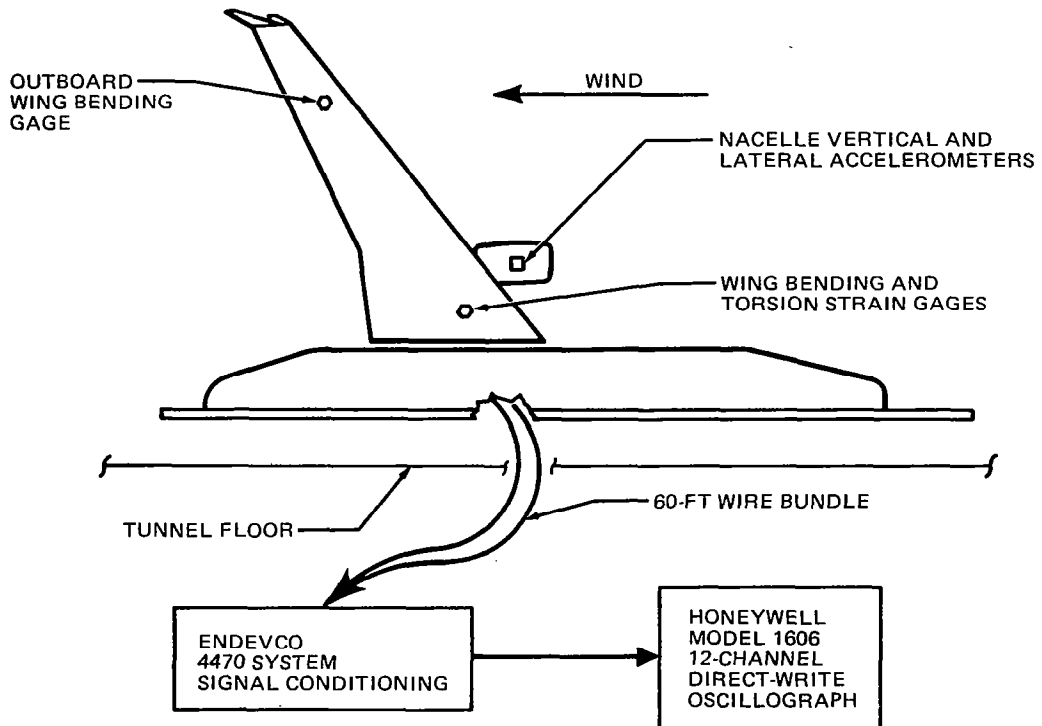
FIGURE 110. WIND TUNNEL INSTRUMENTATION FOR SEMISPAN WINGLET FLUTTER MODEL

Analytical Methodology

Basic data — The model geometric idealization is shown in Figure 111. The figure contains all of the geometric data required to generate oscillatory aerodynamic influence coefficients by the doublet lattice method. These coefficients were generated at a Mach number of 0.20 for reduced frequency of 0.0, 0.1, 0.333, 0.5, and 1.0 based on a reference chord of 33.81 cm (13.31 inches).

In generating the aerodynamic influence coefficients, the plywood base (see Figures 107 and 108) was taken as the symmetry plane. The "fuselage" fairing was idealized simply as a panel, which adequately simulated the significant interference lift. The nacelle was idealized as a flow-through hexagon. The model nacelle pylon is not an aerodynamic panel as on an airplane. Hence, in the model idealization, the nacelle was separated from the wing by a small gap.

The theoretical aerodynamic influence coefficients were not weighted. An analogous set of coefficients was generated without the winglet for use in base case flutter analyses.

The weight and rigidity data were formulated in the elastic axis coordinate system shown in Figure 111. Table 3 lists the location of each bay reference station in elastic axis coordinates. The weight, chordwise unbalance, and pitch moment of inertia for each bay were measured from the model. The roll, yaw, and products of inertia were obtained by extrapolation, using full-scale airplane data as a guide.

Table 4 shows the bay mass and inertia data for the engine and upper winglet. The lower winglet was massless. Tables 5 through 14 list the mass and inertia data for the wing bays in each fuel configuration. The mass properties are about the bay reference station in the elastic axis coordinate system. The sketch and notes at the bottom of Table 4 document the sign convention for the mass and inertia data.

The rigidity data for the wing are shown in Figures 112 through 114. The model wing normal bending and torsion rigidities accurately simulated scaled airplane values, but the longitudinal bending rigidity was significantly higher than scaled airplane values. The implication is discussed later.

Pylon rigidity is not presented. Instead, the cantilevered nacelle/pylon normalized mode shapes and frequencies are given directly in Table 15.

Modal vibration analysis — The mass representation of the wing/winglet/nacelle flutter model consisted of "lumping" the mass and inertia properties of the model into 16 bays. The mass and inertia data are shown in Tables 4 through 14; the lower winglet was massless. Each bay was capable of six inertial degrees of freedom.
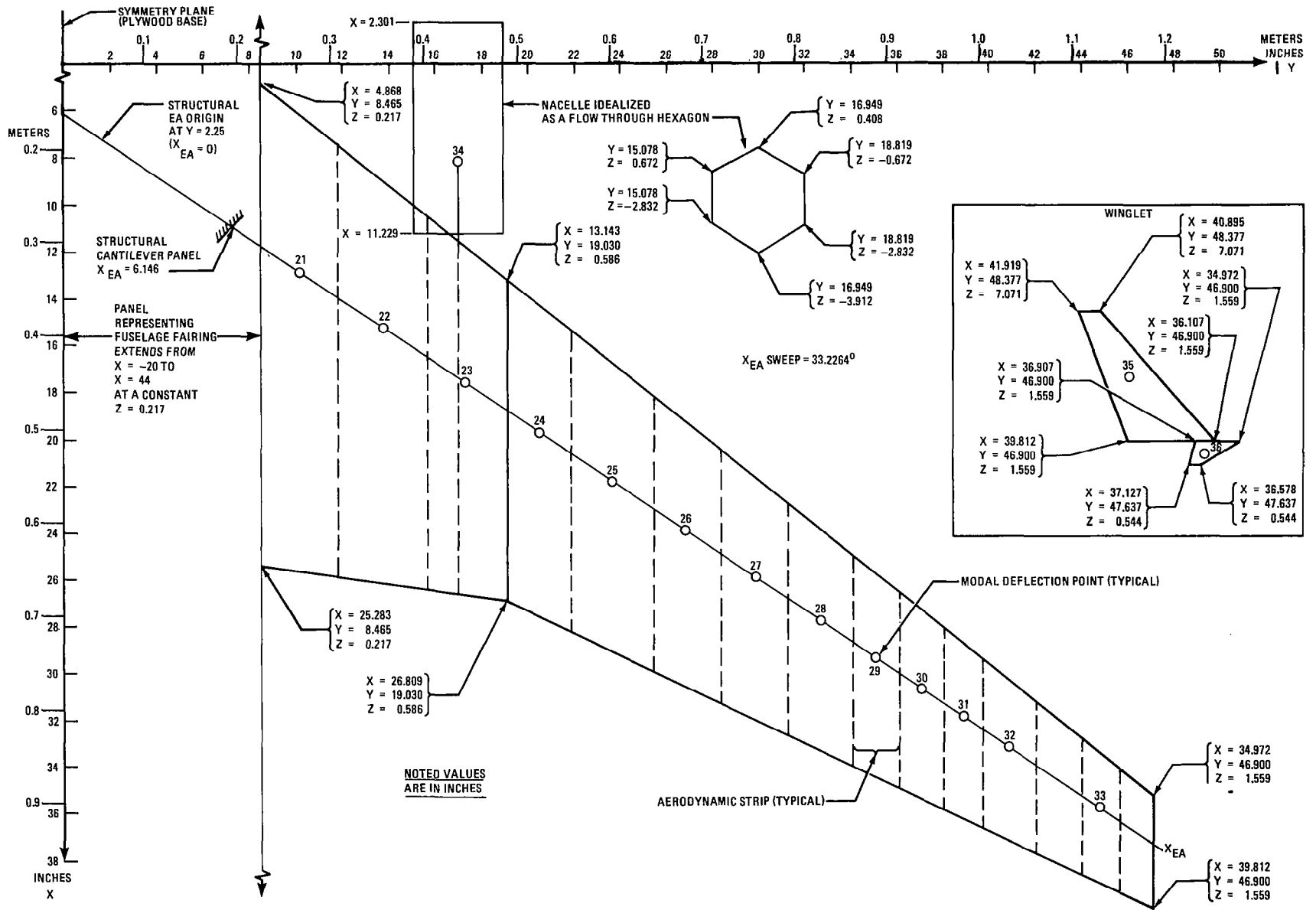
FIGURE 111. MODEL GEOMETRIC IDEALIZATION

86

TABLE 3
MODEL BAY COORDINATES — WING ELASTIC AXIS SYSTEM

BAY	COMPONENT	Xea (METERS)	Yea (METERS)	Zea (METERS)
21	WING	0.23896	0	0
22		0.34999		
23		0.45552		
24		0.55044		
25		0.65385		
26		0.75209		
27		0.84003		
28		0.92685		
29		1.00079		
30		1.05951		
31		1.11417		
32		1.17526		
33		1.28626		
34	ENGINE	0.32319	−0.19449	−0.07305
35	UPPER WINGLET	1.39629	0.02068	0.04785
36	LOWER WINGLET	1.35042	−0.01976	−0.01067

NOTES: 1. Xea IS + OUTBOARD ALONG ELASTIC AXIS
2. Yea IS + AFT PERPENDICULAR TO ELASTIC AXIS
3. Zea IS + UP PERPENDICULAR TO WING PLANE

The structural influence coefficient matrix relating static deflections at each bay reference point to applied unit forces and moments at the same set of points was generated from beam equations using the span distributions of rigidity shown in Figures 112 through 114. The pylon was rigid in this matrix. This structural influence coefficient was then used along with the mass matrix of the model to generate component wing modes for the various fuel configurations, where the word "component" signifies that the pylon was rigid in these modes.

Similarly, component pylon modes were generated assuming a rigid wing. A beam structural influence coefficient matrix relating the nacelle bay reference station deflections to applied forces was used with the nacelle mass matrix to generate these modes.

The winglets were assumed to be rigid. As mentioned previously, the lower winglet was also massless.

These component modes provided the basis for the flutter analysis. However, fully coupled orthogonal modes of the wing/winglet/nacelle system were explicitly calculated for the zero- and full-fuel configurations for comparison with model ground vibration test results.

Flutter analysis — The flutter analysis was done by the usual V-g method. The analysis used the calculated mode shapes and frequencies discussed earlier. Theoretical aerodynamic influence coefficients for a Mach number of 0.20 were used. All runs were made at sea level. A structural damping value of g_s equal to 0.02 was used for each mode.

TABLE 4
MODEL MASS AND INERTIA DATA ENGINE (BAY 34)

MODE NO. 19660

BAY	MASS	MX	MY	MZ	IXX
34	0.90899E+00	0.0	0.0	0.0	0.47295E-02

BAY	IYY	IZZ	IXY	IYZ	IXZ
34	0.75832E-03	0.46442E-02	0.12585E-03	0.45552E-04	0.10512E-04

MODEL MASS AND INERTIA DATA UPPER WINGLET (BAY 35)

MODE NO. 19661

BAY	MASS	MX	MY	MZ	IXX
35	0.29573E-01	0.0	0.0	0.0	0.37344E-04

BAY	IYY	IZZ	IXY	IYZ	IXZ
35	0.48346E-04	0.80364E-04	-0.11303E-04	0.0	0.0

NOTES:

MASS — MASS OF BAY — kg

MX ⎫ MASS OF BAY TIMES ΔX, ΔY, ΔZ, WHERE ⎫
MY ⎬ ΔX IS + IF BAY CG IS OUTBOARD OF REFERENCE POINT ⎬ kg-m
      ΔY IS + IF BAY CG IS AFT OF REFERENCE POINT
MZ ⎭ ΔZ IS + IF BAY CG IS ABOVE REFERENCE POINT ⎭

IXX — PITCH MASS MOMENT OF INERTIA — $kg\text{-}m^2$
IYY — ROLL MASS MOMENT OF INERTIA — $kg\text{-}m^2$
IZZ — YAW MASS MOMENT OF INERTIA — $kg\text{-}m^2$
IXY, IYZ, IXZ — PRODUCTS OF INERTIA — $kg\text{-}m^2$
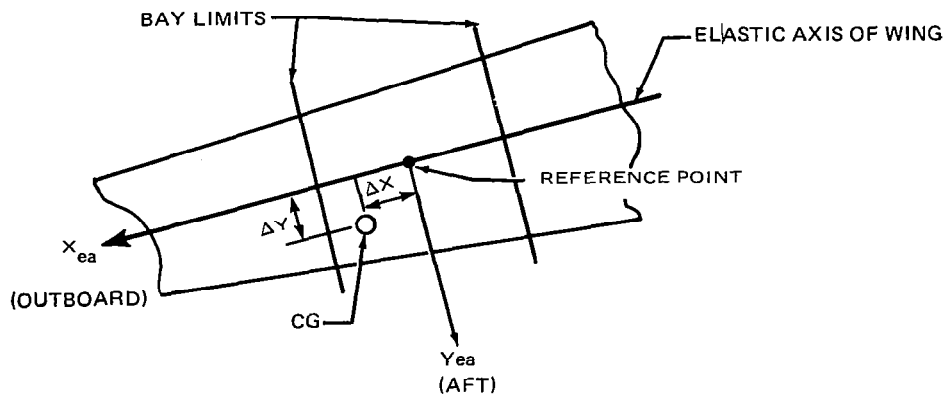
WING PLANFORM
VIEW LOOKING DOWN

TABLE 5
MODEL MASS AND INERTIA DATA WING BAYS ZERO FUEL

MODE NO. 19662

BAY	MASS	MX	MY	MZ	IXX
21	0.40883E+00	0.0	-0.11636E-03	0.0	0.57855E-03
22	0.51873E+00	0.0	0.18881E-01	0.0	0.40829E-02
23	0.24533E+00	0.0	0.56035E-02	0.0	0.16535E-02
24	0.17729E+00	0.0	0.31653E-02	0.0	0.10057E-02
25	0.19368E+00	0.0	0.54109E-02	0.0	0.10473E-02
26	0.12050E+00	0.0	0.18879E-02	0.0	0.51377E-03
27	0.10986E+00	0.0	0.15944E-02	0.0	0.35361E-03
28	0.79487E-01	0.0	0.76481E-03	0.0	0.21649E-03
29	0.44824E-01	0.0	0.58464E-03	0.0	0.12112E-03
30	0.35053E-01	0.0	0.24515E-03	0.0	0.64754E-04
31	0.27755E-01	0.0	0.21876E-03	0.0	0.49906E-04
32	0.33067E-01	0.0	0.21151E-03	0.0	0.59918E-04
33	0.50684E-01	0.0	0.43834E-03	0.0	0.95239E-04

BAY	IYY	IZZ	IXY	IYZ	IXZ
21	0.86724E-04	0.66547E-03	0.0	0.0	0.0
22	0.61232E-03	0.46953E-02	0.0	0.0	0.0
23	0.24791E-03	0.19015E-02	0.0	0.0	0.0
24	0.15096E-03	0.11566E-02	0.0	0.0	0.0
25	0.15710E-03	0.12045E-02	0.0	0.0	0.0
26	0.77088E-04	0.59071E-03	0.0	0.0	0.0
27	0.53144E-04	0.40675E-03	0.0	0.0	0.0
28	0.32412E-04	0.24908E-03	0.0	0.0	0.0
29	0.18104E-04	0.13928E-03	0.0	0.0	0.0
30	0.96360E-05	0.74460E-04	0.0	0.0	0.0
31	0.75920E-05	0.57524E-04	0.0	0.0	0.0
32	0.90520E-05	0.68912E-04	0.0	0.0	0.0
33	0.47596E-04	0.14279E-03	0.0	0.0	0.0

TABLE 6
MODEL MASS AND INERTIA DATA WING BAYS 10-PERCENT FUEL

MODE NO. 19663

BAY	MASS	MX	MY	MZ	IXX
21	0.57640E+00	0.0	-0.11636E-03	0.0	0.24789E-02
22	0.70820E+00	0.0	0.18881E-01	0.0	0.46748E-02
23	0.39454E+00	0.0	0.56035E-02	0.0	0.19210E-02
24	0.19468E+00	0.0	0.31653E-02	0.0	0.10641E-02
25	0.19675E+00	0.0	0.54109E-02	0.0	0.10812E-02
26	0.12050E+00	0.0	0.18879E-02	0.0	0.51377E-03
27	0.10986E+00	0.0	0.15944E-02	0.0	0.35361E-03
28	0.79487E-01	0.0	0.76481E-03	0.0	0.21649E-03
29	0.44824E-01	0.0	0.58464E-03	0.0	0.12112E-03
30	0.35053E-01	0.0	0.24515E-03	0.0	0.64754E-04
31	0.27755E-01	0.0	0.21876E-03	0.0	0.49906E-04
32	0.33067E-01	0.0	0.21151E-03	0.0	0.59918E-04
33	0.50684E-01	0.0	0.43834E-03	0.0	0.95239E-04

BAY	IYY	IZZ	IXY	IYZ	IXZ
21	0.15044E-02	0.17771E-02	0.0	0.0	0.0
22	0.90520E-03	0.51386E-02	0.0	0.0	0.0
23	0.60911E-03	0.22627E-02	0.0	0.0	0.0
24	0.19243E-03	0.11981E-02	0.0	0.0	0.0
25	0.18192E-03	0.12267E-02	0.0	0.0	0.0
26	0.77088E-04	0.59071E-03	0.0	0.0	0.0
27	0.53144E-04	0.40675E-03	0.0	0.0	0.0
28	0.32412E-04	0.24908E-03	0.0	0.0	0.0
29	0.18104E-04	0.13928E-03	0.0	0.0	0.0
30	0.96360E-05	0.74460E-04	0.0	0.0	0.0
31	0.75920E-05	0.57524E-04	0.0	0.0	0.0
32	0.90520E-05	0.68912E-04	0.0	0.0	0.0
33	0.47596E-04	0.14279E-03	0.0	0.0	0.0

TABLE 7
MODEL MASS AND INERTIA DATA WING BAYS 12.5-PERCENT FUEL

MODE NO. 19664

BAY	MASS	MX	MY	MZ	IXX
21	0.61627E+00	0.0	-0.11636E-03	0.0	0.26115E-02
22	0.71751E+00	0.0	0.18881E-01	0.0	0.47192E-02
23	0.39817E+00	0.0	0.56035E-02	0.0	0.19870E-02
24	0.19863E+00	0.0	0.31653E-02	0.0	0.10673E-02
25	0.19744E+00	0.0	0.54109E-02	0.0	0.10812E-02
26	0.12050E+00	0.0	0.18879E-02	0.0	0.51377E-03
27	0.10986E+00	0.0	0.15944E-02	0.0	0.35361E-03
28	0.79487E-01	0.0	0.76481E-03	0.0	0.21649E-03
29	0.87883E-01	0.0	0.58464E-03	0.0	0.13631E-03
30	0.58640E-01	0.0	0.24515E-03	0.0	0.77602E-04
31	0.36977E-01	0.0	0.21876E-03	0.0	0.54578E-04
32	0.35017E-01	0.0	0.21151E-03	0.0	0.60502E-04
33	0.50684E-01	0.0	0.43834E-03	0.0	0.95239E-04

BAY	IYY	IZZ	IXY	IYZ	IXZ
21	0.16034E-02	0.18548E-02	0.0	0.0	0.0
22	0.92739E-03	0.51719E-02	0.0	0.0	0.0
23	0.69759E-03	0.23512E-02	0.0	0.0	0.0
24	0.19476E-03	0.12004E-02	0.0	0.0	0.0
25	0.18192E-03	0.12267E-02	0.0	0.0	0.0
26	0.77088E-04	0.59071E-03	0.0	0.0	0.0
27	0.53144E-04	0.40675E-03	0.0	0.0	0.0
28	0.32412E-04	0.24908E-03	0.0	0.0	0.0
29	0.33580E-04	0.15476E-03	0.0	0.0	0.0
30	0.20148E-04	0.87600E-04	0.0	0.0	0.0
31	0.11680E-04	0.62196E-04	0.0	0.0	0.0
32	0.10103E-04	0.70138E-04	0.0	0.0	0.0
33	0.47596E-04	0.14279E-03	0.0	0.0	0.0

TABLE 8
MODEL MASS AND INERTIA DATA WING BAYS 15-PERCENT FUEL

MODE NO. 19665

BAY	MASS	MX	MY	MZ	IXX
21	0.65373E+00	0.0	-0.11636E-03	0.0	0.30597E-02
22	0.72449E+00	0.0	0.18881E-01	0.0	0.47414E-02
23	0.39817E+00	0.0	0.56035E-02	0.0	0.19870E-02
24	0.19863E+00	0.0	0.31653E-02	0.0	0.10673E-02
25	0.19744E+00	0.0	0.54109E-02	0.0	0.10812E-02
26	0.12050E+00	0.0	0.18879E-02	0.0	0.51377E-03
27	0.10986E+00	0.0	0.15944E-02	0.0	0.35361E-03
28	0.79487E-01	0.0	0.76481E-03	0.0	0.21649E-03
29	0.11727E+00	0.0	0.58464E-03	0.0	0.14331E-03
30	0.82290E-01	0.0	0.24515E-03	0.0	0.84026E-04
31	0.56231E-01	0.0	0.21876E-03	0.0	0.61878E-04
32	0.51092E-01	0.0	0.21151E-03	0.0	0.64590E-04
33	0.52204E-01	0.0	0.43834E-03	0.0	0.95297E-04

BAY	IYY	IZZ	IXY	IYZ	IXZ
21	0.19377E-02	0.21170E-02	0.0	0.0	0.0
22	0.93819E-03	0.51885E-02	0.0	0.0	0.0
23	0.69817E-03	0.46928E-01	0.0	0.0	0.0
24	0.19476E-03	0.12004E-02	0.0	0.0	0.0
25	0.18200E-03	0.12266E-02	0.0	0.0	0.0
26	0.77088E-04	0.59071E-03	0.0	0.0	0.0
27	0.53144E-04	0.40675E-03	0.0	0.0	0.0
28	0.32412E-04	0.24908E-03	0.0	0.0	0.0
29	0.40529E-04	0.16171E-03	0.0	0.0	0.0
30	0.25462E-04	0.94257E-04	0.0	0.0	0.0
31	0.18046E-04	0.69291E-04	0.0	0.0	0.0
32	0.17462E-04	0.78606E-04	0.0	0.0	0.0
33	0.47713E-04	0.14293E-03	0.0	0.0	0.0

TABLE 9
MODEL MASS AND INERTIA DATA WING BAYS 17.5-PERCENT FUEL

MODE NO. 19666

BAY	MASS	MX	MY	MZ	IXX
21	0.68948E+00	0.0	-0.11636E-03	0.0	0.31441E-02
22	0.73203E+00	0.0	0.18881E-01	0.0	0.47860E-02
23	0.39817E+00	0.0	0.56035E-02	0.0	0.19870E-02
24	0.19863E+00	0.0	0.31653E-02	0.0	0.10673E-02
25	0.19744E+00	0.0	0.54109E-02	0.0	0.10812E-02
26	0.12050E+00	0.0	0.18879E-02	0.0	0.51377E-03
27	0.10986E+00	0.0	0.15944E-02	0.0	0.35361E-03
28	0.79487E-01	0.0	0.76481E-03	0.0	0.21649E-03
29	0.13971E+00	0.0	0.58464E-03	0.0	0.15295E-03
30	0.10269E+00	0.0	0.24515E-03	0.0	0.10242E-03
31	0.74575E-01	0.0	0.21876E-03	0.0	0.66258E-04
32	0.72021E-01	0.0	0.21151E-03	0.0	0.69846E-04
33	0.59497E-01	0.0	0.43834E-03	0.0	0.96698E-04

BAY	IYY	IZZ	IXY	IYZ	IXZ
21	0.20005E-02	0.21661E-02	0.0	0.0	0.0
22	0.96039E-03	0.52221E-02	0.0	0.0	0.0
23	0.69817E-03	0.23518E-02	0.0	0.0	0.0
24	0.19476E-03	0.12004E-02	0.0	0.0	0.0
25	0.18200E-03	0.12266E-02	0.0	0.0	0.0
26	0.77088E-04	0.59071E-03	0.0	0.0	0.0
27	0.53144E-04	0.40675E-03	0.0	0.0	0.0
28	0.32412E-04	0.24908E-03	0.0	0.0	0.0
29	0.50253E-04	0.17143E-03	0.0	0.0	0.0
30	0.40588E-04	0.11315E-03	0.0	0.0	0.0
31	0.21871E-04	0.73613E-04	0.0	0.0	0.0
32	0.26922E-04	0.89527E-04	0.0	0.0	0.0
33	0.50487E-04	0.14641E-03	0.0	0.0	0.0

TABLE 10
MODEL MASS AND INERTIA DATA WING BAYS 21.5-PERCENT FUEL

MODE NO. 19667

BAY	MASS	MX	MY	MZ	IXX
21	0.72536E+00	0.0	-0.11636E-03	0.0	0.32912E-02
22	0.74164E+00	0.0	0.18881E-01	0.0	0.48602E-02
23	0.39817E+00	0.0	0.56035E-02	0.0	0.19870E-02
24	0.19863E+00	0.0	0.31653E-02	0.0	0.10673E-02
25	0.19744E+00	0.0	0.54109E-02	0.0	0.10812E-02
26	0.12050E+00	0.0	0.18879E-02	0.0	0.51377E-03
27	0.10986E+00	0.0	0.15944E-02	0.0	0.35361E-03
28	0.79487E-01	0.0	0.76481E-03	0.0	0.21649E-03
29	0.15890E+00	0.0	0.58464E-03	0.0	0.17894E-03
30	0.12669E+00	0.0	0.24515E-03	0.0	0.10739E-03
31	0.10422E+00	0.0	0.21876E-03	0.0	0.10334E-03
32	0.11466E+00	0.0	0.21151E-03	0.0	0.81030E-04
33	0.81936E-01	0.0	0.43834E-03	0.0	0.10111E-03

BAY	IYY	IZZ	IXY	IYZ	IXZ
21	0.21104E-02	0.22524E-02	0.0	0.0	0.0
22	0.99709E-03	0.52775E-02	0.0	0.0	0.0
23	0.69808E-03	0.23517E-02	0.0	0.0	0.0
24	0.19476E-03	0.12004E-02	0.0	0.0	0.0
25	0.18200E-03	0.12266E-02	0.0	0.0	0.0
26	0.77088E-04	0.59071E-03	0.0	0.0	0.0
27	0.53144E-04	0.40675E-03	0.0	0.0	0.0
28	0.32412E-04	0.24908E-03	0.0	0.0	0.0
29	0.76475E-04	0.19765E-03	0.0	0.0	0.0
30	0.44705E-04	0.11823E-03	0.0	0.0	0.0
31	0.54283E-04	0.11011E-03	0.0	0.0	0.0
32	0.47041E-04	0.11271E-03	0.0	0.0	0.0
33	0.59276E-04	0.15745E-03	0.0	0.0	0.0

TABLE 11
MODEL MASS AND INERTIA DATA WING BAYS 40-PERCENT FUEL

MODE NO. 19668

BAY	MASS	MX	MY	MZ	IXX
21	0.10093E+01	0.0	-0.11636E-03	0.0	0.56894E-02
22	0.93042E+00	0.0	0.18881E-01	0.0	0.53584E-02
23	0.59461E+00	0.0	0.56035E-02	0.0	0.22264E-02
24	0.39006E+00	0.0	0.31653E-02	0.0	0.12823E-02
25	0.32463E+00	0.0	0.54109E-02	0.0	0.11805E-02
26	0.14028E+00	0.0	0.18879E-02	0.0	0.55699E-03
27	0.10986E+00	0.0	0.15944E-02	0.0	0.35361E-03
28	0.79487E-01	0.0	0.76481E-03	0.0	0.21649E-03
29	0.15890E+00	0.0	0.58464E-03	0.0	0.17894E-03
30	0.12669E+00	0.0	0.24515E-03	0.0	0.10739E-03
31	0.10422E+00	0.0	0.21876E-03	0.0	0.10334E-03
32	0.11466E+00	0.0	0.21151E-03	0.0	0.81030E-04
33	0.81936E-01	0.0	0.43834E-03	0.0	0.10111E-03

BAY	IYY	IZZ	IXY	IYZ	IXZ
21	0.38994E-02	0.36553E-02	0.0	0.0	0.0
22	0.12437E-02	0.56507E-02	0.0	0.0	0.0
23	0.10213E-02	0.26749E-02	0.0	0.0	0.0
24	0.34757E-03	0.13240E-02	0.0	0.0	0.0
25	0.25497E-03	0.12915E-02	0.0	0.0	0.0
26	0.91863E-04	0.61329E-03	0.0	0.0	0.0
27	0.53144E-04	0.40675E-03	0.0	0.0	0.0
28	0.32412E-04	0.24908E-03	0.0	0.0	0.0
29	0.76475E-04	0.19765E-03	0.0	0.0	0.0
30	0.44676E-04	0.11823E-03	0.0	0.0	0.0
31	0.54283E-04	0.11011E-03	0.0	0.0	0.0
32	0.47041E-04	0.11271E-03	0.0	0.0	0.0
33	0.59276E-04	0.15745E-03	0.0	0.0	0.0

TABLE 12
MODEL MASS AND INERTIA DATA WING BAYS 60-PERCENT FUEL

MODE NO. 19669

BAY	MASS	MX	MY	MZ	IXX
21	0.12567E+01	0.0	-0.11636E-03	0.0	0.62921E-02
22	0.10995E+01	0.0	0.18881E-01	0.0	0.57140E-02
23	0.74229E+00	0.0	0.56035E-02	0.0	0.22375E-02
24	0.54260E+00	0.0	0.31653E-02	0.0	0.13646E-02
25	0.47899E+00	0.0	0.54109E-02	0.0	0.12941E-02
26	0.24384E+00	0.0	0.18879E-02	0.0	0.61480E-03
27	0.17625E+00	0.0	0.15944E-02	0.0	0.39245E-03
28	0.97621E-01	0.0	0.76481E-03	0.0	0.22531E-03
29	0.15890E+00	0.0	0.58464E-03	0.0	0.17894E-03
30	0.12669E+00	0.0	0.24515E-03	0.0	0.10739E-03
31	0.10422E+00	0.0	0.21876E-03	0.0	0.10334E-03
32	0.11466E+00	0.0	0.21151E-03	0.0	0.81030E-04
33	0.81936E-01	0.0	0.43834E-03	0.0	0.10111E-03

BAY	IYY	IZZ	IXY	IYZ	IXZ
21	0.43490E-02	0.40079E-02	0.0	0.0	0.0
22	0.14197E-02	0.59170E-02	0.0	0.0	0.0
23	0.10363E-02	0.26899E-02	0.0	0.0	0.0
24	0.40611E-03	0.14118E-02	0.0	0.0	0.0
25	0.33846E-03	0.13656E-02	0.0	0.0	0.0
26	0.11163E-03	0.64345E-03	0.0	0.0	0.0
27	0.66430E-04	0.42714E-03	0.0	0.0	0.0
28	0.39186E-04	0.25813E-03	0.0	0.0	0.0
29	0.76504E-04	0.19768E-03	0.0	0.0	0.0
30	0.44676E-04	0.11823E-03	0.0	0.0	0.0
31	0.54283E-04	0.11011E-03	0.0	0.0	0.0
32	0.47041E-04	0.11271E-03	0.0	0.0	0.0
33	0.59276E-04	0.15745E-03	0.0	0.0	0.0

TABLE 13
MODEL MASS AND INERTIA DATA WING BAYS 80-PERCENT FUEL

MODE NO. 19670

BAY	MASS	MX	MY	MZ	IXX
21	0.14902E+01	0.0	-0.11636E-03	0.0	0.68805E-02
22	0.12481E+01	0.0	0.18881E-01	0.0	0.60279E-02
23	0.82825E+00	0.0	0.56035E-02	0.0	0.22466E-02
24	0.65909E+00	0.0	0.31653E-02	0.0	0.14697E-02
25	0.63690E+00	0.0	0.54109E-02	0.0	0.13174E-02
26	0.37166E+00	0.0	0.18879E-02	0.0	0.62561E-03
27	0.31218E+00	0.0	0.15944E-02	0.0	0.44588E-03
28	0.17414E+00	0.0	0.76481E-03	0.0	0.24715E-03
29	0.15890E+00	0.0	0.58464E-03	0.0	0.17894E-03
30	0.12669E+00	0.0	0.24515E-03	0.0	0.10739E-03
31	0.10422E+00	0.0	0.21876E-03	0.0	0.10334E-03
32	0.11466E+00	0.0	0.21151E-03	0.0	0.81030E-04
33	0.81936E-01	0.0	0.43834E-03	0.0	0.10111E-03

BAY	IYY	IZZ	IXY	IYZ	IXZ
21	0.47879E-02	0.43521E-02	0.0	0.0	0.0
22	0.15751E-02	0.61522E-02	0.0	0.0	0.0
23	0.10485E-02	0.27021E-02	0.0	0.0	0.0
24	0.48086E-03	0.14865E-02	0.0	0.0	0.0
25	0.35563E-03	0.13809E-02	0.0	0.0	0.0
26	0.11534E-03	0.64908E-03	0.0	0.0	0.0
27	0.84709E-04	0.45520E-03	0.0	0.0	0.0
28	0.55976E-04	0.28049E-03	0.0	0.0	0.0
29	0.76504E-04	0.19768E-03	0.0	0.0	0.0
30	0.44676E-04	0.11823E-03	0.0	0.0	0.0
31	0.54283E-04	0.11011E-03	0.0	0.0	0.0
32	0.47041E-04	0.11271E-03	0.0	0.0	0.0
33	0.59276E-04	0.15739E-03	0.0	0.0	0.0

TABLE 14
MODEL MASS AND INERTIA DATA WING BAYS 100-PERCENT FUEL

MODE NO. 19671

BAY	MASS	MX	MY	MZ	IXX
21	0.20752E+01	0.0	-0.11636E-03	0.0	0.74645E-02
22	0.15826E+01	0.0	0.18881E-01	0.0	0.65015E-02
23	0.82941E+00	0.0	0.56035E-02	0.0	0.23015E-02
24	0.67140E+00	0.0	0.31653E-02	0.0	0.14986E-02
25	0.66596E+00	0.0	0.54109E-02	0.0	0.14050E-02
26	0.40270E+00	0.0	0.18879E-02	0.0	0.69277E-03
27	0.33769E+00	0.0	0.15944E-02	0.0	0.48151E-03
28	0.19288E+00	0.0	0.76481E-03	0.0	0.26204E-03
29	0.15890E+00	0.0	0.58464E-03	0.0	0.17894E-03
30	0.12669E+00	0.0	0.24515E-03	0.0	0.10739E-03
31	0.10422E+00	0.0	0.21876E-03	0.0	0.10334E-03
32	0.11466E+00	0.0	0.21151E-03	0.0	0.81030E-04
33	0.81936E-01	0.0	0.43834E-03	0.0	0.10111E-03

| BAY	IYY	IZZ	IXY	IYZ	IXZ
21	0.52259E-02	0.46951E-02	0.0	0.0	0.0
22	0.18095E-02	0.65057E-02	0.0	0.0	0.0
23	0.11239E-02	0.27775E-02	0.0	0.0	0.0
24	0.50136E-03	0.15070E-02	0.0	0.0	0.0
25	0.41989E-03	0.14381E-02	0.0	0.0	0.0
26	0.13841E-03	0.68415E-03	0.0	0.0	0.0
27	0.96944E-04	0.47391E-03	0.0	0.0	0.0
28	0.67452E-04	0.29580E-03	0.0	0.0	0.0
29	0.76504E-04	0.19768E-03	0.0	0.0	0.0
30	0.44676E-04	0.11826E-03	0.0	0.0	0.0
31	0.54312E-04	0.11008E-03	0.0	0.0	0.0
32	0.47012E-04	0.11271E-03	0.0	0.0	0.0
33	0.59276E-04	0.15739E-03	0.0	0.0	0.0
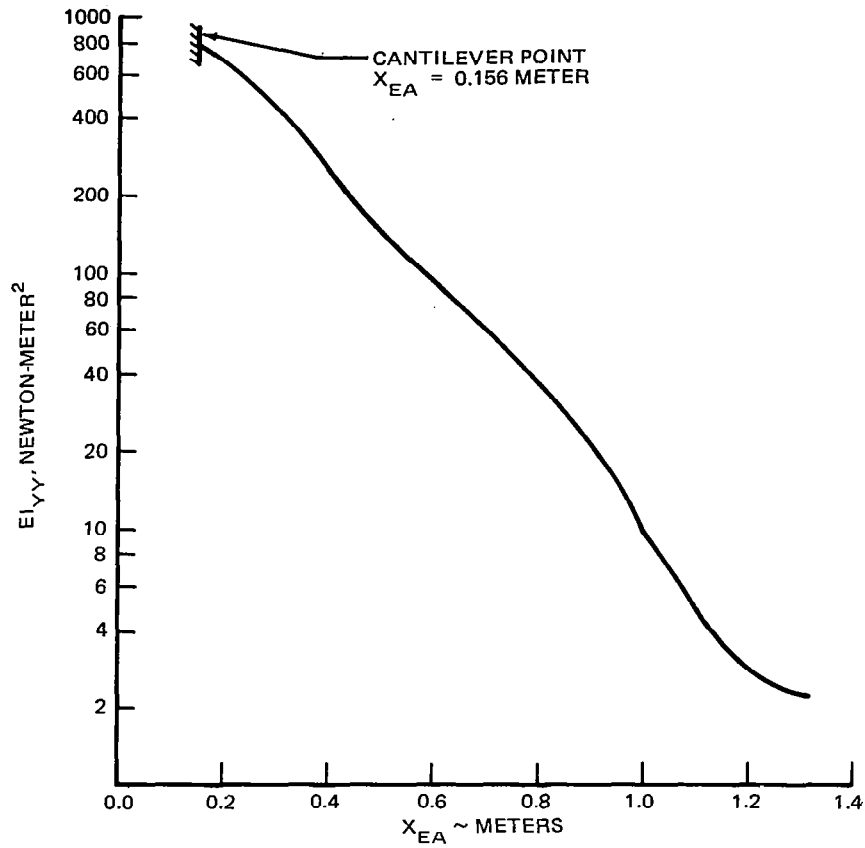
FIGURE 112. WING VERTICAL BENDING RIGIDITY FOR WINGLET FLUTTER MODEL
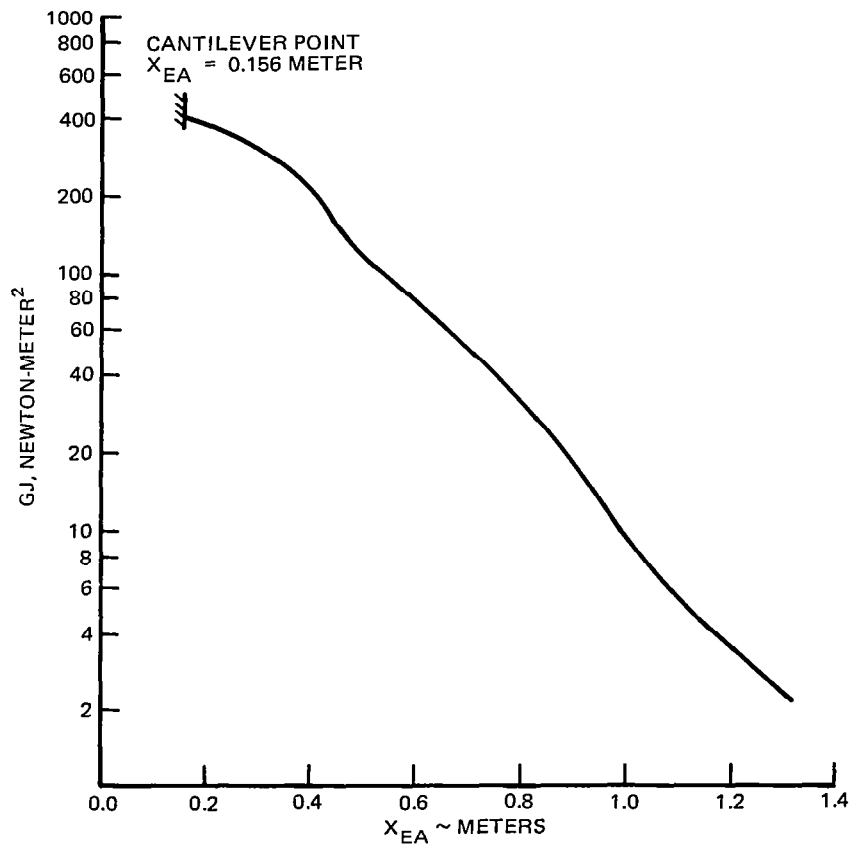
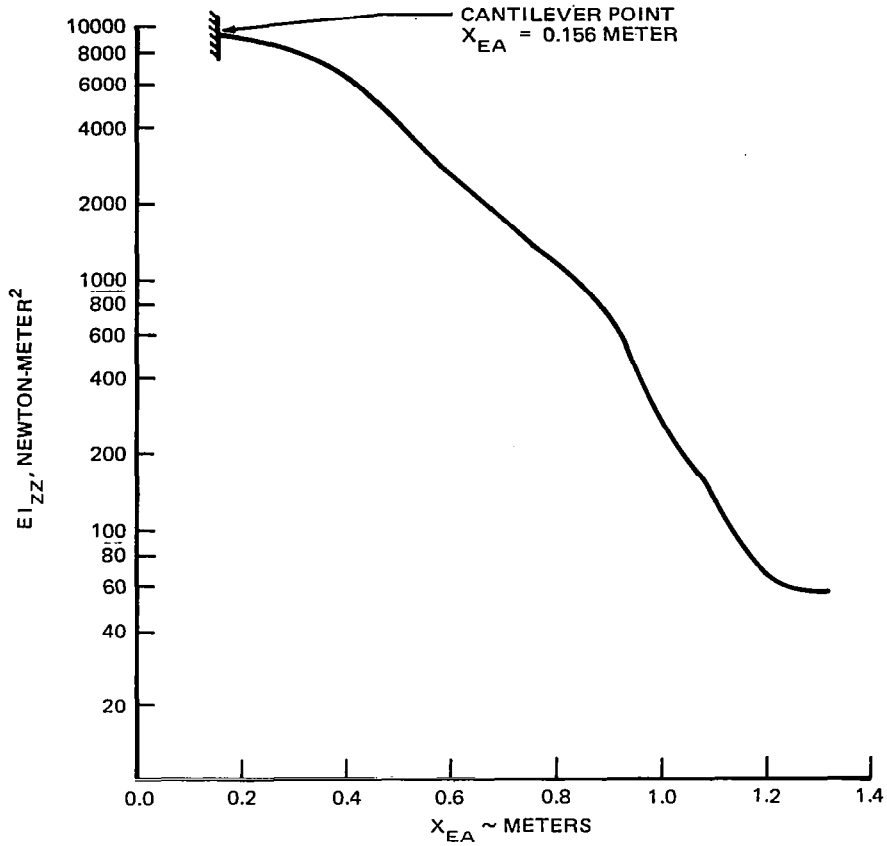**FIGURE 113. WING TORSIONAL RIGIDITY FOR WINGLET FLUTTER MODEL**

CANTILEVER POINT
X_{EA} = 0.156 METER

EI$_{ZZ}$, NEWTON-METER^2

10000
8000
6000
4000
2000
1000
800
600
400
200
100
80
60
40
20

0.0   0.2   0.4   0.6   0.8   1.0   1.2   1.4

X_{EA} ~ METERS

FIGURE 114. WING LONGITUDINAL BENDING RIGIDITY FOR WINGLET FLUTTER MODEL

TABLE 15

COMPONENT PYLON MODE SHAPES AND FREQUENCIES[1]

MODE	1	2	3
FREQUENCY	6.655	16.244	22.794
h	2.125×10^{-4}	1.0	7.757×10^{-2}
α_F	$- 5.513 \times 10^{-5}$	-2.296×10^{-1}	$- 1.557 \times 10^{-2}$
θ	$- 5.586 \times 10^{-2}$	-1.879×10^{-2}	1.0
f	$- 8.806 \times 10^{-5}$	-3.644×10^{-1}	$- 2.473 \times 10^{-2}$
l	1.0	8.61×10^{-3}	$- 8.196 \times 10^{-1}$
ψ	$- 2.052 \times 10^{-1}$	7.672×10^{-3}	$- 5.56 \times 10^{-1}$

(1) ALL FREQUENCIES IN Hz; RIGID WING

The entire fuel schedule was analyzed without the winglets, with the basic winglets at 75 degrees dihedral, and with winglet mass only (no winglet aerodynamic effects). Results were summarized in plots of flutter speed as a function of fuel state for each configuration. Typical frequency and damping trends were summarized.

A further case was analyzed and tested at 10 percent fuel with a softer-than-design engine pylon. This was done to stabilize the lower frequency flutter mode and thereby measure the flutter speed of the high-frequency mode at low fuel states. Parametric studies which were tested but not analyzed included winglet dihedral variations, wing angle-of-attack variation, and engine weight variation.

Results and Discussion

Vibration modes — Table 15 shows the calculated component pylon mode shapes and frequencies used in the analysis. The frequencies shown are the base case values. For pylon flexibility parametric studies, the tabulated shapes were retained and the modal frequencies varied. The base frequencies were verified by measurement.

Tables 16 and 17 show the calculated component wing frequencies for each fuel case, with and without winglets. These intermediate results were with a rigid pylon, and hence were not directly verified by measurement. The names applied are somewhat subjective since all the modes are fully coupled; i.e., they all exhibit normal and longitudinal bending and torsion simultaneously.

The orthogonal modes of the entire flexible system were calculated for zero and full fuel for comparison with ground vibration test results. Table 18 presents a comparison of theoretical and measured coupled orthogonal mode frequencies. The calculated and measured relative deflection shapes and mode lines for each mode are shown in Figures 115 through 118. The data show good agreement for all modes.

Flutter characteristics — In general, the flutter analyses showed that there were two significant flutter modes. The first, with a frequency varying between 11.2 and 12.9 Hertz depending on the fuel state, is known as "inner panel torsion" or "engine pitch." This remained the critical flutter mode for the configuration without winglets. Most of the strain energy in the mode is in the twist of the "inner panel" of the wing (inboard of the pylon) and in the pylon vertical bending. The flutter instability is caused by the coupling of this mode with wing first bending.

TABLE 16
COMPONENT WING MODE FREQUENCIES [1] FOR WINGLET CASES

FUEL MODE	MODE FREQUENCY				
	0%	10%	12-1/2%	15%	17-1/2%
1ST WING VERT BEND	5.64	5.64	5.37	5.00	4.64
2ND WING VERT BEND	14.98	14.89	14.13	13.61	13.18
INNER PANEL TORSION	20.44	20.33	20.27	20.22	20.17
WING FORE & AFT BEND	27.02	26.99	26.07	24.53	23.20
3RD WING VERT BEND	32.85	32.09	30.71	29.28	28.28
WING TORSION	36.20	36.06	35.00	33.88	33.06
MODE 7	58.86	56.66	55.19	52.83	50.53
MODE 8	60.27	59.80	58.71	59.39	57.11
MODE 9	74.84	73.83	72.68	69.05	70.33
MODE 10	90.03	85.79	82.04	79.39	77.20

FUEL MODE	21-1/2%	40%	60%	80%	100%
1ST WING VERT BEND	4.12	4.10	4.04	3.92	3.89
2ND WING VERT BEND	12.57	12.27	11.47	10.47	10.29
INNER PANEL TORSION	20.04	19.90	19.77	19.43	19.29
WING FORE & AFT BEND	20.96	20.82	20.43	19.91	19.80
3RD WING VERT BEND	27.06	24.44	22.13	20.77	20.53
WING TORSION	31.59	31.29	31.01	30.71	30.59
MODE 7	47.41	44.64	41.91	38.44	37.64
MODE 8	55.59	54.54	52.39	49.78	48.89
MODE 9	67.49	64.91	61.19	58.11	56.97
MODE 10	74.09	69.42	63.91	60.25	58.94

(1) ALL FREQUENCIES IN Hz; RIGID PYLON

The second flutter mode is an outer wing bending/torsion for the baseline (no winglet) case. However, the winglet, with its large offset center-of-gravity relative to the wing plane, caused a significant coupling with wing longitudinal bending. The large additional tip inertia about the wing elastic axis from the winglet also caused the frequency to be significantly lower than the baseline configuration.

The analysis/test correlation will be discussed first for the baseline configuration, then for the basic winglet configuration, and finally for the dummy (mass only) configuration. Following this discussion, the test results that were not analyzed — i.e., variations in winglet dihedral, wing angle of attack, and engine weight — will be addressed.

TABLE 17
COMPONENT WING MODE FREQUENCIES[1] FOR BASELINE (NO WINGLET) CASES

	MODE FREQUENCY				
MODE \ FUEL	0%	10%	12-1/2%	15%	17-1/2%
1ST WING VERT BEND	6.75	6.74	6.25	5.67	5.15
2ND WING VERT BEND	18.58	18.42	18.01	17.57	16.84
INNER PANEL TORSION	20.72	20.57	20.48	20.42	20.38
WING FORE & AFT BEND	33.40	33.31	30.96	27.90	25.85
3RD WING VERT BEND	40.16	38.86	36.23	34.44	33.05
WING TORSION	42.51	42.45	41.71	41.01	39.95
MODE 7	68.95	67.36	65.44	62.44	59.66
MODE 8	70.69	68.68	68.48	68.16	67.80
MODE 9	83.13	81.58	80.95	74.83	77.58
MODE 10	98.96	95.32	92.83	88.91	85.94

MODE \ FUEL	21-1/2%	40%	60%	80%	100%
1ST WING VERT BEND	4.46	4.44	4.36	4.19	4.15
2ND WING VERT BEND	15.49	14.85	13.52	12.13	11.90
INNER PANEL TORSION	20.30	20.13	20.02	19.93	19.83
WING FORE & AFT BEND	22.65	22.47	21.87	20.82	20.61
3RD WING VERT BEND	31.15	27.96	25.81	24.48	24.20
WING TORSION	37.70	37.49	37.18	36.84	36.54
MODE 7	55.47	52.33	48.11	43.65	42.66
MODE 8	66.65	65.14	62.54	58.08	57.18
MODE 9	72.99	69.22	64.28	62.25	50.88
MODE 10	81.35	76.29	71.76	67.97	66.20

(1) ALL FREQUENCIES IN Hz; RIGID PYLON

TABLE 18
SUMMARY OF TEST AND ANALYSIS MODAL FREQUENCIES FOR 0-PERCENT AND 100-PERCENT FUEL CASES[1]

MODE NAME	0% FUEL				100% FUEL			
	WITH WINGLET		WITHOUT WINGLET		WITH WINGLET		WITHOUT WINGLET	
	TEST	ANALYSIS	TEST	ANALYSIS	TEST	ANALYSIS	TEST	ANALYSIS
ENG YAW	6.65	6.64	6.58	6.57	6.66	6.64	6.67	6.64
1ST WG H	5.69	5.64	6.82	6.82	4.00	3.89	4.27	4.15
ENG PITCH[2]	13.22	13.02	13.22	13.06	13.12	13.02	13.14	13.05
2ND WG H	15.12	15.12	18.62	18.82	10.67	10.31	12.33	11.91
ENG ROLL	22.63	22.63	22.75	22.72	22.73	22.83	NOT MEASURED	22.51
WING F&A	27.68[3]	26.87[3]	34.05	33.80	19.95[3]	19.45[3]	21.25	20.71
3RD WG H	32.13	33.14	37.38	39.33	20.60	20.45	24.50	24.50
WG TORSION	37.47[3]	35.64[3]	NOT MEASURED	41.32	28.27[3]	29.25[3]	30.85	33.00

(1) ALL FREQUENCIES IN Hz
(2) ALSO REFERRED TO AS INNER PANEL TORSION MODE
(3) LARGE LONGITUDINAL BENDING/OUTER WING TORSION COUPLING

110

**ENGINE YAW
(PYLON SIDE BENDING)**

	MODEL	ANALYSIS
FUEL	0%	0%
FREQ	6.58	6.57
NODE	○——○	△——△
SHAPE	▬ ▬ ▬	▬ ▬ ▬ ▬
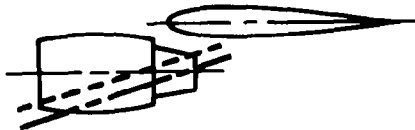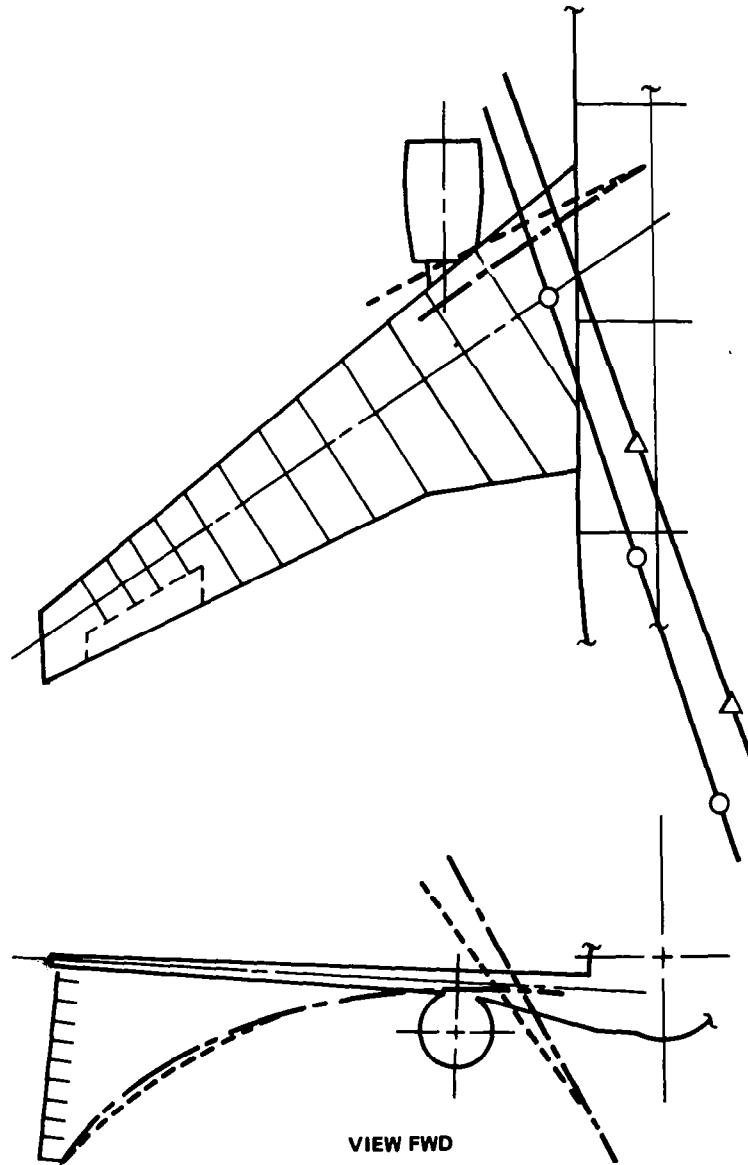
WING-ENGINE

VIEW FWD

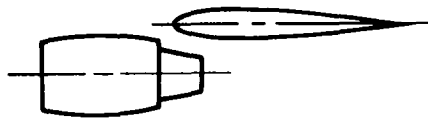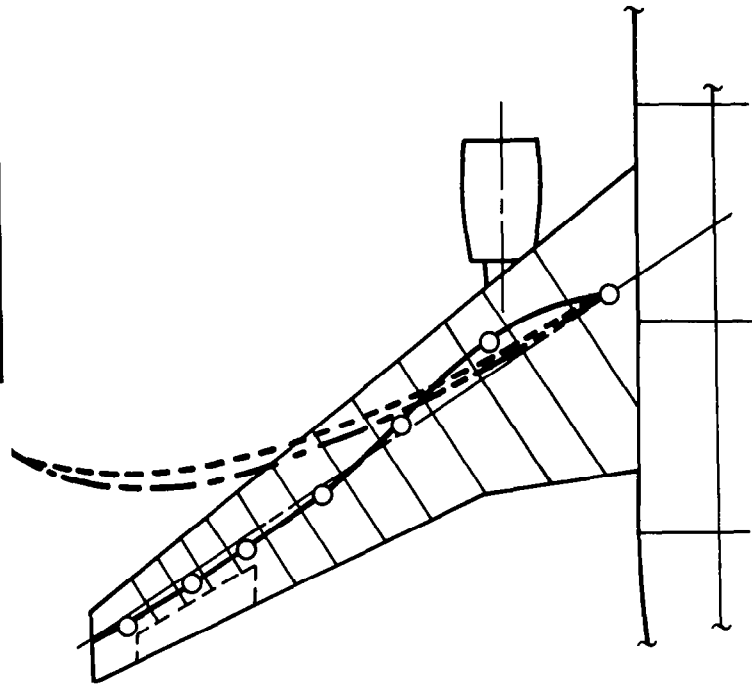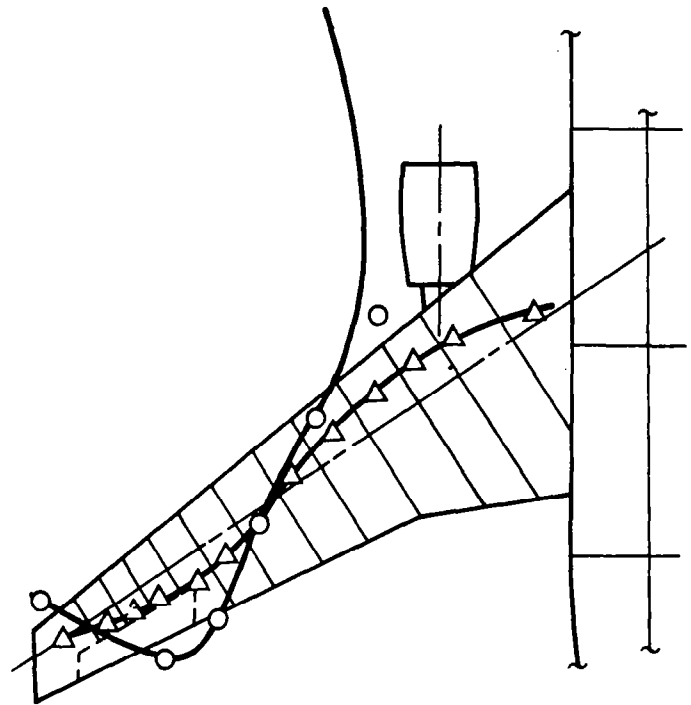FIGURE 115. FLUTTER MODEL VIBRATION MODES; ZERO FUEL WITHOUT WINGLETS (1 OF 8)
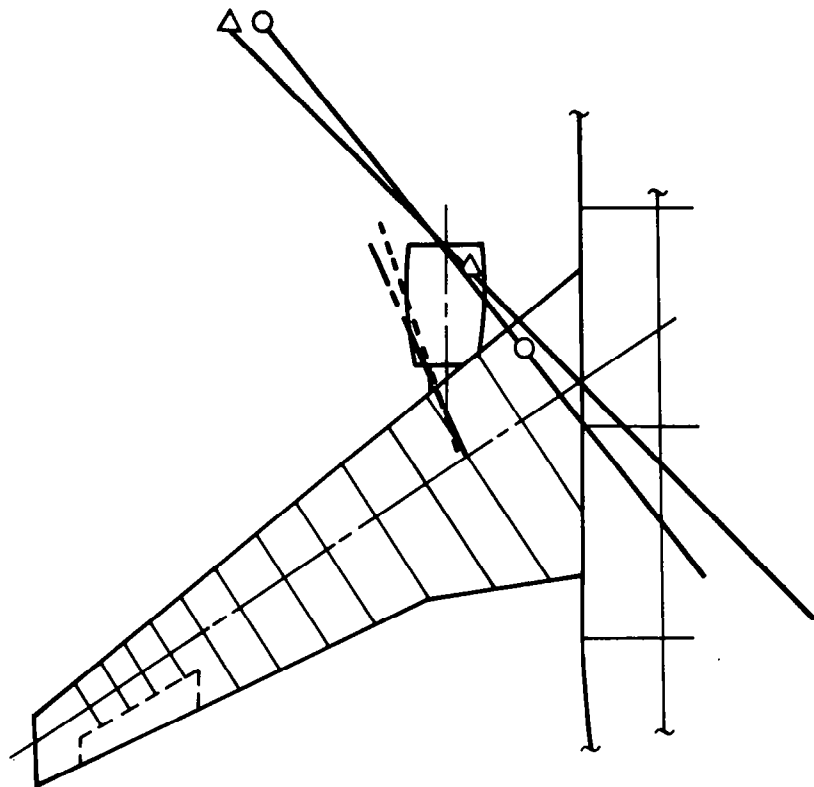
1ST WING BENDING

	MODEL	ANALYSIS
FUEL	0%	0%
FREQ	6.82	6.82
NODE	○———○	△———△
SHAPE	— — — —	— — — —

WING-ENGINE

VIEW FWD

FIGURE 115. FLUTTER MODEL VIBRATION MODES; ZERO FUEL WITHOUT WINGLETS (2 OF 8)

**ENGINE PITCH
(PYLON VERTICAL BENDING)**

	MODEL	ANALYSIS
FUEL	0%	0%
FREQ	13.22	13.06
NODE	○——○	△——△
SHAPE	▬ ▬ ▬	▬ ▬ ▬
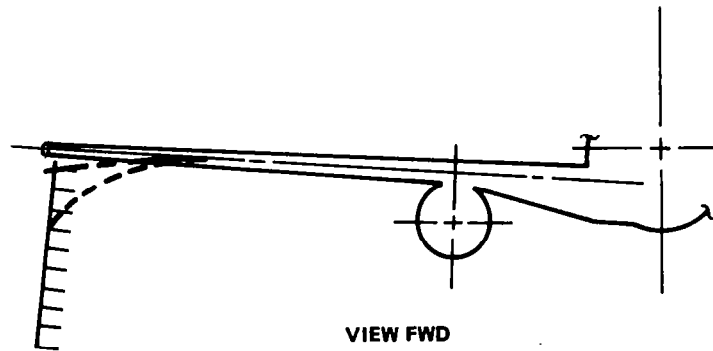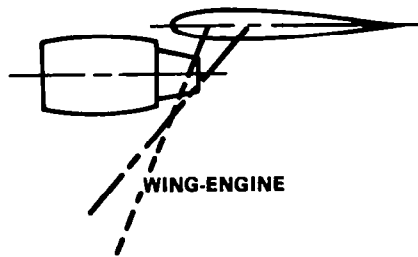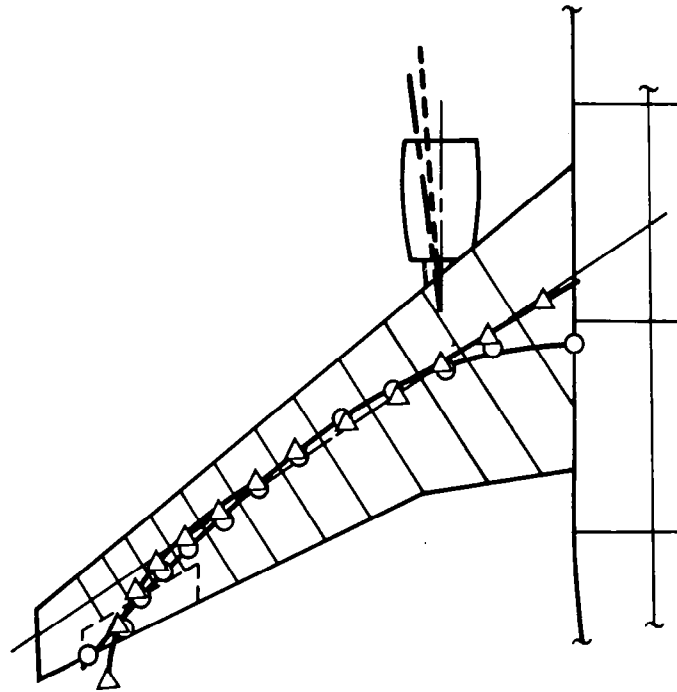
WING-ENGINE

VIEW FWD

FIGURE 115. FLUTTER MODEL VIBRATION MODES; ZERO FUEL WITHOUT WINGLETS (3 OF 8)

2ND WING BENDING

	MODEL	ANALYSIS
FUEL	0%	0%
FREQ	18.62	18.82
NODE	O———O	△———△
SHAPE	▬ ▬ ▬	▬ ▬ ▬
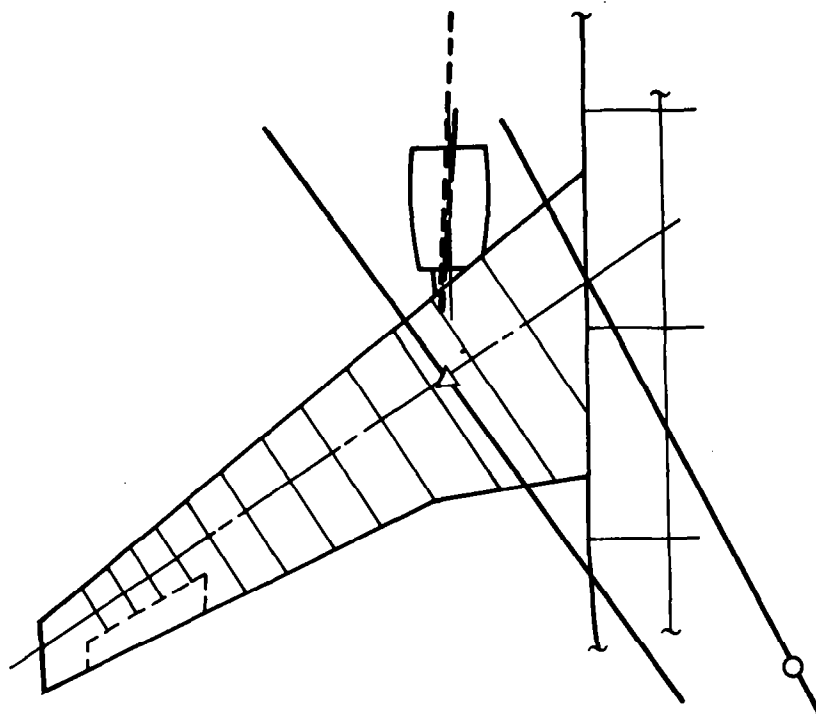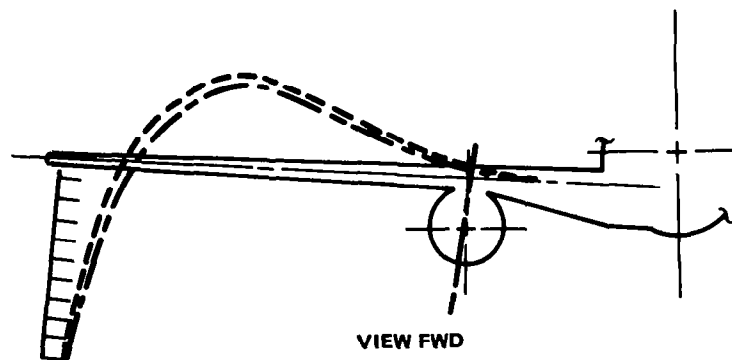
WING-ENGINE

VIEW FWD

FIGURE 115. FLUTTER MODEL VIBRATION MODES; ZERO FUEL WITHOUT WINGLETS (4 OF 8)

ENGINE ROLL
(PYLON TORSION)

	MODEL	ANALYSIS
FUEL	0%	0%
FREQ	22.75	22.72
NODE		
SHAPE		

WING-ENGINE

VIEW FWD

FIGURE 115. FLUTTER MODEL VIBRATION MODES; ZERO FUEL WITHOUT WINGLETS (5 OF 8)

1ST WING LONGITUDINAL BENDING

	MODEL	ANALYSIS
FUEL	0%	0%
FREQ	34.05	33.80
NODE	○——○	△——△
SHAPE	▬ ▬ ▬	▬ ▬ ▬

WING-ENGINE
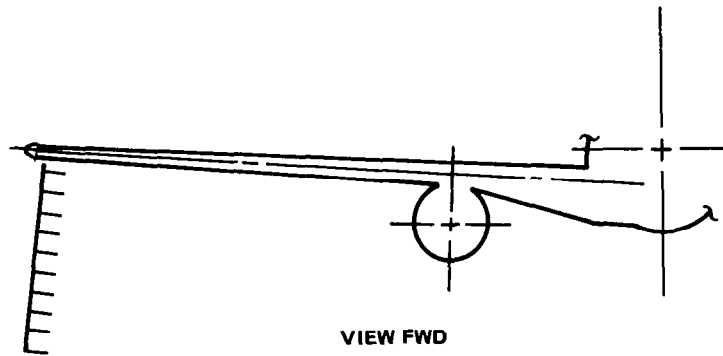
VIEW FWD

FIGURE 115. FLUTTER MODEL VIBRATION MODES; ZERO FUEL WITHOUT WINGLETS (6 OF 8)

3RD WING BENDING

	MODEL	ANALYSIS
FUEL	0%	0%
FREQ	37.38	39.33
NODE	O——O	△——△
SHAPE	— — —	— — —
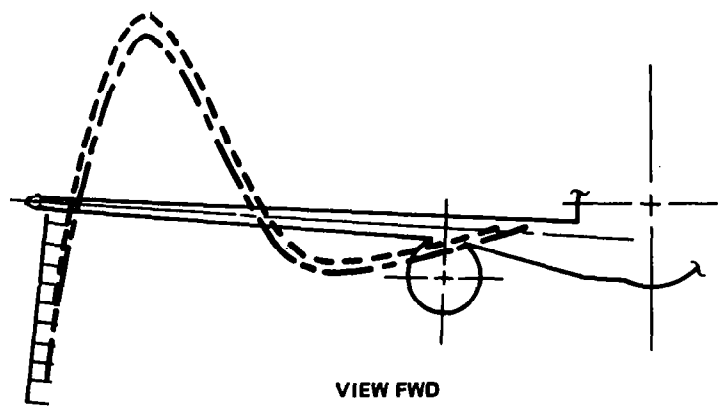
WING-ENGINE

VIEW FWD

FIGURE 115. FLUTTER MODEL VIBRATION MODES; ZERO FUEL WITHOUT WINGLETS (7 OF 8)

WING TORSION

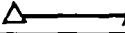|	MODEL	ANALYSIS
FUEL		0%
FREQ	NOT MEASURED	41.32
NODE	O———O	△———△
SHAPE	▬ ▬▬ ▬	▬ ▬ ▬ ▬
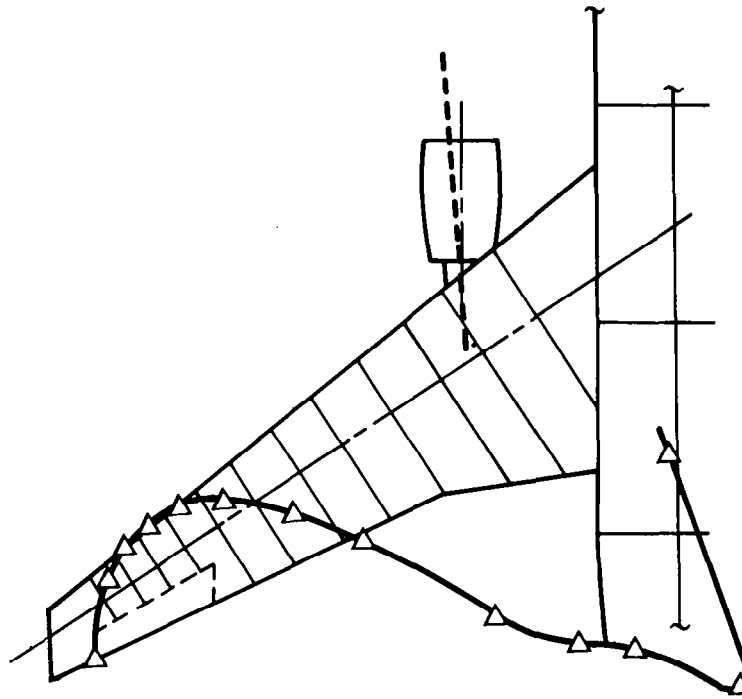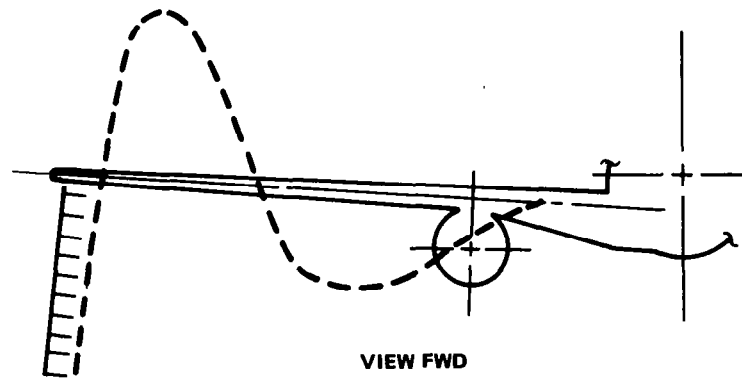
WING-ENGINE

VIEW FWD

FIGURE 115. FLUTTER MODEL VIBRATION MODES; ZERO FUEL WITHOUT WINGLETS (8 OF 8)

118

ENGINE YAW
(PYLON SIDE BENDING)

	MODEL	ANALYSIS
FUEL	0%	0%
FREQ	6.65	6.64
NODE	O———O	△———△
SHAPE	▬ ▬▬ ▬	▬ ▬ ▬ ▬

WING-ENGINE

VIEW FWD

FIGURE 116. FLUTTER MODEL VIBRATION MODES; ZERO FUEL WITH WINGLETS (1 OF 8)

1ST WING BENDING

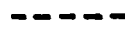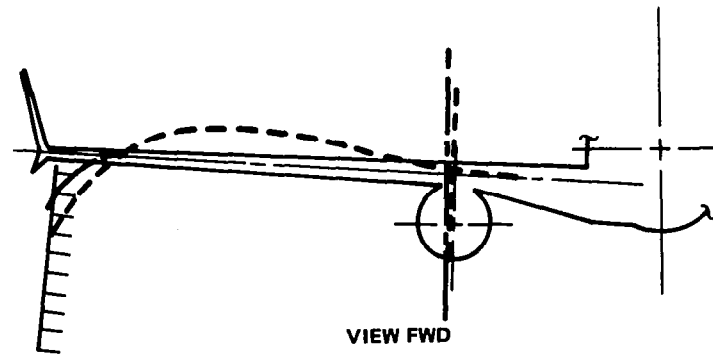|	MODEL	ANALYSIS
FUEL	0%	0%
FREQ	5.69	5.64
NODE	O——O	△——△
SHAPE	▬ ▬ ▬	▬ ▬ ▬ ▬

WING-ENGINE

VIEW FWD

FIGURE 116. FLUTTER MODEL VIBRATION MODES; ZERO FUEL WITH WINGLETS (2 OF 8)

ENGINE PITCH
(PYLON VERTICAL BENDING)

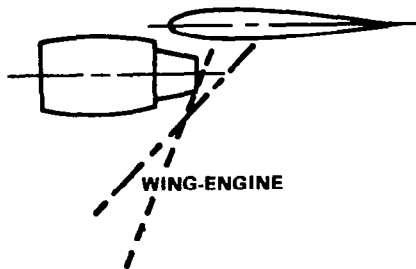|	MODEL	ANALYSIS
FUEL	0%	0%
FREQ	13.22	13.02
NODE	O——O	△——△
SHAPE	— — —	– – – –

WING-ENGINE

VIEW FWD

FIGURE 116. FLUTTER MODEL VIBRATION MODES; ZERO FUEL WITH WINGLETS (3 OF 8)

2ND WING BENDING

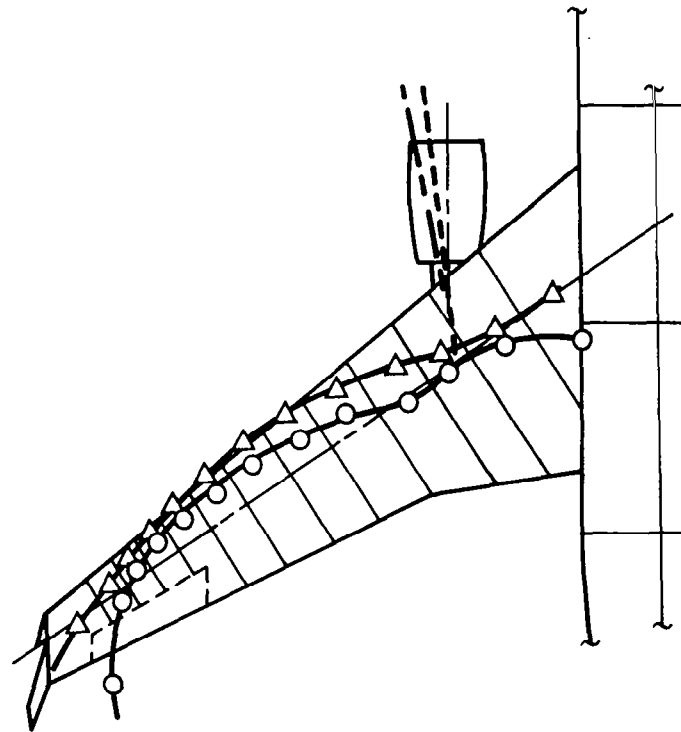|	MODEL	ANALYSIS
FUEL	0%	0%
FREQ	15.12	15.12
NODE	O———O	△————△
SHAPE	▬ ▬ ▬	▬ ▬ ▬ ▬

WING-ENGINE

VIEW FWD

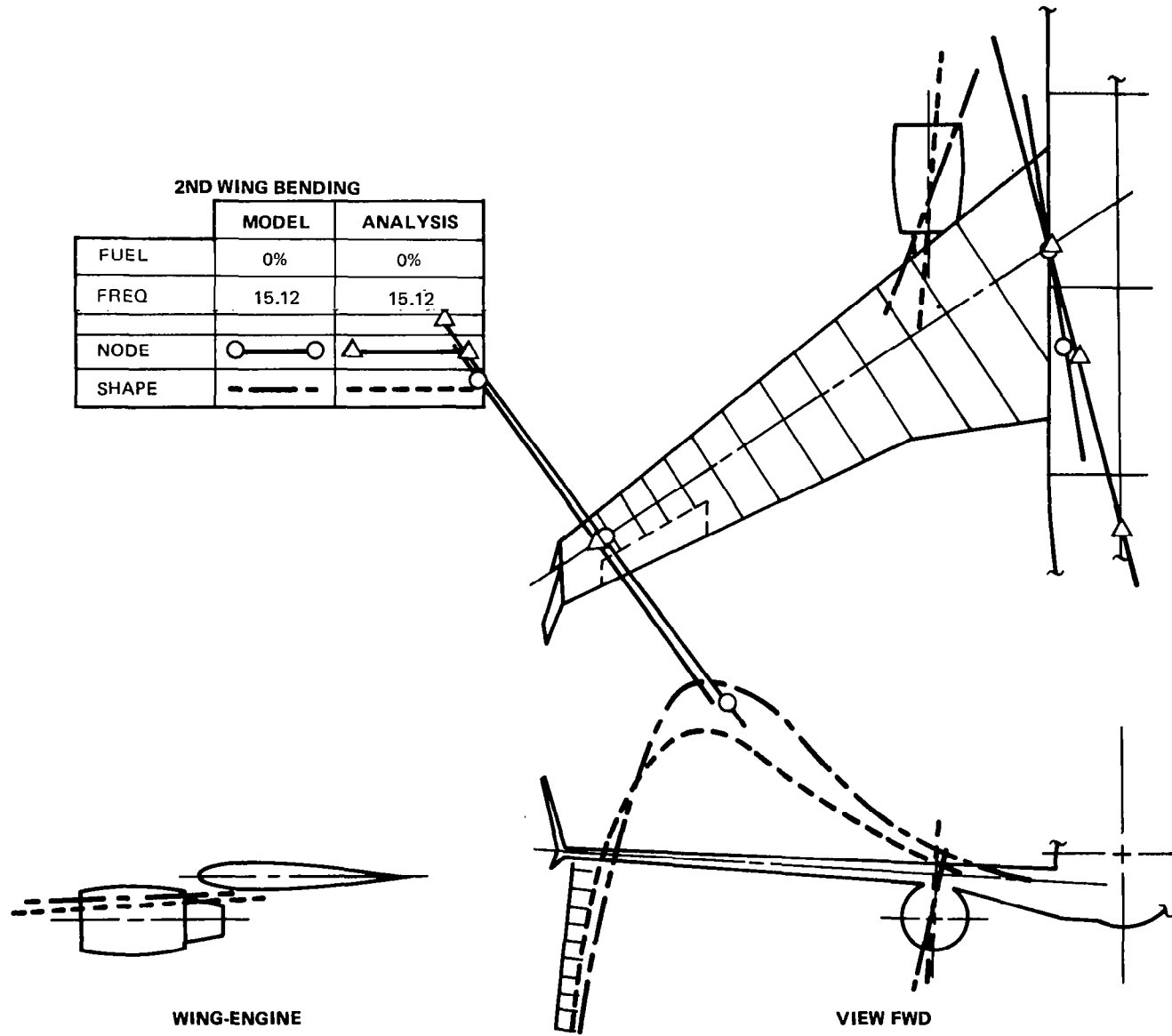**FIGURE 116. FLUTTER MODEL VIBRATION MODES; ZERO FUEL WITH WINGLETS (4 OF 8)**

ENGINE ROLL
(PYLON TORSION)

	MODEL	ANALYSIS
FUEL	0%	0%
FREQ	22.63	22.63
NODE	O———O	△———△
SHAPE	▬ ▬ ▬	▬ ▬ ▬

MODEL AND ANALYSIS

MODEL
ANALYSIS

WING-ENGINE

VIEW FWD

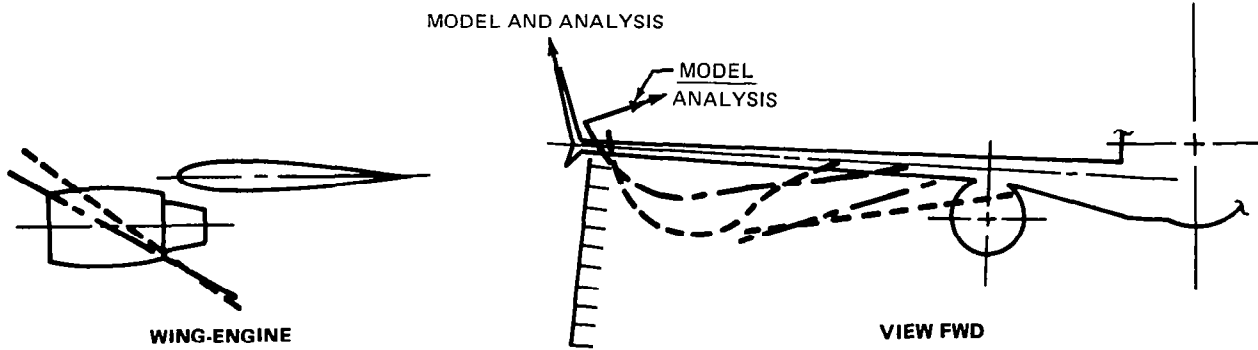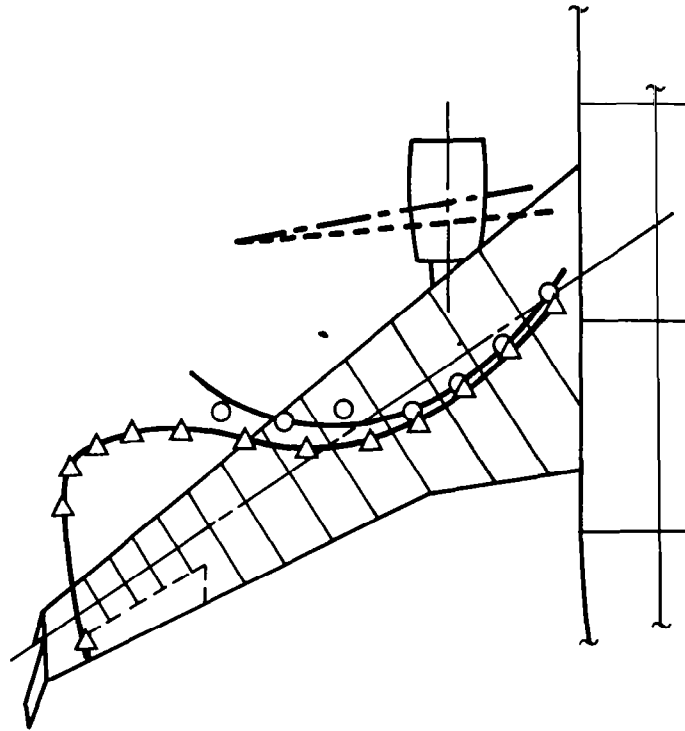FIGURE 116. FLUTTER MODEL VIBRATION MODES; ZERO FUEL WITH WINGLETS (5 OF 8)

1ST WING LONGITUDINAL BENDING

	MODEL	ANALYSIS
FUEL	0%	0%
FREQ	27.68	26.87
NODE	O———O	△————△
SHAPE	–––––	––––––

ANALYSIS

MODEL

MODEL
ANALYSIS

MODEL

ANALYSIS

WING-ENGINE

VIEW FWD

FIGURE 116. FLUTTER MODEL VIBRATION MODES; ZERO FUEL WITH WINGLETS (6 OF 8)

3RD WING BENDING

	MODEL	ANALYSIS
FUEL	0%	0%
FREQ	32.13	33.14
NODE	O——O	△——△
SHAPE	— — —	— — —
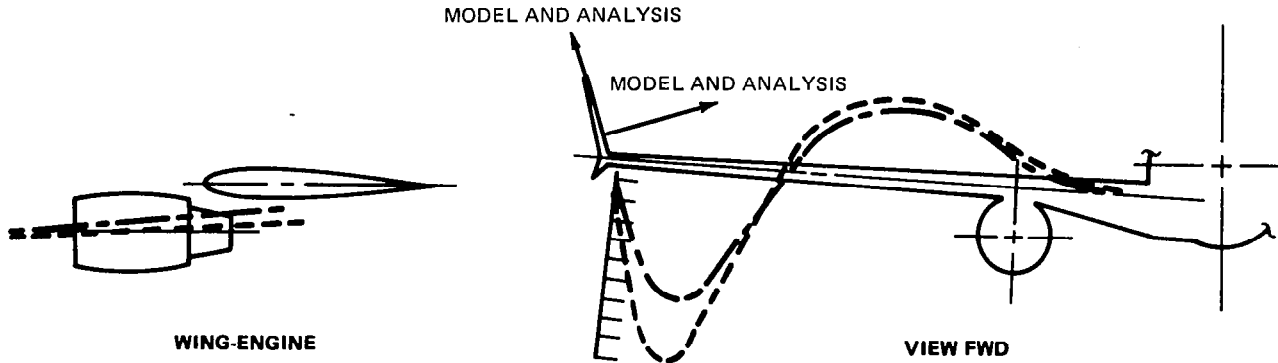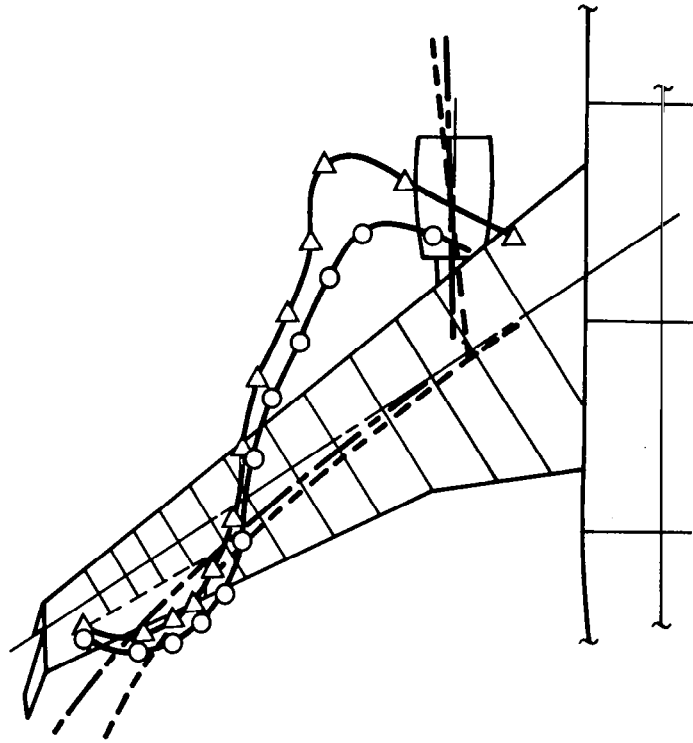
MODEL AND ANALYSIS

MODEL AND ANALYSIS

WING-ENGINE

VIEW FWD

FIGURE 116. FLUTTER MODEL VIBRATION MODES; ZERO FUEL WITH WINGLETS (7 OF 8)

WING TORSION

	MODEL	ANALYSIS
FUEL	0%	0%
FREQ	37.47	35.64
NODE	○——○	△——△
SHAPE	— - — - —	— — — — —

MODEL

ANALYSIS

MODEL AND ANALYSIS

MODEL

ANALYSIS

WING-ENGINE

VIEW FWD

FIGURE 116. FLUTTER MODEL VIBRATION MODES; ZERO FUEL WITH WINGLETS (8 OF 8)

ENGINE YAW
(PYLON SIDE BENDING)

	MODEL	ANALYSIS
FUEL	100%	100%
FREQ	6.67	6.64
NODE	O——O	△——△
SHAPE	▬ ▬ ▬ ▬	▬ ▬ ▬ ▬

WING-ENGINE

VIEW FWD

FIGURE 117. FLUTTER MODEL VIBRATION MODES; FULL FUEL WITHOUT WINGLETS (1 OF 8)

1ST WING BENDING

	MODEL	ANALYSIS
FUEL	100%	100%
FREQ	4.27	4.15
NODE	O—————O	△—————△
SHAPE	▬ ▬▬ ▬	▬▬▬▬ ▬
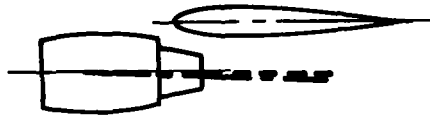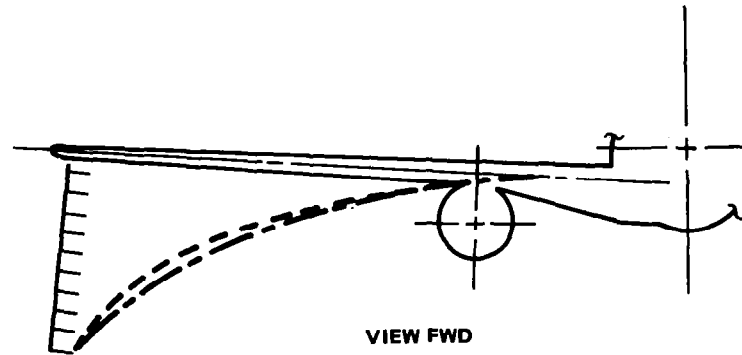
WING-ENGINE

VIEW FWD

FIGURE 117. FLUTTER MODEL VIBRATION MODES; FULL FUEL WITHOUT WINGLETS (2 OF 8)

ENGINE PITCH
(PYLON VERTICAL BENDING)

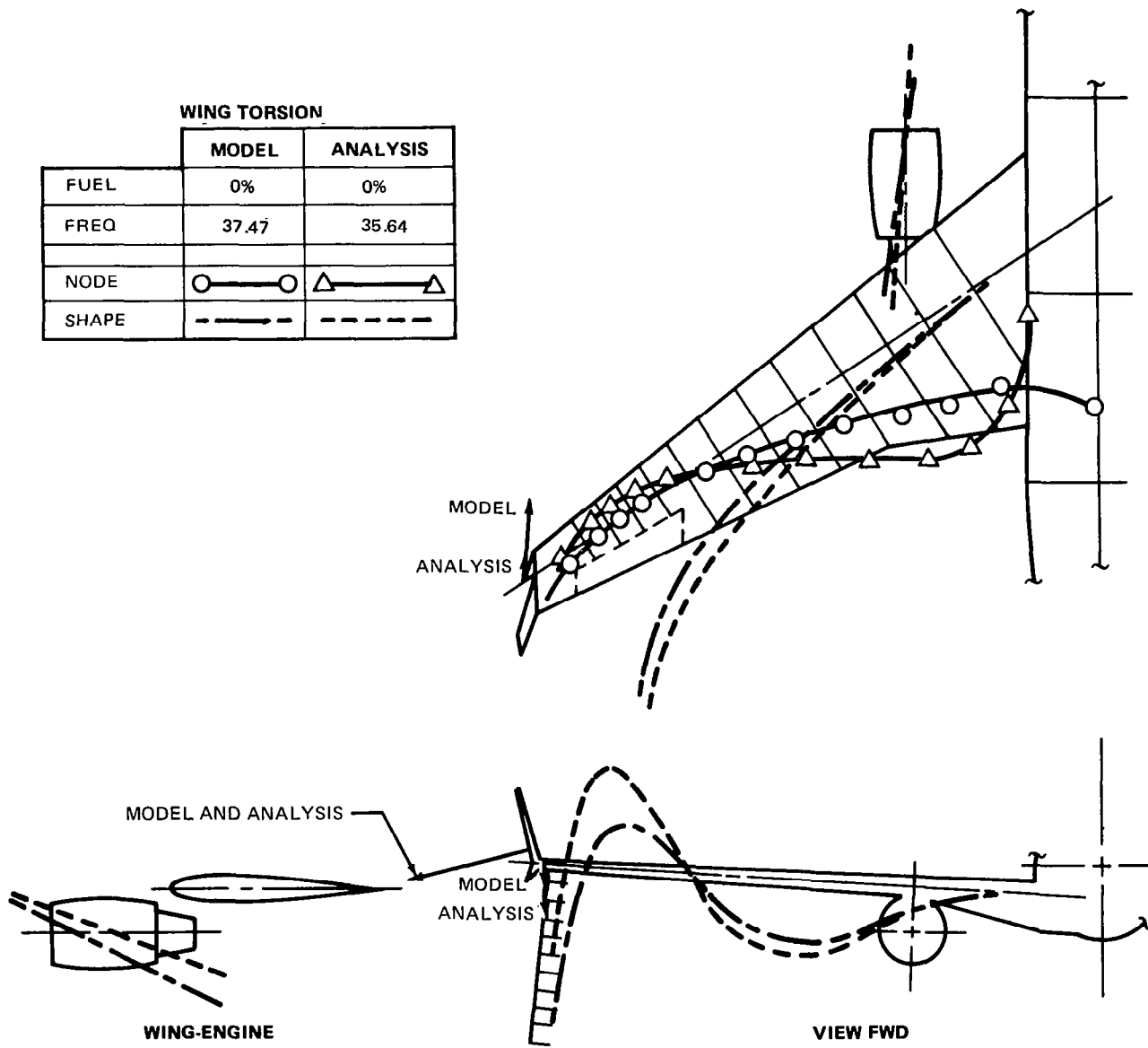|	MODEL	ANALYSIS
FUEL	100%	100%
FREQ	13.14	13.05
NODE	O———O	△———△
SHAPE	▬ ▬▬ ▬	▬ ▬ ▬ ▬

WING-ENGINE

VIEW FWD

FIGURE 117. FLUTTER MODEL VIBRATION MODES; FULL FUEL WITHOUT WINGLETS (3 OF 8)

2ND WING BENDING

	MODEL	ANALYSIS
FUEL	100%	100%
FREQ	12.33	11.91
NODE	O———O	△———△
SHAPE	— ·· — ·· —	— — — —

WING-ENGINE

VIEW FWD

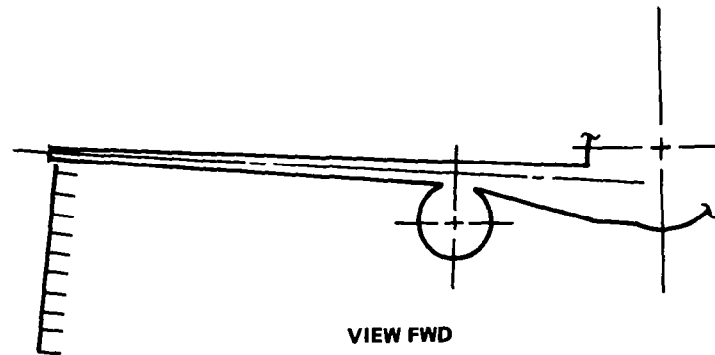FIGURE 117. FLUTTER MODEL VIBRATION MODES; FULL FUEL WITHOUT WINGLETS (4 OF 8)

ENGINE ROLL
(PYLON TORSION)

	MODEL	ANALYSIS
FUEL		100%
FREQ	NOT MEASURED	22.51
NODE	○——○	△——△
SHAPE	▬ ▬ ▬	▬ ▬ ▬ ▬

WING-ENGINE
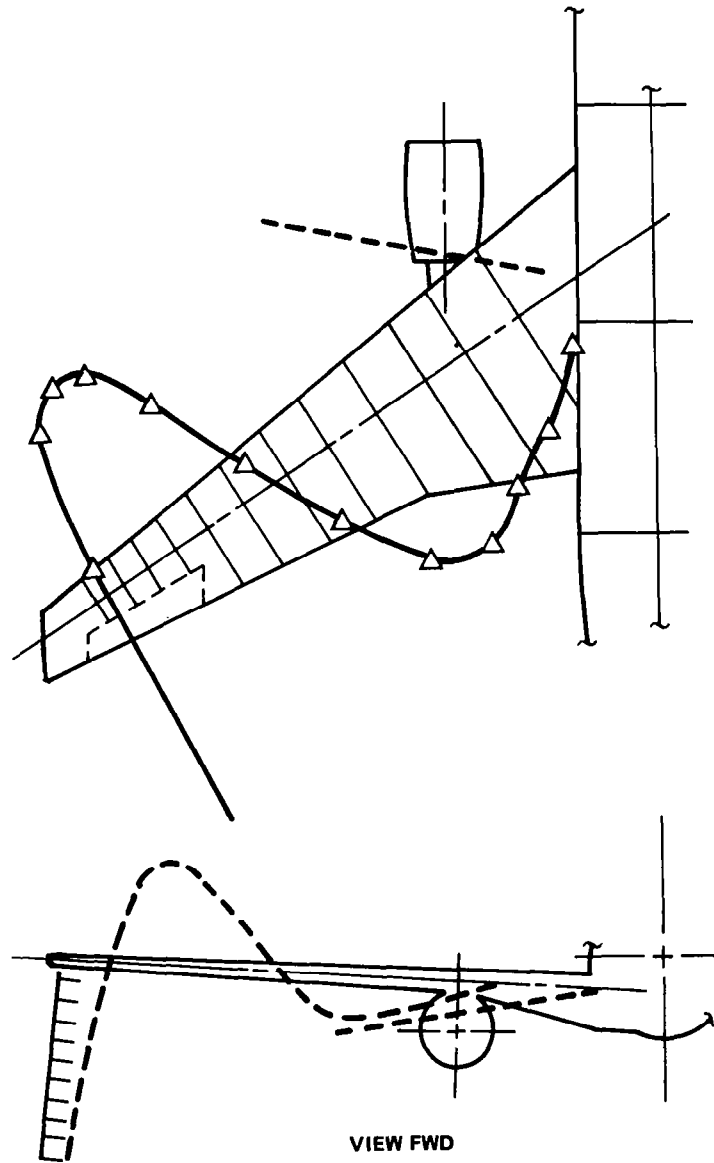
VIEW FWD

FIGURE 117. FLUTTER MODEL VIBRATION MODES; FULL FUEL WITHOUT WINGLETS (5 OF 8)

1ST WING LONGITUDINAL BENDING

	MODEL	ANALYSIS
FUEL	100%	100%
FREQ	21.25	20.71
NODE	O———O	△———△
SHAPE	▬ ▬ ▬ ▬	▬ ▬ ▬ ▬ ▬

WING-ENGINE

VIEW FWD

FIGURE 117. FLUTTER MODEL VIBRATION MODES; FULL FUEL WITHOUT WINGLETS (6 OF 8)

3RD WING BENDING

	MODEL	ANALYSIS
FUEL	100%	100%
SYM		
FREQ	24.5	24.5
NODE	○——○	△——△
SHAPE	—— —	—— ——

WING-ENGINE

VIEW FWD

FIGURE 117. FLUTTER MODEL VIBRATION MODES; FULL FUEL WITHOUT WINGLETS (7 OF 8)

WING TORSION

	MODEL	ANALYSIS
FUEL	100%	100%
FREQ	30.85	33.0
NODE	O———O	△———△
SHAPE	▬ ▬ ▬	▬ ▬ ▬ ▬

WING-ENGINE
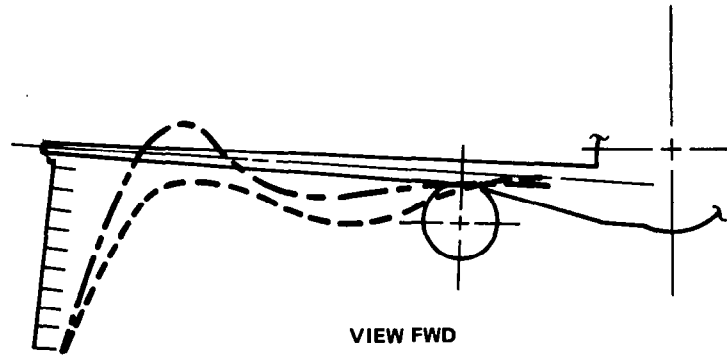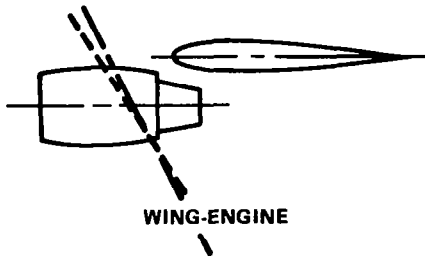
VIEW FWD

FIGURE 117. FLUTTER MODEL VIBRATION MODES; FULL FUEL WITHOUT WINGLETS (8 OF 8)

ENGINE YAW
(PYLON SIDE BENDING)

	MODEL	ANALYSIS
FUEL	100%	100%
FREQ	6.66	6.64
NODE	O———O	△———△
SHAPE	——————	——————
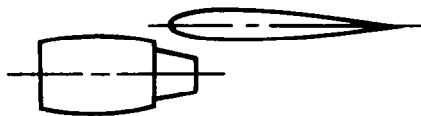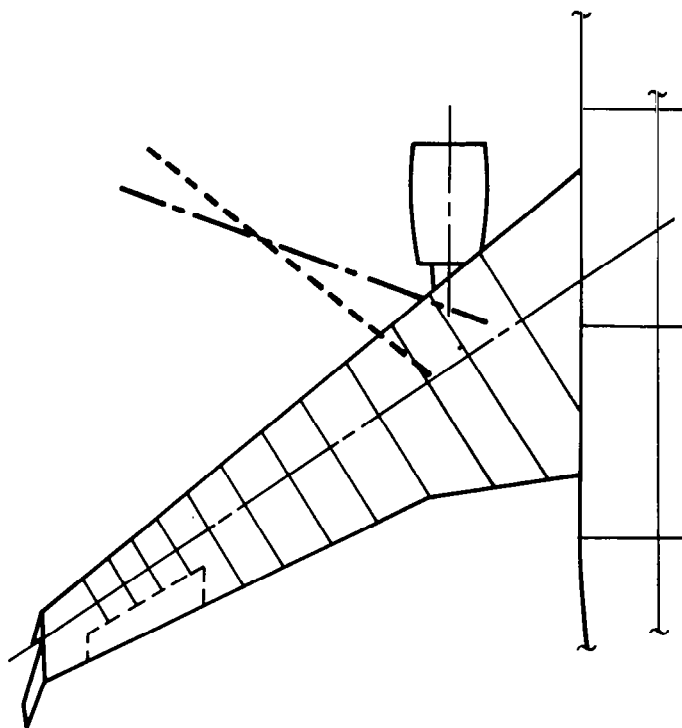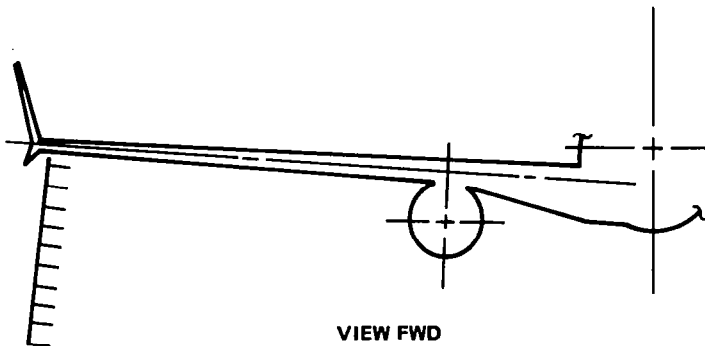
WING-ENGINE
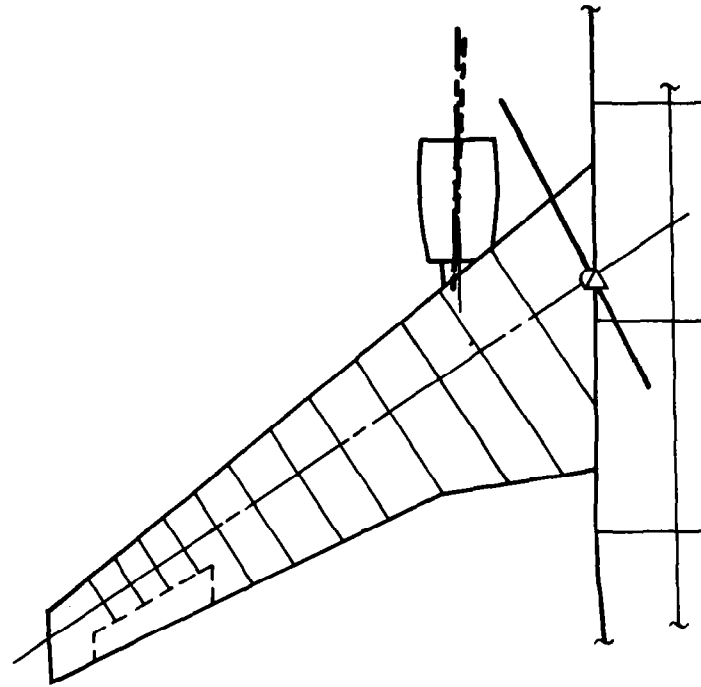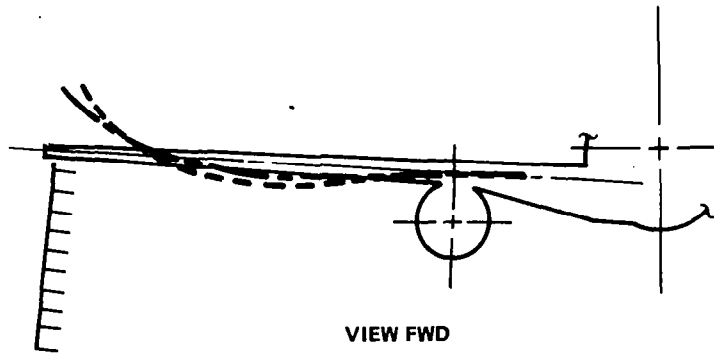
VIEW FWD

FIGURE 118. FLUTTER MODEL VIBRATION MODES; FULL FUEL WITH WINGLETS (1 OF 8)

1ST WING BENDING

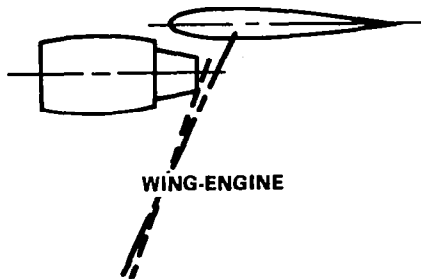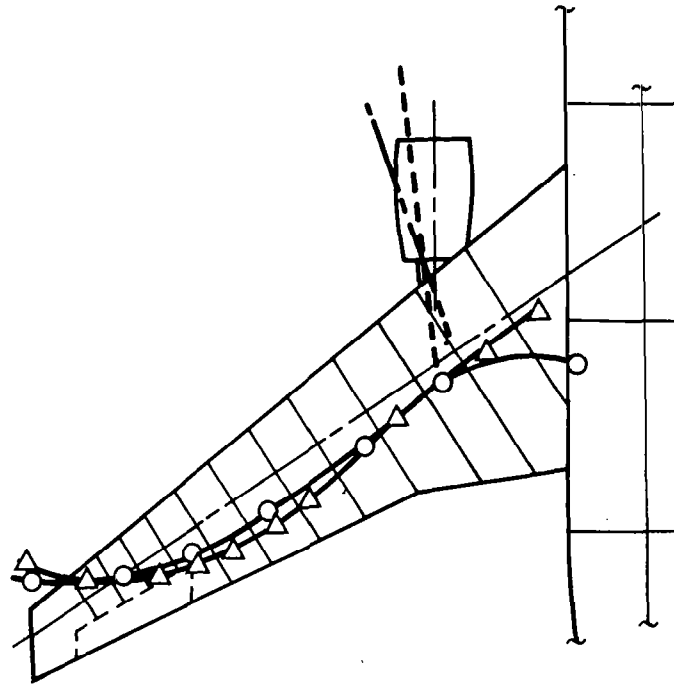|	MODEL	ANALYSIS
FUEL	100%	100%
FREQ	4.00	3.89
NODE	○──○	△──△
SHAPE	▬ ▬ ▬	▬ ▬ ▬ ▬
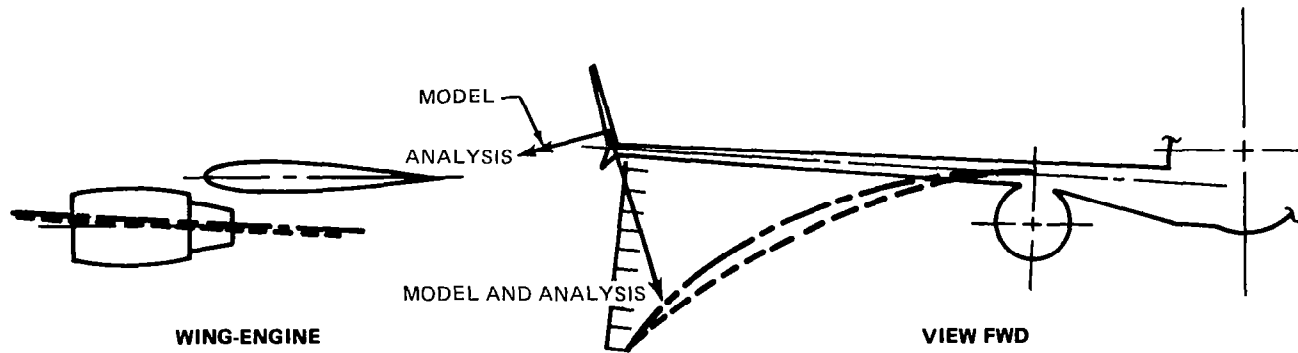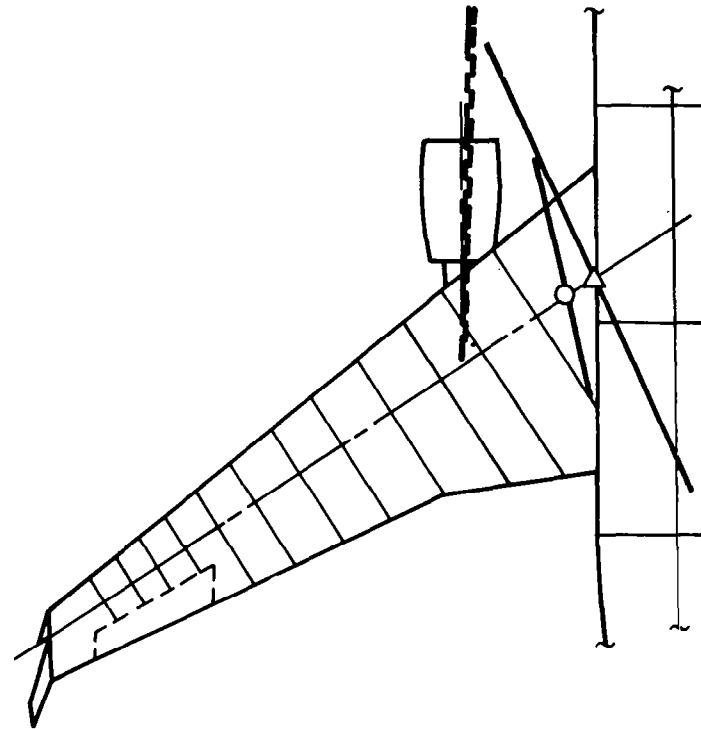
MODEL
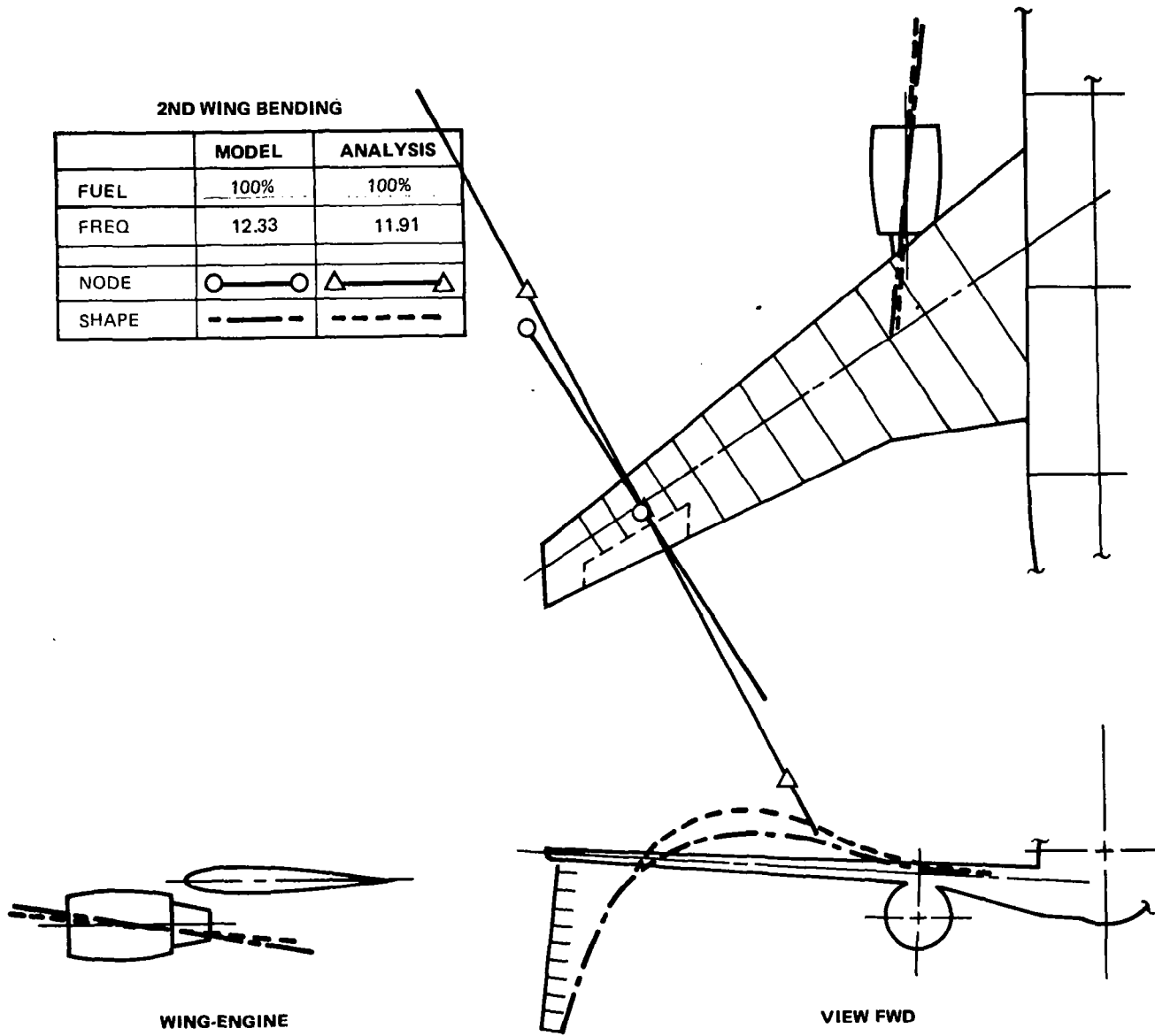
ANALYSIS

MODEL AND ANALYSIS

WING-ENGINE

VIEW FWD

FIGURE 118. FLUTTER MODEL VIBRATION MODES; FULL FUEL WITH WINGLETS (2 OF 8)

ENGINE PITCH
(PYLON VERTICAL BENDING)

	MODEL	ANALYSIS
FUEL	100%	100%
FREQ	13.12	13.02
NODE	O——O	△——△
SHAPE	▬ ▬▬ ▬▬	▬ ▬ ▬ ▬ ▬
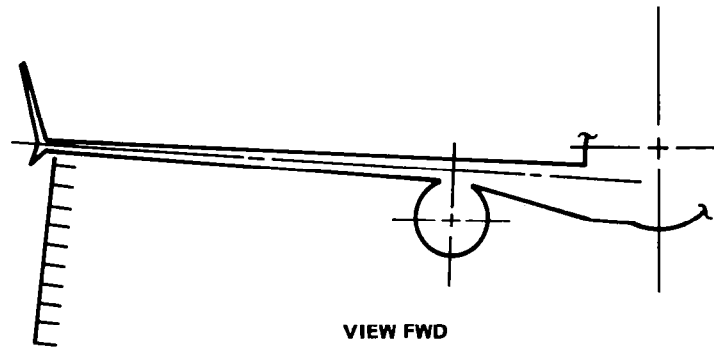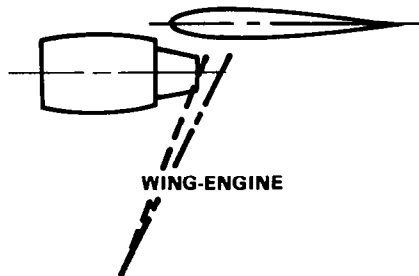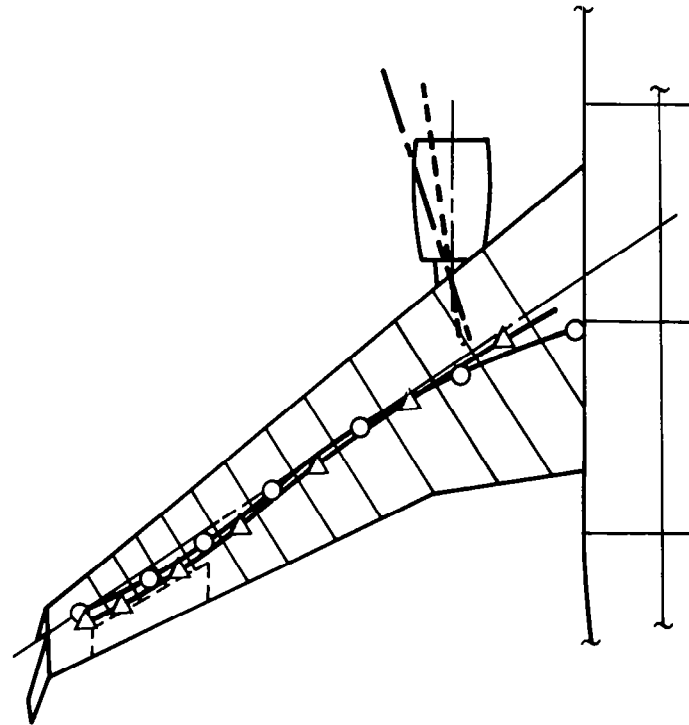
WING-ENGINE

VIEW FWD

FIGURE 118. FLUTTER MODEL VIBRATION MODES; FULL FUEL WITH WINGLETS (3 OF 8)

2ND WING BENDING

	MODEL	ANALYSIS
FUEL	100%	100%
FREQ	10.67	10.31
NODE	O———O	△———△
SHAPE	▬ ▬ ▬	▬▬ ▬▬
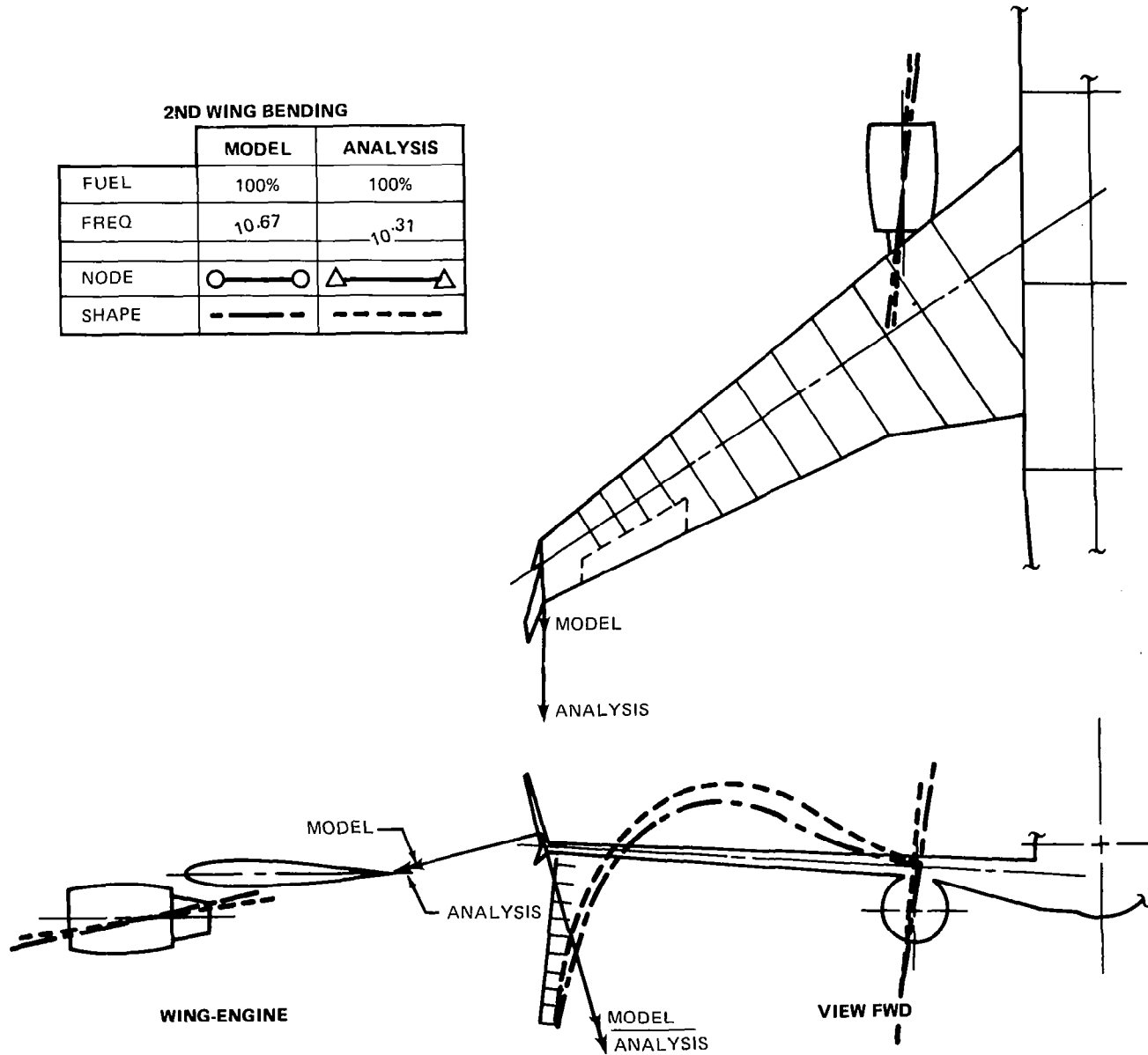
MODEL

ANALYSIS

MODEL

ANALYSIS

WING-ENGINE

MODEL
ANALYSIS

VIEW FWD
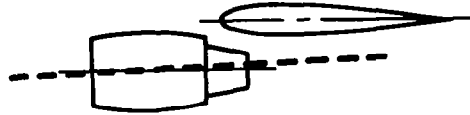
FIGURE 118. FLUTTER MODEL VIBRATION MODES; FULL FUEL WITH WINGLETS (4 OF 8)

ENGINE ROLL
(PYLON TORSION)

	MODEL	ANALYSIS
FUEL	100%	100%
FREQ	22.73	22.83
NODE	O———O	△———△
SHAPE	— · —	— — — —

MODEL

ANALYSIS

MODEL

ANALYSIS

MODEL

ANALYSIS

WING-ENGINE

VIEW FWD

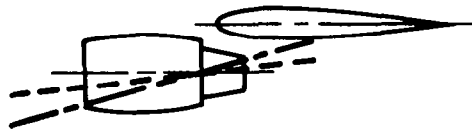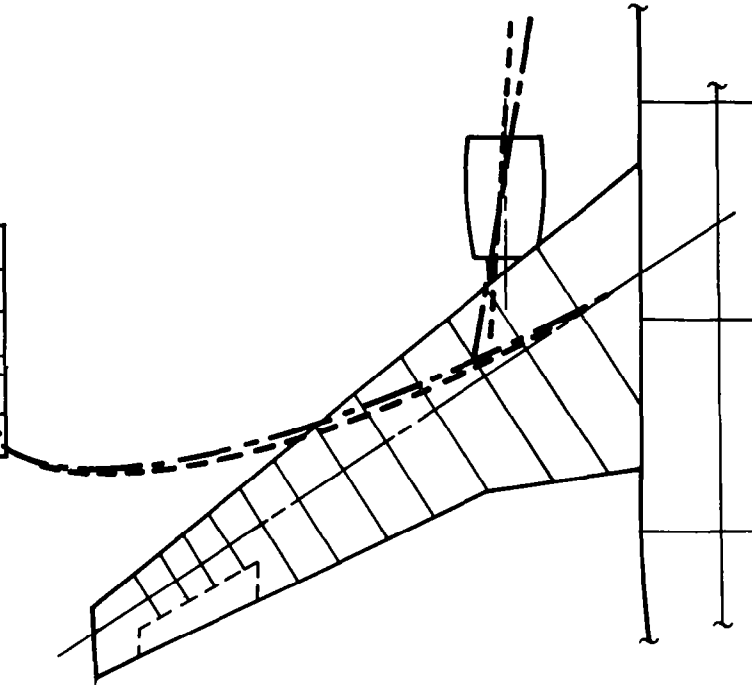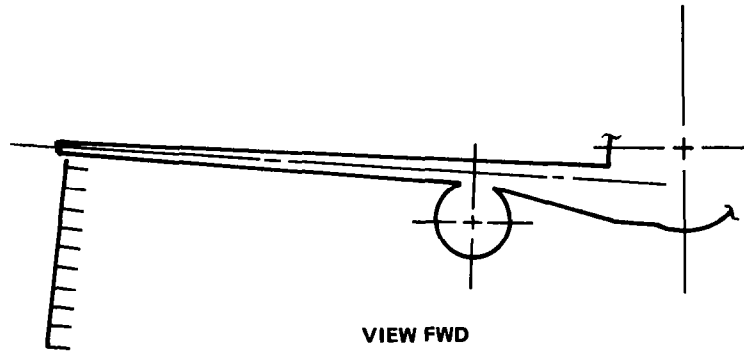**FIGURE 118. FLUTTER MODEL VIBRATION MODES; FULL FUEL WITH WINGLETS (5 OF 8)**

1ST WING LONGITUDINAL BENDING

	MODEL	ANALYSIS
FUEL	100%	100%
FREQ	19.95	19.45
NODE	○——○	△——△
SHAPE	▬ ▬ ▬	▬ ▬ ▬

MODEL
ANALYSIS

MODEL
ANALYSIS

MODEL
ANALYSIS

WING-ENGINE

VIEW FWD

FIGURE 118. FLUTTER MODEL VIBRATION MODES; FULL FUEL WITH WINGLETS (6 OF 8)

3RD WING BENDING

	MODEL	ANALYSIS
FUEL	100%	100%
FREQ	20.60	20.45
NODE	O——O	△——△
SHAPE	— — —	— — — —

MODEL

ANALYSIS

MODEL

ANALYSIS

MODEL

ANALYSIS

MODEL

ANALYSIS

WING-ENGINE

VIEW FWD

FIGURE 118. FLUTTER MODEL VIBRATION MODES; FULL FUEL WITH WINGLETS (7 OF 8)

141
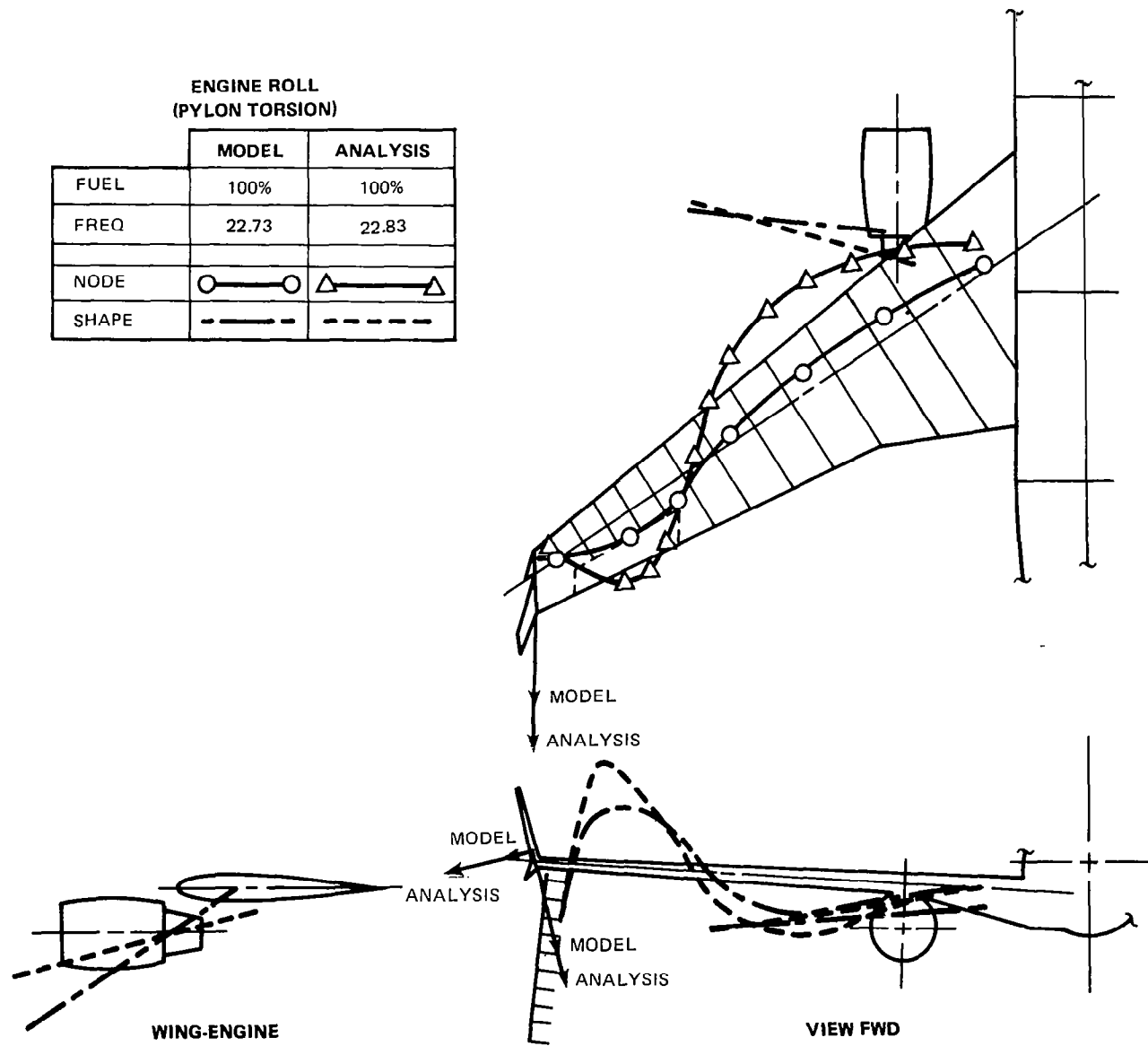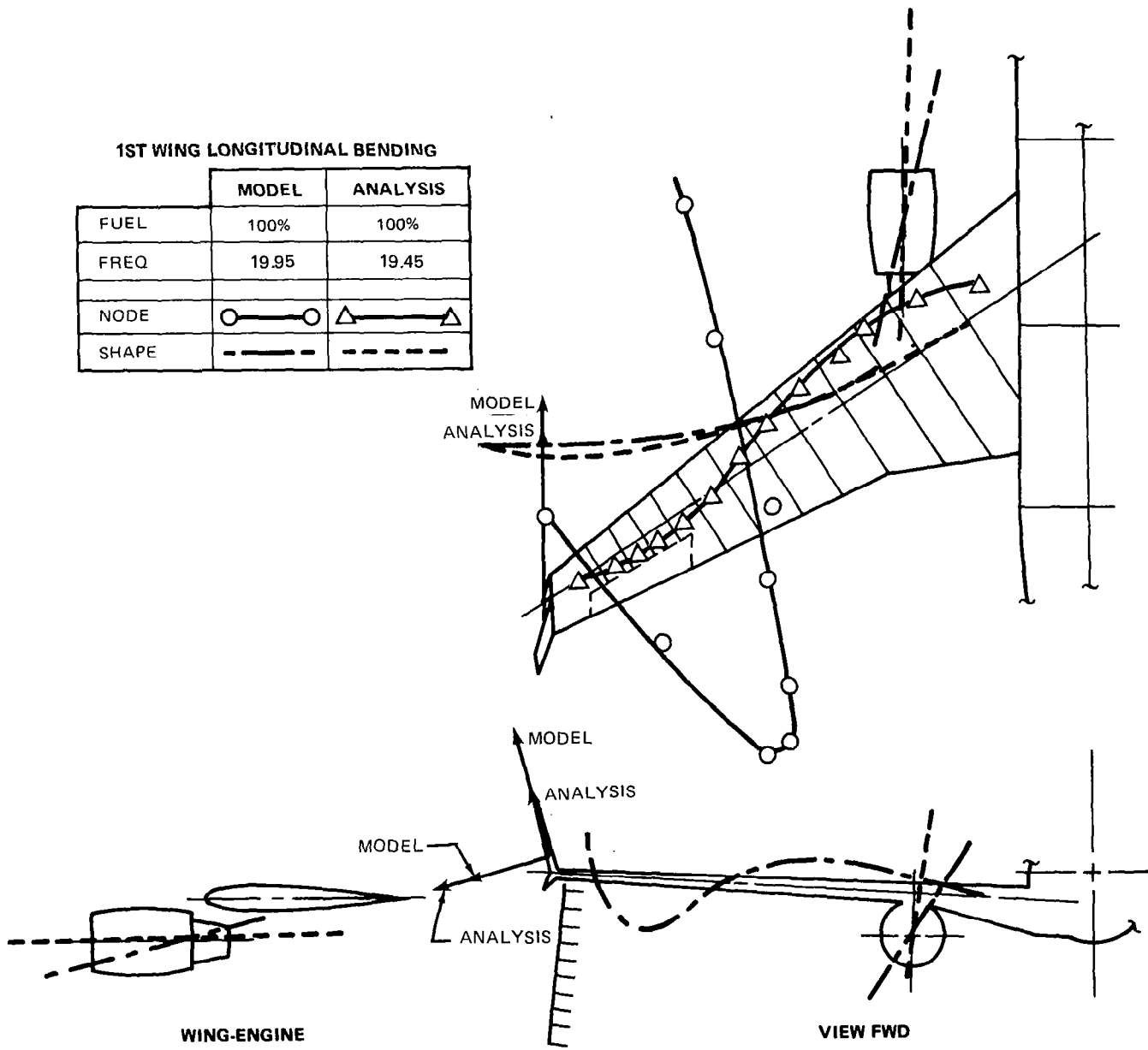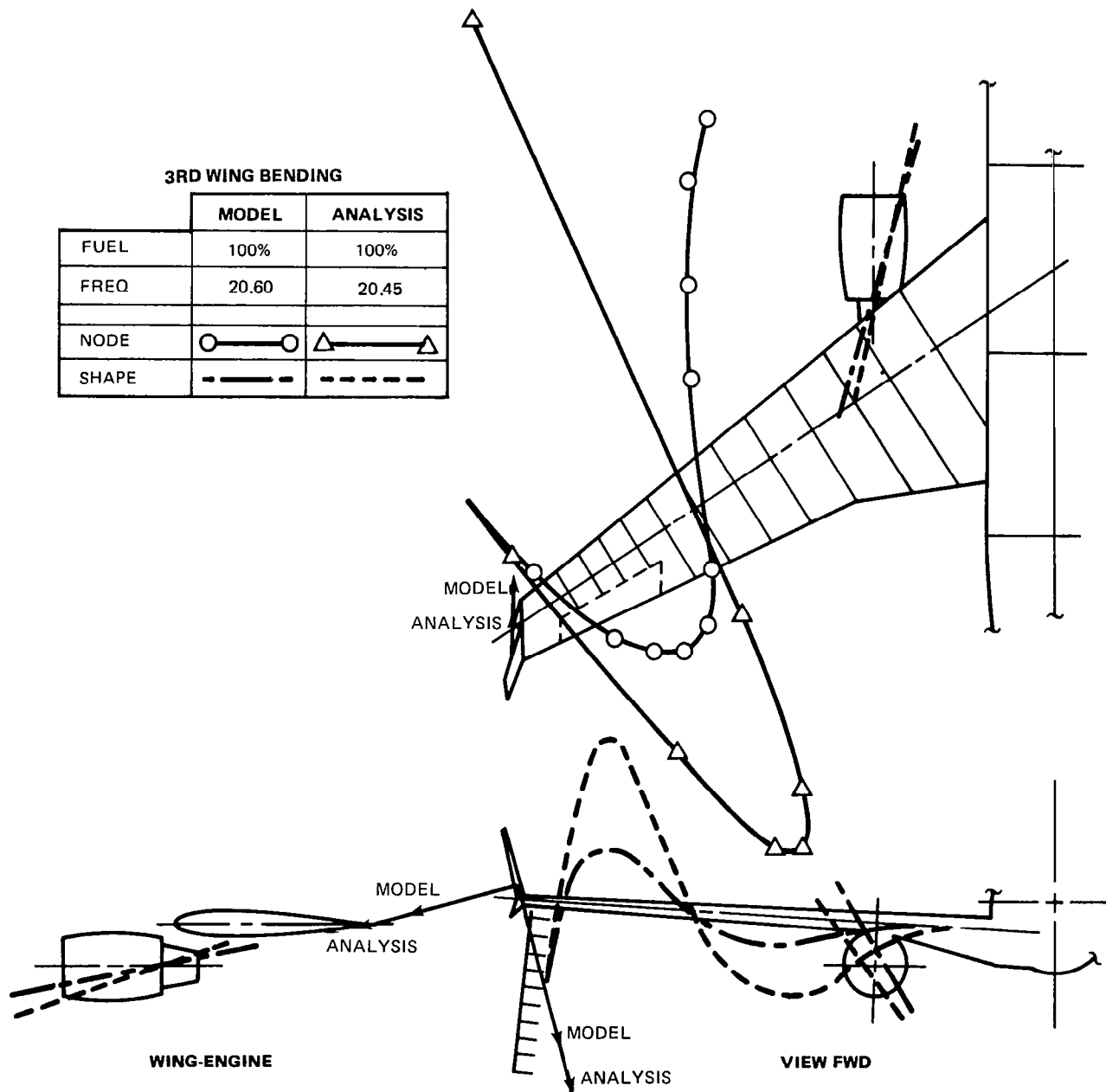
WING TORSION	MODEL	ANALYSIS
FUEL	100%	100%
FREQ	28.27	29.25
NODE	○——○	△——△
SHAPE	▬ ▬ ▬ ▬	▬ ▬ ▬ ▬

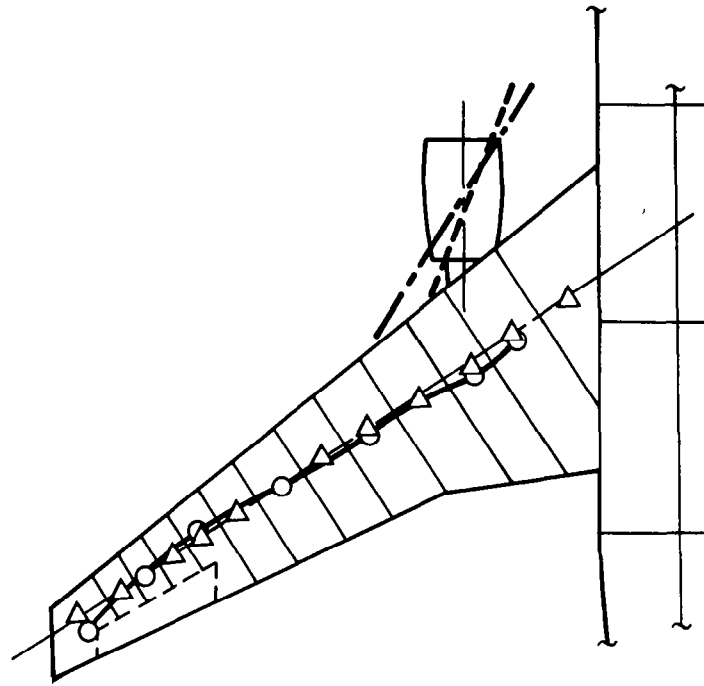ANALYSIS

MODEL

MODEL

ANALYSIS

ANALYSIS

MODEL

WING-ENGINE

VIEW FWD
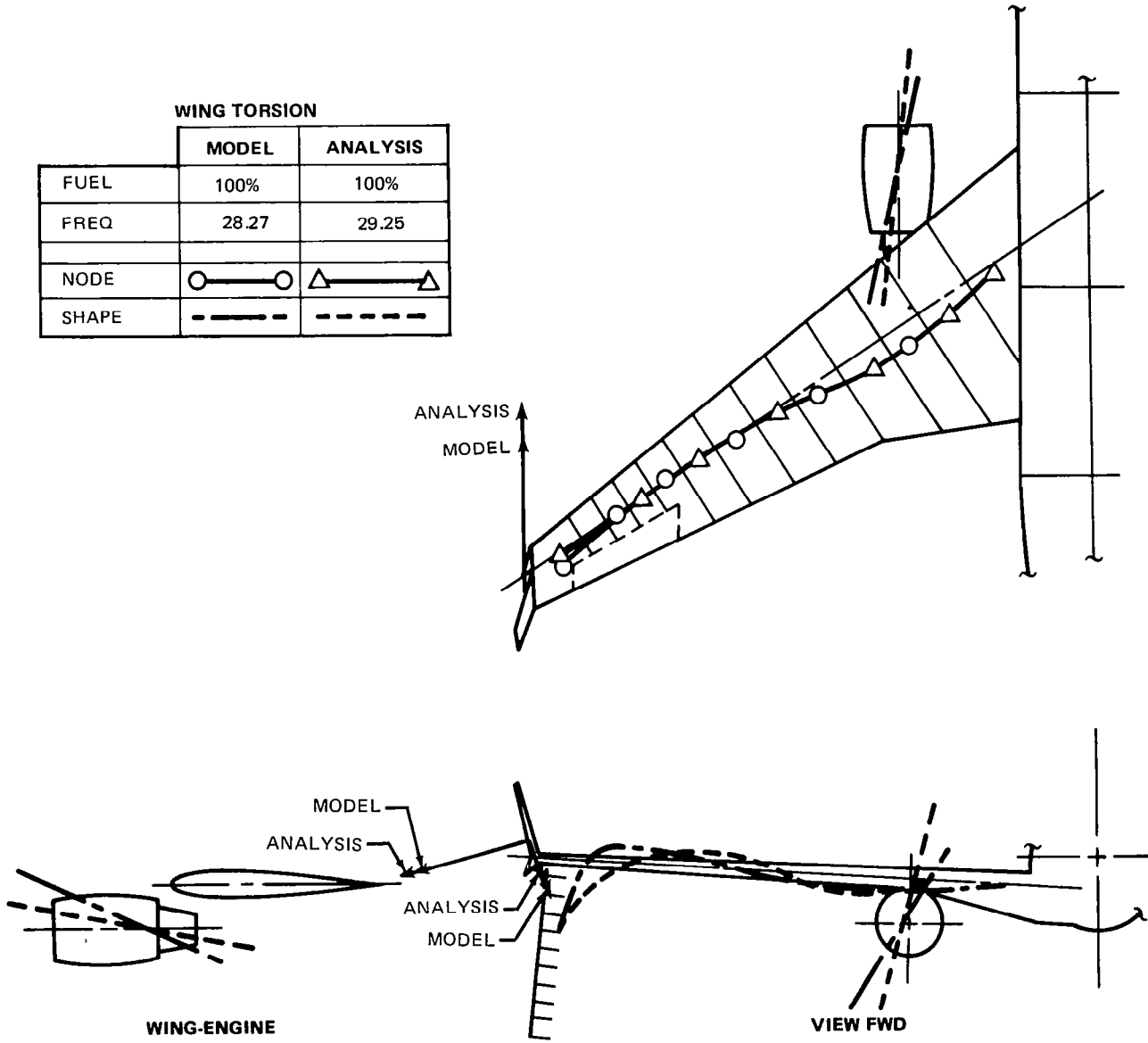
FIGURE 118. FLUTTER MODEL VIBRATION MODES; FULL FUEL WITH WINGLETS (8 OF 8)

As noted above, the structural damping coefficient, g_s, was assumed to be 0.02 for all modes since this is the usual practice in design analysis before ground vibration tests are conducted. On actual aircraft, the lowest values for g_s are, in fact, about 0.02. However, the model exhibited structural damping for the "inner-panel torsion" mode of less than 0.02. At low-fuel states, the damping as a function of velocity curve for this mode is one of the shallow hump type where a small change in structural damping has a noticeable effect on the flutter speed. For heavier fuel states, the crossing is steeper and hence less sensitive to structural damping. This explains the phenomenon shown in Figures 119 and 120 where the analysis is slightly unconservative at low-fuel states. For heavier fuel states, where small changes in structural damping have a negligible effect, the analysis is slightly conservative.
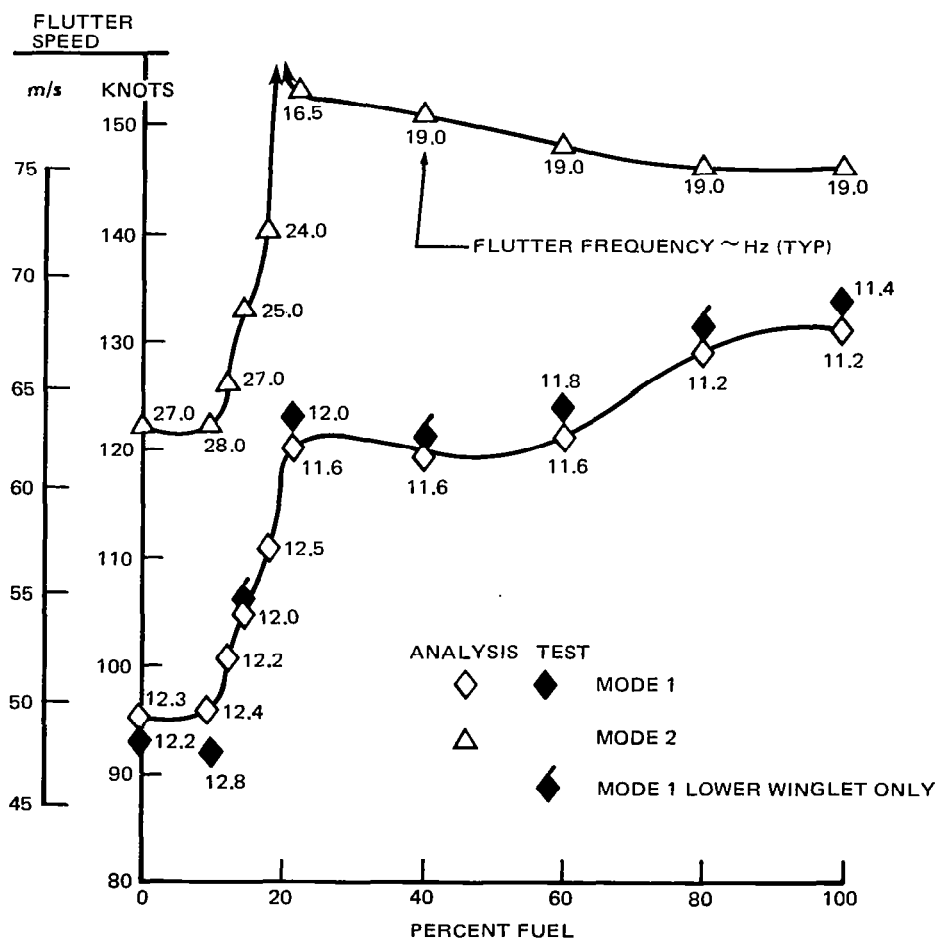
FIGURE 119. EFFECT OF FUEL STATE ON FLUTTER SPEED FOR BASELINE AIRCRAFT
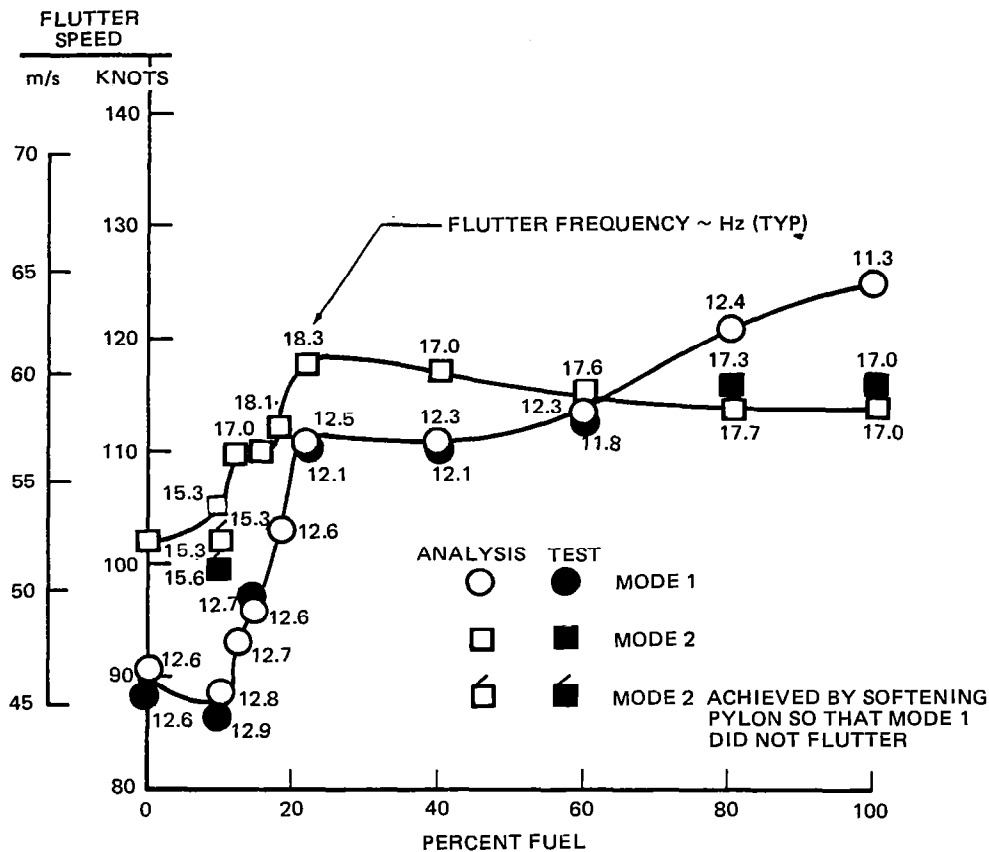
FIGURE 120. EFFECT OF FUEL STATE ON FLUTTER SPEED FOR WINGLET AIRCRAFT

Baseline configuration — Figure 119 shows a summary of flutter speed as a function of fuel state for the baseline (no winglet) configuration. As indicated, the inner panel torsion mode (Mode 1) is the critical mode at all fuel states, and good agreement between test and analysis was obtained. Some of the fuel state test points shown are for the lower winglet only. This is because the baseline configuration was not tested at these fuel states. However, the test flutter speed for the lower-winglet-only configuration was always within 1 meter per second (2 knots) of the baseline configuration for those fuel states in which both configurations were tested. The lower winglet was much smaller than the basic winglet, and was essentially massless. No analysis was made of the lower-winglet-only configuration.

Also shown in Figure 119 are the calculated flutter speeds for the next-highest-speed flutter mode (Mode 2), which is the outer wing bending/torsion mode. Of course, no experimental confirmation of this mode was obtained since the model could not be tested beyond the speed of the lower mode flutter case.

Figure 121 shows the typical calculated frequency and damping as functions of velocity variations for the two flutter modes at zero and full fuel.
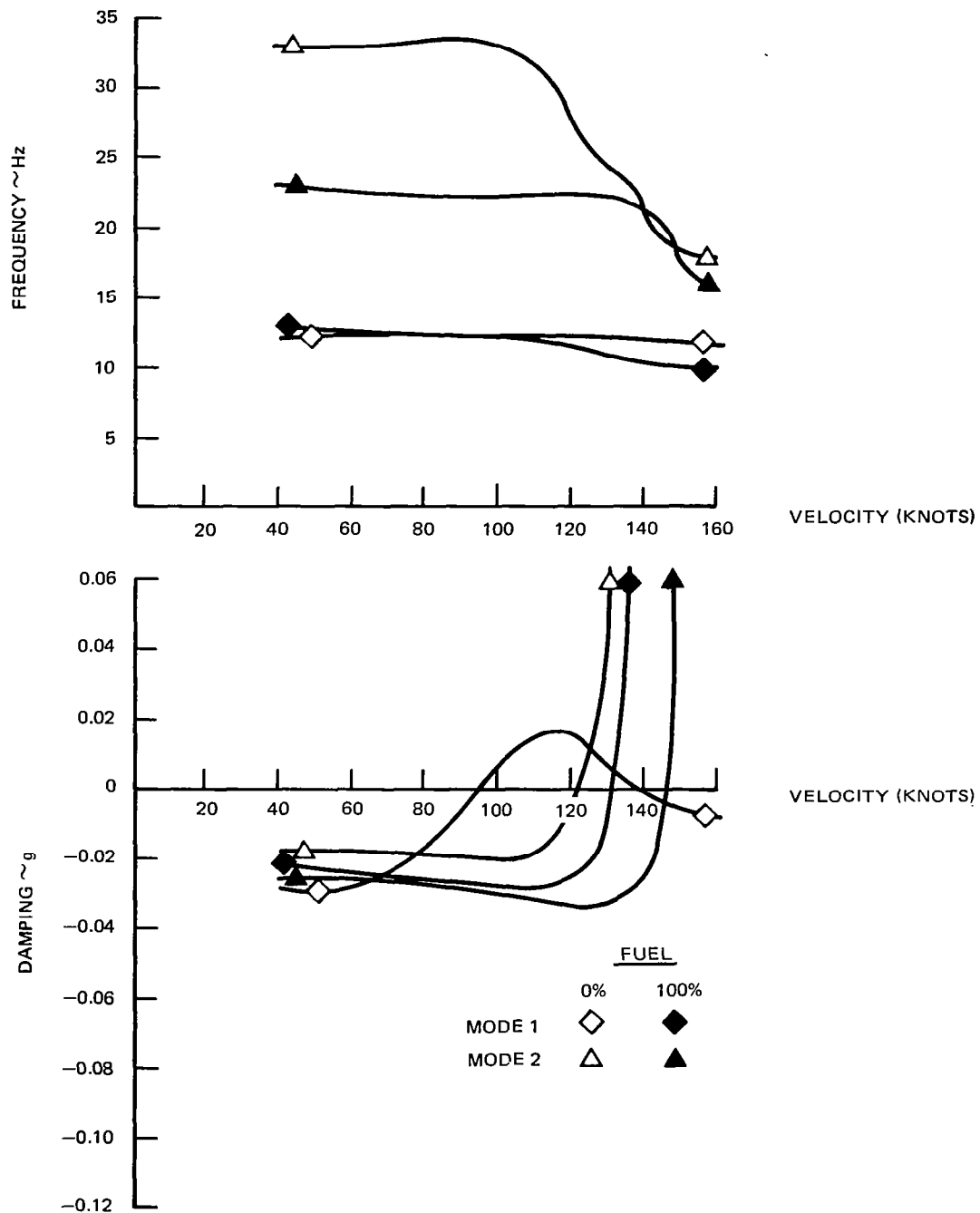
FIGURE 121. FREQUENCY AND DAMPING ANALYSIS RESULTS FOR BASELINE AIRCRAFT

Basic winglet configuration — Figure 120 shows a summary of flutter speed as a function of fuel level for the basic winglet case. As indicated, the inner panel torsion mode (Mode 1) is critical from zero to approximately 60-percent fuel and the outer panel mode (Mode 2) is critical from 60 percent to full fuel. Very good agreement is seen to exist between theory and experiment. Further scrutiny of test results also showed, in agreement with theory, that the higher frequency flutter speed was imminent when the inner panel flutter case was obtained at 60-percent fuel.

Also shown in Figure 120 is a test point at 10-percent fuel for Mode 2. This was achieved by reducing the cantilevered engine pitch frequency from 16.2 to 11.8 Hertz, thereby stabilizing Mode 1. The corresponding change was made in the analysis and, as shown, the agreement with test was again excellent. The ability of the theory to accurately predict these higher frequency flutter speeds for the winglet configurations is the main result of this study.

Figure 122 shows frequency and damping as functions of velocity for the two flutter modes at zero and full fuel.

According to Figure 120, the critical flutter mode is still the inner panel torsion mode (Mode 1). Comparison of Figures 119 and 120 would appear to indicate that the winglets, in effect, reduced the lowest flutter speed (using test results at 10-percent fuel) by 5 percent. This extrapolation is not valid for the following reasons:

- As previously noted, the wing longitudinal bending rigidity of the model is significantly higher than scaled values representative of actual transport aircraft. This parameter is important for the winglet configuration. Futher analysis showed that if the model had realistic longitudinal bending rigidity, the high-frequency winglet configuration flutter speeds would have been about 51 meters per second (100 knots) or less over most of the fuel range.

- Experience shows that releasing the cantilever constraint and including the rest of the airplane flexibility raises the lowest flutter speed of the inner panel torsion mode to more than 57 meters per second (110 knots). No such effect would be expected for the higher frequency flutter mode since the higher frequency wing modes involve only small amounts of fuselage and empennage motion.

Hence, on an actual free-flying aircraft with winglets installed, the higher frequency flutter mode may exhibit significantly lower flutter speeds than the inner panel torsion mode.
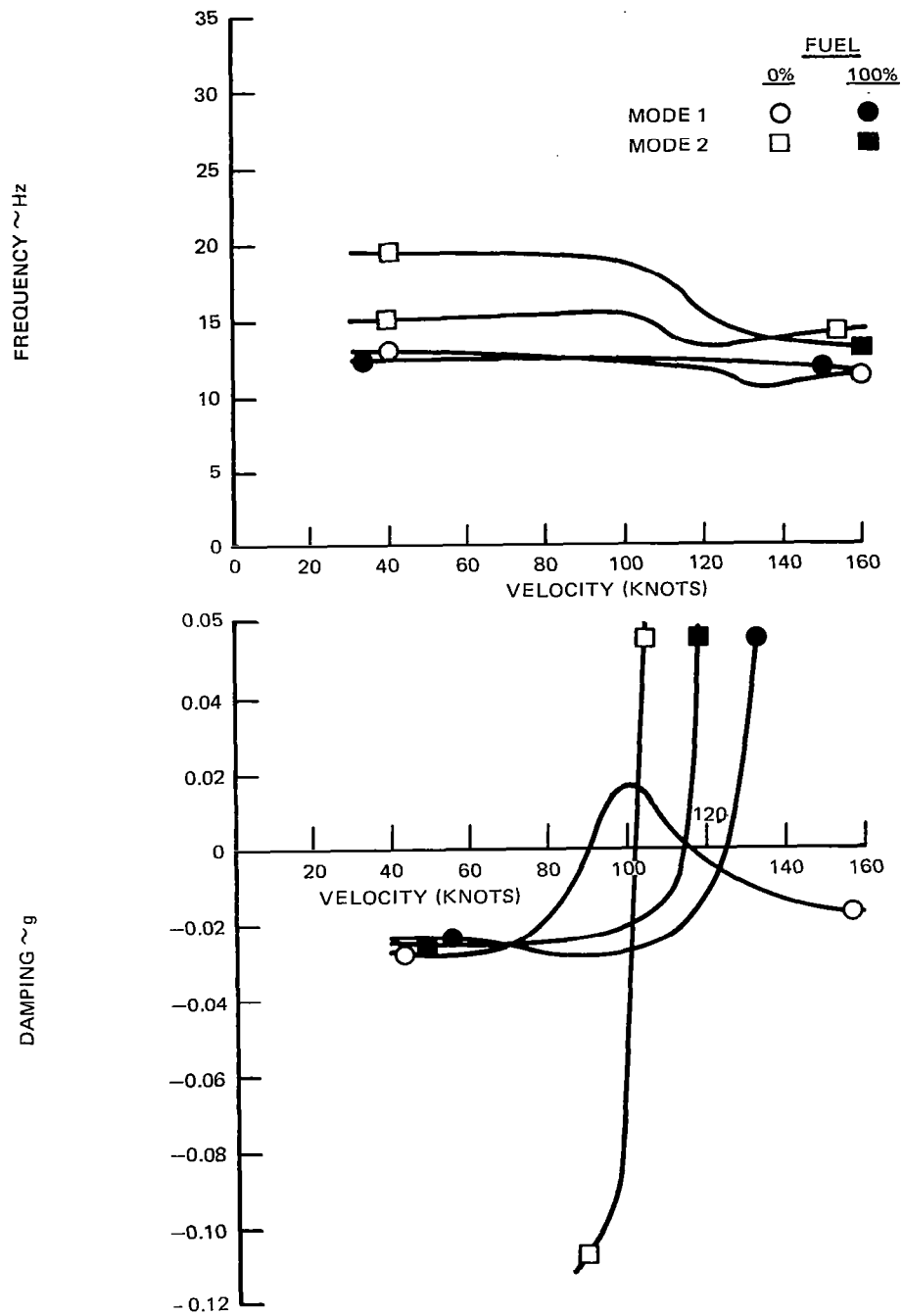
FIGURE 122. FREQUENCY AND DAMPING ANALYSIS RESULTS FOR WINGLET AIRCRAFT

This study shows that standard flutter analysis techniques predict the wing/winglet flutter speeds with sufficient accuracy, at least at subsonic Mach numbers. It should be noted, however, that the transonic regime is usually critical for flutter. It is accepted practice that whenever a high-speed aerodynamic design significantly different from previous experience is considered, confidence in the flutter integrity of the design is achieved by correlating the tests with analysis of a transonic flutter model. This correlation determines the adjustments which must be made to the theory for further application to the design flutter analyses.

Winglet-mass-only configuration — The question is sometimes posed as to how much of the reduction in flutter speed is due to the mass and inertia of the winglet, and how much is due to the aerodynamics of the winglet. This question is addressed in the flutter model by the fabrication of a dummy winglet, as described previously. This dummy winglet closely approximated the mass and inertia properties of the actual winglet, but was constructed of circular tubes with lead ballast in an attempt to minimize aerodynamic lift forces on the winglet. Analysis was also performed with the mass and inertia for the winglet included, but with the winglet aerodynamics deleted.

Figure 123 shows a summary of flutter speed as a function of fuel loading for the winglet mass and inertia only (dummy winglet) configuration. Agreement between theory and experiment, while good in this case, was not as good as for either the baseline or the basic winglet configurations. The probable reason for this is that the dummy winglet generated some small, unknown aerodynamic forces that were not accounted for in the analysis. The detrimental effect of these (Mode 2) forces would explain why the predicted flutter speeds at higher fuel states and higher frequency were slightly nonconservative with the dummy winglets (Figure 123), while they were slightly conservative with the actual winglets (Figure 120). The analysis showed that, for the higher frequency flutter mode, the mass and inertia effect and the aerodynamic effect would both be detrimental and roughly of equal magnitude. This would imply that, for a lighter winglet, the detrimental effect of the winglet on the higher frequency flutter mode would be alleviated.

Other parametric variations — Two additional significant variations were tested on the model but were not analyzed. These were winglet dihedral angle and wing angle of attack. The nominal winglet dihedral angle was 75 degrees. Additional tests were run with dihedral angles of 90 and 65 degrees. Figure 124 shows that changing the winglet dihedral angle had only a small effect on the flutter speed.

Also, only slight changes in the flutter speed of both flutter modes occurred for wing angle-of-attack variations from −1.5 to +1.0 degrees.
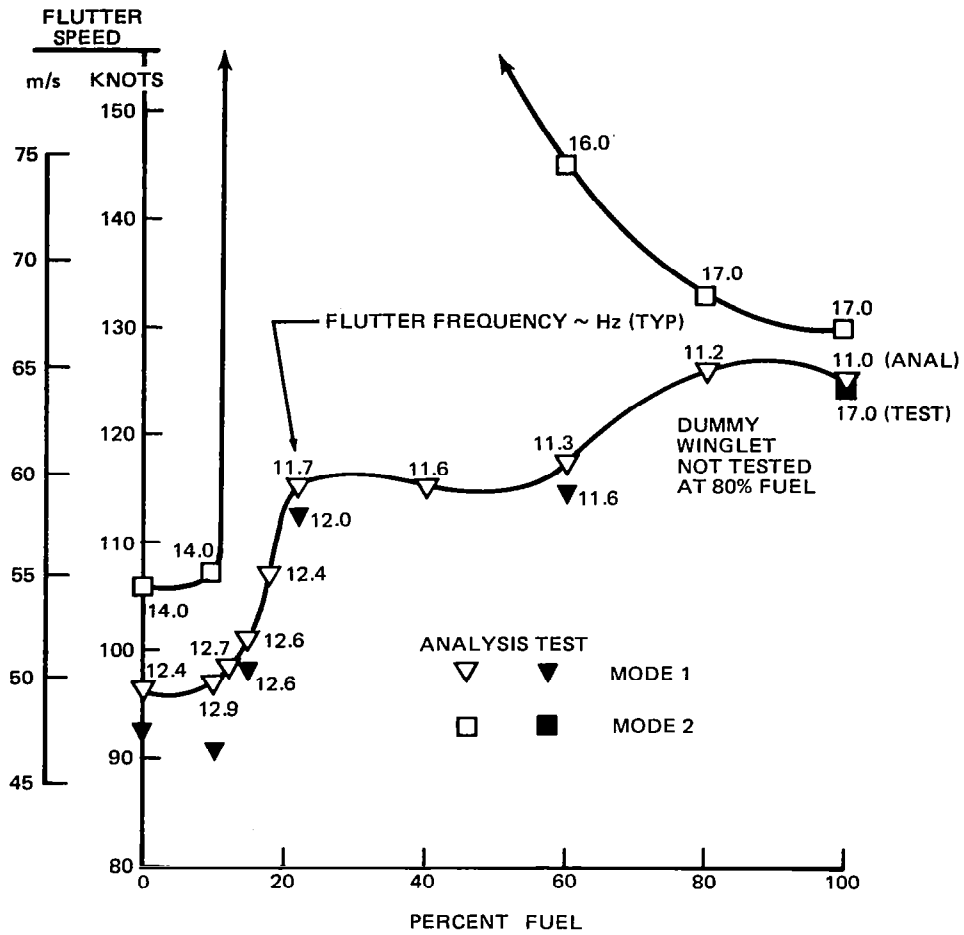
FIGURE 123. EFFECT OF FUEL STATE ON FLUTTER SPEED FOR WINGLET MASS AND INERTIA ONLY
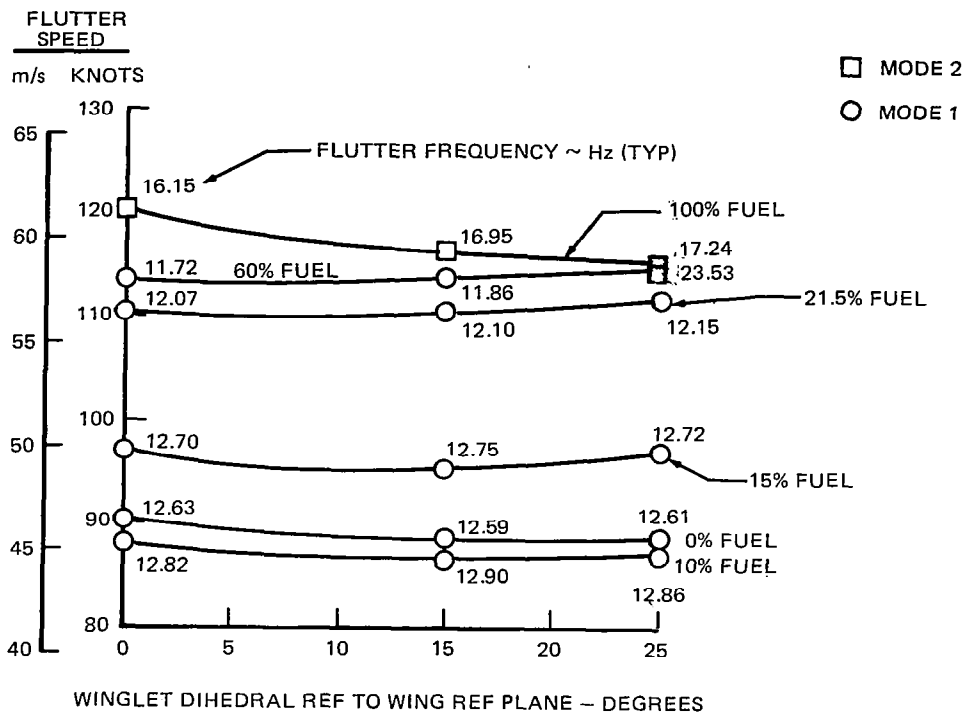
FIGURE 124. EFFECT OF WINGLET DIHEDRAL ON FLUTTER SPEED

Conclusions

Based upon this subsonic investigation, the winglets had generally detrimental effects on the flutter characteristics of the given wing. These include both a small-to-moderate degradation in the basic existing wing flutter mode and a large degradation in a higher frequency wing flutter mode, so that this second mode may become critical.

The mass and inertia effect and the aerodynamic effect of the winglets are both detrimental and roughly of equal magnitude in the higher frequency wing flutter mode.

Production flutter analysis methodology, using unsteady aerodynamics generated by the doublet lattice method, accurately predicts the effect of winglets on the subsonic flutter speed of both flutter modes.

Wing fore and aft bending rigidity is an important flutter parameter for winglet configurations.

Winglet dihedral variations within the test range (65 to 90 degrees) produced minimal effects on flutter speed.

CONFIGURATION INTEGRATION ANALYSIS

Investigation Objective

The objective of the configuration integration study was to determine the impact of findings of the aerodynamic, flutter, structural, and configuration investigation conducted by Douglas on the most significant performance parameters of the DC-10.

Initial Structural and Application Studies

The baseline configuration used was a DC-10 Series 30 with a 259,000 kilogram (572,000 pound) maximum takeoff gross weight, using General Electric CF6-50C1 engines. For the winglet installation, the required structural modifications were determined from the results of a preliminary design study. The structural design was based on the choice of conservative materials and concepts. No advanced systems such as wing load alleviation were considered.

Performance data were taken from the results of the wind tunnel tests and analyses reported in Reference 5 and elsewhere in this report. From these data, and using estimates of the operational weight change due to the winglet installation and structural modifications, the saving in fuel burned compared with the baseline was estimated. At a typical range of 7,400 kilometers (4,000 nautical miles) the fuel saving was 2.9 percent. With a payload of 277 passengers and baggage, the range was increased by 269 kilometers (145 nautical miles). The drag reduction of the winglet resulted in a reduction in field length, which was small for the DC-10 Series 30: 31 meters (100 feet) for the maximum takeoff weight at 30°C (86° F).

It was also estimated that the winglets would result in a small reduction in noise level at takeoff and approach, amounting to 0.5 effective perceived noise level decibel in the approach.

The installation of the winglets was estimated to add 1,374 kilograms (3,030 pounds) to the baseline operational empty weight. Of this weight increase, 865 kilograms (1,908 pounds) resulted from modifications to the wing, 111 kilograms (244 pounds) from adding the wing tip unit, and 361 kilograms (795 pounds) from adding the upper and lower winglets. Also, 38 kilograms (83 pounds) were added for contingencies. It was concluded that the structure added for wing modifications would enable the flutter speed of the basic aircraft to be maintained.

The fuel saving benefits were considered to be sufficiently attractive to warrant continuation of the technology development. At this stage of the aerodynamic and flutter studies, it was also considered that the most beneficial next major step for the winglet development would be a full-scale flight evaluation. The preliminary design phase for such an activity was authorized by NASA. In addition, the structural and application studies were continued by Douglas at a greater level of detail.

Additional Structural and Application Studies

Further structural studies were conducted using data from the EET wind-tunnel tests described in this report. These studies widened the investigation to include the DC-10 Series 10 medium-range aircraft, and introduced an investigation of winglet retrofit to existing fleet aircraft.

The new studies included a more detailed investigation of the effects of aeroelastic deflections. The effect of the winglet loads on the wing deflection was reestimated and was found to result in an 0.2-percent reduction in cruise drag improvement. The aeroelastic effects were also considered in the reestimate of wing loads. For a given condition, the loads at the base of the winglet, as evolved from the wind tunnel data, were applied to the wing tip as a system of concentrated forces and moments. The standard analytical wing loads program was modified so that this system of loads could be changed to account for aeroelastic deflection of the wing. Two degrees of aeroelastic freedom were considered; the first due to aeroelastic wing twist, and the second due to aeroelastic yawing of the wing tip. The derivatives used for this process were determined using wind tunnel data adjusted by theoretical data. The winglet loads were modified iteratively until the incremental changes were within 1 percent of the previous values.

A detailed wing loads analysis for a DC-10 Series 30 winglet aircraft, using the maximum gross weight, was conducted with the revised methods. Rigid winglet loads were calculated for a variety of conditions: symmetric maneuvers; lateral gusts; rudder kick maneuvers at high and low speeds; and maneuvers at a load factor of −1. The low-speed, high-angle-of-attack symmetric maneuvers gave the highest winglet normal force, with the low-speed rudder kick maneuver producing a marginally higher winglet root moment.

The results indicated a larger effect on the wing root bending moment than had previously been estimated, requiring more than double the amount of structural strengthening to the wing. Even though some of the previously estimated loads had been reduced substantially by the aeroelastic analysis, it was found that a significant part of the increase was due to the horizontal component of the winglet normal force.

The net effect of the winglet drag reduction benefit, aeroelastic losses, and weight penalty was to reduce the fuel burned savings from that of the original study. The fuel burned savings for the new configuration is shown in Figure 125 and the payload-range comparison is shown in Figure 126. It was concluded that a winglet installation could be justified on a new production version of this aircraft if substantial wing modifications and other improvements were to be incorporated at the same time. Retrofit of winglets to existing fleet aircraft was considered infeasible.

For the DC-10 Series 10, it was found that a winglet retrofit installation for fleet aircraft could be feasible and economical provided a smaller winglet than the basic design was used. Such a design would sacrifice some aerodynamic drag reduction in favor of reducing the incremental wing loads. In such a way, the extent of the modifications to existing structure would be minimized.
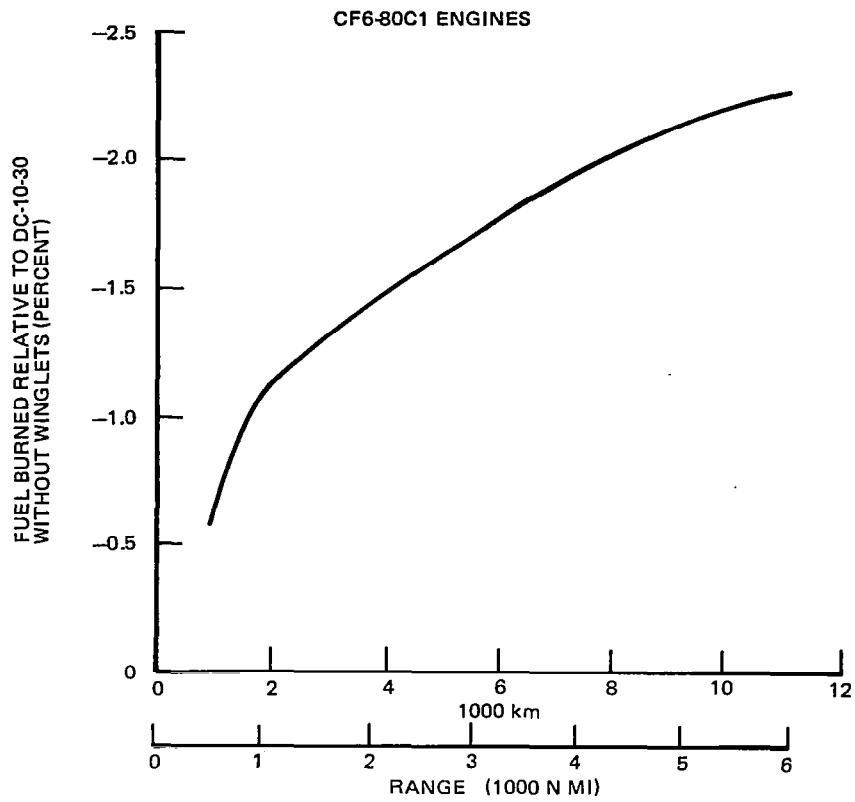
FIGURE 125. FUEL-BURNED SAVINGS DUE TO WINGLETS
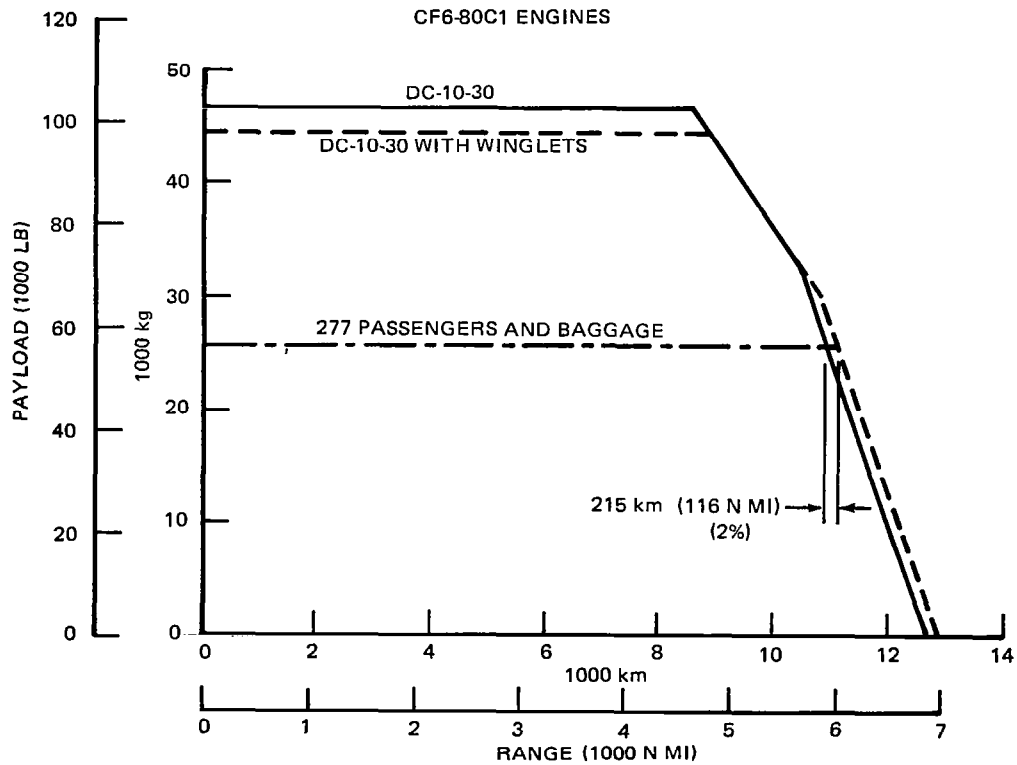
FIGURE 126. PAYLOAD-RANGE WITH AND WITHOUT WINGLETS

153

The reduced-span winglet could also be considered for new production derivatives. If new production only were to be considered, assuming that more changes in the wing structure would be acceptable, the use of the basic winglet would offer slightly higher performance.

The proposed reduced-span winglet is compared with the basic shape in Figure 127. The smaller winglet span was 62 percent of the larger span. No attempt was made to optimize the new shape or to alter the setting on the wing. The purpose of the shape variation was to establish the performance gain and weight penalty tradeoff.

For the DC-10 Series 10 with basic winglet, the installation which could be considered for new production derivatives, the fuel burned savings at maximum range with a full load of passengers (297) and baggage was estimated to be 3.5 percent, including the weight effect. This resulted in a range increase of 121 kilometers (65 nautical miles). The low-speed lift-to-drag ratio increase produced by the winglets resulted in a substantial field length reduction of 198 meters (950 feet) at a takeoff gross weight of 206,388 kilograms (455,000 pounds).

With the reduced-span winglet, assuming a takeoff gross weight of 195,048 kilograms (430,000 pounds) which is typical for candidate retrofit aircraft, the fuel burned savings at maximum range with a full load of passengers and baggage was estimated to be 3.0 percent. Although low-speed performance benefits from the reduced-span winglets were not estimated, it would be expected that a field performance benefit slightly less than that of the basic winglet would be obtained. With the basic winglet at the given gross weight and conditions, a field length reduction of 198 meters (650 feet) resulted.
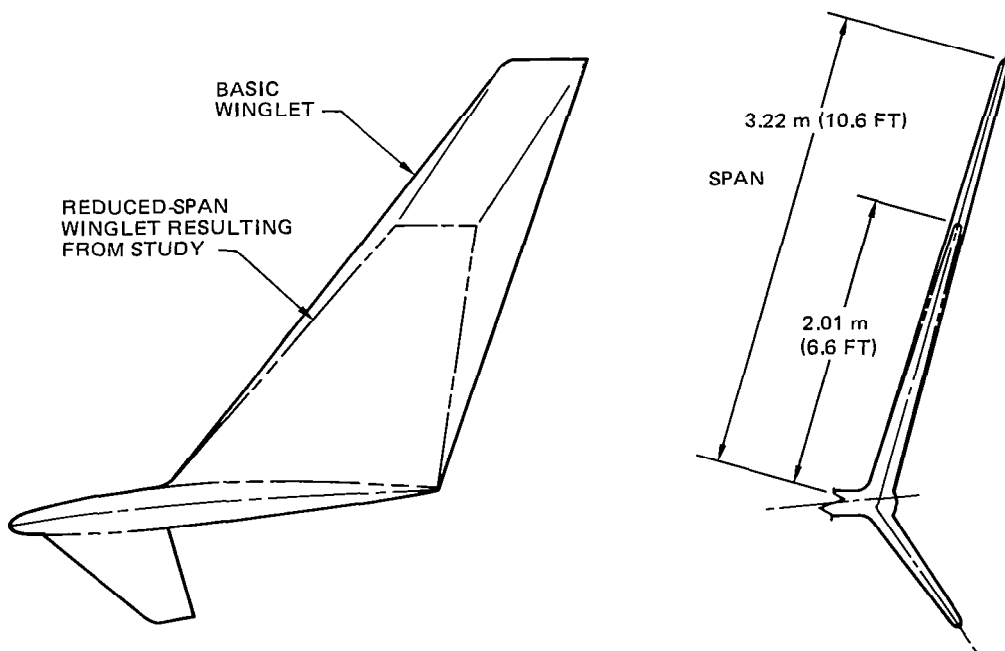
FIGURE 127. BASIC AND REDUCED-SPAN WINGLETS

Given these results, it was considered that an important parameter to be included in a flight evaluation program would be winglet span. Therefore, it was proposed (and accepted by NASA) to change the originally planned flight evaluation program to include a reduced-span winglet so that a back-to-back comparison could be obtained. It was decided to obtain the reduced-span configuration at the appropriate time during the flight test by simply cutting off the outer portion of the basic winglet, so that a truncated shape would be obtained. Such a shape was included in the low-speed test program previously discussed.
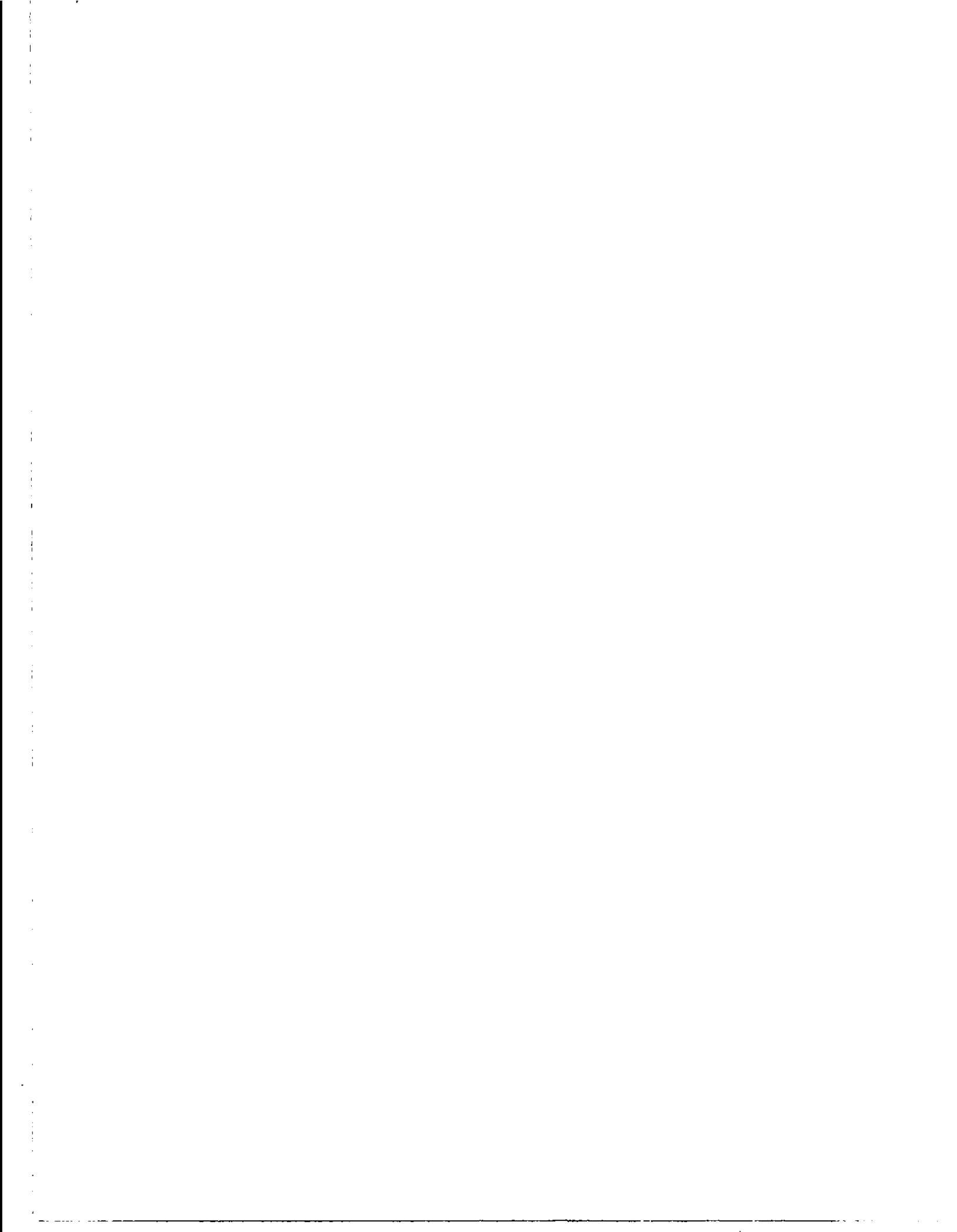
SUMMARY OF CONCLUSIONS AND RECOMMENDATIONS

A series of wind tunnel tests and analyses has been completed to investigate winglet installation effects on the DC-10 aircraft. Four wind-tunnel tests (a high-speed and two low-speed tests to evaluate aerodynamic characteristics and a subsonic flutter test) were included in the investigation in addition to the original development test (Reference 5). Also, a configuration study integrated the results of the wind tunnel tests to provide an overall evaluation of winglet impact on the DC-10. Although the test programs employed models of the DC-10 Series 30 aircraft, the results of this study are believed to be sufficiently general to apply to all models of the DC-10 aircraft. Detailed conclusions for each of the individual investigations have been listed separately in each section. A synopsis of these results follows.

High-speed investigations — Based on the results of the DC-10 winglet configuration development test (Reference 5), a significant high-speed drag improvement was realized from the installation of winglets. The present investigation showed that winglets had a negligible effect on the DC-10 cruise buffet or stability and control characteristics but offered some improvement to outboard aileron effectiveness at high speeds for possible active control applications.

Low-speed investigations — Results indicate that the DC-10 stall speed would be unchanged by the addition of winglets but that considerable winglet low-speed drag reduction would favorably impact takeoff climb performance. No adverse effects of winglet-related low-speed stability, control, or flying qualities were apparent for either of the two winglet configurations examined. Upper winglet flow separation was apparent prior to wing stall, leading to concern of possible winglet-induced low-speed buffet which can be conclusively investigated only in flight. While it is anticipated that winglet flow separation would be different in flight than in wind tunnel tests because of Reynolds number effects, a winglet leading edge device should be included as a contingency in a flight evaluation program.

Subsonic flutter investigations — Addition of winglets to the DC-10 resulted in detrimental effects on DC-10 flutter characteristics originating from both winglet mass/inertia and aerodynamic properties. Winglets degraded the basic existing DC-10 wing flutter mode and introduced a new critical mode. Winglet flutter effects were accurately predicted by present analysis methods, thereby providing confidence in the application of the methods to analyze winglet configurations.

Configuration integration analysis — Performance benefits, structural modifications, retrofit feasibility, development cost, and economics of winglet applications to the DC-10 aircraft were evaluated and determined to be of sufficient merit to indicate further development.

In general, the winglet installation effects on the DC-10 have been evaluated and determined to be acceptable. Consequently, the DC-10 winglet technology has been advanced to a level which indicates that the winglet cruise drag benefit is obtainable. Further development should include flight evaluation to substantiate the potential winglet cruise drag and low-speed drag reduction as well as to investigate areas (such as low-speed buffet) which cannot be conclusively evaluated in wind tunnel investigations. Flight evaluation is recommended as the next logical step to build on the accomplishments of the present study in order to bring the DC-10 winglet technology to fruition.

REFERENCES

1. Flechner, S. G.; Jacobs, P. F.; and Whitcomb, R. T.: A High Subsonic Speed Wind-Tunnel Investigation of Winglets on a Representative Second-Generation Jet Transport Wing. NASA TN D-8264, July 1976.

2. Whitcomb, R.T.: A Design Approach and Selected Wind-Tunnel Results at High Subsonic Speeds for Wing-Tip Mounted Winglets. NASA TN D-8260, July 1976.

3. Anon.: 747 Product Development, Boeing Commercial Airplane Company: Selected Advanced Aerodynamics and Active Controls Technology Concepts Development on a Derivative B-747 Aircraft. NASA CR-3295, January 1980.

4. Shollenberger, C. A.: Application of an Optimized Wing-Winglet Configuration to an Advanced Commercial Transport. NASA CR-159156, November 1979.

5. Gilkey, R. D.: Design and Wind Tunnel Tests of Winglets on a DC-10 Wing. NASA CR-3119, April 1979.

6. Crowder, J. P.; Hill, E. G.; and Pond, C. R.: Selected Wind Tunnel Testing Techniques at the Boeing Aerodynamics Laboratory. AIAA Paper 80-0458, March 1980.

1. Report No. NASA CR-3677	2. Government Accession No.	3. Recipient's Catalog No.
4. Title and Subtitle RESULTS OF WINGLET DEVELOPMENT STUDIES FOR DC-10 DERIVATIVES		5. Report Date March 1983
		6. Performing Organization Code
7. Author(s) C. A. Shollenberger, J. W. Humphreys, F. S. Heiberger, and R. M. Pearson		8. Performing Organization Report No. ACEE-17-FR-1682
		10. Work Unit No.
9. Performing Organization Name and Address Douglas Aircraft Company McDonnell Douglas Corporation 3855 Lakewood Boulevard Long Beach, California 90846		11. Contract or Grant No. NAS1-15327
		13. Type of Report and Period Covered
12. Sponsoring Agency Name and Address National Aeronautics and Space Administration Washington, DC 20546		Contractor Report
		14. Sponsoring Agency Code

15. Supplementary Notes

Langley Technical Monitor: Thomas G. Gainer
Final Report

16. Abstract

The results of investigations into the application of winglets to the DC-10 aircraft are presented. The DC-10 winglet configuration was developed and its cruise performance determined in a previous investigation. This study included high-speed and low-speed wind tunnel tests to evaluate aerodynamic characteristics, and a subsonic flutter wind tunnel test with accompanying analysis and evaluation of results. Additionally, a configuration integration study employed the results of the wind tunnel studies to determine the overall impact of the installation of winglets on the DC-10 aircraft. Conclusions derived from the high-speed and low-speed tests indicate that the winglets had no significant effects on the DC-10 stability characteristics or high-speed buffet. It was determined that winglets had a minimal effect on aircraft lift characteristics and improved the low-speed aircraft drag under high-lift conditions. The winglets affected the DC-10 flutter characteristics by reducing the flutter speed of the basic critical mode and introducing a new critical mode involving outer wing torsion and longitudinal bending. The overall impact of winglets was determined to be of sufficient benefit to merit flight evaluation.

17. Key Words (Suggested by Author(s)) DC-10 Buffet Flutter Winglets Configuration integration Low speed drag improvement Stability and control characteristics Aileron effectiveness	18. Distribution Statement FEDD Distribution Subject Category 05		
19. Security Classif. (of this report) Unclassified	20. Security Classif. (of this page) Unclassified	21. No. of Pages 174	22. Price